

# **A biotechnological approach to understanding the interactions between endothelial cell integrins and neuropilin-2 in Angiogenesis**

---

**Abdullah Asser A Alghamdi**

A thesis submitted for the degree of Doctor of Philosophy  
(Ph.D.) in Biomolecular Science

University of East Anglia  
School of Biological Sciences

**June 2019**

© This copy of the thesis has been supplied on condition that anyone who consults it is understood to recognise that its copyright rests with the author and that use of any information derived there from must be in accordance with current UK Copyright Law. In addition, any quotation or extract must include full attribution.

## Abstract

---

Although a number of studies have focused on the role of neuropilin-2 (NRP2) in early embryological development and in various cancer cells, very little is known about the biological roles of NRP2 in microvascular endothelial cells (ECs). Here, we show that siRNA depletion of NRP2 decreases fibronectin (FN)-dependent migration, adhesion and focal adhesion assembly and disassembly in murine lung microvascular endothelial cells (ECs). Compared to control cells, NRP2-depleted cells exhibit elevated levels of total cellular integrin- $\alpha$ 5 (ITGA5 - the main FN receptor in ECs), but this increase does not translate to the cell surface. MS analysis identified the major FN receptors  $\alpha$ 5 $\beta$ 1 as NRP2 binding partners. However, ITGA5 internalization and recycling assays revealed that NRP2 knockdown suppress ITGA5 recycling to the cell surface and a direct interaction between NRP2 and ITGA5 is observed by co-immunoprecipitation. This suggests that NRP2 controls microvascular EC behaviour on FN by regulating ITGA5 function.

## **Dedication**

---

To my parents,  
**Asser and Fatima,**  
Without whom I would not be who I am

# Table of Contents

Abstract.....	2
Dedication.....	3
List of Figures.....	9
List of Tables.....	10
Chapter 1: Introduction.....	11
1.1 Circulatory system.....	11
1.1.1 Blood vessel function and architecture.....	12
1.1.2 Endothelium.....	15
1.1.3. Extracellular matrix.....	17
1.2. Blood vessel development/formation.....	20
1.2.1 Vasculogenesis.....	20
1.2.2. Angiogenesis.....	22
1.2.2.1. Mechanism of sprouting angiogenesis.....	22
1.2.2.2. The VEGF family and their receptors.....	25
1.2.2.2.1. VEGF.....	29
1.2.2.2.2. VEGFR2.....	32
1.2.2.2.2.1. VEGF and VEGFR2 during early stage of angiogenesis.....	33
1.2.2.2.2.2. VEGF/VEGFR2 signalling mechanism.....	34
1.2.3. Additional molecular players in angiogenesis.....	38
1.2.3.1 Neuropilin.....	38
1.2.3.1.1 History of neuropilin.....	38
1.2.3.1.2. NRP structure.....	39
1.2.3.1.3. Neuropilins in embryonic development.....	42
1.2.3.1.4 Post-embryonic Neuropilin expression.....	43
1.2.3.1.4.1. Neuropilins in nerve cells.....	43
1.2.3.1.4.2. Neuropilins in ECs.....	44
1.2.3.1.4.2.1 NRP1.....	45
1.2.3.1.4.2.2 NRP2.....	51
1.2.3.1.4.2.2.1. NRP2's function in cancer.....	54
1.2.3.2. Integrins.....	59
1.2.3.2.1. Integrin structure and ligands.....	60
1.2.3.2.2. Integrin activation.....	64

1.2.3.2.2.1. Outside-in signalling.....	66
1.2.3.2.2.2. Inside-out signalling.....	67
1.2.3.2.2.3. Cross talk between integrin and growth factor receptors to control downstream signalling pathways during outside-in signalling .....	70
1.2.3.2.3. Integrins in angiogenesis.....	73
1.2.3.2.3.1. $\alpha\beta3$ integrin.....	75
1.2.3.2.3.1.1. $\alpha\beta3$ -VEGFR2 complex and NRP1 functions in ECs.....	76
1.2.3.2.3.2. $\alpha5\beta1$ integrin.....	81
1.2.3.2.4. Integrin trafficking .....	86
1.2.3.2.4.1. Examples of $\alpha\beta3$ and $\alpha5\beta1$ trafficking .....	91
1.3 Research Aims and Objectives .....	94
Chapter 2: Materials and Methods.....	95
2.1. Chemicals, antibodies, restriction enzymes and VEGF <sub>164</sub> .....	95
2.2. Lung microvascular ECs isolation .....	98
2.3. Microvascular EC immortalisation .....	99
2.4. Freezing and thawing cells.....	99
2.5. Tissue culture .....	100
2.6. Mouse genotyping.....	101
2.6.1. DNA extraction.....	101
2.6.1.1. <i>Itgb3</i> knockout genotype.....	101
2.6.1.2. <i>Pdgfb.CreER</i> genotyping .....	102
2.6.2. Agarose gel electrophoresis .....	103
2.6.2.1. 8% gel preparation .....	103
2.7. Endothelial cells Electroporation (Nucleofection).....	103
2.7.1. General procedure .....	103
2.8. Reusing cuvettes .....	104
2.9. Western blot analysis .....	104
2.9.1. Lysate preparation.....	104
2.9.2. Preparing SDS-PAGE gels .....	105
2.9.3. Electrophoretic separation of proteins and transferring proteins to a membrane .....	106
2.9.4. Primary/secondary antibody incubation and chemiluminescence detection .....	106
2.9.5. Western blot analysis .....	107
2.10. Signalling assays.....	107
2.11. EC detachment assay .....	108

2.11.1. Trypsin .....	108
2.11.2. Other cell detachment reagents .....	108
2.12. Adhesion assay.....	108
2.13. Random migration assay .....	109
2.14. Wound healing migration assay .....	110
2.15. Proliferation assays .....	111
2.15.1. WST-1.....	111
2.15.2. BrdU.....	111
2.16. Protein and FA turnover assay .....	112
2.17. Immunocytochemistry .....	113
2.18. Immunoprecipitation.....	113
2.18.1. Silver staining .....	114
2.18.2. Mass spectrometry .....	115
2.19. Flow cytometry (FC).....	115
2.20. Subcellular protein fractionation assay .....	116
2.21. Protein stability assay .....	117
2.22. Protein cell surface internalisation assay .....	118
2.23. Protein cell surface recycling assay .....	119
2.24. Building shRNA constructs .....	120
2.24.1. Target sequence selection .....	120
2.24.2. Oligomer design.....	121
2.24.3. Vector digestion and extraction .....	121
2.24.4. Oligo annealing.....	121
2.24.5. Vector-oligo (pconstruct) ligation.....	122
2.24.6. Bacterial transformation and colony selection.....	122
2.24.7. Plasmid miniprep .....	123
2.24.8. Plasmid digestion and positive clone detection .....	123
2.24.9. Sequencing and plasmid maxiprep .....	123
2.24.10. Lentivirus production.....	124
2.24.11. Concentrating lentivirus.....	125
2.24.12. Lentivirus titering.....	125
2.24.13. Plasmid transfection and infection.....	126
2.24.13.1. Immortalised mLMCEs transfection with shRNAs constructs.....	126

2.24.13.2. Primary lung ECs infection with lentivirus .....	126
2.25. <i>ex vivo</i> aortic ring assay .....	126
2.26. Graphics and statistical significance analysis .....	127
Chapter 3: An introduction to investigating potential links between ITGB3 and NRP2.....	128
3.1. Examining ITGB3 levels across a panel of polyomavirus middle-T-antigen immortalized ECs.....	128
3.2. Analysis of NRP2 knockdown efficiency in immortalised ECs.....	131
3.3. Discussion.....	133
3.4. Conclusion .....	135
Chapter 4: Investigating the roles of NRP2 in ECs .....	136
4.1. Upregulation of NRP2 in $\beta$ 3HET cells; ITGB3 depletion upregulates the expression of NRP2, similar to what was previously reported with NRP1. ....	136
4.2. There is no link between NRP2 and ITGB3 in response to VEGF <sub>164</sub> stimulation, but NRP2 depletion marginally impairs VEGFR2/ERK phosphorylation in response to VEGF-stimulation.....	139
4.3. NRP2-depletion reduces random migration in ECs, but the effects are not linked to ITGB3. ....	143
4.4. NRP2 does not regulate EC proliferation. ....	147
4.5. NRP2 is Trypsin sensitive; and siRNA-mediated depletion of NRP2 reduces the relative number of ECs adhered on Fibronectin. ....	149
4.6. NRP2 knockdown slows the rate of focal adhesion turnover .....	154
4.7. Identifying the potential NRP2 binding partners using Mass Spectrometry (MS).....	157
4.8. SiRNA-mediated knockdown of NRP2 upregulates ITGA5 expression.....	163
4.9. ITGA5 subunit interacts with NRP2.....	165
4.10. Discussion .....	168
4.11. Conclusion .....	173
Chapter 5: Investigating how NRP2 regulates ITGA5 function in mouse lung endothelial cells .....	175
5.1. NRP2 knockdown disrupts the structural formation of ITGA5 on FN; and attempting to localise NRP2 with ITGA5 in mLMECs. ....	175
5.2. Subcellular protein fractionation revealed NRP2 is localized in cellular membranes....	179
5.3. NRP2 seems to regulate ITGA5 turnover.....	182
5.4. NRP2 knockdown does not change ITGA5 levels on the cell surface .....	182
5.5. NRP2 does not regulate the total ITGA5 subunit internalization. ....	184
5.6. NRP2 knockdown supresses ITGA5 subunit recycling.....	188

5.7. Discussion .....	191
5.8. Conclusion .....	194
Chapter 6: Investigating NRP2 silencing effect in the angiogenesis <i>ex vivo</i> aortic ring model .....	195
6.1. Selection of NRP2 targeting sequences, designing the short hairpin RNA (shRNA) oligonucleotides, and generating conditional lentiviral vectors. ....	196
6.2. Inefficient mLMECs uptake of pSicoR constructs introduced by electroporation.....	201
6.3. Infecting primary ECs with pSico lentiviruses induced marginal NRP2 knockdown....	204
6.4. Infecting aortic rings with the pSico lentivirus provided inconclusive results.....	206
6.5. Discussion .....	208
6.6. Conclusion .....	209
Chapter 7: Summary and Conclusion .....	210
7.1. Novelty and Significance .....	210
7.2. Summary of the Findings and discussion .....	210
7.3. Final Conclusion .....	214
7.4. Priority future work.....	214
7.5. Other future work.....	216
Publication: .....	219
Abbreviations:.....	220
References:.....	225

## List of Figures

<b>Figure 1.1</b>	The basic structure of the blood vessels and the direction of the blood flow.....	14
<b>Figure 1.2</b>	Endothelial morphology and transmembrane junctional adhesive proteins between adjacent ECs.....	18
<b>Figure 1.3</b>	Pericyte interactions with endothelium along small blood vessels	19
<b>Figure 1.4</b>	Development of blood vessels through vasculogenesis and angiogenesis processes.....	21
<b>Figure 1.5</b>	Mechanisms of formation of new blood vessel from a pre-existing vessel.....	24
<b>Figure 1.6</b>	Structure of VEGF receptors and their ligands.....	28
<b>Figure 1.7</b>	VEGF-A pre-mRNA isoforms.....	31
<b>Figure 1.8</b>	VEGFR2 downstream signalling via its tyrosine phosphorylation sites.....	32
<b>Figure 1.9</b>	Neuropilin structure and ligand interactions.....	41
<b>Figure 1.10</b>	Contribution of NRP1 function in VEGF-A165/VEGFR2 vs VEGF-A121/VEGFR2 signalling in ECs.....	50
<b>Figure 1.11</b>	Differential VEGFR2 activation driven by NRP1-binding in <i>cis</i> -vs. <i>trans</i> .....	50
<b>Figure 1.12</b>	The integrin subfamilies and their ligands.....	62
<b>Figure 1.13</b>	Integrin structure and conformational changes to integrin $\alpha\beta$ subunits during activation.....	63
<b>Figure 1.14</b>	Anatomical section of a migrating cell adhered to a 2D ECM.....	65
<b>Figure 1.15</b>	The bi-directional signalling of integrins.....	69
<b>Figure 1.16</b>	Downstream signalling of clustered integrin.....	72
<b>Figure 1.17</b>	Structure of Arf and Rab G proteins on the plasma membrane.....	90
<b>Figure 1.18</b>	Trafficking mechanisms of $\alpha V\beta 3$ and $\alpha 5\beta 1$ to regulate cell adhesion and migration of adherent cells.....	93
<b>Figure 3.1</b>	$\beta 3$ -integrin genotyping and expression level analyses of immortalised EC lines.....	129
<b>Figure 3.2</b>	Establishing optimised NRP2 knockdown and Western blotting conditions.....	132
<b>Figure 4.1</b>	Upregulation of NRP2 expression in $\beta 3$ HET ECs.....	138
<b>Figure 4.2</b>	NRP2 silencing attenuates VEGFR2 phosphorylation in response to VEGF <sub>164</sub> .....	142
<b>Figure 4.3</b>	NRP2-siRNA significantly reduces ECs migration in both WT and $\beta 3$ HET ECs.....	146
<b>Figure 4.4</b>	NRP2 doesn't regulate mouse microvascular ECs proliferation...	148
<b>Figure 4.5</b>	NRP2 is Trypsin sensitive, and siRNA-mediated depletion of NRP2 reduces the relative number of microvascular ECs adhered on FN.....	153
<b>Figure 4.6</b>	NRP2 regulate FAs turnover.....	156
<b>Figure 4.7</b>	Mass Spectrophotometry to identify NRP2's binding partners.....	159
<b>Figure 4.8</b>	siRNA-mediated silencing of NRP2 upregulates ITGA5 expression, but not ITGB1.....	164
<b>Figure 4.9</b>	ITGA5 is a partner binding with NRP2.....	167
<b>Figure 5.1</b>	NRP2 knockdown disrupts the structural formation of ITGA5	

	subunit on FN.....	177
<b>Figure 5.2</b>	Measuring the elongated shape of the ITGA5 formed in the NRP2-depleted ECs compared to control cells.....	178
<b>Figure 5.3</b>	NRP2 resides only in the cellular membranes in which only the compartment NRP2 was localised with ITGA5.....	181
<b>Figure 5.4</b>	NRP2 does not regulate ITGA5's synthesis.....	183
<b>Figure 5.5</b>	NRP2 does not change the mount of ITGA5 on the plasma membrane.....	183
<b>Figure 5.6</b>	NRP2 doesn't regulate the total ITGA5 internalization.....	186
<b>Figure 5.7</b>	NRP2 knockdown supresses total ITGA5 Recycling.....	189
<b>Figure 6.1</b>	Selection of NRP2 targets and cloning the shRNA oligonucleotides in conditional vectors.....	197
<b>Figure 6.2</b>	The percentage prediction formation of the short hairpin structures of the four designed shRNAs oligonucleotides targeting different domains of NRP2.....	199
<b>Figure 6.3</b>	pSico and pSicoR constructs digestions with restriction enzymes to detect the positive cloned shRNAs.....	200
<b>Figure 6.4</b>	Inefficient uptake of pSiocR constructs by electroporation.....	203
<b>Figure 6.5</b>	Testing pSico lentivirus of primary ECs.....	205
<b>Figure 6.6</b>	Infecting aortic rings with the pSico lentivirus provided inconclusive results.....	207
<b>Figure 7.1</b>	Model mechanism.....	213

## List of Tables

<b>Table 1.1</b>	Vascular Integrins in Angiogenesis.....	74
<b>Table 2.1</b>	List of primary conjugated antibodies.....	96
<b>Table 2.2</b>	List of primary antibodies.....	96
<b>Table 2.3</b>	List of secondary conjugated antibodies.....	97
<b>Table 2.4</b>	List of restriction enzymes and buffers.....	97
<b>Table 2.5</b>	Summarisation of EC tissue culture conditions.....	100
<b>Table 2.6</b>	Recipes for preparing the resolving and stacking buffer gels.....	105
<b>Table 4.1</b>	Label-Free quantitative (LFQ) mass spectrometry results of NRP2 immunoprecipitation in two mLMEC clones.....	160
<b>Table 6.1</b>	Selecting four different NRP2 targeting sequences starting with (G) and indicating the position, length, score, exon number and the targeting domain of each target.....	198
<b>Table 6.2</b>	Designing NRP2-siRNA (sense & anti-sense) oligonucleotides containing hairpin sequences.....	198

# Chapter 1: Introduction

---

## 1.1 Circulatory system

The circulatory systems of vertebrates and invertebrates differ according to the presence of a true endothelium, which is a continuous layer of adluminal epithelial cells connected by a specialised junctional complex. The circulatory system is responsible for the transport and exchange of fluids containing gases, nutrients and metabolic waste products to and from each cell in the body (Muñoz-Chápuli, Carmona et al. 2005). In diploblastic animals, such as jellyfish, the circulatory system is open to the environment, whereas in triploblastic animals (from flat worms to humans), the circulatory fluids travel through either the body cavity or a complex network of vessels, sinuses and the central macular pump (Monahan-Earley, Dvorak et al. 2013). Acoelomates are small animals, such as flat worms, that lack a body cavity (coelom) and a blood vascular system in which the space between the ectoderm and endoderm is filled with a meshwork of *parenchyma*, which allows them to obtain food and oxygen by simple diffusion across the skin and gut. Small coelomates are animals, such as sea stars, that possess a coelomic circulatory system in which the body cavity provides a connective flow of gas, food and waste products, thus allowing the organ to move freely. Large coelomates, including mice and humans, possess a vascular system that circulates both blood and lymph throughout the body (Monahan-Earley, Dvorak et al. 2013). In large coelomates, fluid flows through two circulatory systems: 1) the cardiovascular system, which circulates blood that is mainly composed of plasma, erythrocytes (red blood cells), leukocytes (white blood cells), and thrombocytes (platelets); 2) lymphatic circulation, which collects lymph that is derived from the interstitial fluid and returns it to the blood circulation (Pugsley and Tabrizchi 2000).

In the cardiovascular system, which is also called systemic circulation, the blood is circulated in a “closed loop” through two circulatory systems: systemic circulation and pulmonary circulation. In systemic circulation, oxygenated blood is circulated from the heart through arteries that branch into arterioles until it reaches the arterial capillaries. Because the hydrostatic pressure within these capillaries is greater, the blood is diffused from these capillaries to the interstitial tissues that take up the oxygen and nutrients. Simultaneously, the

waste products, including carbon dioxide, that are secreted by these surrounding tissues, are diffused back to the venial capillaries because of the greater osmotic pressure within these capillaries. The deoxygenated blood then is circulated through venules and large veins back to the heart. In pulmonary circulation, the deoxygenated blood in the heart is pumped to the lung capillaries. Because the oxygen partial pressure (OPP) of CO<sub>2</sub> in the lungs is lower than that within the capillaries, the CO<sub>2</sub> is diffused into the lungs. Simultaneously, the greater OPP of oxygen in the lungs leads to the diffusion of oxygen from the lungs to the capillaries where it is bound by haemoglobins. The oxygenated blood then returns into the heart where it is pumped again throughout the body to supply oxygen to the tissues.

In contrast, the lymphatic system is an 'open' and one-way transport system. The purpose of this system is to collect the excess interstitial fluid, proteins, white blood cells and microorganisms from the interstitial space via lymphatic capillaries and circulate it as lymph. The lymphatic capillaries merge with large lymphatic vessels called lymphatic ducts, which recycle lymph via the lymph nodes back into the cardiovascular circulation. (Riley and Courmand 1951), (Pugsley and Tabrizchi 2000), (Swartz 2001), (Monahan-Earley, Dvorak et al. 2013)

### **1.1.1 Blood vessel function and architecture**

In vertebrates, the blood vessels are the conduits of the cardiovascular system, which allows the movement of the blood. Based on their diameters, blood vessels are categorised into five classes that are connected in series: artery, arteriole, capillary, venule and vein (**Figure 1.1**). The smallest blood vessels (capillaries) consist of only one layer, *tunica interna* (intima), whereas all the larger blood vessels are composed of three layers: *tunica interna*, *tunica media* and *tunica externa* (adventitia). The *tunica interna* is made up of a single layer of endothelial cells surrounded by a basement membrane (BM) that lines the entire circulatory system from the heart to the capillaries. The *tunica media* is located between the innermost and the outermost layer, and it is made up of vascular smooth muscles (vSMC) and elastic fibres. The *tunica externa* is the outermost layer, which is made up of fibro-elastic connective tissues that anchor the vessels to the surrounding tissue.

The function and architecture of the arteries differ from those of veins (see **Figure 1.1**). The arteries transport the oxygenated blood away from the heart (except in the pulmonary artery), whereas veins carry the deoxygenated blood toward the heart (except in the pulmonary vein).

Arteries have narrow lumens and a greater number of muscles and elastic fibres, which allow them to transport the blood under high pressure, whereas veins have wider and fewer muscles and elastic fibres for transporting blood under low pressure. Finally, the arteries do not contain valves (except the semilunar valves of the aorta and the pulmonary artery), whereas veins possess valves that prevent the backflow of the blood. (Pugsley and Tabrizchi 2000), (McConnell 2013), (Potente and Mäkinen 2017)

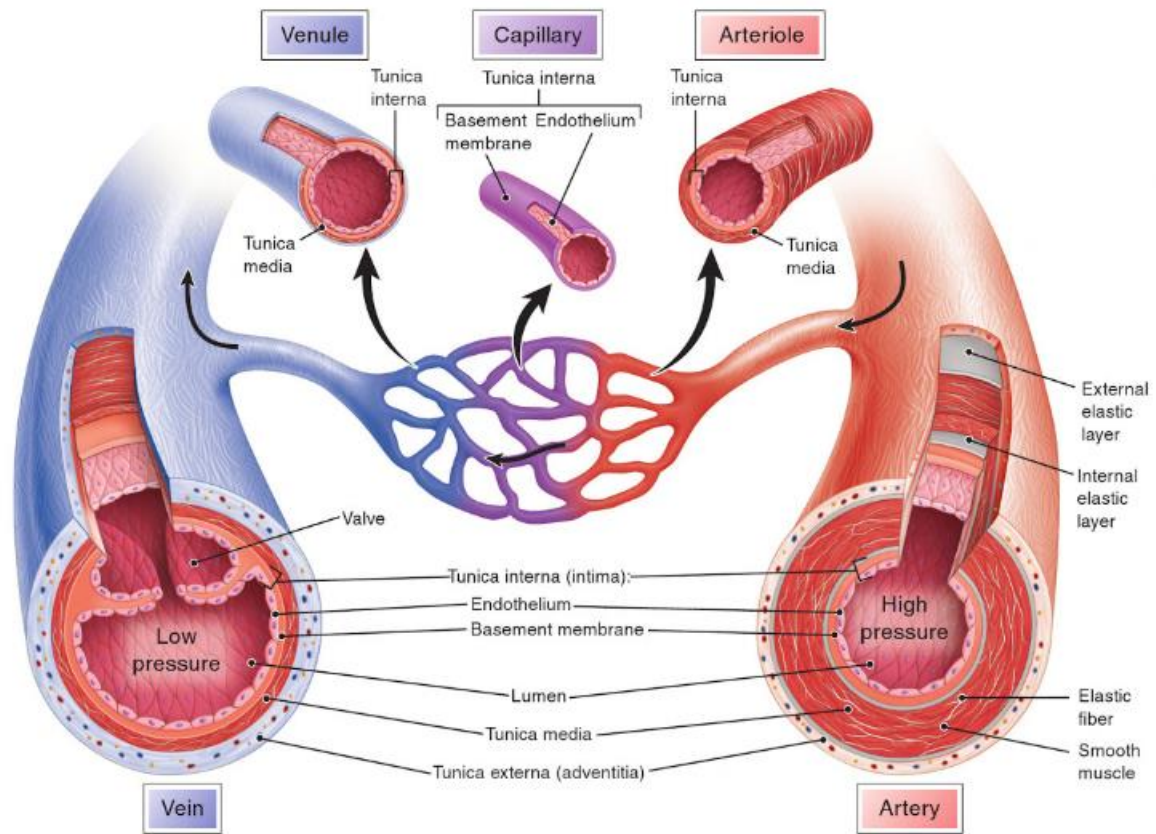


**Figure 1.1 The basic structure of the blood vessels and the direction of the blood flow.** The capillaries consist of only *tunica intema*, whereas the large blood vessels (arteries, arterioles, veins and venules) consist of *tunica intema*, *tunica media* and *tunica externa*. The oxygenated blood flows from the heart into arteries that branch off into arterioles until it reaches the capillaries where the oxygen is diffused. The deoxygenated blood then flows back to the heart after passing through the venules and veins in that order (McConnell 2013).

### 1.1.2 Endothelium

The endothelium consists of a monolayer of cells that line the blood vessels (vascular endothelial cells) and lymphatic vessels (lymphatic endothelial cells), allowing them to interact not only with the circulating blood/lymph but also with the cells in the vessel walls. (Félétou 2011), (Cahill and Redmond 2016). These interactions are achieved because of the presence of three surfaces in the endothelial cells (ECs): cohesive, adhesive and luminal. Cohesive surfaces consist of intracellular gap, tight and adherent junctions that connect ECs to one another and promote crosstalk between adjacent cells. The function of adhesive surfaces is to adhere the endothelium to a sheet-like structure called the basement membrane (BM). Luminal surfaces contain specific binding proteins that regulate the trafficking of the circulating blood cells (Favero, Paganelli et al. 2014).

Although the cells in the endothelium share many common characteristics, they vary in size and shape across the blood vessel network (Setyawati, Tay et al. 2015). Because of these differences, the endothelium is remarkably heterogeneous in structure and function not only in different organs but also within the same organ (e.g. the kidney). The heterogeneity of the endothelium is the most notable at the morphological level, where it can be classified into three types: continuous nonfenestrated, continuous fenestrated, and discontinuous endothelium (Setyawati, Tay et al. 2015) (**Figure 1.2 A**). In the continuous nonfenestrated endothelium, the ECs are joined to one another by intracellular junctions to form a sheet of continuous ECs surrounded by an uninterrupted BM that allows only the passage of small molecules (e.g. water and ions). The plasmalemma also contains a distinct invaginations called caveolae (see **Figure 1.2 A**). This type of endothelium lines the interior surface of arteries, veins and capillaries in the brain, lungs, skin and heart. In continuous fenestrated endothelium, the EC sheet contains ~70nm pores (fenestra), which are sealed by a thin 5–6 nm non-membranous diaphragm and are surrounded by a continuous BM, thus allowing the filtration and transport of certain sizes of solutes. This fenestrated endothelium is found in organs that are involved in filtration or secretion, such as the capillaries of the exocrine and endocrine glands, gastric and intestinal mucosa, choroids plexus, glomeruli and renal tubules. The discontinuous endothelium possesses fenestrations with larger diameters (100–200 nm) that lack a diaphragm but contain pores or “gaps” within individual ECs and an absent or partially formed underlying BM such as that present in the liver. (Cleaver and Melton 2003), (Favero, Paganelli et al. 2014), (Setyawati, Tay et al. 2015), (Kim, Faix et al. 2017). This heterogeneity allows ECs to play central roles in many physiological functions, including

thrombosis, fibrinolysis, inflammation, white cell trafficking, vascular tone, vascular permeability, vascular smooth muscle proliferation, metabolism and angiogenesis (Galley and Webster 2004), (Aird 2007), (Aird 2012), (Setyawati, Tay et al. 2015)

ECs adhere to one another through intracellular junctions (tight, adherent and gap) (**Figure 1.2 B**) formed by transmembrane junctional adhesive proteins, which are linked to the actin cytoskeletal through intracellular signalling proteins. These proteins not only stabilise the junctions but also regulate permeability, haemostasis and apoptosis as well as maintaining their shape and polarity (Dejana 2004), (Bazzoni and Dejana 2004). Some junctional adhesive proteins are specifically expressed in ECs (e.g. VE-cadherins, claudins-5), while others are also expressed in epithelial cells, such as occludin, junctional adhesion molecules (JAM)-A, CD99, and melanoma cell-associated molecules (MCAM), which are also known as (S-endo-1/CD146) or VE-caderin-2 (Wallez and Huber 2008). Tight junctions (TJ) act as either para-cellular passage “gates” for selected ions, water and various macromolecules or “fences” that maintain cell polarity between the luminal side and the outer side of ECs (e.g. claudins and occludins) (Galley and Webster 2004). The adherens junction (AJ) is mainly mediated by vascular endothelial cadherins (VE-cadherins), which interact with several signalling partners to inhibit growth and decrease permeability (Dejana 2004), (Evans, De Vuyst et al. 2006). Nectin is involved in the organisation of both TJ and AJ (Wallez and Huber 2008). The gap junction (GJ) directly connects the cytoplasm of two adjacent cells, mediating cell-to-cell communication through the assembly of connexin hemichannel proteins (connexons), which act as bi-directional channels for the intracellular passage of small molecular weight molecules and ions (Bazzoni and Dejana 2004), (Evans, De Vuyst et al. 2006). Other proteins, such as Platelet endothelial cell adhesion molecule-1 (PECAM-1, CD31), cluster of differentiation (CD99), surface glycoprotein MUC18 (MCAM) and protocadherin-12, also connect adjacent ECs independently of the intracellular junctions (Wallez and Huber 2008). In contrast to epithelial cells, the organisation of endothelial junctions is less defined because the TJs are mingled with the AJs, and the junctional compositions are varied along the vascular tree in different organs (Bazzoni and Dejana 2004), (Wallez and Huber 2008).

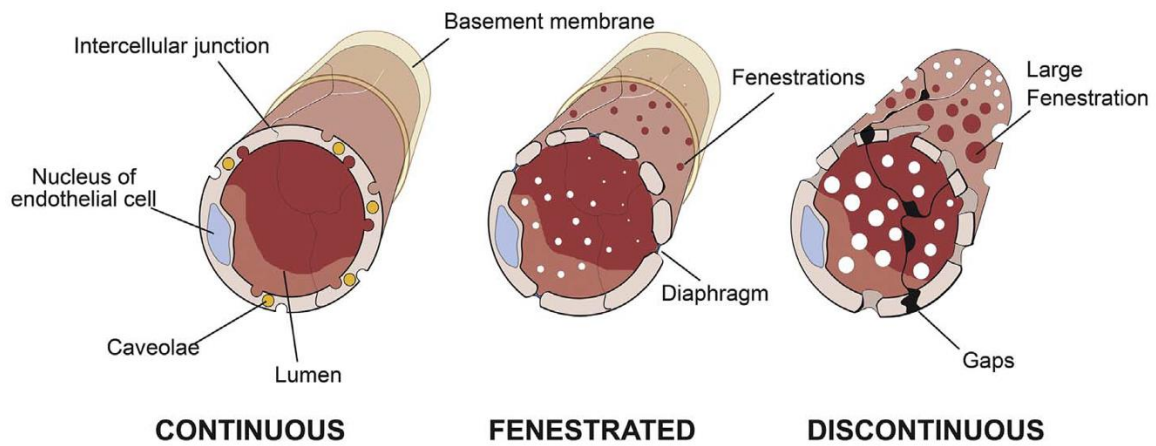
The blood flow within the small vascular vessels (arterioles, venules and capillaries in particular) is not only controlled by the ECs and the surrounding BM but also by contractile small cells called pericytes (**Figure 1.3 A**), which are embedded in the BM and communicate with the ECs through both direct physical interactions and paracrine signalling. For example,

ions and small molecules are exchanged directly between the cytoplasm of the pericytes and the ECs through gap junctions in the peg-socket junctional complex, while the adhesion plaques serve to anchor pericytes to the ECs (**Figure 1.3 B**) (Rucker, Wynder et al. 2000), (Gerhardt and Betsholtz 2003), (Bergers and Song 2005), (Armulik, Genové et al. 2011), (Munde, Khandekar et al. 2014), (Yang, Jin et al. 2017).

### **1.1.3. Extracellular matrix**

ECs are embedded in a collection of non-cellular three dimensional macromolecules called the extracellular matrix (ECM), which can be classified into two distinct compartments: the BM (or basal lamina) and the interstitial matrix (Iivanainen, Kähäri et al. 2003), (Theocharis, Skandalis et al. 2016). These two compartments are not isolated from one another; instead, they are interconnected by a series of anchoring fibrils (**Figure 1.3 C**) (Akalu and Brooks 2005). The BMs are large insoluble molecules secreted by the ECs in a sheet-like structure 50–100 nm in thickness, including type IV collagen, laminin, heparan sulphate proteoglycans (HSPGs) and nidogen/entactin (Raghu 2003), (Iivanainen, Kähäri et al. 2003). The difference between the two compartments is that the BM is always in direct contact with the monolayer of the endothelium, lining up the blood vessels to provide structural support and prevent them from ripping apart, whereas the interstitial matrix is found in the interstitial space between the cells and mainly consists of fibrillar collagens and glycoproteins such as fibronectin (FN) (Iivanainen, Kähäri et al. 2003), (Theocharis, Skandalis et al. 2016). The compartments in the ECM not only provide the scaffolded architecture of the ECs but also exhibit dynamic interactions with endothelial receptors (e.g. integrins), as well as initiating intercellular signalling cascades in response to binding to specific ECM molecules (Iivanainen, Kähäri et al. 2003), (Theocharis, Skandalis et al. 2016). Because of these dynamic interactions, the ECM is continually remodelled either enzymatically or non-enzymatically (Streuli 1999), (Frantz, Stewart et al. 2010) (**Figure 1.3 D**), and thus regulates many cellular processes, including proliferation, migration, differentiation, survival, invasion, morphogenesis and angiogenesis (Iivanainen, Kähäri et al. 2003) (Akalu and Brooks 2005), (Theocharis, Skandalis et al. 2016). For example, during angiogenesis, the matrix metalloproteases (MMPs) degrade the BMs, allowing direct interactions between endothelial receptors and the interstitial matrix molecules, which results in the invasion of ECs through the interstitial matrix until new blood vessels are formed with BM surrounding the endothelium (Senger and Davis 2011).

A)



B)

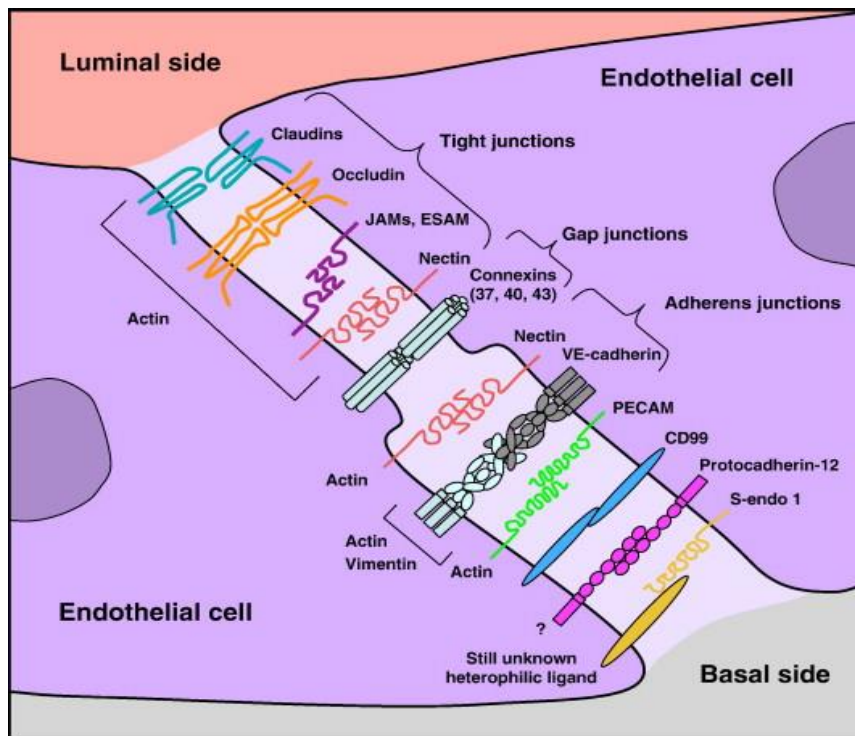


**Figure 1.2 Endothelial morphology and transmembrane junctional adhesive proteins between adjacent ECs.** A) Schematic representation showing the three major types of endothelium. (Kim, Faix et al. 2017) B) Tight junction is mediated by claudins, occludin, JAMs, ESAM and nectin, while the adherens junction is mediated by VE-cadherin and nectin. Tight junctions are formed by hemichannel connexins, whereas PECAM, CD99, protocadherin-12 and S-endo are located outside the intracellular junctions (Wallez and Huber 2008).

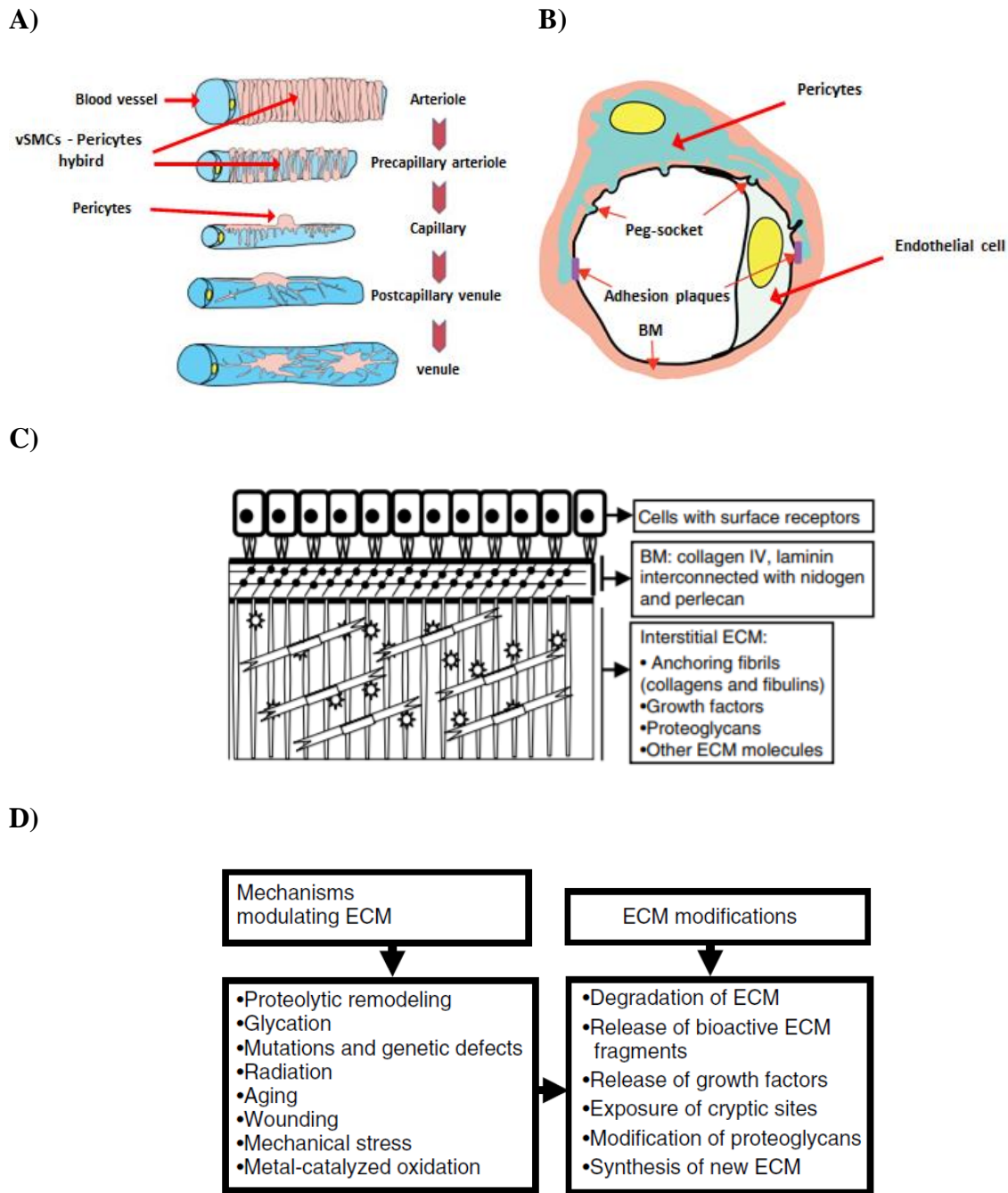


**Figure 1.3 Pericyte interactions with endothelium along small blood vessels.** **A)** All vessels contain a single layer of ECs surrounded by a BM. In contrast to arteries that contain multi layers of vSMCs, the endothelium of arterioles and precapillary arterioles are entirely surrounded by a single layer of vSMCs and pericytes, while capillaries are covered only by pericytes with primary cytoplasmic extensions along the endothelium. On the postcapillaries, the pericytes are flattened, and they produce many slender and secondary branches. The venules are covered by relatively large vSMCs with many branches, and they do not entirely surround the endothelium. **B)** ECs and pericytes are separated by a BM, but they interact with each other at holes in the BM. The number of contacts between a single endothelial cell and pericyte can reach 1,000. These contacts are found at the peg-socket junctional complex and the adhesion plaques that link the actin filaments in the pericyte's cytoplasm to the cytoplasm in the endothelial cell. Figures in A-B are adapted from (Armulik, Genové et al. 2011). **C)** Schematic representation showing ECM organisation and compositions. **D)** Mechanisms by which ECM modifications can alter cellular behaviour (Akalu and Brooks 2005).

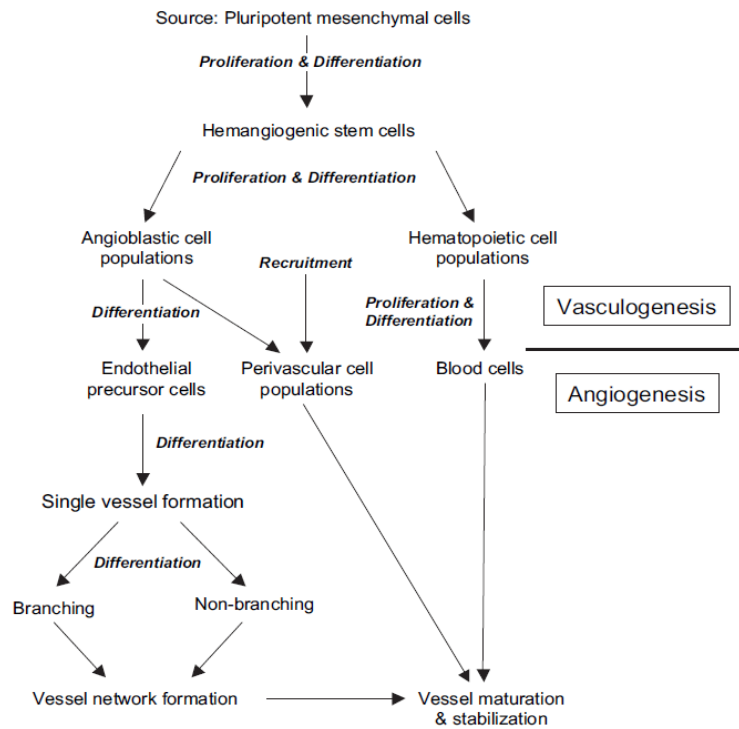
## 1.2. Blood vessel development/formation

Blood vessels are the first functional organ to be developed in the vertebrate embryo (Risau and Flamme 1995). Blood vessels are generally developed through two different processes: vasculogenesis and angiogenesis (**Figure 1.4 A**). In embryonic development, these processes complement each other to eventually form the mature circulatory system. Vasculogenesis refers to the *de novo* formation of primitive blood vessels from vascular progenitor cells, while angiogenesis refers to the formation of new blood vessels by primary and secondary extensions from existing capillaries (Vailhé, Vittet et al. 2001), (Demir, Yaba et al. 2010). Although the formation of the postnatal neovasculature was believed to occur only by angiogenesis, some research suggests that vasculogenesis continues to play an essential role in adults (Asahara, Masuda et al. 1999), (Gehling, Ergün et al. 2000), (Reyes, Dudek et al. 2002), (Balaji, King et al. 2013). For example, endothelial progenitor cells (EPCs), which are derived from bone marrow, circulate in the blood and mobilise to sites of neovascularisation in response to tissue ischaemia, where they differentiate *in situ* into mature ECs to promote tissue repair (**Figure 1.4 B**) (Isner and Asahara 1999).

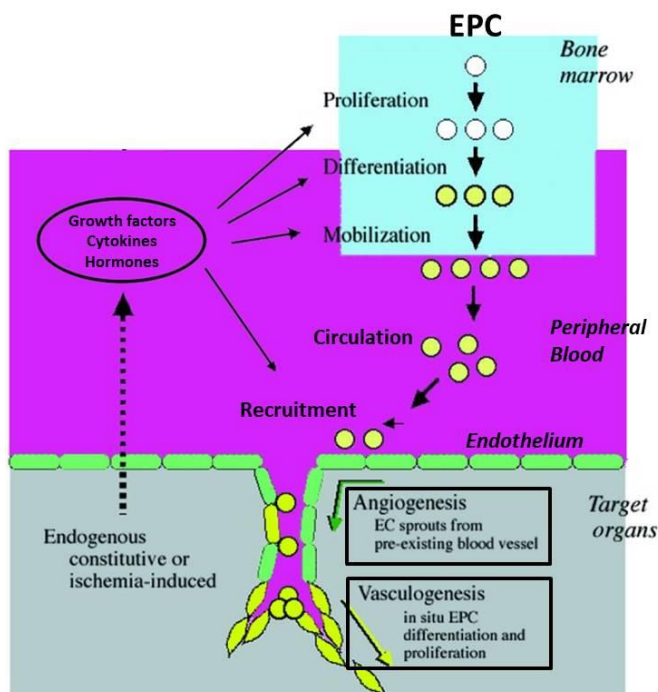
### 1.2.1 Vasculogenesis

During vasculogenesis, primitive blood vessel development is established following the gastrulation process when mesenchymal cell aggregations, known as blood islands, are formed within the mesoderm adjacent to the extra-embryonic yolk sac. These pluripotent mesenchymal cells proliferate and differentiate to multipotent hemangiogenic stem cells (hemangioblasts). The hemangioblasts further proliferate and differentiate into haematopoietic progenitor cells, which give rise to all blood cell types, and angioblastic progenitor cells (angioblasts), which give rise to blood vessels, including endothelial cells and smooth muscle cells (SMC) (**Figure 1.4 C**) (Risau and Flamme 1995), (Conway, Collen et al. 2001), (Kubis and Levy 2003), (Demir, Kayisli et al. 2006), (Failla, Carbo et al. 2018). Therefore, in embryonic development, vasculogenesis is responsible for the formation of the first blood vessels, including the dorsal aorta (Cox and Poole 2000), (Helker, Schuermann et al. 2015), (Jin, Zhu et al. 2017).

A)



B)



C)

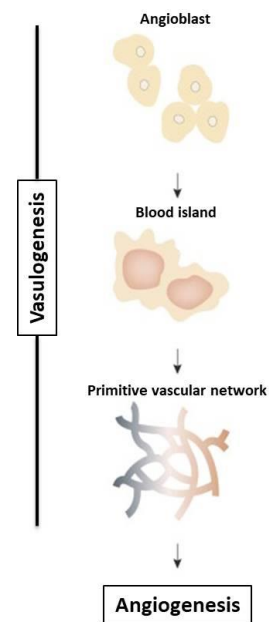


**Figure 1.4 Development of blood vessels through vasculogenesis and angiogenesis processes.** A) The schematic representation shows the complementary step-by-step route of vasculogenesis and angiogenesis to develop a mature vascular network from the mesenchymal cells in the yolk sac during embryonic development (Demir, Kayisli et al. 2006). B) The schematic representation shows the complementarity of vasculogenesis and angiogenesis to develop neovasculature in adults. Adapted from (Isner and Asahara 1999). C) A schematic representation showing the *de novo* formation of the primitive blood vessels from the vascular progenitor cells through vasculogenesis. Adapted from (de Oliveira, Hamm et al. 2011).

## 1.2.2. Angiogenesis

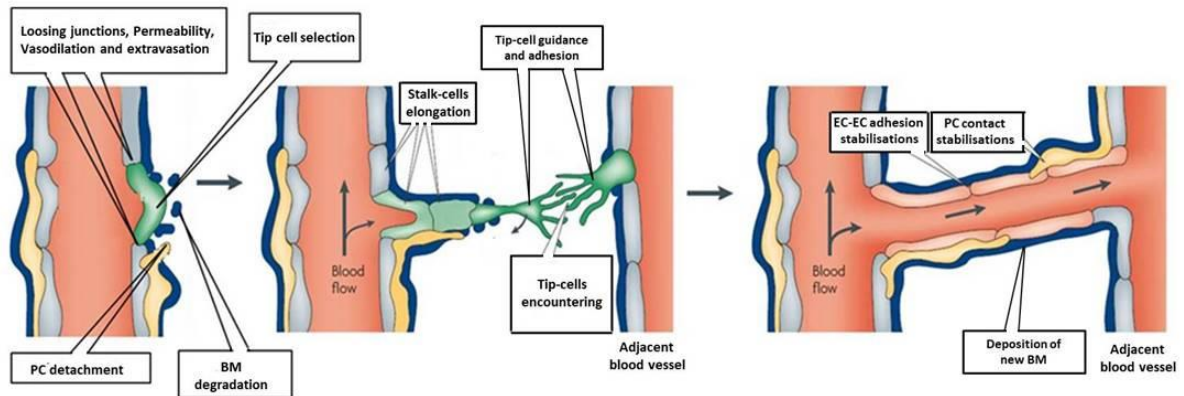
The formation of new blood vessels from already existing vessels (angiogenesis) is achieved by either the migration of endothelial cells from a pre-existing vessel until it eventually forms a mature blood vessel (sprouting angiogenesis) (**Figure 1.5 A**) or by the insertion of the tissue pillar mechanism, which eventually leads to the extension and subdivision of a pre-existing vessel into two mature vessels (intussusceptive or non-sprouting angiogenesis) (**Figure 1.5 B**) (Vailhé, Vittet et al. 2001), (Adams and Alitalo 2007), (Kim, Faix et al. 2017). The main goal of the two types of angiogenesis is to supply blood to newly forming tissue (Demir, Yaba et al. 2010). Angiogenesis normally occurs during embryonic development after the *de novo* formation of the primitive blood vessels by vasculogenesis (see **Figure 1.4**), but it rarely occurs in adults because most blood vessels are quiescent except in wound or fracture healing after an injury, in females during endometrial growth and corpus luteum formation, and in specific diseases (e.g. diabetic retinopathy and tumour growth) (Klagsbrun and Moses 1999), (Demir, Yaba et al. 2010).

### 1.2.2.1. Mechanism of sprouting angiogenesis

Sprouting angiogenesis is a complex process of sequential stages that employ many cellular proteins and growth factors secreted by different cell types. In a healthy adult, quiescent ECs are interconnected through junctional molecules (see **Figure 1.2 B**) and ensheathed by pericytes, which stabilise ECs and suppress EC proliferation and release cell survival growth factors, such as vascular endothelial growth factor (VEGF) and angiotensin 2 (ANG-2). Because ECs are in direct contact with the blood flow, they are equipped with oxygen sensors, such as prolyl hydroxylase domain 2 (PHD2) and hypoxia-inducible factor-2 $\alpha$  (HIF-2 $\alpha$ ), to optimise blood flow within vessels, and re-adjusting their shape accordingly. In a resting state, ECs and pericytes form the BM. However, when these quiescent ECs sense pro-angiogenic growth factors, such as VEGF, angiotensin 2 (ANG-2), basic fibroblast growth factor (bFGF), placental growth factor (PIGF, PLGF or PGF), chemokines, or tumour necrosis factor alpha (TNF $\alpha$ ) (Ferrara, Gerber et al. 2003), the pericytes are first removed from the vessel walls, mainly in response to ANG-2. The ECs are thereby liberated from the BM, increasing permeability and vasodilation in the vessel by proteolytic enzymes, such as MMPs, which degrade the surrounding BM and allow the interstitial provisional matrix components, such as FN, vitronectin and type I collagen, to directly interact and activate the ECs signalling through their cell surface anchors (integrins). Following the disruption of the

intracellular junctions, the ECs are liberated and thereby proliferate, migrate and invade the ECM toward the angiogenic stimuli site. The initial formation of a new blood vessel from a pre-existing one is initiated by the selection of one endothelial cell, known as the tip cell, which leads the growing sprout in response to the secreted growth factor (e.g. binding of VEGF isoforms to their VEGF receptors (VEGFRs) and neuropilins by extending filopodia to explore signals that are present in the tissue environment. Notch receptors and their ligands (e.g. delta like ligand 4 (DLL4) and Jagged1) have also been shown to be essential in sprouting growth during development. At this stage, as well as during other steps in sprouting angiogenesis, changes in the balance between pro- or anti-angiogenic factors may result in pruning the formation of the new vessel. Cells behind the tip cells (known as stalk-cells), divide to elongate the sprout toward the angiogenic stimulus until lumen formation within the endothelial sprout is established, ultimately forming loops by the anastomoses of sprouts to connect blood flow. For the vessel to be functionally mature, ECs first have to regain their BM and intercellular junctions, a process initiated by protease inhibitors called tissue inhibitors of metalloproteinases (TIMPs) and plasminogen activator inhibitor-1 (PAI-1). Finally, mural cells (pericytes and vSMCs) are then recruited, mainly by platelet-derived growth factor-B (PDGF-B) and ANG-1, to stabilise ECs, which then resume their quiescent phalanx state. The blood flow increases oxygen delivery and thus reduces pro-angiogenic attractants (see **Figure 1.5 A**) (Raghu 2003), (Adams and Alitalo 2007), (Demir, Yaba et al. 2010), (Senger and Davis 2011), (Elpek 2015).

A)



B)

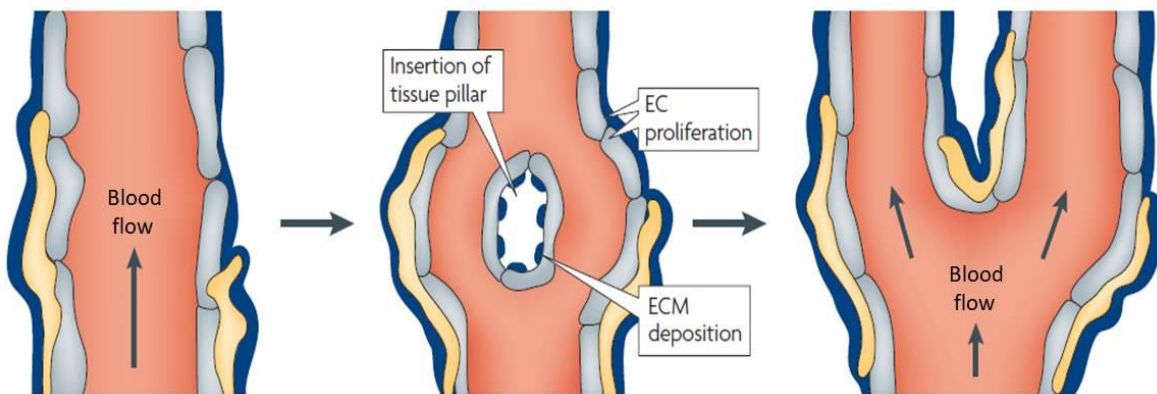


**Figure 1.5 Mechanisms of formation of new blood vessel from a pre-existing vessel. A) Sprouting angiogenesis.** In response to angiogenic factors, the following sequential changes occur during sprouting angiogenesis: 1) de-attachment of pericytes from a blood vessel walls (in response to ANG-2); 2) degradation of BM by enzymatic degradation (e.g. MMPs) as well as disruption of intracellular junctions, which results in increasing vessels permeability and vasodilation; 3) selection of a tip cell (regulated by DLL4 and NOTCH signalling); 4) proliferation of the stalk-cells behind the tip cell; 5) migration of the tip cell toward the source of the angiogenic (guidance) signals, which is mediated by adhesion of integrins to ECM; 6) encountering the tip cell with the tip cell of the adjacent blood vessel; 7) strong EC-EC junctional interactions are established at this joining point; 8) re-establishing BM and intracellular junctions and deposition of ECM protein into the sub-endothelial BM; 9) stabilising ECs by pericyte attachment to resume ECs quiescent phalanx state; 10) Flowing of blood to adjacent blood vessel improves oxygen delivery and thus reduces pro-angiogenic signals. **B) Intussusceptive (Non-sprouting) angiogenesis.** Little is known about the function and regulation of this mechanism but it is believable that it involves ECM degradation, EC proliferation and new ECM deposition (Raghu 2003). Adapted from (Adams and Alitalo 2007), (Carmeliet and Jain 2011).

### 1.2.2.2. The VEGF family and their receptors

VEGFs are disulphide bond-linked soluble secretory glycoproteins. In mammals, five subtype members of the family are designated as VEGF-A (also known as VEGF) to VEGF-D (also known as FIGF) and the placenta growth factor (PLGF), which are characterised by the presence of eight conserved cysteine residues that form a cystine knot structure (Muller, Li et al. 1997), (Holmes and Zachary 2005), (Shibuya 2011), (Iyer and Acharya 2011). Virus-encoded VEGF-E (Meyer, Clauss et al. 1999) and snake venom-derived VEGF-F (Yamazaki, Matsunaga et al. 2009) have also been identified (Iyer and Acharya 2011). The VEGF family regulates the physiological and pathological development of blood and lymph vessels through binding to their transmembrane type III receptor tyrosine kinases (RTKs) (**Figure 1.6**) as well as non-tyrosine kinase receptors (neuropilins), which will be discussed in section **1.2.3.1** (see **Figure 1.9 B**) (Duffy, Bouchier-Hayes et al. 2004), (Demir, Kayisli et al. 2006), (Smith, Fearnley et al. 2015). Following the binding of VEGFs and the dimerisation of VEGFRs, auto-phosphorylation occurs, generating a series of VEGF-associated downstream signals that change and regulate many cellular functions (Arroyo and Winn 2008), (Mesquita, Castro-de-Sousa et al. 2018).

The VEGF/VEGFR-associated signalling pathways play an essential role in orchestrating EC behaviour during the angiogenic process (Harry and Paleolog 2003), (Carmeliet 2003), (Kim, Faix et al. 2017). Three VEGF tyrosine kinase receptor subtypes, which are similar to platelet-derived growth factor receptors (PDGFRs), have been identified: VEGFR1 (flt-1), VEGFR2 (flk-1) and VEGFR3 (flt-4). (Arroyo and Winn 2008), (Peach, Mignone et al. 2018). Both VEGFR1 and VEGFR2 have an extracellular region that consists of seven immunoglobulin-like domains. VEGFR3 has the same composition except in its extracellular region, which consists of only six Ig-homology domains (Ferrara, Gerber et al. 2003), (Shibuya 2011). In the embryos of gene-targeted mice, the knockout of any VEGFR is lethal because of dramatic blood vessel phenotypes. However, in adults, VEGFR3 expression becomes restricted to lymphatic ECs and certain fenestrated blood vessels (Kaipainen, Korhonen et al. 1995), (Partanen, Arola et al. 2000), (Tammela, Enholm et al. 2005). It is noteworthy mentioning that VEGFR1 and VEGFR2 can also exist as soluble secreted forms sVEGFR1 and sVEGFR2, respectively (Arroyo and Winn 2008), (Lal, Puri et al. 2018), (Collet, Lamerant-Fayel et al. 2013).

VEGFR1 and VEGFR2 are predominantly expressed by vascular ECs (Costache, Ioana et al. 2015), whereas (as mentioned above) VEGFR3 expression is limited largely to lymphatic ECs. Among the three subtypes in the family of VEGFRs, VEGFR2 is the major mediator of angiogenic, mitogenic and permeability pathways via its interactions with VEGF-A (Achen, Jeltsch et al. 1998), (Costache, Ioana et al. 2015). VEGF-A binds to VEGFR1 with an affinity that is 10-fold higher than its binding to VEGFR2, but binding to VEGFR2 promotes more potent angiogenic responses than VEGFR1 (Sawano, Takahashi et al. 1996). VEGFR1 is also a receptor for VEGF-B and PLGF, while both VEGFR2 and VEGFR3 are receptors for VEGF-C and VEGF-D (Lal, Puri et al. 2018). The alternative splicing of VEGF-A, VEGF-B and PLGF can form different isoforms, whereas VEGF-C and VEGF-D isoforms are formed through proteolytic processing (Tammela, Enholm et al. 2005).

VEGF-B (also called VEGF-related factor/VRF) and PLGF bind to and activate only VEGFR1 (Lal, Puri et al. 2018). Both VEGF-B-NULL mice and PLGF-NULL mice are viable and develop with no significant angiogenic defects, suggesting that the genes of these two growth factors are dispensable for embryogenesis (Takahashi and Shibuya 2005), (Shibuya 2011). However, some studies showed that these mice do develop mild phenotypes, such as smaller hearts and slower myocardial recovery following ischemia (Bellomo, Headrick et al. 2000), (Li, Tjwa et al. 2008), (Sun, Jin et al. 2004). Although VEGF-B has a wide tissue distribution, it is highly expressed in the heart, skeletal muscles and pancreas (Lal, Chiu et al. 2017), (Mesquita, Castro-de-Sousa et al. 2018). Because VEGF-B is highly related to VEGF-A, it can compete with VEGF-A for VEGFR1 and form heterodimers with VEGF-A to increase its bioavailability (Iyer and Acharya 2011). PLGF is highly expressed in the placenta and other organs, such as heart, lung and ovary (Tammela, Enholm et al. 2005). Although PIGF is known to bind only to VEGFR1, it can also form a heterodimer with VEGF-A and then bind to VEGFR2 (Autiero, Lutun et al. 2003)

VEGF-C and VEGF-D are not essential for blood vessel formation. Instead, they are implicated in lymphatic vessel formation (lymphangiogenesis) (Tammela, Enholm et al. 2005). VEGF-C is expressed during embryonic development, whereas VEGF-D is expressed after birth (Shibuya 2011). Both growth factors are secreted as pro-proteins with long C and N terminals. They do not bind to VEGFR2 or VEGFR3 until they are cleaved by proteolytic processing (Lal, Puri et al. 2018). VEGF-C and its receptor, VEGFR3, are expressed in regions where lymph vessels sprout from blood vessels, and then their expression is decreased in most tissues except in the lymph nodes where expression remains high

(Kaipainen, Korhonen et al. 1995), (Iyer and Acharya 2011). Mouse embryos missing both alleles of VEGF-C, but not of VEGF-D (Baldwin, Halford et al. 2005), die due to a failure in the development of lymphatic vasculature (e.g. lymphedema) (Karkkainen, Haiko et al. 2004), whereas the overexpression of VEGF-C leads to enlarged lymphatic vessels (Shibuya 2011). In adult humans, VEGF-D is localised in smooth muscle cells in many tissues, indicating that it may play an important role in vessel repair after tissue damage (Rutanen, Leppänen et al. 2003). Furthermore, in mice, VEGF-D binds to only VEGFR3, suggesting that it may play a different role in this species (Baldwin, Catimel et al. 2001).

Because of the dominant and overwhelming role of VEGF-A and its main receptor (VEGFR2) in angiogenesis, in this thesis, we focus on these two molecules.

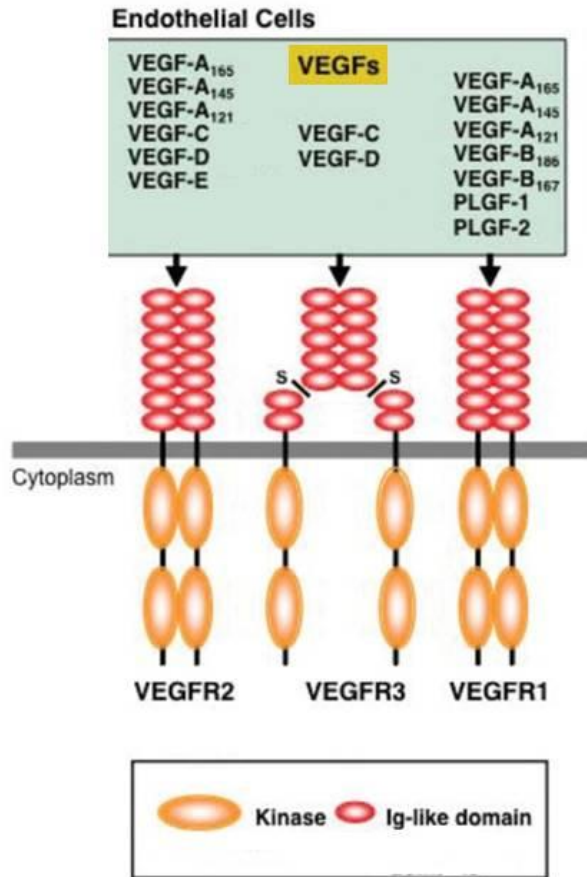


**Figure 1.6 Structure of VEGF receptors and their ligands.** Schematic representation shows VEGFR-1 (flt-1), VEGFR-2 (flk-1) and VEGFR-3 (flt-4). These receptors have the same compositions of the intracellular regions. However, the extracellular regions of VEGFR1 and VEGFR2 consist of seven immunoglobulin (Ig)-like domains, while VEGFR3 consists of six Ig-homology domains. Different isoforms of VEGF recognise different VEGFRs. Adapted from (Zachary, Frankel et al. 2009)

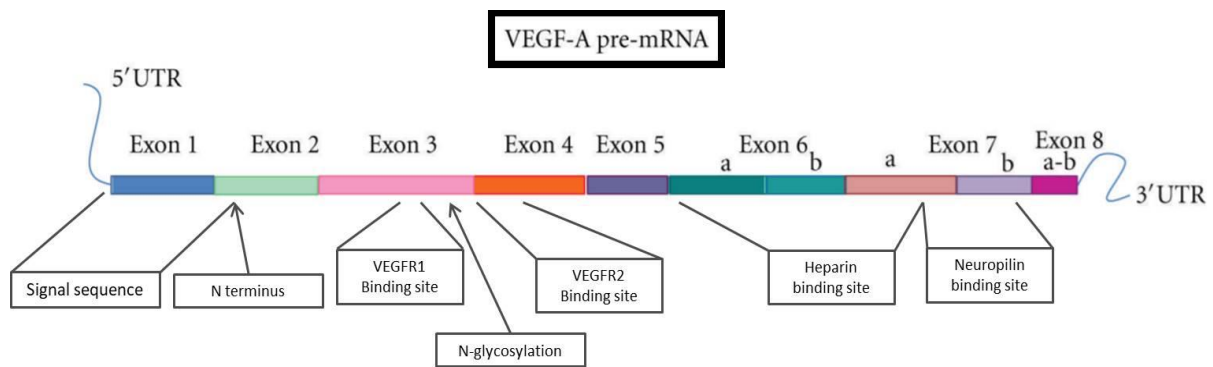
### 1.2.2.2.1. VEGF

VEGF, which is also known as vascular permeability factor (VPF) or (VEGF-A), was first described in 1989 as an endothelial cell-specific mitogen (Leung, Cachianes et al. 1989), (Demir, Kayisli et al. 2006). Subsequent studies showed that non-endothelial cells also expressed VEGF, such as fibroblast, macrophages (Nissen, Polverini et al. 1998), smooth muscle cells (Brogi, Wu et al. 1994) platelets (Banks, Forbes et al. 1998), neutrophils (Gaudry, Br erie et al. 1997), and about 60% of all tumours (Mesquita, Castro-de-Sousa et al. 2018). VEGF is considered the most active and powerful modulator of angiogenic processes that increase the leakage of other proteins and molecules from blood vessels to promote EC proliferation, migration, sprouting, and tube formation (Woolard, Bevan et al. 2009), (Iyer and Acharya 2011), (Dehghanian, Hojati et al. 2014), (Costache, Ioana et al. 2015). For example, among all the pro-angiogenic factors that are upregulated in response to hypoxia, VEGF is released as much as 30 fold within minutes to increase the permeability of ECs (Carmeliet 2003). However, VEGF expression is also stimulated by other factors even in the presence of oxygen (Iyer and Acharya 2011). Additionally, VEGF expression increases the production of nitric oxide (NO), which promotes vasodilation and facilitates blood flow (Hood, Meininger et al. 1998), fibroblast growth factor (FGF) for EC proliferation, and ICAM/VECAM/metalloproteases for EC migration and adhesion, all of which contribute to the formation of new blood vessels (Mesquita, Castro-de-Sousa et al. 2018). After birth, VEGF-A is downregulated (Breier, Albrecht et al. 1992), and it is upregulated during physiological (e.g. injury) or pathological angiogenesis (e.g. tumour growth) (Ferrara, Gerber et al. 2003). Therefore, VEGF has become a target in many anticancer therapies. For example, in 2004, bevacizumab (Avastin<sup>®</sup>), an anti-VEGF monoclonal antibody, was approved for the treatment of cancer (Mesquita, Castro-de-Sousa et al. 2018).

During mouse development, VEGF is first expressed in the anterior portion of the embryo to direct the tissue migration through VEGFR1 and VEGFR2 (Hiratsuka, Kataoka et al. 2005), (Tammela, Enholm et al. 2005). It is essential for the chemotaxis and differentiation of the endothelial progenitor cells (EPCs; angioblasts). It eventually directs ECs to form a vascular structure (vasculogenesis) and angiogenic remodelling (angiogenesis) (Adams and Alitalo 2007). The inactivation of a single *VEGF* allele in mice causes severe defects and abnormalities in the development of the cardiovascular system, which leads to death between E10 and E12 (Carmeliet, Ferreira et al. 1996), (Shibuya 2011).

The alternative splicing of VEGF can generate 16 distinct isoforms, which are distinguished by their number of amino acids (Woolard, Bevan et al. 2009), (Gu, Li et al. 2013), (Eswarappa, Potdar et al. 2014), (Peach, Mignone et al. 2018). These isoforms are divided into two groups: pro-angiogenic, termed VEGF<sub>xxx</sub>, and anti-angiogenic, termed VEGF<sub>xxx<sup>b</sup></sub> (**Figure 1.7 A-B**). The most frequently studied VEGF isoforms are VEGF<sub>111</sub>, VEGF<sub>121</sub>, VEGF<sub>145</sub>, VEGF<sub>165</sub>, VEGF<sub>189</sub>, and VEGF<sub>206</sub> (Mesquita, Castro-de-Sousa et al. 2018); however, VEGF<sub>165</sub> and VEGF<sub>121</sub> were proposed to be the most abundant isoforms (Soker, Takashima et al. 1998). These isoforms differ in the presence or absence of exons 6 and 7, which encode the heparin binding domain that is responsible for the binding affinity to the heparin/heparan sulphate proteoglycan proteins either on the EC's surface or in the surrounding ECM proteins. (Pan, Chathery et al. 2007), (Shibuya 2011), (Iyer and Acharya 2011). Although all VEGF isoforms can bind to VEGFR2, VEGF<sub>165</sub> (in mice known as VEGF<sub>164</sub>) (Stalmans, Ng et al. 2002), is the most VEGFR2-driven signal and therefore is considered the most potent and essential stimulator of angiogenesis (Sun, Liu et al. 2011), (Peach, Mignone et al. 2018), possibly because amongst all VEGF-A isoforms it induces the highest level of the phosphorylation of VEGFR2, extracellular-signal-regulated kinase (ERK) and Protein kinase B (PKB, Akt)(Fearnley, Smith et al. 2016).

A)



B)

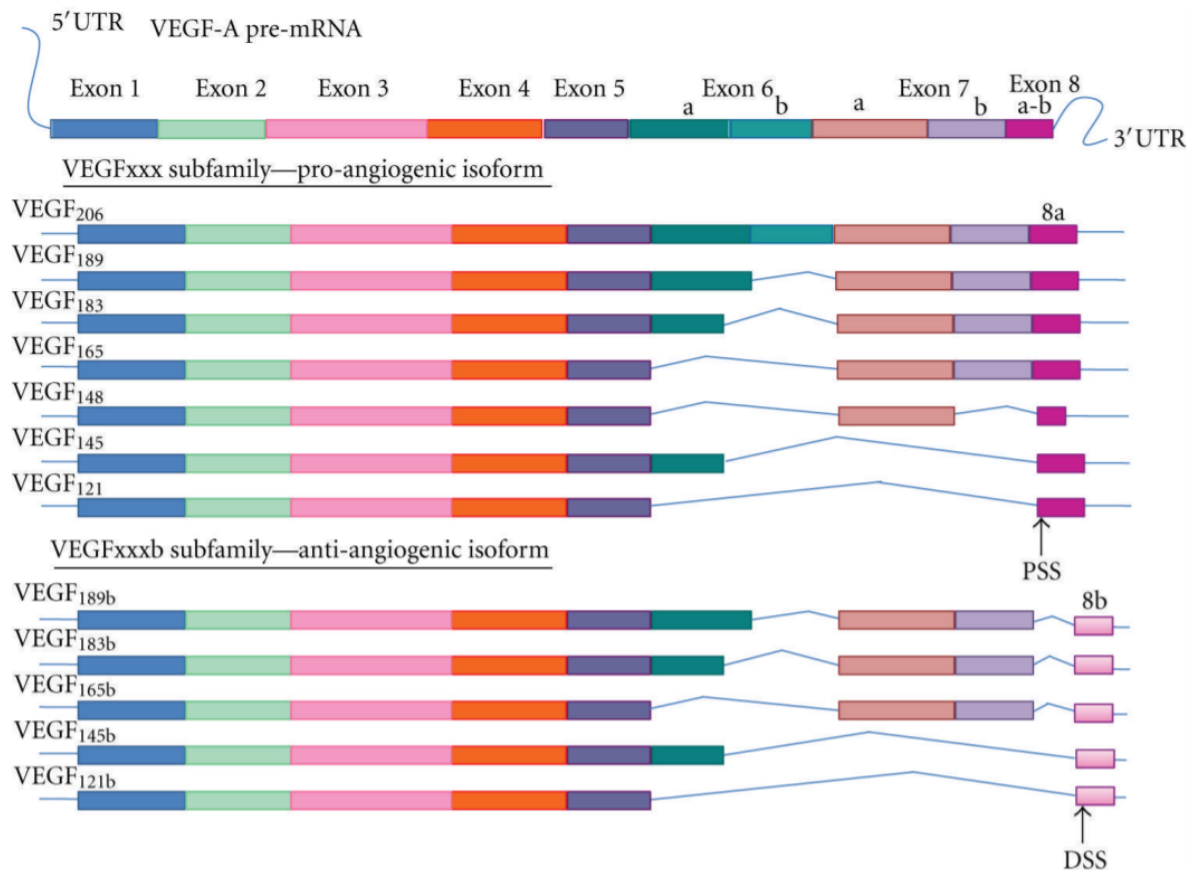


**Figure 1.7 VEGF-A pre-mRNA isoforms.** A) A schematic representation shows the gene structure of human VEGF, which consists of 8 exons (16,272 bp). The protein structure of all VEGF-A isoforms contain binding sites for VEGFR1 (encoded by exon 3), VEGFR2 (encoded by exon 4) and heparin (encoded by exon 6a/b and exon 7b). B) A schematic representation shows that VEGF-A pre-mRNA undergoes alternative splicing into the pro-angiogenic isoform subfamily, of which members are generated by proximal splice site (PSS) selection of exon 8 and anti-angiogenic isoforms, which are generated from exon 8 distal splice site (DSS) choices. These alternative splicing isoforms differ by their extreme carboxy-terminal six amino acids. The six amino acids encoded at exon 8a generate pro-angiogenic VEGF-Axxx isoforms, while those encoded at exon 8b generates anti-angiogenic VEGF-Axxx isoforms. Adapted from (Bates 2011), (Hilmi and Guyot 2012)

#### 1.2.2.2.2. VEGFR2

VEGFR2, which is also known as the kinase-insert domain receptor (KDR) in humans, consists of 1,356 amino acids in humans and 1,345 amino acids in mice. It is separated into four regions: the extracellular-binding domain, the transmembrane domain, the tyrosine kinase region and the carboxyl-terminal region (Guo, Colbert et al. 2010). Its molecular weight is approximately 210–230 kilodalton (kDa). VEGFR2 binds to its cognate angiogenic growth factor (VEGF) with a binding affinity between 75–125pM (Ferrara, Gerber et al. 2003), (Koch and Claesson-Welsh 2012). VEGFR2 is expressed by a range of non-endothelial cells (e.g. megakaryocytes, pancreatic duct cells, osteoblasts, retinal progenitor cells and neurons) but at a lower level than in vascular ECs (Ho and Kuo 2007). VEGFR2 expression increases during embryonic development (vasculogenesis and angiogenesis) as well as during physiological and pathological neovasculogenesis (Koch and Claesson-Welsh 2012), (Zhang, Wang et al. 2018). For example, the mRNA level of VEGFR2 increases during the reproductive period from the middle to the late stage of the luteal phase during the oestrus cycle within the uterus (Tasaki, Nishimura et al. 2010). Similar to VEGF-NULL mice, VEGFR2-NULL mice die *in utero* between 8.5 and 9.5 days because of an early defect in the development of haematopoietic progenitor and endothelial cells (Shalaby, Rossant et al. 1995). The VEGF/VEGFR-associated signalling pathway is the most prominent ligand/receptor complex that orchestrates EC functions during angiogenesis (Harry and Paleolog 2003), (Carmeliet 2003), (Abhinand, Raju et al. 2016), (Kim, Faix et al. 2017). This complex association can occur in cis- or trans-binding fashion (e.g. via HSPGs), forming homo- or hetero-dimerisation with other receptors on adjacent cells (Plein, Fantin et al. 2014). Unlike other tyrosine kinase receptors which use the Ras pathway to activate ERK, VEGFR2 uses mainly the phospholipase C $\gamma$  (PLC $\gamma$ )-protein kinase C (PKC) pathway (Takahashi, Yamaguchi et al. 2001), (Shibuya 2006), (Koch and Claesson-Welsh 2012). Upon VEGF binding, VEGFR2 can internalise within 15–20 minutes, and then it is recycled back to the plasma membrane or is subjected to lysosomal degradation. VEGFR2 endocytosis has been reported to be essential in ERK activation (Gourlaouen, Welti et al. 2013), (Peach, Mignone et al. 2018).

### **1.2.2.2.2.1. VEGF and VEGFR2 during early stage of angiogenesis**

VE-cadherin stabilises EC interactions by activating TGF- $\beta$  receptor signalling, which then inhibits VEGFR2 activation (Lampugnani, Zanetti et al. 2003), (Carmeliet and Jain 2011). Additionally, VE-cadherin alone can prevent VEGFR2 internalisation and proliferative signalling by forming a direct multiprotein complex with VEGFR2 (Lampugnani, Orsenigo et al. 2006). However, in response to VEGF and other growth factors, EC permeability in addition to the production of proteases are increased because of the loss of VE-cadherin and other junctional adhesions between adjacent ECs via rapid VE-cadherin endocytosis, which leads to the formation of fenestrated BM, through which small molecules can pass (Roberts and Palade 1997), (Gavard and Gutkind 2006), (Dejana, Orsenigo et al. 2008), (Koch and Claesson-Welsh 2012). Simultaneously, VE-cadherin in the tip cell that is localised at the filopodia initiates new outreach contacts to establish sprouting (Carmeliet and Jain 2011). HSPGs, which are present in the assembled BM can sequester growth factors, such as VEGF and basic epidermal growth factor (bEGF), and prevent them from playing a pro-angiogenic role. However, when MMP9 is released in response to VEGF stimulation, it effectively degrades type VI collagen in the BM, which results in the disruption of the assembled BM, including HSPG and perlecan, leading to the release of BM-bound VEGF (Kalluri 2003). Protolytic release (e.g. MMP12 and heparanase) has also been shown to increase VEGF–VEGFR2 associations on ECs (Vempati, Popel et al. 2014). Heparin and heparan sulphate proteoglycans (e.g. syndecan) have been also been shown to enhance VEGF–VEGFR2 binding and subsequent downstream signalling through the co-activation of integrins (e.g.  $\alpha 5\beta 1$  on FN and  $\alpha v\beta 3$  on vitronectin) (Jakobsson, Kreuger et al. 2006), (Purushothaman, Uyama et al. 2010), (Wijelath, Murray et al. 2002), (Mahabeleshwar, Feng et al. 2007), (Koch and Claesson-Welsh 2012), (Vempati, Popel et al. 2014).

VEGF orchestrates the sprouting of quiescent ECs in the parent vessel by binding to VEGFR2 and other accessory co-receptors (e.g. neuropilin and integrins) on the selected tip cell and one or more adjacent proliferative stalk cells via DLL4-Notch signalling. The VEGF–VEGFR2 interaction upregulates DLL4 expression in the tip cell, which results in the activation of NOTCH signalling in the trailing stalk-cells. Jagged1 is another protein that is expressed by the stalk cells acting with the NOTCH receptor to promote the selection of tip cell. This action suppresses VEGFR2 expression but increases VEGFR1 signalling (e.g. through PIGF) in the stalk cells, thus preventing the stalk cells from sprouting and allowing the tip cell to lead the sprout in the direction of VEGF cues. The tip cells and the trailing stalk

cells can be dynamically re-assigned based on the direction of the gradient of VEGF cues. Previous research showed that reductions in DLL4 or the blocking of Notch signalling caused significant angiogenic sprouting of ECs during mouse development (Adams and Alitalo 2007), (Jakobsson, Bentley et al. 2009), (Phng and Gerhardt 2009), (Benedito, Roca et al. 2009), (Carmeliet and Jain 2011), (Blanco and Gerhardt 2012). To restrain VEGFR2 production as well as the VEGF-VEGFR2 signalling pathway, VEGFR3 expression is essentially enhanced in the tip EC, which prevents the excessive permeability of vascular ECs (Heinolainen, Karaman et al. 2017), (Zhang, Wang et al. 2018). Furthermore, soluble inhibitor factors (e.g. VEGF<sub>165b</sub>) prevent VEGFR2 dimerisation and the subsequent downstream signalling from being established in the tip cell (Woolard, Wang et al. 2004), (Vempati, Popel et al. 2014).

#### **1.2.2.2.2. VEGF/VEGFR2 signalling mechanism**

VEGF/VEGFR2 signalling is essential in four main biological functions of ECs during angiogenesis: EC permeability, proliferation, migration and survival (Guo, Colbert et al. 2010), (Dellinger and Brekken 2011). In a recent study, a comprehensive VEGF/VEGFR2 signalling map was developed to depict all the proteins and pathways involved in ECs during angiogenesis. Briefly, the study identified 70 proteins that are involved in cell proliferation, 103 proteins that participate in cell migration function, 95 proteins that are implicated in cell survival, and 31 proteins that engage in the internalisation and recycling of receptors [reviewed by (Abhinand, Raju et al. 2016)]. A change in any of these proteins would change the signalling output and therefore affect EC function during angiogenesis.

Mechanistically, VEGF binds to the 2 and 3 Ig-like domains of VEGFR2, leading to conformational changes in the extracellular region of VEGFR2, which subsequently results in the rotation of the transmembrane helices (Fuh, Li et al. 1998), (Dell'Era Dosch and Ballmer-Hofer 2010), (Koch and Claesson-Welsh 2012). Conformational changes in the intracellular regions of VEGFR2 then occur, leading to VEGFR2 dimerisation through tyrosine auto-phosphorylation at five major tyrosine (Tyr) sites: Tyr 951 (in the kinase-insert domain), Tyr 1054 and Tyr 1059 (in the kinase domain), and Tyr1175 and Tyr1214 (in the carboxyl-terminal domain) (Takahashi, Yamaguchi et al. 2001), (Matsumoto, Bohman et al. 2005). Other phosphorylation positions have also been identified, including 801, 1223, 1305, 1309 and 1319 (Matsumoto, Bohman et al. 2005), (Koch and Claesson-Welsh 2012). All these phosphorylated tyrosines then recruit the cytoplasmic adaptor proteins to bind the VEGFR2

cytoplasmic tail and initiate the complex downstream signalling pathways required for angiogenesis (**Figure 1.8**).

For example, **Tyr951** phosphorylation serves as a binding site for the T-cell-specific-adaptor molecule (TSAd) (Matsumoto, Bohman et al. 2005), which is also known as the VEGF receptor associated protein (VRAP) (Wu, Mayo et al. 2000), thus activating Src. The substrates of Src, including the SHB adaptor domain, then activate phosphatidylinositol 3-kinase (PI3-kinase)/Akt pathway required for actin reorganisation and migration (Koch and Claesson-Welsh 2012). **Tyr 1175** phosphorylation recruits SHB (Holmqvist, Cross et al. 2004), which activates focal adhesion kinase (FAK) and PI3-kinase for cell attachment and migration (Holmqvist, Cross et al. 2004). Additionally, the recruitment of the nucleotide-exchange factor Son of sevenless (SOS) to the phosphorylated VEGFR2 at Tyr 1175 is mediated by either Src homology collagen homology (SHC) or growth factor receptor-bound protein 2 (GRB2) (Warner, Lopez-dee et al. 2000). Subsequently, the phosphorylated Tyr 1175 binds to PLC $\gamma$ , which releases Ca<sup>2+</sup> from the smooth endoplasmic reticulum (ER). Then, the Ca<sup>2+</sup> activates protein kinase C (PKC) and the subsequent downstream signalling ERK. This signalling cascade is believed to be an important pathway leading to cell proliferation during angiogenesis (Takahashi, Yamaguchi et al. 2001), (Koch and Claesson-Welsh 2012). When PLC $\gamma$  is phosphorylated, it hydrolyses the membrane phospholipid phosphatidylinositol (4, 5)-bisphosphate (PIP<sub>2</sub>), resulting in production of two products, which act as second messengers, diacylglycerol (DAG) and inositol 1,4,5-triphosphate (IP<sub>3</sub>). Subsequently, DAG remains on the cell membrane and activates PKC, which sequentially activates other cytosolic proteins by phosphorylating them, while IP<sub>3</sub> binds to the IP<sub>3</sub> receptors on the smooth ER and opens calcium channels and release Ca<sup>2+</sup>, which in turn activates other protein signalling cascades (see **Figure 1.8**). **Tyr 1214** phosphorylation creates a direct binding site to the cytoplasmic adaptor protein NCK, which then forms a complex with FYN (Lamalice, Houle et al. 2006). This complex then phosphorylates p21-activated protein kinase-2 (PAK2) and the subsequent sequential activation of cell division cycle 42 (CDC42), P38 mitogen-activated protein kinases (p38 MAPK, p38), MAPK-activated protein kinase 2 (MAPKAPK2) and Heat shock protein 27 (HSP27) for cell migration regulation (Lamalice, Houle et al. 2004), (Koch and Claesson-Welsh 2012) (see **Figure 1.8**). It was reported that **Tyr1059** phosphorylation binds to Src, and the complex can then phosphorylate the Tyr 1175 as well as other downstream signalling, such as IQGAP1 (IQ-motif containing GTPase-activating protein 1), which regulates cell–cell adhesion, proliferation and migration

(Yamaoka-Tojo, Tojo et al. 2006), (Meyer, Sacks et al. 2008), (Koch and Claesson-Welsh 2012). Additionally, in response to VEGF induction, the p85 subunit of the phosphoinositide 3-kinase (PI3K) enzyme is activated through binding to GAP1. The activated PI3K then catalyses the production of phosphatidylinositol-3,4,5-trisphosphate (PIP3) (Cantley 2002), which then activates the small GTPase Rac for the membrane ruffle and cell motility (Cain and Ridley 2009). EC survival during VEGF/VEGFR2 signalling is also regulated by the PI3K pathway. The activated PI3K can activate Akt through two kinase proteins: PDK (phosphoinositide-dependent kinase)-1 and PDK-2. Consequently, Akt can inhibit cell apoptosis by phosphorylating cysteine-aspartic proteases-9 (caspase-9) and BAD [Bcl (Bcell lymphoma)-2-associated death promoter] (Cardone, Roy et al. 1998), (Koch and Claesson-Welsh 2012). The VEGF-induced activation of VEGFR2 promotes EC permeability through NO generation via endothelial NO synthase (eNOS) activation, which can be activated by either PLC $\gamma$ -dependent Ca<sup>2</sup> release or Akt phosphorylation (Fukumura, Gohongi et al. 2001), (Dimmeler, Fleming et al. 1999), (Koch and Claesson-Welsh 2012) (see **Figure 1.8**). It is worth noting that angiogenesis is regulated not only by the binding of the secreted growth factors to their receptors; EC adhesion mediated by the interaction of integrins with ECM ligands can also regulate angiogenesis (Dietrich, Onderka et al. 2007).

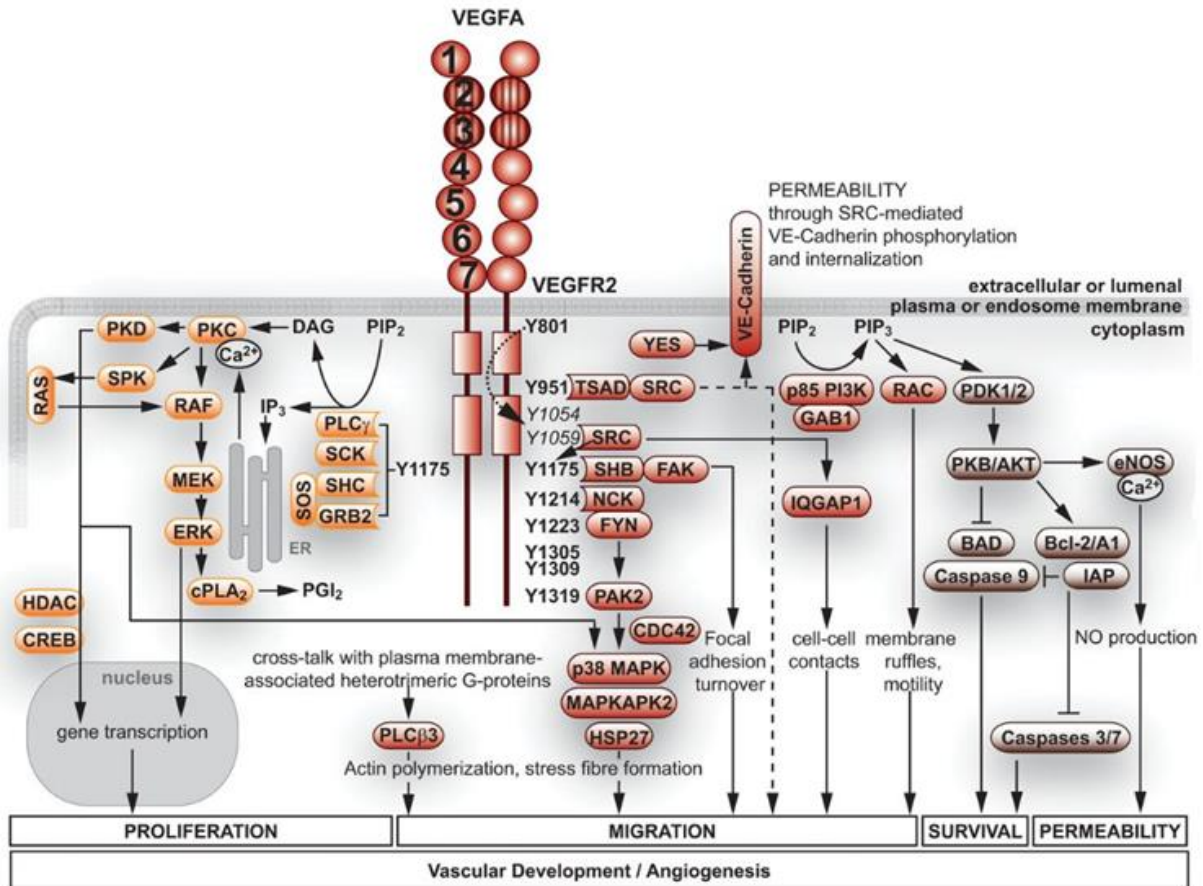


**Figure 1.8 VEGFR2 downstream signalling via its tyrosine phosphorylation sites.** Upon VEGF-A isoform binding to the extracellular Ig-like domains 2 and 3 of VEGFR2, the cytoplasmic tyrosine sites (indicated by numbers) of VEGFR2 are phosphorylated, in which each site recognises specific signalling molecules and then recruits other downstream signalling molecules needed for controlling ECs proliferation, migration, survival and permeability during vascular development and angiogenesis. See the main text for details. Cell division cycle 42 (CDC42); diacylglycerol (DAG); inositol 1,4,5-trisphosphate (IP3); MAPK/ERK kinase (MEK); phosphatidylinositol 4,5-bisphosphate (PIP2); Son of sevenless (SOS) (Koch and Claesson-Welsh 2012).

## **1.2.3. Additional molecular players in angiogenesis**

### **1.2.3.1 Neuropilin**

#### **1.2.3.1.1 History of neuropilin**

In 1987, the antigen A5 was first identified in the nervous system of *Xenopus* embryos by using a monoclonal antibody (MAb-AS) against the optic tectum of *Xenopus laevis* tadpoles as an axonal adhesion protein (Takagi, Tsuji et al. 1987). In 1991, the deduced amino acid sequence of A5 protein revealed that the structure of this protein was a novel neuronal cell surface protein with at least five different extracellular domains (Takagi, Hirata et al. 1991). The A5 protein was then found to be expressed in vertebrates, including chicken and mouse. Specifically, the A5 protein is expressed in a particular neuron circuit at particular developmental stage when axonal growth is active, which was subsequently named neuropilin (NRP) (Fujisawa, Takagi et al. 1995). NRP was found to regulate axon guidance through its binding to class III semaphorin family members (Sema-3). Subsequent studies found that ECs also express NRP; here it plays an essential role in sprouting angiogenesis through the selective binding to members of the VEGF family (Soker, Takashima et al. 1998), (Miao, Soker et al. 1999). Furthermore, early studies in this field discovered that NRP has a very small cytoplasmic tail, which lacks any known catalytic activities (Fujisawa, Kitsukawa et al. 1997), suggesting that NRP is unlikely to be able to transduce intracellular signalling on its own (Fujisawa, Kitsukawa et al. 1997), (Gluzman-Poltorak, Cohen et al. 2000). Instead, neuronal Sema-3 and endothelial VEGF-induced intracellular signalling require the formation of a NRP/ligand complex with other receptors, such as plexins or VEGFRs, in neurons or ECs, respectively. It has become widely accepted that the endothelial NRP1, the first NRP to be discovered, binds to VEGF<sub>165</sub> with high affinity (Soker, Takashima et al. 1998), (Miao, Soker et al. 1999). This complex then binds to VEGFR2 to enhance the VEGF<sub>165</sub>-induced activation of many intracellular pathways, including ERK signalling (Prahst, Héroult et al. 2008). However, subsequent studies in this field found that the function of NRPs extend beyond augmenting VEGF-signalling. For example, it was revealed that NRPs (NRP1 and NRP2) play important roles independently of VEGFRs (Wang, Zeng et al. 2003), (Wang, Mukhopadhyay et al. 2006), (Guo and Vander Kooi 2015), (Ou, Wei et al. 2015) . Subsequent studies found that endothelial NRPs can also bind and control many other cell surface receptors, including transforming growth factor- $\beta$ 1 (TGF- $\beta$ 1),

hepatocyte growth factor (HGF), FGF, Placental growth factor-B (PGF-B), platelet-derived growth factor (PDGF) etc. (Parker, Guo et al. 2012), (Djordjevic and Driscoll 2013). Furthermore, NRP's expression was shown to extend beyond ECs and neuron cells. Many other cells were shown to express NRPs, including immune (Delgoffe, Woo et al. 2013) and tumour cells (Guo and Vander Kooi 2015). To exacerbate the complexity of these receptors, ECs were reported to express different members of the neuronal Sema-3 family, which function with NRPs as competitors for VEGFs and therefore inhibit angiogenic signalling (Miao, Soker et al. 1999). In addition to the regulation of the plexin and VEGF receptors, NRPs can also regulate integrin functions and influence cell adhesion, migration and permeability in physical and pathological conditions (Fukasawa, Matsushita et al. 2007), (Valdembri, Caswell et al. 2009), (Ellison, Atkinson et al. 2015). Because accumulating studies have been found that NRPs participate in many cellular functions depending on the type of cells that express these receptors, the publications in this field defined NRPs as multifunctional and versatile cell surface receptors (Neufeld, Cohen et al. 2002), (Parker, Guo et al. 2012), (Prud'homme and Glinka 2012), (Li, Parker et al. 2014), (Guo and Vander Kooi 2015).

### **1.2.3.1.2. NRP structure**

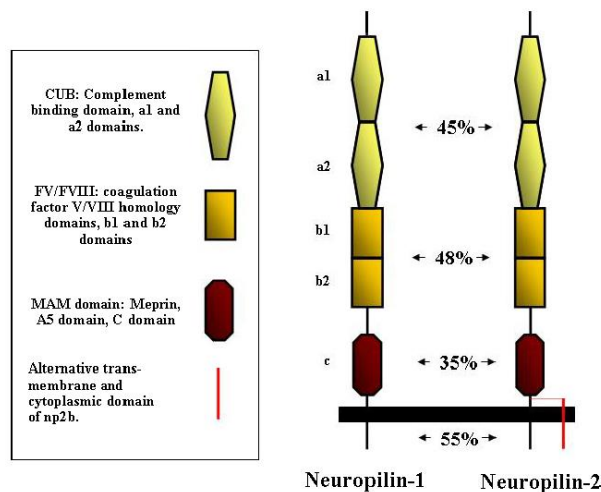
NRP, which is also known as Nrp, Npn or Np, is a single multifunctional non-tyrosine kinase receptor belonging to type I transmembrane glycoprotein receptor of about 130–140 kDa (Soker, Takashima et al. 1998). To date, only two NRPs have been identified in vertebrates, NRP1 and NRP2, which are composed of 923 and 926 amino acids, respectively. NRP2 shares a very similar domain structure and an overall 44% amino acid identity with NRP1 (**Figure 1.9 A**) (Pellet-Many, Frankel et al. 2008), (Zachary 2014). Both NRPs are comprised of a large single extracellular region consisting of five domains: two complement C1r/C1s, Uegf, Bmp1 (CUB) domains, two coagulation factor V/VIII homology domains, and one meprin, A-5 protein domain, and a receptor protein-tyrosine phosphatase mu (MAM) domain of 170 amino acids. This extracellular region is connected to a single helical transmembrane domain (TMD) and a short cytoplasmic tail of 44 amino acids in NRP1 and 43 amino acids in NRP2 (Nakamura, Tanaka et al. 1998), (Pellet-Many, Frankel et al. 2008), (Zachary 2014).

The CUB domains (a1 and a2) serve as binding sites for the Sema-3 family, while the V/VIII domains (b1 and b2) serve as binding sites for certain isoforms of the VEGF family (**Figure 1.9 B**) and heparins. It was reported that the b2 domain is required for both Sema-3 binding

and glycosaminoglycan (GAG) binding. The MAM domain is similar to other MAM domains that are present in many proteins. Its function is believed to be required for both receptor dimerisation and homophilic interaction with other receptors (Schwarz and Ruhrberg 2010), (Zachary 2014), (Plein, Fantin et al. 2014). The short cytoplasmic domain contains three conserved amino acids at the carboxyl-terminal (SEA-COOH) of NRP1 and NRP2a, forming a consensus PDZ domain binding motif that can bind to the cytoplasmic adaptor protein RGS-GAIP interacting protein C-terminus (GIPC), which is also called neuropilin-interacting protein-1 (NIP-1) or synectin, a molecule that modulates endocytic trafficking (De Vries, Lou et al. 1998), (Cai and Reed 1999), (Ballmer-Hofer, Andersson et al. 2011), (Lanahan, Zhang et al. 2013), (Zachary 2014).

Although both NRPs are glycoproteins, their glycosylation differs depending on the cell type (Shintani, Takashima et al. 2006), (Zachary 2014). In addition to the normal molecular weight of NRP1 (130kDa), some tumours, vSMCs and cultured ECs express high glycosylated molecular weights of NRP1 (> 250 kDa) (Shintani, Takashima et al. 2006), (Frankel, Pellet-Many et al. 2008), (Pellet-Many, Frankel et al. 2011). The modification of NRP1 occurs in the linker region between the V/VIII (b2) domain and the MAM domain at Ser 612 by the addition of an O-linked heparan sulphate and/or chondroitin sulphate GAGs (Zachary 2014). NRP1 also exists in a soluble form (sNRP1) because the truncation that occurs in the linker region between the second V/VIII (b2) domain and MAM domain, ending with the 3 amino acids GlyIsoLys (GIK) (Rossignol, Gagnon et al. 2000), (Mamluk, Klagsbrun et al. 2005), (Neufeld, Shraga-Heled et al. 2007), (Zachary 2014). In contrast, no highly glycosylated, high molecular weight isoform of NRP2 has been identified. NRP2 is divided into the two major forms NRP2a and NRP2b, but NRP2a has received the most attention in research because it possesses the SEA domain. In mice, NRP2a can have three variants, which are generated by the insertion of 5, 7 or 22 amino acids at position 809. However, only one isoform has been identified in humans, which is generated by the insertion of 7 amino acids at position 808. In mice, NRP2b is missing the SEA domain, and it can exist in two isoforms that differ in the sequence of the transmembrane and the intracellular region starting from position 809 (Gluzman-Poltorak, Cohen et al. 2000). Soluble NRP2 (sNRP2) has also been identified (Rossignol, Gagnon et al. 2000), (Neufeld, Shraga-Heled et al. 2007).

A)



B)

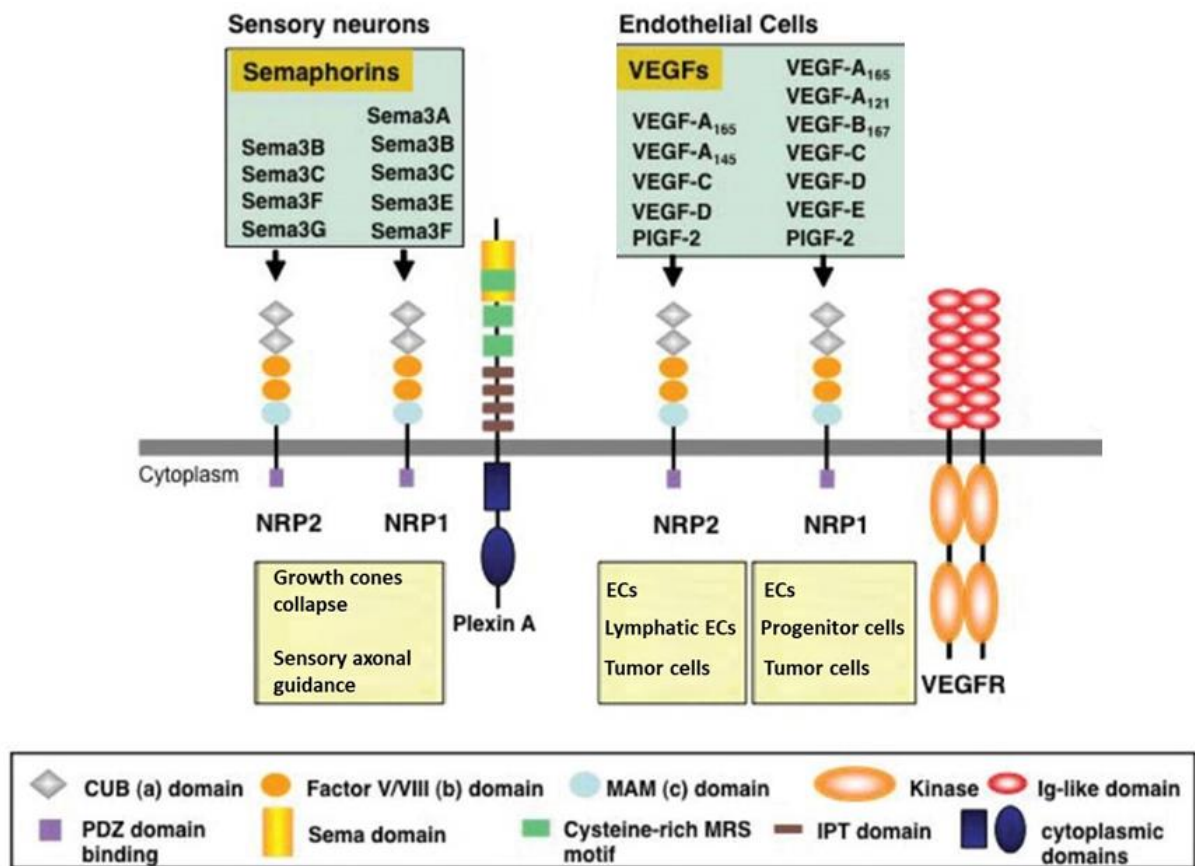


**Figure 1.9 Neuropilin structure and ligand interactions.** A) NRP1 and NRP2 consist of two CUB domains that are 45% homologous, two FV/FVIII domains that are 48% homologous, a single MAM domain that is 35% homologous, and a cytoplasmic tail that is 55% homologous. B) Schematic representation showing that neuropilins can transduce signalling of two distinct classes of growth factors (Sema-3 and VEGFs) by forming a complex with plexin-A or VEGFRs, respectively. In neuron cells, neuropilins bind to major receptors (Plexin A1 and A2) and transduce signalling of different isoforms of Sema-3 to promote growth cone collapse and sensory axonal guidance. NRP1 transduces the signalling of Sema-3A, Sema-3B, Sema-3C, Sema-3E And Sema-3F, while NRP2 transduces the signalling of Sema-3B, Sema-3C, Sema-3F and Sema-3G. In endothelial cells, neuropilins bind to major receptors (VEGFR1, VEGFR2 and VEGFR3) and transduce the signalling of different isoforms of VEGF to promote vascular maturation/branching, cardiac development or lymphogenesis. Adapted from (Zachary, Frankel et al. 2009), (Gaur, Bielenberg et al. 2009), (Lange, Storkebaum et al. 2016)

### 1.2.3.1.3. Neuropilins in embryonic development

During mouse embryonic development, NRP1 is predominantly expressed on the ECs of arteries and capillaries as well as in the mouse embryo hindbrain. NRP2 is mainly expressed in venous and lymphatic vessels (Plein, Fantin et al. 2014). Transgenic mouse studies revealed that NRP1-NULL mice die between E10.5 and E13.5, as a result of an impairment in the heart outflow tract as well as severe defects in the yolk sac and neuronal vacuolisation, especially in the brain and spinal cord (Kawasaki, Kitsukawa et al. 1999), (Gu, Rodriguez et al. 2003), (Jones, Yuan et al. 2008). The overexpression of NRP1 leads to hyper-vascularisation in the growth of capillaries and blood vessels, which were leaky and haemorrhagic (Klagsbrun, Takashima et al. 2002), (Kitsukawa, Shimono et al. 1995). Transgenic mice lacking the short intracellular domain of NRP1 survive, but the mutation impairs arteriogenesis, a process that involves the growth of the luminal vessels (Fantin, Schwarz et al. 2011), (Lanahan, Zhang et al. 2013). Another study reported that targeting NRP1 only in ECs, but not other cell types, caused severe disruption of vascular development (Gu, Rodriguez et al. 2003). The same study also reported that the disruption of the CUB domain, which is essential for Sema binding, did not affect general vascular development, but there was a bilateral atrial enlargement in the heart, suggesting that both VEGF-NRP1 and Sema-3A-NRP1 signalling in endothelial cells are essential in the development of the heart (Gu, Rodriguez et al. 2003). The results of another study indicated that the phenotypic defects seen in vascular development upon NRP1 deletion occurred because of the disruption of EC migration, not EC proliferation (Jones, Yuan et al. 2008). These previous studies confirmed that NRP1 plays critical roles in embryonic vascular development.

On the other hand, studies on NRP2 revealed that NRP2-NULL mice are viable with normal arterial development; however, the animals exhibit markedly small veins and lymphatic vessels in addition to abnormalities of sensory axons in the spinal cord, hippocampal and olfactory bulb (Chen, Bagri et al. 2000), (Yuan, Moyon et al. 2002). The double knockout of both NRPs is lethal, and mice die *in utero* earlier than NRP1 knockout mice at E8.5 (Takashima, Kitakaze et al. 2002). Transgenic mice with the targeted deletion in one NRP while the other one was heterozygous died at E10 to E10.5 (Takashima, Kitakaze et al. 2002). Interestingly, mice lacking the NRP2 gene and containing only one functional NRP1 gene exhibited more severe defects in vascular development than those reported in mice lacking both NRP1 alleles (Takashima, Kitakaze et al. 2002). Another study compared the expression of both NRPs during embryonic vascular development of chicks and showed both NRPs are

expressed in the blood islands of 24-hours old chick embryos. However, between 48 and 72 hours, the expression of NRP1 was restricted to the arteries as well as the smaller branches of these arteries, whereas NRP2 was preferentially expressed in veins as well as in the smaller venous branches that merged with the arteries (Herzog, Kalcheim et al. 2001). Overall, these results indicate that the expressions of both NRPs are required in the early development of embryonic vessels (Takashima, Kitakaze et al. 2002).

#### **1.2.3.1.4 Post-embryonic Neuropilin expression**

NRP expression is not only restricted to nerve cells and ECs. Their expression and function has been implicated in many other cells, including immune cells, epithelial cells, osteoblasts, and tumour cells (Bielenberg, Hida et al. 2004).

##### **1.2.3.1.4.1. Neuropilins in nerve cells**

Semaphorins are a large family of transmembrane and secreted proteins characterised by the expression of conserved 500 amino acids called the Sema domain. Semaphorins are grouped into eight major subclasses in which classes 1 and 2 are expressed in invertebrates, and classes 3 to 7 are expressed in vertebrates. Semaphorin class 8 was also identified, but it is only encoded by a virus. Transmembrane semaphorin proteins are in classes 1 and 4–7, whereas secreted semaphorin proteins are in classes 2, 3 and 8 (Raper 2000), (Suzuki, Kumanogoh et al. 2008). Although semaphorins are expressed by other cells, their functions are best illustrated in the nerve cells where they guide the growing axons to the target and simultaneously deflect or repel them from an inappropriate target (Yazdani and Terman 2006). Transmembrane and viral semaphorin signalling occur through binding with the plexin family of transmembrane proteins, whereas secreted semaphorins, specifically Sema-3 family members, transduce signalling through complex formations with plexins and NRPs, which act as co-receptors to enhance signalling (Tamagnone, Artigiani et al. 1999).

It was believed that only the Sema-3 subfamily binds and utilises NRPs to transduce signalling, but subsequent studies reported that Sema-4A can also signal through NRP1 expressed by the regulatory T-cells (Treg cells) (Delgoffe, Woo et al. 2013), (Guo and Vander Kooi 2015). Seven Sema-3 members are designated from Sema-3A to Sema-3G, all of which require NRP binding to mediate repulsive signals during neuronal axon guidance with the exception of Sema-3E, which has been reported to signal through plexin D1 independently of NRPs (Gu, Yoshida et al. 2005), (Serini, Bussolino et al. 2013). The CUB

(a1/a2) domains of NRPs selectively bind different members of the secreted Sema-3 family, in which NRP1 binds to Sema-3A, Sema-3B, Sema-3C and Sema-3F, while NRP2 binds to Sema-3B, Sema-3C, Sema-3D and Sema-3F (Neufeld, Cohen et al. 2002), (Djordjevic and Driscoll 2013). However, Sema-3A binds to NRP1 with the highest affinity, while Sema-3F is the best characterised ligand for NRP2 binding (Zachary 2014).

#### **1.2.3.1.4.2. Neuropilins in ECs**

Based on early transgenic mouse studies in this field (see above), it was speculated that NRP1 is mainly expressed in arteries, arterioles and capillaries, whereas NRP2 is expressed in veins, venules and lymphatic vessels (Herzog, Kalcheim et al. 2001), (Yuan, Moyon et al. 2002). However, subsequent studies revealed that both NRPs are expressed in normal blood and lymphatic endothelial cells, and both play essential roles in forming blood and lymphatic vasculature networks (Jurisic, Maby-El Hajjami et al. 2012), (Bouvrée, Brunet et al. 2012), (Mucka, Levonyak et al. 2016). Additionally, both EC types express the soluble Sema-3 subfamily, which signal through NRPs, thus adding another layer to the complexity of NRP functions in ECs (Jurisic, Maby-El Hajjami et al. 2012). With regard to angiogenesis, both NRPs were described to act as co-receptors for selective forms of VEGFs to enhance VEGFR phosphorylation (Fuh, Garcia et al. 2000), (Gluzman-Poltorak, Cohen et al. 2001), (Kärpänen, Heckman et al. 2006), (Xu, Yuan et al. 2010), (Ballmer-Hofer, Andersson et al. 2011), (Fearnley, Smith et al. 2016), (Fuh, Garcia et al. 2000), (Herzog, Pellet-Many et al. 2011), (Tiwari, Jung et al. 2012). There is also evidence that NRPs can mediate ligand signalling independently of VEGFRs (Wang, Zeng et al. 2003), (Favier, Alam et al. 2006). Furthermore, there is strong evidence that NRPs can regulate VEGFRs independently of VEGF binding (Fantin, Schwarz et al. 2011), (Fantin, Herzog et al. 2014). In another group of studies, NRP functions were implicated in EC adhesion and migration independently of both VEGF and VEGFR by modulating other transmembrane receptors (e.g. integrins) (Murga, Fernandez-Capetillo et al. 2005), (Valdembri, Caswell et al. 2009), (Raimondi, Fantin et al. 2014), which also play critical roles in modulating the biological function of ECs during angiogenesis.

Understanding the different mechanisms by which NRPs are implicated in angiogenesis is required to improve therapeutic inhibitors in cancer treatment. In the following sections, we will discuss the different functions of NRPs in endothelial cells and cancer cells.

### 1.2.3.1.4.2.1 NRP1

In 1996, an immunoprecipitation experiment revealed for the first time that NRP1 protein is a receptor of VEGF<sub>165</sub> but not of the soluble VEGF<sub>121</sub> because it lacks the exon 6 and 7-encoded domains (Soker, Fidder et al. 1996), (Soker, Takashima et al. 1998), which contain HSPG- and NRP1-binding regions (Tiwari, Jung et al. 2012), (Vempati, Popel et al. 2014). Ten years later, studies demonstrated that VEGF<sub>121</sub> binds directly to NRP1 and regulates both EC migration and sprouting, but unlike VEGF<sub>165</sub>, VEGF<sub>121</sub> does not form a NRP1-VEGF<sub>121</sub>-VEGFR2 complex (Pan, Chathery et al. 2007), (Shraga-Heled, Kessler et al. 2007). Not all VEGF-A isoforms can bind to NRP1; for example, VEGF<sub>165b</sub> (Suarez, Pieren et al. 2006) and VEGF<sub>145</sub> do not bind to NRP1, whereas VEGF<sub>189</sub> (Tillo, Erskine et al. 2015) can bind to NRP1, but VEGF<sub>165</sub> is believed to be the only VEGF-A isoform that can form a heterocomplex with VEGFR2 and NRP1 and increase VEGFR2 signalling and recycling. VEGF<sub>165b</sub> acts negatively through binding to VEGFR2 and preventing NRP1 from binding to VEGFR2, thus leading to VEGFR2 degradation (Ballmer-Hofer, Andersson et al. 2011), (Fearnley, Smith et al. 2016). In particular, Ballmer *et. el* showed that in response to VEGF<sub>165</sub>, NRP1 is essential in mediating VEGFR2 internalisation, phosphorylation and recycling back to the plasma membrane through the Rab11 vesicles, whereas VEGF<sub>165b</sub>, which lacks NRP1-binding, inactivated VEGFR2 and rapidly promoted the accumulation of VEGFR2 in Rab7 vesicles (not in Rab11 vesicles) and trafficking to lysosomes for degradation because of the absence of NRP1 (Ballmer-Hofer, Andersson et al. 2011). Therefore, because of this key role, VEGFR2 signalling driven by VEGF<sub>165</sub> is the most potent angiogenic factor function during angiogenesis (Sun, Liu et al. 2011), (Peach, Mignone et al. 2018).

An *in vitro* binding analysis showed that the extracellular domain of NRP1 does not interact directly with VEGFR2, but the density of NRP1 on the cell membrane increases the interaction between VEGF<sub>165</sub> and VEGFR2 (Fuh, Garcia et al. 2000). Additionally, targeting the Tyr297 residue within the extracellular b1 domain of NRP1 prevented the VEGF<sub>165</sub>-induced complex formation between VEGFR2 and NRP1 (Herzog, Pellet-Many et al. 2011), suggesting that the VEGF<sub>165</sub>-VEGFR2 complex is dependent on NRP1 (Fuh, Garcia et al. 2000), (Herzog, Pellet-Many et al. 2011), (Tiwari, Jung et al. 2012). Furthermore, another study showed that NRP1 and VEGFR2 are highly expressed in the tip cell during sprouting angiogenesis (Fantin, Vieira et al. 2013), which supports a mechanism whereby VEGF<sub>165</sub>-induced angiogenic signalling occurs through binding to NRP1 and its main receptor

(VEGFR2) in the tip cell. This mechanism requires the formation of the VEGF-NRP1 pre-complex (Soker, Fidler et al. 1996) to enhance VEGF binding to VEGFR2, and thus potentiate VEGFR2-mediated ECs signalling, migration and permeability during angiogenesis (Pan, Chathery et al. 2007). This mechanism was validated using an antibody that blocks the extracellular (b1/b2) domains within NRP1, which resulted in a significant reduction in: (1) VEGF-induced VEGFR2 complex formation; (2) migration; (3) *in vitro* sprouting; (4) and *in vivo* neovasciogenesis (Pan, Chanthery et al. 2007). Another study used RNA interference silencing of NRP1 or VEGFR2 to show that NRP1 and VEGFR2 are required for VEGF-induced signalling as well as for the proliferation and migration of ECs (Murga, Fernandez-Capetillo et al. 2005). Consistent with these findings, NRP1-siRNA knockdown (Fearnley, Odell et al. 2014), (Raimondi, Fantin et al. 2014) or NRP1 inhibition (Becker, Waltenberger et al. 2005) reduce VEGF<sub>165</sub>-induced phosphorylation of VEGFR2, ERK1/2, and p38. Another study also strongly supported this mechanism, indicating that VEGF<sub>165</sub>-VEGFR2-NRP1 complex formation induces angiogenic sprouting and EC organisation *in vitro* and *in vivo* through the activation of VEGFR2, ERK1/2, Akt and p38, whereas VEGF<sub>121</sub> failed to activate p38 (Kawamura, Li et al. 2008) (**Figure 1.10**). It is worth noting that HSPGs can also enhance VEGF<sub>165</sub>-VEGFR2-NRP1 complex formation and ERK1/2 phosphorylation (Kawamura, Li et al. 2008), (Teran and Nugent 2015). Many other proteins are also upregulated in response to hypoxia, and they are involved directly or indirectly in angiogenesis (e.g. VEGFR1, NRP2, Ang-2, eNOs, TGF- $\beta$ 1 and PDGF-BB), thus adding another layer of complexity to VEGF-VEGFR2 signalling (Conway, Collen et al. 2001). In brief, the extracellular region of NRP1 does not directly bind to VEGFR2, and the complex formation of VEGF<sub>165</sub>-VEGFR2 is, at least partially, dependent on NRP1.

Although the extracellular region of NRP1 has become a model for mediating the VEGF<sub>165</sub>-VEGFR2 complex, another group of studies provided strong evidence that the short intracellular region of NRP1 is also required for VEGF<sub>165</sub>-VEGFR2 downstream signalling, and it can even regulate EC migration, adhesion and the functions of other cell membrane receptors, including VEGFR2, independently of VEGF-stimulation (Wang, Zeng et al. 2003). In fact, this suggestion was published only three years after the discovery of NRP1 by Cai and Reed, who isolated the cytoplasmic-bound adaptor GIPC from the C-terminal PDZ-binding domain of NRP1, suggesting that GIPC-NRP1 may participate in membrane trafficking machinery (Cai and Reed 1999). This suggestion was supported by a study showing that PLC $\gamma$  phosphorylation, one of the downstream signals directly activated by

VEGFR2, was decreased when the cytoplasmic C-terminal PDZ domain-binding SEA motif of NRP1 was mutated, suggesting that one or more sites in the NRP1 cytoplasmic tail play an essential regulatory role in PLC $\gamma$ -1 phosphorylation (Ballmer-Hofer, Andersson et al. 2011). Interestingly, the same study also found that p38, a required molecule in vascular sprouting (Kawamura, Li et al. 2008), phosphorylation was diminished when the entire NRP1 cytoplasmic tail, including the last three amino acids (SEA), was missing, indicating that not only the SEA motif in NRP1 mediates signalling but the entire cytoplasmic tail is also required in VEGF<sub>165</sub>-VEGFR2 signalling (Ballmer-Hofer, Andersson et al. 2011). Another study showed that binding  $\beta$ 3-integrin subunit (ITGB3) to NRP1 via its cytoplasmic PDZ-binding domain limited the interaction between NRP1-VEGFR2 and the subsequent VEGF<sub>165</sub>-VEGFR2 downstream signalling, thereby significantly reducing the number of microvessel sprouting in *ex vivo* aortic ring assays (Robinson, Reynolds et al. 2009).

The cytoplasmic tail of NRP1 can also regulate EC functions independently of VEGF-induction. This statement is supported by two studies. Valdembri *et al.* showed that silencing NRP1 with siRNA in human umbilical artery ECs (HUAECs) reduced ECs adhesion to FN and impaired endogenous soluble FN (sFN) incorporation into a dense fibrillar network (Valdembri, Caswell et al. 2009). By transfecting the NRP1-siRNA depleted ECs with retrovirus carrying full-length mouse NRP1 (mNRP1) or lacking either the C-terminal SEA amino acids (mNrp1dSEA) or the whole cytoplasmic domain (mNrp1dCy), the authors found that, in comparison to full-length mNRP1, cytoplasmic deletion constructs of mouse NRP1 failed to rescue the adhesion and fibrilogenesis defects seen in NRP1-siRNA depleted ECs, suggesting that NRP1 through its cytoplasmic tail promotes EC adhesion to FN and FN matrix formation. Importantly, NRP1-siRNA blocked VEGF<sub>165</sub>-induced human EC adhesion to FN stimulation, but all the three constructs (mNRP1, mNrp1dSEA and mNrp1dCy) rescued the adhesion of NRP1-siRNA depleted EC in response to VEGF<sub>165</sub> stimulation with similar efficiency, suggesting that the NRP1 cytoplasmic tail regulates EC adhesion to FN independently of VEGF<sub>165</sub> (Valdembri, Caswell et al. 2009). Fantin *et al.* showed that targeting the Tyr 297A within the extracellular b1 domain of NRP1, which is a required site for VEGF binding and NRP1VEGFR2 complex formation, resulted in no severe embryonic defects in full or endothelial-specific NRP1 knockout, but these mice displayed significant impairment in arterial morphogenesis during development and in adulthood, suggesting that VEGF binding to NRP1 is not essential for embryonic angiogenic development. Therefore,

NRP1 must have a VEGF-independent role, which is likely through its cytoplasmic tail (Fantin, Herzog et al. 2014).

NRP1 interacts with VEGFR2 not only in a *cis*-binding fashion but also in *trans*, mediating interactions between adjacent cells. For example, the investigations of the effects of NRP1 on VEGFR2 function in *cis*- and *trans*-binding showed results that were consistent with previous observations. The study found that VEGF-induced rapid VEGFR2-NRP1 complex formation and internalisation when the receptors were expressed in the same cell. However, when NRP1 was expressed by adjacent cells (e.g. tumour cells), it showed distinct effects on VEGFR2 function by causing a delay in complex formation and a reduction in ERK1 phosphorylation, while the prolonged expression of PLC $\gamma$ -1 and ERK2 resulted in preventing and reducing sprouting angiogenesis (**Figure 1.11**) (Koch, van Meeteren et al. 2014).

A group of other studies demonstrated that NRP1 regulated EC function and extracellular remodelling independently of VEGFR2. For example, transducing EGNRP-1, a chimeric receptor generated by fusing the extracellular region of the epidermal growth factor receptor (EGFR) to the transmembrane/intracellular domains of NRP1, promoted HUVEC migration in response to EGF when VEGFR2 was mutated, indicating that the cytoplasmic tail of NRP1 alone could mediate ligand-dependent ECs migration, but not proliferation, independently of VEGFR2 (Wang, Zeng et al. 2003). Murga *et al.* showed that VEGFR2-siRNA displayed no significant effect on HUVEC adhesion on FN, laminin or gelatin, whereas NRP1-siRNA significantly impaired HUVEC adhesion on these matrices. Additionally, the pattern of filamentous actin (F-actin) over 24 hours incubation in VEGFR2-siRNA depleted HUVECs were not different compared to control HUVECs, whereas NRP1-siRNA depleted HUVECs displayed a significant reduction in F-actin organisation over 48 hours of incubation. Only after this time did NRP1-siRNA depleted HUVECs display F-actin organisation similar to control cells, suggesting that NRP1 controls endothelial cell adhesion independently of VEGFR-2 (Murga, Fernandez-Capetillo et al. 2005). Four years later, this finding was strongly supported by another study showing that NRP1, independently of VEGF<sub>165</sub> and SEMA-3A signalling, promotes  $\alpha$ 5 $\beta$ 1 integrin-mediated EC adhesion to FN via the interaction of the SEA domain at the C-terminal of NRP1 with the endocytic adaptor protein GIPC. Specifically, the interaction of NRP1-GIPC with the active form of  $\alpha$ 5 $\beta$ 1 is mediated by another associated molecule called motor myosin VI (Myo-6), which then promotes active  $\alpha$ 5 $\beta$ 1 integrin endocytosis and EC adhesion to FN. This study suggested that vascular phenotypes resulting from the loss of the *NRP1* gene or its cytoplasmic tail could be due to

the role of NRP1 in mediating EC adhesion to ECM. (Valdembri, Caswell et al. 2009). Consistent with these results, another study showed that NRP1 regulates angiogenesis independently of VEGF-VEGFR2 system by regulating FN matrix remodelling and phosphorylation of paxillin, a focal adhesion multifunctional adaptor molecule that links the cell surface protein-ECM to the actin cytoskeleton during cell migration, activation and actin remodelling (Raimondi, Fantin et al. 2014). In contrast to earlier studies, which showed that NRP1 depletion decreased HUVEC adhesion to FN (Murga, Fernandez-Capetillo et al. 2005), (Valdembri, Caswell et al. 2009), Raimondi and Fantin reported that NRP1-siRNA-depletion did not affect EC adhesion to FN substrates in either HUVECs or HDMECs. However, NRP1-silencing reduced the migration of these ECs on FN. NRP1 knockdown led to abnormal cytoskeletal morphology with abundant cortical actin as well as a significant reduction in paxillin phosphorylation, when cells were plated on FN. In contrast, control siRNA-treated or VEGFR2-siRNA treated ECs exhibited normal elongated stress fibres with paxillin localised to focal adhesion (FAs) at the end of the actin filament fibres stimulated with VEGF<sub>165</sub>. Additionally, VEGF<sub>165</sub>-induced paxillin phosphorylation was not changed in NRP1-depleted ECs compare to control siRNA ECs, whereas NRP1 knockdown showed a downregulation of paxillin phosphorylation in FN-stimulated ECs. Interestingly, the co-immunoprecipitation experiment showed that NRP1 formed a complex with paxillin as well as ABL1 (Raimondi, Fantin et al. 2014), a non-receptor tyrosine kinase whose activity and recruitment from the nucleus to FAs is regulated by integrins (Lewis, Baskaran et al. 1996), (Lewis and Schwartz 1998), (Cui, Chen et al. 2009). These findings showed that NRP1 regulates FN-dependent actin remodelling, cell migration, and paxillin activation via ABL1 independently of VEGF-VEGFR signalling (Raimondi, Fantin et al. 2014).

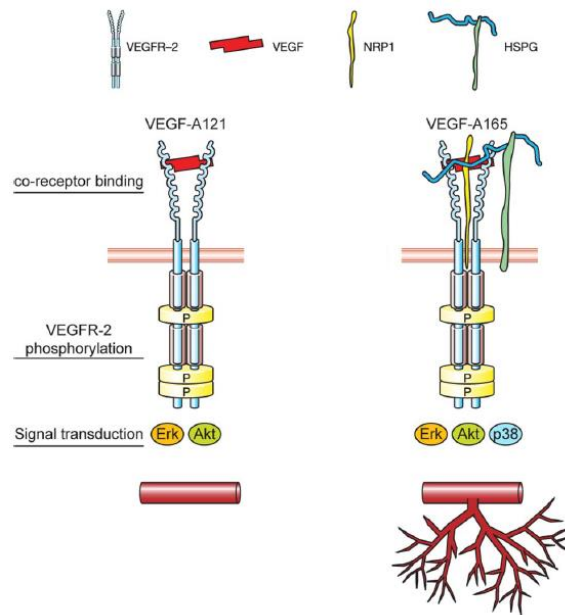


**Figure 1.10 Contribution of NRP1 function in VEGF-A<sub>165</sub>/VEGFR2 vs VEGF-A<sub>121</sub>/VEGFR2 signalling in ECs.** Schematic representation showing that the complex formation of NRP1-VEGFR2 as well as HSPG enhance VEGFR2 binding to VEGF<sub>165</sub> and transduce the downstream signalling activation of ERK1/2, Akt and p38 MAPK, which results in angiogenic sprouting/branching, whereas VEGF-A<sub>121</sub> does not induce stable complex formation between NRP1 and VEGFR2 and thus fails to transduce the downstream signalling activation of p38 MAPK and endothelial angiogenic sprouting/branching. The P symbol in yellow indicates VEGFR2 phosphorylation. Note that NRP1 interacts directly with VEGFR2, but for better visualisation, they are shown separately. Adapted from (Kawamura, Li et al. 2008).

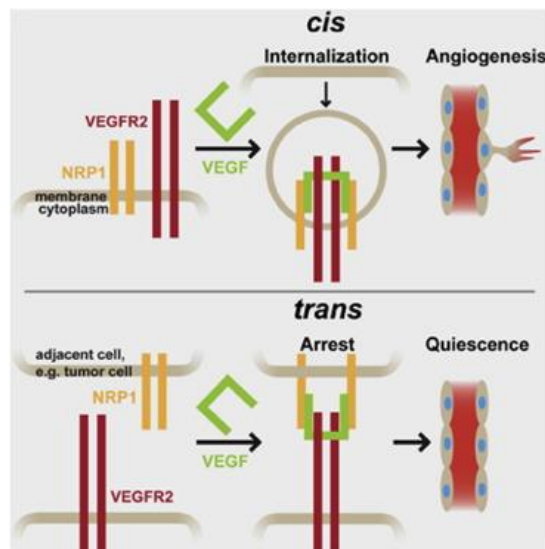


**Figure 1.11 Differential VEGFR2 activation driven by NRP1-binding in *cis*- vs. *trans*.** The schematic representation shows that the complex formation of NRP1-VEGFR2 in response to VEGF in the same cell (*cis*-binding) promotes rapid VEGFR2 activation, internalisation and angiogenic sprouting/branching; whereas a *trans*-binding formation between non-endothelial (e.g. tumour cells) NRP1 and endothelial VEGFR2 in response to VEGF results in a delay of NRP1-VEGFR2 complex formation, arrests internalisation and prevents angiogenic sprouting/branching (Koch, van Meeteren et al. 2014).

### 1.2.3.1.4.2.2 NRP2

A role for NRP2 in regulating neuron cells axon guidance was discovered only one year after the discovery that NRP1 regulates this same process. NRP2's domain structure is highly similar to NRP1 (Chen, Chédotal et al. 1997); however, studies on neuropilins were mainly focused on NRP1 (Zachary 2014), (Wittmann, Grubinger et al. 2015). This focus was possibly due to the observations of early transgenic mice studies in which NRP1-NUL mice were embryonically lethal (Kawasaki, Kitsukawa et al. 1999), whereas NRP2-NUL mice were viable with only small defects in venous/lymphatic vessels and the minor brain defects described above (Giger, Cloutier et al. 2000), (Chen, Bagri et al. 2000), (Yuan, Moyon et al. 2002). To date, there are only a few studies that have examined the role of NRP2 in ECs; these will be summarised below. A few more studies have focused on NRP2 function in cancer cells perhaps because its upregulation is consistent with cancer progression (e.g. neuroblastomas (Fakhari, Pullirsch et al. 2002), nonsmall cell lung carcinoma [NSCLC] (Kawakami, Tokunaga et al. 2002), human prostate carcinoma, melanoma (Bielenberg, Hida et al. 2004), lung cancer (Tomizawa, Sekido et al. 2001), (Kawakami, Tokunaga et al. 2002), (Lantuéjoul, Constantin et al. 2003), myeloid leukaemia (Vales, Kondo et al. 2007), breast cancer (Bachelder, Crago et al. 2001) and pancreatic cancer (Fukahi, Fukasawa et al. 2004)). Perhaps it is not surprising that NRP2 has become a biomarker for some cancers, including endocrine pancreatic (Cohen, Herzog et al. 2002) and bladder cancer progression (Sanchez-Carbayo, Socci et al. 2003), or a prognostic indicator in osteosarcoma (Handa, Tokunaga et al. 2000).

In 2000, NRP2 expression was reported for the first time in HUVECs, suggesting that it may play a role in cardiovascular biology (Gluzman-Poltorak, Cohen et al. 2000). Interestingly, this study reported two important findings: 1) Similar to NRP1, NRP2 binds to VEGF<sub>165</sub> and PlGF-2 with high affinity; 2) VEGF<sub>145</sub>, which lacks exon 7, but contains exon 6 (Poltorak, Cohen et al. 1997), is able to bind only to NRP2, not to NRP1; however, the affinity between NRP2 and VEGF<sub>145</sub> is five-fold lower than that between NRP2 and VEGF<sub>165</sub>. This initial study concluded that NRP2 may initiate signal transduction through VEGF receptors in ECs (Gluzman-Poltorak, Cohen et al. 2000). A study conducted the following year supported this hypothesis by showing that NRP2 binds to VEGF<sub>165</sub>. The disruption of the cytoplasmic tail of NRP2 by inserting myc-epitope in frame after the conserved SEA domain of NRP2 caused NRP2 to lose most of its binding affinity with VEGF<sub>165</sub> but not with Sema-3F, indicating that the cytoplasmic tail of NRP2 is required for VEGF<sub>165</sub> but not for Sema-3F signalling

(Gluzman-Poltorak, Cohen et al. 2001). This study also reported that both NRP1 and NRP2 form a complex with VEGFR1 (Fuh, Garcia et al. 2000), and this interaction allows NRPs to bind to VEGF<sub>121</sub> (Gluzman-Poltorak, Cohen et al. 2001).

NRP2 has also been implicated in lymphogenesis, by forming a complex with VEGFR3, which is exclusively expressed in lymphatic ECs (Kärpänen, Heckman et al. 2006). This study reported several important findings: 1) NRP2 is expressed in both human lymphatic dermal microvascular endothelial cells (HLDMVECs) and in human blood dermal microvascular endothelial cells (HBDMVECs), indicating directly that NRP2 may play roles in both lymphatic and blood ECs; 2) Human embryonic kidney 293 cells expressing the SV40 large T antigen (HEK293 cells) transfected with plasmids encoding human VEGF-C or VEGF-D **and** NRP1 or NRP2 showed that VEGFC could interact with NRP2 and that this interaction was slightly enhanced with the addition of HSPGs, while the interaction of VEGFC with NRP1 was entirely dependent on HSPGs. VEGF-D could also bind to both NRP1 and NRP2, but both interactions were dependent on HSPGs; 3) Sema-3F, whose binding was believed to be restricted to NRP2 (Bielenberg, Hida et al. 2004), binds to NRP1 and NRP2 and competes with VEGF-C in binding to both NRPs, indicating that these different ligands interact with NRPs through overlapping binding sites; 4) HEK293 cells transfected with a plasmid encoding NRP2 and then stimulated with VEGF-C did not induce NRP2 internalisation. However, if the cells were additionally transfected with VEGFR3, NRP2 was internalised, indicating that NRP2 internalisation is dependent on the presence of both VEGFR3 and VEGF-C; 5) endogenous NRP2 binds directly to VEGFR3 in a ligand-independent manner, but VEGF-C or VEGF-D is required for NRP2-VEGFR3 complex to co-internalise and co-localise in endocytic vesicles (Kärpänen, Heckman et al. 2006). Another study published in the same year examined HEK293 cells transfected with NRP2-flag and HA-VEGFR2 or HA-VEGFR3. Immunoprecipitation studies showed that NRP2 interacts with not only VEGFR3 but also VEGFR2. Interestingly, stimulation with VEGF-A or VEGF-C increased the association of flag-NRP2/VEGFR2, while flag-NRP2/VEGFR3 was increased only in the presence of VEGF-C, indicating that NRP2 binds to VEGFR2 or VEGFR3 in both ligand-dependent and -independent fashions (Favier, Alam et al. 2006). By using porcine aortic endothelial cells (PAEC), the authors also showed that VEGFR2 phosphorylation was increased when the cells were transfected with human pCDNA hygro-NRP2 and stimulated with either VEGF-A or VEGF-C compared to low VEGFR2 phosphorylation in the absence of NRP2. This observation was confirmed by NRP2-siRNA

silencing experiments in human microvascular endothelial cells (hMVECs). VEGF-C or VEGF-D induced phosphorylation of VEGFR2 was inhibited upon NRP2 knockdown. Interestingly, the overexpression of NRP2 in hMVECs increased cell survival induced by either VEGF-A or VEGF-C compared to cells transfected with an empty vector (Favier, Alam et al. 2006), whereas NRP2 knockdown significantly inhibited VEGF-A- and VEGF-C-induced migration (Favier, Alam et al. 2006), supporting the hypothesis that NRP2 knockdown might help in cancer therapy. Consistent with this concept, another report studied the effect NRP2 inhibition in three different lymphogenesis models of adult mice, where the injection of a function-blocking anti-NRP2 antibody resulted in a significant reduction in the number of: 1) superficial dermal tail lymphatic network; 2) lymphatic villi with lacteals in the small intestinal; and 3) epicardial lymphatic branch points in the heart. Interestingly, NRP2 was also shown to be highly expressed in lymphatic tip cells, but not in stalk cells. Moreover, blocking the VEGF-C binding to NRP2 with anti-NRP2 antibody inhibited the sprouting of the lymphatic endothelial tip cells, indicating that NRP2-VEGF-C plays a critical role in inducing filopodia extension in this system. The same study also showed that LECs, including tip cells, expressed both VEGFR2 and VEGFR3, but the lymphatic vessels sprouting in the double-heterozygous *NRP2<sup>+/-</sup> VEGFR2<sup>+/-</sup>* mice developed normally without detectable defects, whereas in the double-heterozygous *NRP2<sup>+/-</sup> VEGFR3<sup>+/-</sup>* mice, lymphatic sprouting was reduced in the three lymphogenesis models. The authors concluded that the NRP2-VEGFR3 interaction induced by VEGF-C in the tip cells mediates the sprouting of lymphatic vessels during lymphogenesis (Xu, Yuan et al. 2010).

In contrast to the findings of the above studies, a recent study showed that the siRNA-mediated depletion of NRP2 in HUVEC resulted in a ~1.5-fold increase in both cell migration and invasion, and the overexpression of NRP2 reduced HUVEC migration and invasion. Similarly, EC infiltration into a matrigel implant plug treated with NRP2-siRNA was increased compared to an implant containing control siRNA (German, Mammoto et al. 2014). Furthermore, this study showed that VEGF alone or soluble tumour-driven factors induces cell migration and micro-vessel sprouting by decreasing the expression levels of NRP2 and paxillin, (German, Mammoto et al. 2014). This observation is inconsistent with many other studies that show VEGF, NRP2, and paxillin (Jagadeeswaran, Surawska et al. 2008), (Mackinnon, Tretiakova et al. 2010), (Deakin, Pignatelli et al. 2012), (Sen, De Castro et al. 2012) are all highly expressed in tumours and their expression is correlated with cancer progression. Nevertheless, the same study reported that the deletion of paxillin resulted in a

50% reduction in both NRP2 protein and mRNA, indicating that NRP2-paxillin signalling plays a significant role in cell migration, but how is still under investigation. The findings of this study suggested that the amino-terminus (N-terminus) of paxillin binds to NRP2 indirectly through other adaptor proteins, including vinculin, to regulate cell migration (German, Mammoto et al. 2014).

#### **1.2.3.1.4.2.2.1. NRP2's function in cancer**

Similar to NRP1 expression, NRP2 expression has been implicated in cancer progression. A previous study showed that the NRP2-VEGF-C complex is required to promote the survival of prostate cancer cells (PC3 cells) by activating Akt signalling and preventing these cells from oxidative stress-induced cell death. The study found that by increasing the concentration of VEGF-C in the presence of oxidative stress hydrogen peroxidase ( $H_2O_2$ ), Akt phosphorylation as well as the phosphorylation of its downstream signalling proteins Forkhead box protein O1 (FOXO1) and Glycogen synthase kinase 3 beta (GSK-3 $\beta$ ) were increased compared to unstimulated cells. NRP2 knockdown inhibited the VEGF-C-induced phosphorylation of these proteins, indicating that VEGF-C promotes cell survival through binding to NRP2 (Muders, Zhang et al. 2009). To further understand the potential mechanism involved in VEGF-C-induced survival, three years later, the same group conducted a microarray study and identified two molecules that were consistently upregulated when VEGF-C or NRP2 were separately knocked down in PC3 cells: 1) WD Repeat and FYVE domain containing 1 (WDFY1), a vesicle trafficking protein; 2) Lysosome-associated membrane protein 2 (LAMP2), a lysosomal membrane protein that functions as a downstream effector of WDFY1 and facilitates the fusion of autophagosomes to the late endosomes during autophagy. Additionally, the deletion of VEGF-C or NRP2 decreased autolysosomal turnover and thus inhibited autophagy trafficking in PC3 cells. Furthermore, the overexpression of VEGF-C in other prostate cancer cell lines (LNCaP C4-2B and LNCaP C4-2) that contain high levels of NRP2 enhanced autophagy and thus prevented cell death, whereas the overexpression of VEGF-C in VEGF-C-depleted PC3s increased cell survival. Interestingly, the depletion of VEGF-C or NRP2 in cancer cells after treatment with chemotherapy enhanced cell death compared to the untreated cells, suggesting that VEGF-C and NRP2 depletion in cancer cells could ameliorate the resistance to cancer treatment. Overall, this study showed that the upregulation of VEGF-C and NRP2 in prostate cancer cells reduce the expression of WDFY1 and LAMP2, which resulted in the activation of

autophagy and therefore enhanced cancer cell survival. These two studies indicated that VEGF-C-NRP2 can regulate both autophagic pathways and antiapoptotic pathways (Stanton, Dutta et al. 2012). Because VEGF-C-NRP2 was shown to induce autophagic and antiapoptotic signalling pathways, a follow-up longitudinal study analysed the prognostic effects of NRP2 and VEGF-C expression in 247 bladder cancer patients over a period of 15 years. When NRP2 was highly expressed, the cancer-specific survival (CSS) rate dropped from 166 months to 85 months. When VEGF-C was highly expressed, the CSS rate dropped from 170 months to 88 months, suggesting that NRP2 alone or in combination with VEGF-C expression is a prognostic marker that can predict outcomes before transurethral resection (TURBT) and radio-chemotherapy (RCT). Their expression can also be used as a biomarker to predict the response to therapy for bladder cancer or other cancer types (Keck, Wach et al. 2015). Another study provided a molecular mechanism by which NRP2 regulated WDFY1 synthesis in prostate cancer. In this study, NRP2 knockdown did not alter the protein stability of WDFY1 in PC3 prostate cancer cells, but it did increase the transcriptional activity of WDFY1 as well as both mRNA and protein levels of WDFY1. Similar to the NRP2 knockdown effect, the deletion of foetal ALZ50-reactive clone 1 (FAC1), a transcriptional repressor protein that presents in the cytosol and in the nucleus of PC3 cells, also increased the mRNA level of WDFY1. Interestingly, NRP2 knockdown shifts the localisation of FAC1 from the nucleus to the cytosol and thus reduces the recruitment of FAC1 to bind and suppress WDFY1 transcription in the nucleus, which results in the continual transcription of WDFY1, indicating that NRP2 inhibits the transcription of WDFY1 by controlling the subcellular localisation of FAC1 repressor protein (Dutta, Roy et al. 2016). Another study identified a correlation between the elevation of NRP2 expression in aggressive prostate cancer cells, including PC3 cells, and the hindrance of the tumour suppressor protein phosphatase and tensin homolog (PTEN). The findings also revealed a novel molecular mechanism by which NRP2 suppresses PTEN function. These aggressive prostate cancer cells also exhibited high levels of VEGF protein, polycomb complex protein (Bmi-1), c-Jun N-terminal kinases (JNKs), and focal adhesion kinase (FAK) phosphorylation but downregulation of Insulin-like growth factor-1 receptor (IGF-1R). Silencing any of these proteins serves to rescue the IGF-1R and PTEN expression, which then inhibits NRP2 expression as well as other molecules implicated in prostate cancer cells (Goel, Chang et al. 2012).

NRP2 also has been implicated in many other cancers. For example, NRP2 is highly expressed in breast cancer, and its expression is correlated with aggressiveness (Yasuoka,

Kodama et al. 2009). In this study, the NRP2 immunostaining of breast cancer tissues showed that the NRP2 protein is expressed not only in the vascular ECs of cancer tissue but also in the cytoplasm of the cancer cells. This study showed that NRP2 expression tended to be co-localised or adjacent to endogenous VEGF-C expression on cell surface, whereas the cytoplasmic NRP2 was co-localised to chemokine receptor 4 (CXCR4), which was previously shown to promote lymph node metastasis. Interestingly, anti-NRP2 antibody inhibited both cytoplasmic CXCR4 expression and CXCR4-endogenous VEGF-C-induced migration, suggesting that there is a correlation between NRP2-VEGF-C-CXCR4 expression in breast cancer (Yasuoka, Kodama et al. 2009). Another study correlated the upregulation of NRP2 levels in lung cancer with TGF- $\beta$ -mediated epithelial mesenchymal transition (EMT), a process by which cells lose their cell-cell interaction allowing tumour cells to migrate and invade. Mechanistically, TGF- $\beta$  induced NRP2 upregulation through activation of the zinc finger E-box-binding homeobox-1 (ZEB-1) transcription repressor, which inhibits SEMA-3F and downregulates E-cadherin. Consequently, this caused tumour progression, migration and invasion through activating the downstream signalling of TGFR- $\beta$ , including the ERK and Akt pathways. Interestingly, blocking the canonical TGF- $\beta$  signalling (e.g. SNAIL protein) by mothers against decapentaplegic homolog 7 (Smad7) antagonist did not change NRP2 expression at the protein or mRNA levels, while inhibiting non-canonical TGF- $\beta$  signalling (e.g. ERK or Akt) by U0126 or MKK-2206 inhibitors, respectively, reduced NRP2 levels, indicating that NRP2 upregulation in lung cancers is mediated by non-canonical TGF- $\beta$  signalling (Nasarre, Gemmill et al. 2013). A similar mechanism was also observed in hepatocellular carcinoma (HCC), in which NRP2 upregulation in HCC enhanced both cell migration and invasion, whereas NRP2 knockdown reduced cell migration and invasion, but not proliferation. However, this study showed that NRP2 is upregulated in the HCC that undergo EMT induced by the canonical Smad2/3-Smad4 signalling cascade, indicating that TGF- $\beta$  induces NRP2 expression in a Smad-dependent fashion. The authors concluded that NRP2 could be used as a biomarker for cancer progression in patients with HCC (Wittmann, Grubinger et al. 2015). Furthermore, NRP2 was also overexpressed in a human pancreatic adenocarcinoma cell line. The depletion of NRP2 in these cells reduced VEGFR1 phosphorylation as well as Akt phosphorylation, indicating that NRP2 knockdown inhibited the survival signalling pathway. Additionally, NRP2 knockdown also reduced pancreatic cancer cell migration and invasion *in vitro*, but not proliferation. However, in a cross-sectional analysis, an *in vivo* study showed that NRP2 depletion significantly reduced the number of proliferative nuclei evaluated by cell nuclear staining and smaller blood vessels.

Interestingly, this study also showed that NRP2 depletion decreased tumour volume and altered the tumour vasculature. To further understand the effects observed in the development of tumour vasculature, the study investigated the protein level of several angiogenic mediators, including VEGF, VEGF-C, DLL4 and Jagged-1. Only Jagged-1, a cell surface protein that functions in Notch signalling to control tip cell selection, was significantly reduced by NRP2 knockdown. The overall findings of this study suggested that NRP2 expression may serve as a therapeutic target for pancreatic cancer (Dallas, Gray et al. 2008). As in pancreatic cancer, NRP2 is also overexpressed in human colorectal tumours. NRP2 depletion also resulted in reductions in VEGFR1 phosphorylation, Akt phosphorylation, invasiveness and tumour volume, but not proliferation. In addition, NRP2 knockdown resulted in less metastasis and increased apoptosis compared to the control cells. The overall findings of this study suggested that NRP2 expression may serve as a potential therapeutic target for colorectal cancer (Gray, Van Buren et al. 2008). Recently, another study demonstrated that NRP2 overexpression acts as a mediator in VEGF-C/VEGFR3 activation to promote aggressive oral squamous cell carcinoma (OSCC) (Ong, Gokavarapu et al. 2017). The immunofluorescence experiments performed in this study revealed that NRP2 was co-localised with VEGF-C expression and that it was associated with regional lymph node metastasis, whereas Sema-3F was not detected in these cancer cells. Interestingly, the NRP2 knockdown reduced cell proliferation, migration and invasion, whereas the overexpression of VEGFR3 with VEGF-C supplementation did not 'rescue' these cellular behaviours when NRP2 was depleted, indicating that NRP2 overexpression plays a central role in aggressive cellular biological behaviour and tumour progression. In this study, it was also concluded that the overexpression of NRP2 may be used as a biomarker for predicting lymph node regional metastasis in patients with OSCC (Ong, Gokavarapu et al. 2017).

Because NRP1 was shown to interact with integrins (Fukasawa, Matsushita et al. 2007), (Valdembri, Caswell et al. 2009), (Robinson, Reynolds et al. 2009) another group of studies demonstrated that NRP2 can also play a role in cancer through its interaction with integrins. For example, in line with previous studies showing that the NRP2 (Yasuoka, Kodama et al. 2009) and  $\alpha 6\beta 1$  integrin (Friedrichs, Ruiz et al. 1995), (Wewer, Shaw et al. 1997) are implicated in aggressive breast cancer, a subsequent study also found that aggressive breast cancers express high levels of both NRP2 and  $\alpha 6\beta 1$  integrin. This study led to the discovery of a potential mechanism whereby NRP2 regulates  $\alpha 6\beta 1$  signalling to promote the association of  $\alpha 6\beta 1$  with laminin allowing for the formation of stable adhesions required for breast

cancer cells to spread (Goel, Pursell et al. 2012). Via co-immunoprecipitation experiments, this study revealed a biochemical interaction between NRP2 and  $\alpha 6$ -integrin subunit (ITGA6). Furthermore, immunofluorescence microscopy substantiated the co-localisation of the two proteins in FAs, specifically with active FAK at the leading edge on laminin containing matrices. Interestingly, the adhesion of the breast cancer cells on laminin was reduced by NRP2-siRNA depletion or by blocking ITGA6 function with the anti-ITGA6 antibody. These findings indicate that these two proteins are important in the adhesion of breast cancer cells on laminin. Additionally, the separate depletion of endogenous VEGF or NRP2 expression reduced FAK activation. The stimulation of VEGF<sub>165</sub>-depleted cells by exogenous VEGF in the presence of NRP2 restored FAK activation, which led to the conclusion that NRP2-VEGF<sub>165</sub> signalling is necessary for  $\alpha 6\beta 1$  to activate FAK and that this activation is crucial for promoting robust FA formations at the leading edge of cells migrating on laminin (Goel, Pursell et al. 2012). NRP2 expression is also high in human renal cancer cell carcinoma (RCC) and pancreatic adenocarcinoma and its level of expression correlates with cancer progression (Cao, Hoepfner et al. 2013). This study revealed a unique mechanism through which NRP2 highly expressed on these cancer cells binds with  $\alpha 5$ -integrin subunit (ITGA5) expressed on the surface of ECs (in *trans* binding fashion) to promote vascular adhesion, extravasation and tumour metastasis (Cao, Hoepfner et al. 2013). Unlike NRP1 (Cao, Wang et al. 2008), NRP2 knockdown did not affect primary tumour growth (Cao, Hoepfner et al. 2013). However, metastatic nodules in the lung were much fewer in mice subcutaneously injected with shRNA directed against NRP2, compared to mice in the control group. Additionally, NRP2 expression at the metastatic site was much greater than in the primary tumour. Interestingly, RCCs or pancreatic adenocarcinoma cells injected into the pericardium of zebrafish embryos extravasated in the extravascular space (adjacent tissues), whereas NRP2-depleted cancer cells remained in the intersegment vessels, indicating that NRP2 plays a central role in tumour cell extravasation (Cao, Hoepfner et al. 2013). The author showed that NRP-2 blocking antibody impaired cancer cell adhesion to a monolayer of ECs. This suggests that NRP2 expressed on cancer cells mediates adhesion through a NRP2 *trans*-interacting partner that is expressed on ECs. Interestingly, NRP2 co-immunoprecipitation in a co-culture of cancer cells and ECs showed a biochemical interaction between NRP2 and the ITGA5 integrin subunit. The pre-treatment of cancer cells with function-blocking anti-ITGA5 did not inhibit their adhesion to ECs; whereas the pre-treatment of ECs with anti-ITGA5 antibody significantly reduced cancer cell adhesion to

ECs, suggesting that ITGA5 is a trans-binding partner for NRP-2 to promote vascular adhesion, extravasation and metastasis (Cao, Hoepfner et al. 2013).

### 1.2.3.2. Integrins

Integrins were first characterised in 1986 as transmembrane glycoproteins that integrate the extracellular matrix with the actin cytoskeleton (Tamkun, DeSimone et al. 1986). Subsequent studies discovered that integrins are heterodimeric type I transmembrane glycoprotein receptors composed of non-covalent associations between  $\alpha$  and  $\beta$  subunits. They function as cell adhesion molecules as well as connecting the intracellular environment with the extracellular environment. In the 30 years since their first characterisation, thousands of integrin studies have been published (Hynes 2002); studies which have defined their essential roles in embryonic development (Bouvard, Brakebusch et al. 2001) and increased our understanding of how different subunits of these receptors associate in different tissues, how they transduce adhesion-mediated signalling events, and how they regulate cellular behaviour in both physiological and pathological conditions (Bökel and Brown 2002). Integrins are expressed in metazoans, including sponges, cnidarians and mammals (Burke 1999). In mammals, at least 18  $\alpha$  and 8  $\beta$  subunits are associated in 24 different heterodimer receptors, in which 12 integrins contain the  $\beta 1$  subunit, five integrins contain the  $\alpha v$  subunit, and four integrins contain the  $\beta 2$  subunit, which are restricted to white blood cells (**Figure 1.12 A-B**) (Hynes 2002). The assembly of these distinct 24 hetero-dimerisations occur within the endoplasmic reticulum in an inactive conformation and then undergo post-translation modifications in the Golgi apparatus before they are targeted to the plasma membrane where they perform their myriad functions (Paul, Jacquemet et al. 2015). Integrins sense ECM and change cell behaviour accordingly (Goel and Mercurio 2012). A characteristic of integrins is that they can transduce signalling across the plasma membrane in both directions, either inside-out signals or outside-in signals. Therefore, integrins play essential roles in several cellular processes, including cell adhesion, proliferation, migration, differentiation, survival, apoptosis and shape in certain types of cells (Srichai and Zent 2010), (Pan, Zhao et al. 2016). Integrins also promote ECM protein assembly, cytoskeleton organisation and angiogenesis (Bökel and Brown 2002). For example, integrins may be found in the following locations: in the vascular system, depending on the anatomical origin of vessels; on the abluminal cell membranes of ECs in the BM, where they recognise ligands such as ECM proteins; on the cell membranes of circulating blood cells, where they recognise cell adhesion ligands, including

intercellular adhesion molecule 1 (ICAM 1) and vascular cell adhesion molecule 1 (VCAM 1). Integrins are also involved in guiding circulating blood cells into inflamed tissues by subsequent adhesion and transmigration (Plow, Meller et al. 2014). During angiogenesis, integrins bind to other transmembrane receptors, including VEGFRs and NRPs, to alter cell behaviour (Goel and Mercurio 2012), (Seguin, Desgrosellier et al. 2015).

### 1.2.3.2.1. Integrin structure and ligands

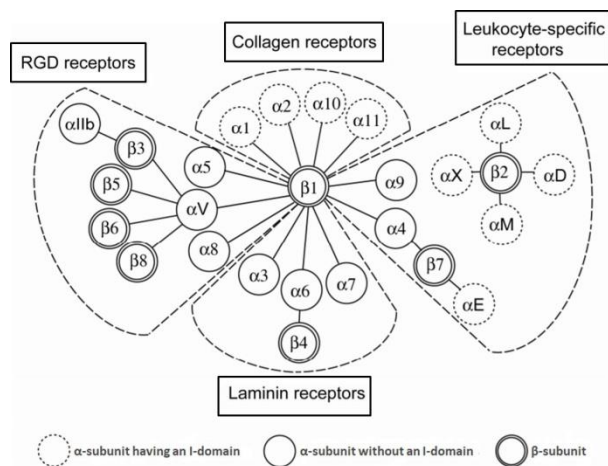
Each integrin is built by the non-covalent association between  $\alpha$ - $\beta$  subunits, each of which is composed of: 1) a large extracellular domain ranging between ~80–150 kDa that is divided into several subdomains, including the N-terminus (headpiece), which is required for extracellular ligand binding and a tailpiece, which function as knee for bending/extension (**Figure 1.13 A**); 2) a single membrane-spanning coiled-coil  $\alpha$  helix of ~25–29 amino acids which allows for bi-directional signal transmission; 3) a short cytoplasmic tail domain of about ~30 to 70 amino acids (with the exception of  $\beta 4$  subunit >1000 amino acids) which acts to transmit or receive intracellular signals (see **Figure 1.13 A**) (Srichai and Zent 2010), (Campbell and Humphries 2011), (Pan, Zhao et al. 2016). The cytoplasmic tail of the  $\alpha$  subunit is generally shorter than the  $\beta$  subunit (Pan, Zhao et al. 2016). The cytoplasmic tails of  $\beta$  subunits are similar, whereas the cytoplasmic tails of  $\alpha$  subunits are diverse (Srichai and Zent 2010). All mammalian cells express integrins. For example, ECs express at least 11 different integrins ( $\alpha 1\beta 1$ ,  $\alpha 2\beta 1$ ,  $\alpha 3\beta 1$ ,  $\alpha 4\beta 1$ ,  $\alpha 5\beta 1$ ,  $\alpha 6\beta 1$ ,  $\alpha v\beta 1$ ,  $\alpha v\beta 3$ ,  $\alpha v\beta 5$ ,  $\alpha v\beta 8$ , and  $\alpha 6\beta 4$ ), whereas platelets express five integrins ( $\alpha II\beta 3$ ,  $\alpha v\beta 3$ ,  $\alpha 2\beta 1$ ,  $\alpha 5\beta 1$ , and  $\alpha 6\beta 1$ ). Mature erythrocytes express very few or no integrins, however their precursor erythroblastoid proerythroblast cells do (Plow, Meller et al. 2014).

Unlike VEGFRs and other growth factor receptors, the cytoplasmic tails of integrin subunits lack enzymatic and kinase activity. Instead, they effectively transduce signalling by co-clustering with protein kinases (e.g. FAK) and adaptor proteins (e.g. tailin, vinculin and paxillin) in FA complexes. The extracellular regions of integrins have the ability to bind to a wide variety of ligands, including ECM deposition proteins (Srichai and Zent 2010) and cell surface adhesion molecules (Hynes 2002), (Campbell and Humphries 2011). The extracellular regions of integrins undergo conformational changes to transduce signalling or initiate apoptosis (Avraamides, Garmy-Susini et al. 2008). Typically, when a heterodimeric ligated integrin exists in an upright and unbent conformation upon ligand binding (active state), the transmembrane and cytoplasmic tails are separated between the  $\alpha$ - $\beta$  subunits, and

the kinases and adaptor proteins are bound to the cytoplasmic tails, allowing the integrins to cluster in transducing signalling pathways. However, when the binding to ligands is lost, integrins undergo conformational changes that lead to a close association between the transmembrane and the cytoplasmic tails of  $\alpha$ - $\beta$  subunits. Then bending of the extracellular regions occurs (in an inactive state), allowing the integrins to initiate apoptosis (**Figure 1.13 B**). (Srichai and Zent 2010), (Nevo 2011).

The number of ligands that are recognised by integrins is extensive, and it depends on the different combinations of  $\alpha$ - $\beta$  subunits. For example, integrins can bind to ECM proteins, including FN, laminin, collagen and other receptor proteins (Srichai and Zent 2010). Some integrins can only bind to a single ligand, such as  $\alpha 5\beta 1$ , whereas others can bind to multiple ligands, such as  $\alpha v\beta 3$ . Many integrins bind to specific sequences presented in the ligands (Avraamides, Garmy-Susini et al. 2008). These short peptide sequences can be classified into four major types: arginine-glycine-aspartic acid tripeptide (RGD) motif-binding integrins, leucine-aspartic acid-valine (LDV) motif-binding integrins,  $\alpha I$ -domain containing-integrins, and non- $\alpha I$ -domain-containing laminin-binding integrins (Humphries, Byron et al. 2006). For example, all five  $\alpha v$  integrins ( $\alpha v\beta 1$ ,  $\alpha v\beta 3$ ,  $\alpha v\beta 5$ ,  $\alpha v\beta 8$ ,  $\alpha v\beta 4$ ), two  $\beta 1$  integrins ( $\alpha 5\beta 1$ ,  $\alpha 8\beta 1$ ) and  $\alpha II\beta 3$  can recognise ligands containing the RGD motif. All  $\beta 2$  integrins ( $\alpha L\beta 2$ ,  $\alpha D\beta 2$ ,  $\alpha M\beta 2$ ,  $\alpha X\beta 2$  as well as  $\alpha 4\beta 1$ ,  $\alpha 4\beta 7$ ,  $\alpha 9\beta 1$ ,  $\alpha E\beta 7$ ) can recognise ligands containing the LDV motif. Regarding the  $\alpha I$ -domain,  $\beta 1$  subunit heterodimers or combine with some  $\alpha$  subunits that possess the  $\alpha I$ -domain to form integrins for laminin/collagen binding ( $\alpha 1\beta 1$ ,  $\alpha 2\beta 1$ ,  $\alpha 10\beta 1$ ,  $\alpha 11\beta 1$ ), whereas other integrins lack the  $\alpha I$ -domain but have highly selective binding to laminin ( $\alpha 3\beta 1$ ,  $\alpha 6\beta 1$ ,  $\alpha 7\beta 1$ ,  $\alpha 6\beta 4$ ) (see **Figure 1.12 A-B**) (Humphries, Byron et al. 2006). Previous studies have also shown that integrins function as receptors for the internalisation of bacteria and viruses (Triantafilou and Triantafilou 2001), (Hoffmann, Ohlsen et al. 2011), (Hussein, Walker et al. 2015).

A)



B)

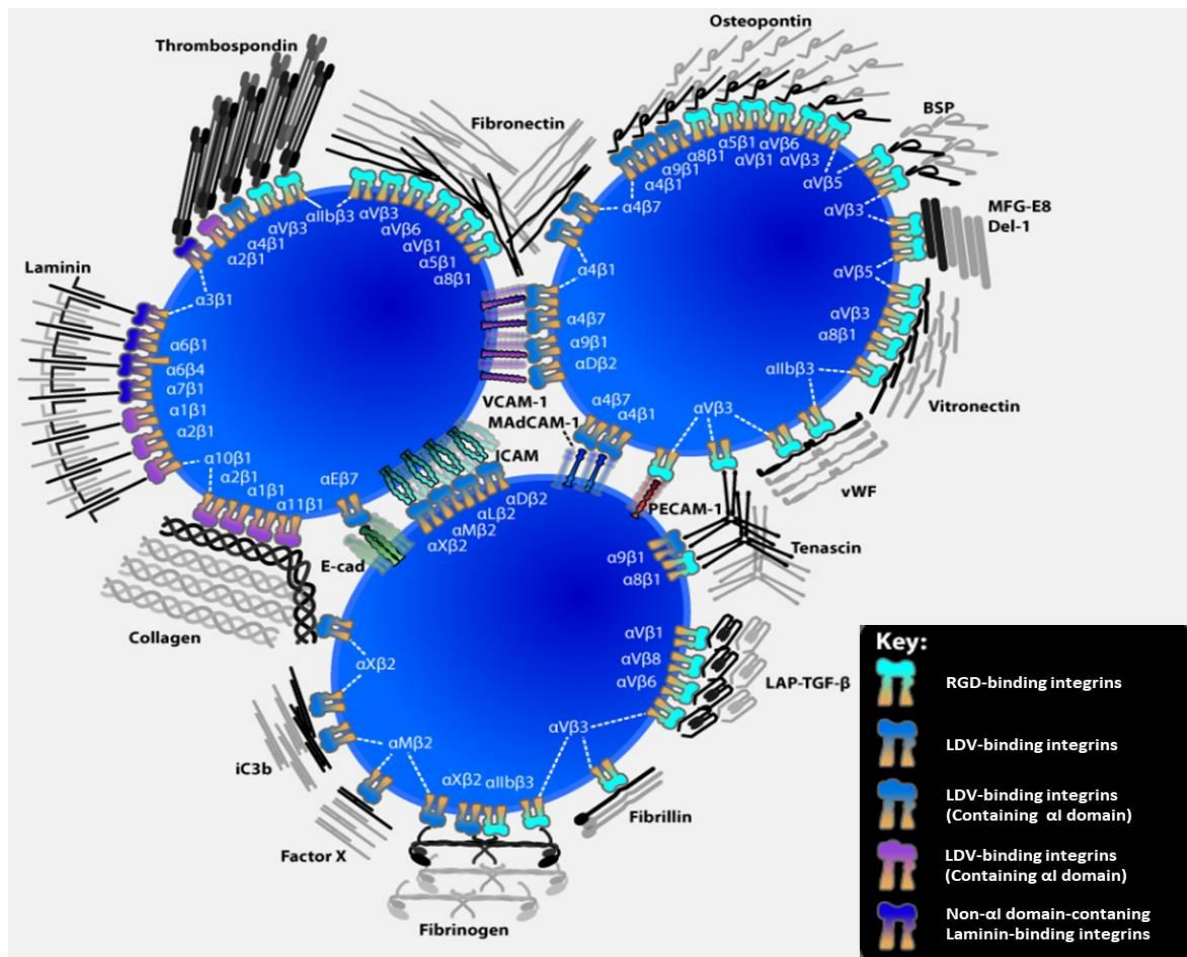
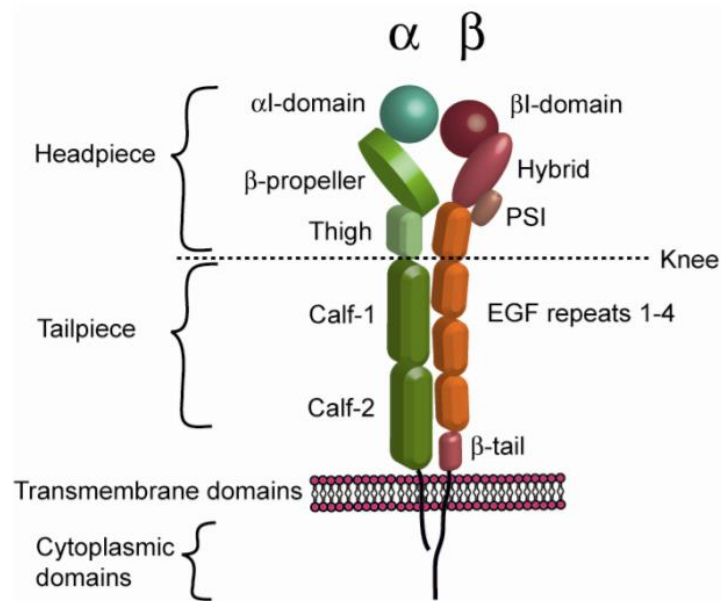


**Figure 1.12 The integrin subfamilies and their ligands.** A) The schematic illustration shows 24  $\alpha$ - $\beta$  forms of integrins based on their ligand specificity. Note that only 9 of 18  $\alpha$  subunits contain the  $\alpha$ I-domain, such as those in collagen and leukocyte receptors, whereas none of the RGD and laminin receptors contain the  $\alpha$ I-domain (Nevo 2011). B) The schematic illustration shows integrins recognising different short peptide sequences (see the integrins in the key on the right) as well as how the multivalent ligands recognise and cluster different integrins (Humphries, Byron et al. 2006).

A)



B)

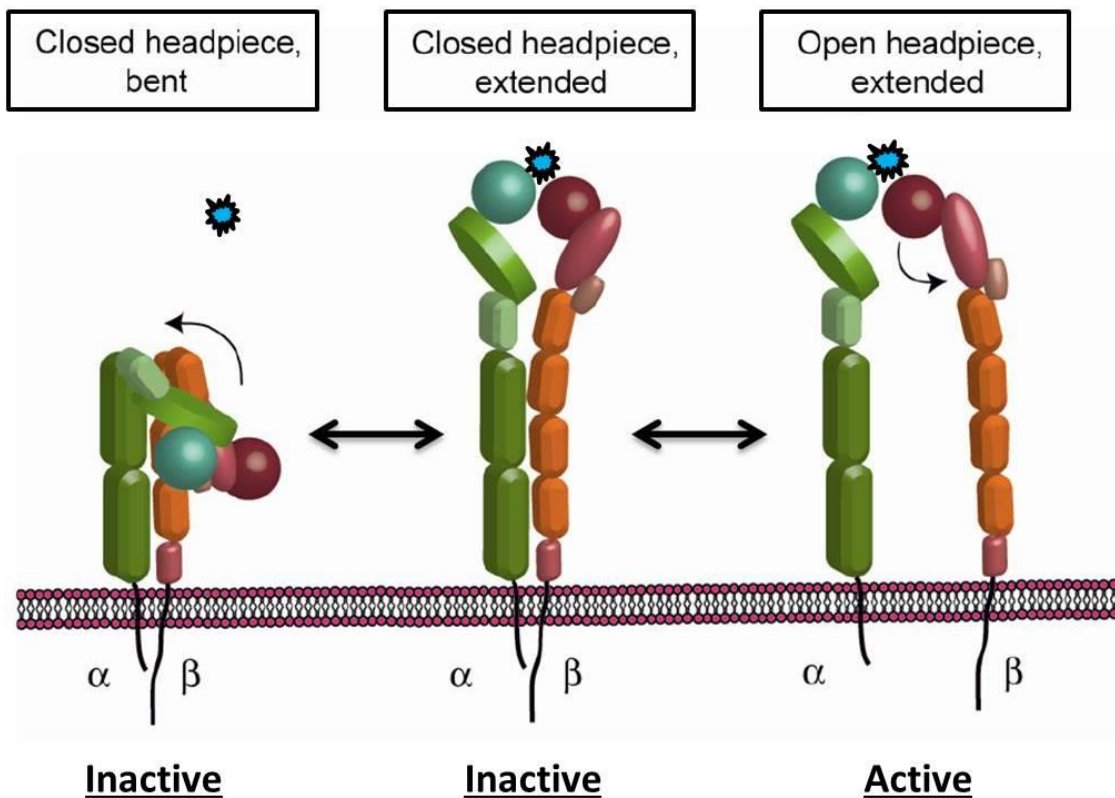


**Figure 1.13 Integrin structure and conformational changes to integrin  $\alpha$ - $\beta$  subunits during activation.** A) Integrins are built of associations between different  $\alpha$ - $\beta$  subunits. Each subunit consists of a large extracellular region, which can be divided into a headpiece and a tail piece, a transmembrane helical region and the intracellular domain. Generally, the cytoplasmic domain of the  $\beta$  subunit is longer than  $\alpha$  subunit. Note that not all  $\alpha$  subunits have the  $\alpha$ I domain. B) The schematic illustration shows the three conformational changes that  $\alpha$ - $\beta$  subunits undergo during integrin activation: closed headpiece/bent (inactive); closed headpiece/extended (inactive); and open headpiece/extended (active). It is worth noting that the activated integrin requires the clustering of integrins as well as intracellular adaptor proteins to transmit signals (not illustrated here). Adapted from (Nevo 2011).

### 1.2.3.2.2. Integrin activation

Integrins promote cell adhesion, angiogenesis, tumour growth and metastasis by sensing, integrating and interspersing outside-in and inside-out signalling between cells and their environments (Jia, Choi et al. 2018). Integrin activation occurs through two major regulation processes: affinity and avidity. The affinity process involves the conformational changes to an individual integrin, which can be further divided into two states: inactive “bent state” and the primed “extended or upright state”. In the bent state, the extracellular headpiece of an individual integrin points to the plasma membrane with a closed headpiece, and the integrin is unable to bind to the extracellular ligands because of the close association between  $\alpha$ - $\beta$  subunits (see **Figure 1.13 B**) (Nevo 2011). It is worth noting, however, that there is some evidence that integrins can bind to matrix even when they are in a bent state (e.g. on FN) (Adair, Xiong et al. 2005). In the primed state, the headpiece swings away from the plasma membrane, which is referred to as a “switchblade motion” and the headpiece is still closed with a close association between the  $\alpha$ - $\beta$  subunits, but the headpiece is able to bind to extracellular ligands. In contrast, the avidity process involves the disassociation between  $\alpha$ - $\beta$  subunits after the clustering interaction of the integrins and other cell surface transmembrane receptors. In the affinity process, the  $\alpha$ - $\beta$  subunits are closely associated, whereas in the avidity process, the  $\alpha$ - $\beta$  subunits are dissociated (Nevo 2011), (Plow, Meller et al. 2014), (Li and Springer 2017). Bi-directionality means that signalling that is generated by the ligands binding to the extracellular domain of integrins is transmitted to the intracellular space to influence the organisation of the actin cytoskeleton (outside-in signalling) while signalling that is generated by binding of the intracellular proteins to the cytoplasmic tails of integrins is transmitted to the extracellular environment to influence the interaction of the extracellular domain with the ligands (inside-out signalling) (Hu and Luo 2013). As a result of integrin activation and depending on the stage of maturation of the integrin, subcellular distribution and ECM composition, different types of adhesion complexes can form in the migrated cells: nascent adhesions, focal complexes, focal adhesions (FAs) and fibrillar adhesions (**Figure 1.14**) (Paul, Jacquemet et al. 2015), (De Pascalis and Etienne-Manneville 2017).

	Nascent adhesions	Focal Complexes	Focal adhesions	Fibrillar adhesions
Dimensions ( $\mu\text{m}$ )	< 0,25	1	2 -10	> 10
Half-life	1 min	2 - 3 min	20 min	very stable
Localization	Lamellipodium	Lamellipodium lamellum interface	Ends of actin bundles	Large actin bundles and fibrillar FN

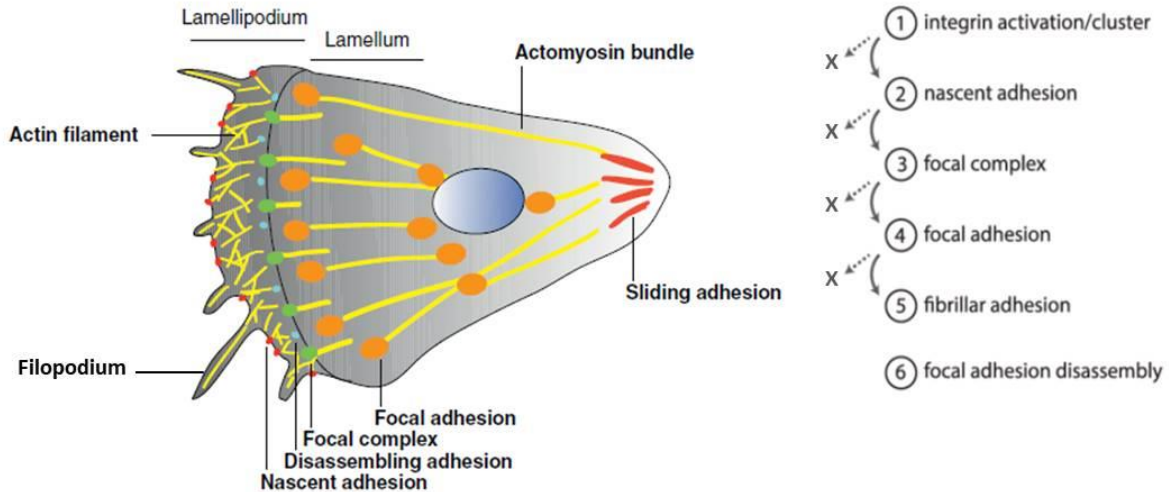


**Figure 1.14 Anatomical section of a migrating cell adhered to a 2D ECM.** Cell migration requires the coordination of a complex integrated process involving the integrins, signalling/adapting molecules and actin-binding proteins, which are activated temporally and spatially at different locations in the cell to achieve the correct balance in the assembly and disassembly of adhesions during cell migration. These adhesions are classified into four groups: nascent adhesion, focal complex, focal adhesion and fibrillar adhesion based on the morphology or the way they are formed (Webb, Parsons *et al.* 2002). Generally, after a cell defines its polarity, polymerisation of actin then occurs by adding new G-actin to the pre-existing actin filaments at the leading edge, where the retrograde flow is rapid, of lamellipodium, which results in the generation of several protrusions (filopodia). Small adhesions, called nascent adhesions, are initiated through the binding of integrins on the cell surface to their ECM ligands at the cell periphery. These small nascent adhesions either disappear within 60 s or grow in size to 1  $\mu\text{m}$  to form a focal complex at the boundary between the lamellipodium and lamellum. They then increase up to 10  $\mu\text{m}$  in mature focal adhesions in the lamellum region, where the retrograde flow and the turnover is slower than in nascent adhesions (up to a 20-minutes half-life). At the lamellum, the accumulation of stable focal adhesions increases, acting as handgrips to tether the cell front. These focal adhesions are rich in integrins that connect the ECM to the actin filaments mediated by intracellular adaptor molecules (e.g. paxillin, tailin, vinculin etc.). At the rear of the cell, the interaction of integrins with their ECM ligands via the adapting molecules becomes weak because the elevation of integrin turnover. This is resulting in the sliding of these focal adhesions toward the cell body until they disperse and eventually move the cell tail forward. Regarding a migrated cell on FN,  $\alpha 5\beta 1$  can drive the formation of very long stable fibrillary adhesion (longer than 10  $\mu\text{m}$ ) (Small, Rottner *et al.* 1998), (Webb, Parsons *et al.* 2002), (Li, Guan *et al.* 2005), (Valdembri and Serini 2012), (De Pascalis and Etienne-Manneville 2017). Adapted from (Valdembri and Serini 2012), (De Pascalis and Etienne-Manneville 2017).

### 1.2.3.2.2.1. Outside-in signalling

The outside-in signalling of integrins is similar to the classical activation of growth factor receptors by their growth factors, in which the receptors on the plasma membrane transmit the extracellular signals into the intracellular space through activating a wide array of intracellular signalling pathways. In fact, integrins require the interaction with growth factor receptors to enhance signal transduction (Menter and DuBois 2012). Typically, outside-in integrin signalling begins when ligands (ECM proteins in the case of basal surfaces or ICAM-1/VECAM in the case of freely circulating cells) bind to the extracellular domain of integrins at the intersection between  $\alpha$ - $\beta$  subunits. Here, the  $I\alpha$  and  $I\beta$  subdomains in the headpiece of both subunits become involved in the ligand binding process (Plow, Meller et al. 2014). However, in  $\alpha$  subunits without  $I\alpha$ , the  $\beta$  propeller of the  $\alpha$  subunit takes over and triggers the conformational changes in the extracellular domains to transform from the bent conformation to the upright active state (see **Figure 1.13 A-B**) (Srichai and Zent 2010). Subsequently, ligand–integrin interactions trigger separations between  $\alpha$ - $\beta$  subunits in the membrane-spanning helix and cytoplasmic tail regions. These conformational changes result in clustering of more integrin binding at the integrin adhesion sites and activation of the cytoplasmic tails of integrins. Over 150 different intracellular accessory proteins are recruited to the cytoplasm tail in order to assemble the small nascent adhesions that may disassemble or mature into bigger FAs complex. These FA complexes connect integrins to the cytoskeletal actin and mediate the mechanical force needed to transmit the extracellular signals and activate multiple intracellular pathways “outside-in”, including proliferation, migration, differentiation and survival (Srichai and Zent 2010), (Nevo 2011).

Three different classes of accessory adaptor proteins are found in FA complexes: 1) structural or scaffolding adaptors (e.g. talin, kindlin, filamin and tensin) that bind to F-actin and thus link integrin directly to the actin cytoskeleton; 2) catalytic adaptors (e.g. FAK, integrin linked kinase [ILK] and Src family kinase [Src]), which substitute for the lack of catalytic activity in the integrin cytoplasmic tail; 3) protein phosphatase 2A (PP2A), which propagates the transduced signals (Legate and Fässler 2009), (Nevo 2011). Briefly, when the cytoplasmic tails of the activated integrins are separated, FAK, a major non-tyrosine receptor kinase protein, undergoes phosphorylation at its tyrosine 397, and then it binds directly to the cytoplasmic tails of integrins or indirectly through the talin adaptor proteins (**Figure 1.15 A**). FAK contains the FERM domain (F for 4.1 protein, E for ezrin, R for radixin and M for moesin) at the N-terminus, and the focal adhesion targeting domain (FAT) at the C-terminal,

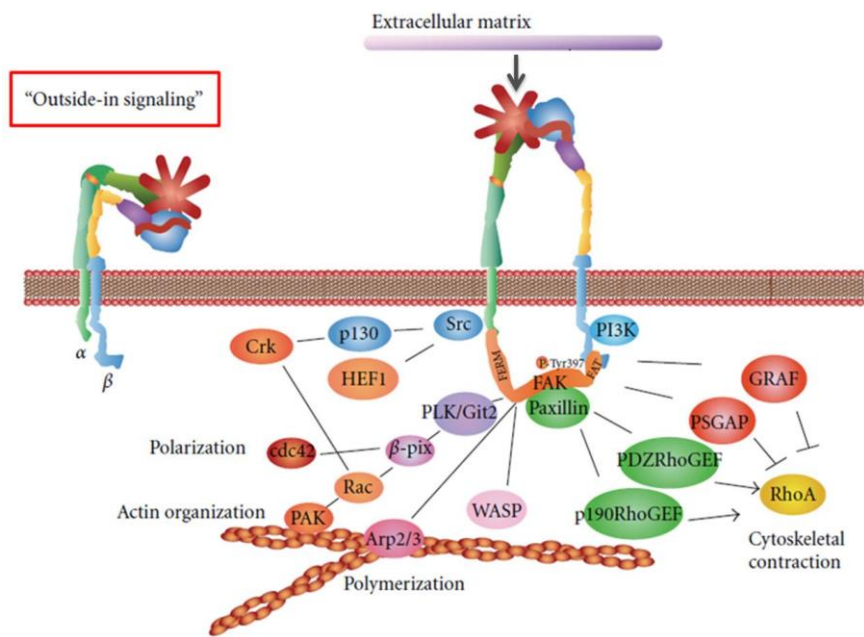
which functions to localise other intracellular adaptor proteins to FAs. The activated FAK then phosphorylates paxillin at tyrosines 31 and 118 which creates binding sites for other adaptor proteins, including Src. Phosphorylated paxillin regulates actin contraction by activating Rho GTPase protein. Phosphorylated Src interacts with scaffold proteins, such as p130 CRK-associated substrate (p130Cas), to enhance the FAK-Src complex. Furthermore, phosphorylated FAK transduces extracellular signalling and regulates actin polymerisation and organisation (see **Figure 1.15 A**) (Menter and DuBois 2012).

#### **1.2.3.2.2.2. Inside-out signalling**

In this type of signalling, integrins are activated by binding the intracellular adaptor proteins to the cytoplasmic tail, which drives both the affinity and avidity regulation processes. These conformational changes guide the integrin headpiece to open, which then interacts with extracellular environmental ligands. Large numbers of intracellular signalling proteins participate indirectly in inside-out signalling while others directly bind to the cytoplasmic tails of integrins, including  $\alpha$ -actinin, talin, filamin, paxillin, kindlin and tensin. However, talin and kindlin are thought to be the most important adaptor proteins in  $\alpha$ - $\beta$  subunit separation and the subsequent integrin activation (Moser, Nieswandt et al. 2008), (Hu and Luo 2013), (Campbell and Humphries 2011), (Pan, Zhao et al. 2016). Typically, talin binds to the membrane-proximal NpxY motif of  $\beta$  subunits, whereas kindlin binds to the distal membrane motif NxxY (Srichai and Zent 2010). The N-terminus of talin possesses a FERM domain, which contains three subdomains (F1, F2, F3) that are essential in integrin cytoplasmic tail binding, while its C-terminus has additional binding sites for the adaptor protein vinculin and additional cytoplasmic tail binding proteins. F3, which resembles a phosphotyrosine binding (PTB) domain, is the subdomain through which talin binds to the proximal NpxY motif of integrin  $\beta$  subunit (Campbell and Humphries 2011), (Menter and DuBois 2012). Other adaptor proteins can also bind to the NpxY motif, such as tensin and docking protein 1 (Dok1). However, only talin promotes the disassociation between  $\alpha$ - $\beta$  subunits (Srichai and Zent 2010). Talin is present in the cytoplasm in an inactive state. Its activation involves PIP<sub>2</sub>, a phospholipid component of the cell membrane, which disrupts the interaction between the head domain and tail rod domains of talin. It thus exposes the FERM domain and its subdomains to allow talin to recognise and bind to the proximal NpxY sequence of integrin  $\beta$  subunits (Goksoy, Ma et al. 2008), (Nevo 2011). G protein-coupled receptors (GPCRs), such as protease-activated receptors-1 (PAR-1), are involved also in the

agonist-induced activation of integrins (**Figure 1.15 B**). Mechanistically, integrin activation begins following stimulation of GPCRs, which results in increased cytosolic levels of  $\text{Ca}^{2+}$ . This is followed by recruitment of guanine nucleotide-exchange factors (GEF) combined with Ras-proximate-1/Ras-related-protein-1- (Rap1-) GTPase to the GPCRs. Subsequently, Rap1 activates the Rap1-GTP-interacting adaptor molecule (RIAM), which recruits talin to the cytoplasmic tail of integrins (Menter and DuBois 2012) (Plow, Meller et al. 2014) (see **Figure 1.15 B**). There is evidence that vinculin has a binding site for RIAM, and the vinculin-RIAM complex binds to talin to promote integrin activation (Goult, Zacharchenko et al. 2013). Similar to talin, kindlin has a FERM domain, and its expression is essential for stabilising the activation state of the integrin cytoplasmic tail. The expression of kindlin or talin alone is insufficient to drive the separation of  $\alpha$ - $\beta$  subunits and subsequent integrin activation (Srichai and Zent 2010), indicating that both adaptor proteins are required for the activation of integrins.

A)



B)

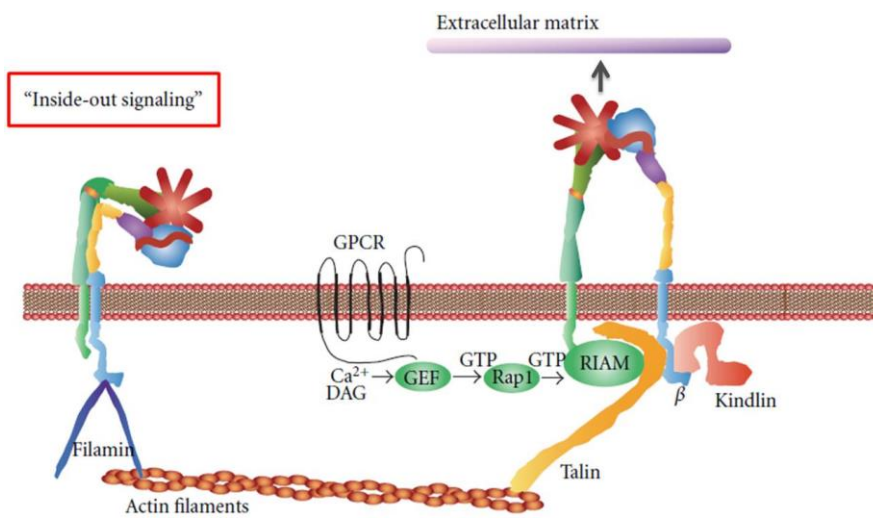


**Figure 1.15 The bi-directional signalling of integrins.** The schematic illustration shows **A)** outside-in signalling and **B)** inside-out signalling (See text). Note that both types of signalling require the clustering of integrins and other transmembrane receptors (not shown) (Menter and DuBois 2012).

### 1.2.3.2.2.3. Cross talk between integrin and growth factor receptors to control downstream signalling pathways during outside-in signalling

Integrin signalling involves more than transmitting signals bi-directionally to adhere cells to extracellular ligands and connect the extracellular environment to the actin cytoskeleton. Integrins also cluster with growth factor receptors, including VEGFRs, fibroblast growth factor receptor 1 (FGFR1) and transforming growth factor receptor- $\beta$  (TGFR- $\beta$ ), to activate complicated downstream signalling pathways that elicit complex cellular responses, such as proliferation, survival and migration (Soldi, Mitola et al. 1999), (Eliceiri 2001), (Reynolds, Wyder et al. 2002), (Masson-Gadais, Houle et al. 2003), (Mahabeleshwar, Feng et al. 2006), (Mahabeleshwar, Feng et al. 2007) (Strieth, Eichhorn et al. 2006), (Robinson, Reynolds et al. 2009), (Valdembri, Caswell et al. 2009), (Somanath, Ciocea et al. 2009), (Srichai and Zent 2010), (Ellison, Atkinson et al. 2015), (Jia, Choi et al. 2018) (**Figure 1.16**). One of the best-known examples of cross talk between growth factor receptors and integrins is shown by VEGFR2 and  $\alpha\beta3$  integrins (Mahabeleshwar, Feng et al. 2007), (Ravelli, Mitola et al. 2013) (Plow, Meller et al. 2014). An early study in this field showed that an antibody directed against ITGB3 reduced VEGFR2 phosphorylation induced by VEGF<sub>165</sub> in human ECs. This direct interaction between ITGB3-VEGFR2 was confirmed by the results of a biochemical immunoprecipitation experiment (Soldi, Mitola et al. 1999). Moreover, the anti-ITGB3 antibody and the anti-VEGFR2 antibody had the same effect of reducing PI-3 kinase phosphorylation, an early downstream kinase protein of VEGF-VEGFR2 pathway (see **Figure 1.16**) (Dellinger and Brekken 2011), when cells were VEGF<sub>165</sub>-stimulated (Soldi, Mitola et al. 1999). Furthermore, the anti-ITGB3 antibody significantly reduced EC migration and proliferation induced by VEGF<sub>165</sub>, indicating that the VEGF<sub>165</sub>-ITGB3-VEGFR2 complex regulates the downstream signalling required for the biological activities in ECs (Soldi, Mitola et al. 1999). A subsequent study demonstrated that the VEGF<sub>165</sub>-induced stimulation of HUVECs enhanced the interaction between VEGFR2 and ITGB3 of  $\alpha\beta3$ , but not  $\alpha\beta5$ ,  $\alpha\text{IIb}\beta3$ , or  $\alpha\beta1$ , integrins and that this cross talk is required for the full phosphorylation of VEGFR2, in order to transduce the intracellular signalling pathways essential for the adhesion and migration of HUVECs. At the molecular level, this study found that the addition of VEGF<sub>165</sub> to HUVECs also increased the phosphorylation of two downstream signal proteins: stress-activated protein kinase-2/p38 (SAPK2/p38) and FAK. Anti-VEGFR2 or anti-ITGB3 inhibited the phosphorylation of both proteins, indicating that the VEGF-induced phosphorylation of SAPK2/p38 and FAK requires a synergistic complex

interaction between VEGFR2 and  $\alpha\text{v}\beta\text{3}$  (Masson-Gadais, Houle et al. 2003). The biological functions and interactions between ITGB3 and VEGFR2 will be discussed in detail in the next section. Other studies demonstrated the complex association between  $\alpha\text{v}\beta\text{3}$  and another TKR, PDGFR- $\beta$  and this complex formation is dependent on growth factor stimulation of the receptors (Schneller, Vuori et al. 1997), (Woodard, García-Cardena et al. 1998). In line with these previous studies, another study showed that ITGB3, but not ITGB1 or ITGB5, formed a complex with VEGFR2 only in the presence of ITGAV, while PDGFR- $\beta$  did not require ITGAV to be co-immunoprecipitated with ITGB3 (Borges, Jan et al. 2000). In contrast to previous studies, this study also demonstrated that associations between ITGB3 and VEGFR2 or PDGFR- $\beta$  are independent of growth factor stimulation and the phosphorylation of these TKRs (Borges, Jan et al. 2000). The binding of fibroblast growth factors-1 (FGF-1) to their receptors results in GRB2-SOS complex formation, which activates the Ras/ERK/MERK pathway (LaVallee, Prudovsky et al. 1998), (Kwabi-Addo, Ozen et al. 2004) (see **Figure 1.16**). Another study demonstrated the direct interaction between  $\alpha\text{v}\beta\text{3}$  integrins and FGFR1. The study showed that compared to control cells,  $\alpha\text{v}\beta\text{3}$ -binding to defective FGF mutant cells reduced cell proliferation and migration, suggesting that the  $\alpha\text{v}\beta\text{3}$ -FGF1 complex is critical in the late FGF signalling pathway (Mori, Wu et al. 2008), (Yamaji, Saegusa et al. 2010).

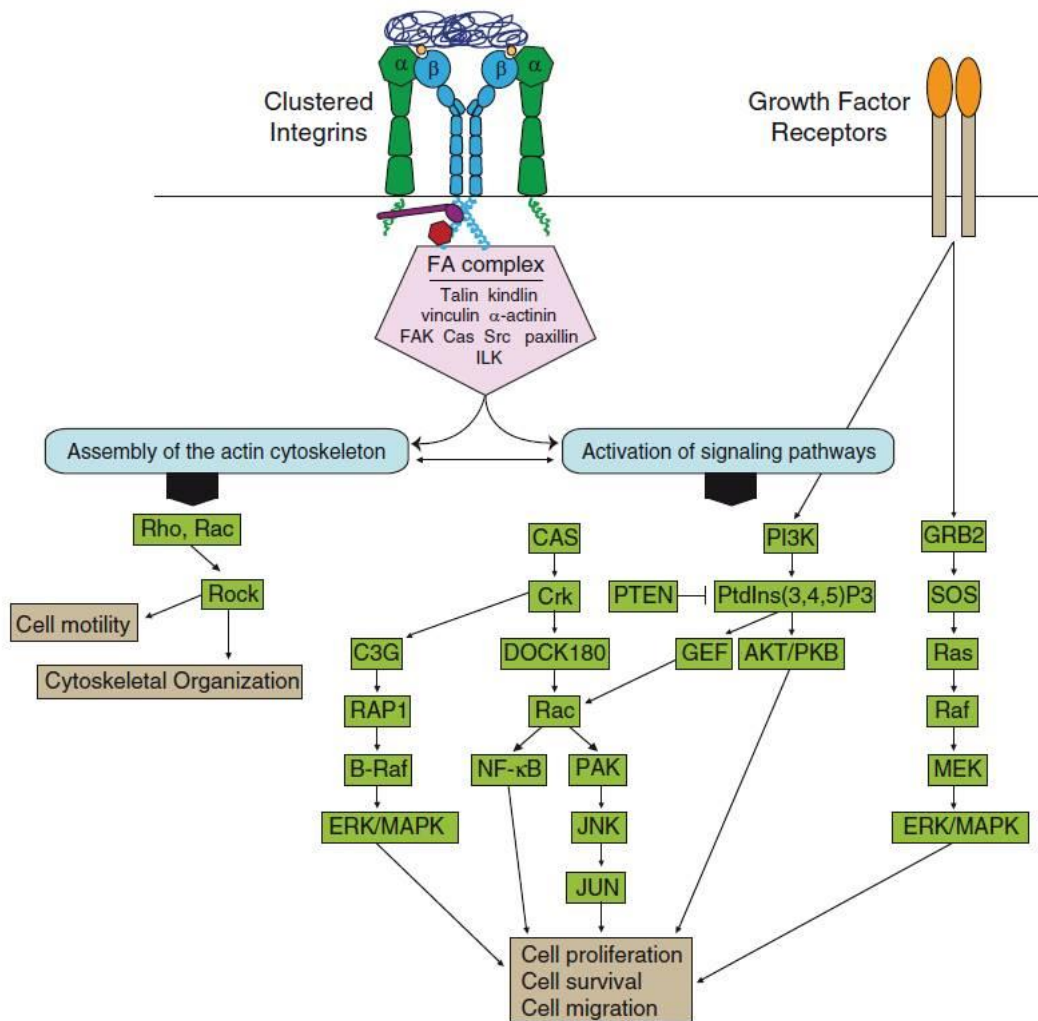


**Figure 1.16 Downstream signalling of clustered integrin.** The schematic illustration shows the contribution of the clustered integrins to transmitting extracellular signals by first recruiting FA complex formation, which promotes actin cytoskeleton assembly and activates the downstream signalling pathways essential for cell proliferation, survival and migration through cross-talking with growth factor receptors (Srichai and Zent 2010).

### 1.2.3.2.3. Integrins in angiogenesis

Clustered integrins (see **Figure 1.16**) can cross talk with VEGFRs and their NRP co-receptors to transmit VEGF signals and regulate the biological functions of ECs during angiogenesis. There is also strong evidence that integrins, through interactions to their ECM ligands, are essential angiogenic players in the development of blood vessels during embryonic and adult tissue neo-vascularisation and pathological angiogenesis (Serini, Valdembri et al. 2006). Integrin expression modulates angiogenic processes in many cell types, including, ECs, perivascular cells (pericytes and vSMCs), fibroblasts and bone marrow-derived dendritic cells (BMDCs) (Desgrosellier and Cheresh 2010). Several previous studies were in agreement that ECs express  $\alpha 1\beta 1$ ,  $\alpha 2\beta 1$ ,  $\alpha 5\beta 1$ ,  $\alpha \nu\beta 3$ ,  $\alpha \nu\beta 5$ ,  $\alpha 6\beta 1$  and  $\alpha 6\beta 4$ , and others found that ECs also express  $\alpha 3\beta 1$ ,  $\alpha 4\beta 1$ ,  $\alpha \nu\beta 1$ ,  $\alpha \nu\beta 8$ ,  $\alpha 8\beta 1$  and  $\alpha 9\beta 1$ . (Rüegg and Mariotti 2003), (Hodivala-Dilke, Reynolds et al. 2003), (Serini, Valdembri et al. 2006), (Zovein, Luque et al. 2010), (Carmeliet and Jain 2011). All these integrins have been implicated in angiogenesis. The embryonic vascular phenotypes generated from gene deletion in each subunit are summarised in **Table 1.1** (Rüegg and Mariotti 2003), (Alghisi and Rüegg 2006), (Desgrosellier and Cheresh 2010). The major integrins in ECs are  $\alpha \nu\beta 3$ ,  $\alpha 5\beta 1$ ,  $\alpha \nu\beta 5$  and  $\alpha 6\beta 4$  (Somanath, Ciocea et al. 2009). For the purpose of this thesis, we will focus on the function of the two major endothelial FN receptors  $\alpha \nu\beta 3$  and  $\alpha 5\beta 1$  (van der Flier, Badu-Nkansah et al. 2010) and their cooperative interaction with VEGFR2 and NRPs.

**Table 1.1: Vascular Integrins in Angiogenesis**

Integrin	Major ECM ligands	Gene deletion	Vascular phenotype in mice with constitutive gene deletion
$\alpha 1\beta 1$	CO, LM	$\alpha 1$	No defects in vascular development + reduced tumour angiogenesis
$\alpha 2\beta 1$	CO, LM	$\alpha 2$	Defects in vascular development
$\alpha 3\beta 1$	LM, TSP	$\alpha 3$	Perinatal lethality because of defects in kidney, lung, skin but no vascular defects
$\alpha 4\beta 1$	FN	$\alpha 4$	Lethal at E11–14 because of placental fusion defect and coronary arteries defect
$\alpha 5\beta 1$	FN, fibrin	$\alpha 5$	Lethal at E10 vasculogenesis but no maturation/angiogenesis
$\alpha 6\beta 1$	LM, CCN1	$\alpha 6$	Lethal at birth but no defects in vascular development
$\alpha 8\beta 1$	FN, TN-C	$\alpha 8$	Partial embryonic lethality but no defects in vascular development
$\alpha 9\beta 1$	TN-C	$\alpha 9$	Lethal at birth because of defects in large lymphatic vessels
$\alpha v\beta 1$	FN, VN	$\beta 1$	Lethal at E5.5 because of the failure to organise the embryonic inner mass
$\alpha v\beta 3$	FN, VN, LM, FB, Fibrin, TSP, TN-C, vWF, dCO, OPN, MMP-2, Del-1, BSP, FGF-2, thrombin, CCN1	$\beta 3$	No defects in vascular development + enhanced postnatal angiogenesis
$\alpha v\beta 5$	VN, Del-1, CCN1	$\beta 5$	No defects in vascular development Enhanced postnatal angiogenesis
$\alpha 6\beta 4$	LM	$\beta 4$	Lethal at birth but no vascular defects in development
$\alpha v\beta 8$	VN	$\beta 8$	Lethal at E12—perinatal vascular defects in the placenta and brain
		$\alpha v$	Lethal at E12—perinatal because of vascular defects in the placenta, brain, and intestine

*Note.* ECs express at least 13 different integrins. Vascular phenotypes are reviewed in (Alghisi and Rüegg 2006).

*Abbreviations:* CCN1, cysteine rich protein 61; CO, collagen; Del-1, developmental locus-1; LM, laminin; VN, vitronectin; TNC, tenascin-C; TSP, thrombospondin; EL, elastin; FN, fibronectin; OPN, osteopontin; FB, fibrinogen; vWF, von Willebrand factor; MMP, matrix metalloproteinase; dCO, denatured collagen; BSP, bone sialo protein.

### 1.2.3.2.3.1. $\alpha v\beta 3$ integrin

$\alpha v\beta 3$  is a unique integrin that recognises a wide variety of ECM proteins, including vitronectin, FN, laminin, fibrinogen, fibrin, thrombospondin, tenascin-C, von Willebrand factor, denatured collagen, osteopontin, matrix metalloproteinase, developmental locus-1, bone sialo protein, thrombin, and cysteine rich protein 61. However, vitronectin is considered the canonical ECM ligand for  $\alpha v\beta 3$  (Avraamides, Garmy-Susini et al. 2008), (Mahabeleshwar, Chen et al. 2008). In ECs, the ITGAV subunit can pair with the  $\beta 1$ ,  $\beta 3$ ,  $\beta 5$  and  $\beta 8$  subunits, whereas the ITGB3 subunit can only pair with the  $\alpha v$  subunit, which means that the investigation of endothelial  $\alpha v\beta 3$  functions in ECs can be best achieved by manipulating the ITGB3 subunit (Hynes 2002) (see **Figure 1.12 A**).

In ITGAV subunit-deficient mice, the formation of dorsal aortae, primary plexus (vasculogenesis) and capillary sprouting (angiogenesis) develop normally without any defects until E9.5; ~80% of the embryos die in uterus between E10.5 and E11.5 because of pericardial oedema, whereas the surviving embryos die immediately after birth because of intracerebral haemorrhage (Bader, Rayburn et al. 1998), (McCarty, Monahan-Earley et al. 2002). The genetic deletion of *Itgb3* did not inhibit angiogenesis and vascular development; instead, these knockout mice showed excessive angiogenesis, ostensibly attributed to increased EC expression of VEGFR2, which may occur developmentally to compensate for the loss of ITGB3 (Reynolds, Wyder et al. 2002), (Reynolds, Reynolds et al. 2004) (Mahabeleshwar, Feng et al. 2006), (Mahabeleshwar, Chen et al. 2008).

In adult mice,  $\alpha v\beta 3$  expression is upregulated in sprouting capillaries during physiological conditions (e.g. wound healing and inflammation) and pathological conditions (e.g. tumours), whereas the expression of the integrin is barely detected in quiescent capillaries (Hodivala-Dilke, Reynolds et al. 2003), (Somanath, Malinin et al. 2009), which indicates that  $\alpha v\beta 3$  functions as a pro-angiogenic molecule (Somanath, Malinin et al. 2009). Therefore,  $\alpha v\beta 3$  antagonists have been designed to inhibit angiogenesis (Miller, Keenan et al. 2000), (Posey, Khazaeli et al. 2001), (Wilder 2002), (Burke, DeNardo et al. 2002), (Marugán, Manthey et al. 2005), (D'andrea, Del Gatto et al. 2006). For example, vitaxin, also known as LM609, was the first monoclonal antibody against  $\alpha v\beta 3$ . Vitaxin functions by blocking ECM ligands from interacting with the RGD binding site on the integrin, thus blocking cell adhesion, migration and sprouting. Brooks *et al.* showed that Vitaxin induces apoptosis without affecting pre-existing quiescent blood vessels *in vitro*, in *in vivo* chicken chorioallantoic membrane models

(CAM) assays (Brooks, Clark et al. 1994), (Brooks, Montgomery et al. 1994), and in a chimeric human/mouse model (Brooks, Strömblad et al. 1995). Vitaxin has entered phase II clinical trials for use in the treatment of several cancers and a recent study demonstrated that Vitaxin specifically binds to the  $\alpha\beta3$  headpiece region during all integrin conformational states, including the bent state. Interestingly, Vitaxin binding does not overlap with the RGD ligand-binding pocket, which makes it highly selective for  $\alpha\beta3$  (Borst, James et al. 2017). Cilengitide, also known as EMD121974, is a small cyclic peptide that shows highly selective inhibition of  $\alpha\beta3$  and  $\alpha\beta5$  binding to vitronectin (Dechantsreiter, Planker et al. 1999). It inhibits angiogenesis in *in vivo* animal models (MacDonald, Taga et al. 2001) as well as in *in vitro* bovine aortic endothelial (BAE) angiogenesis assays (Nisato, Tille et al. 2003). In phase I and II clinical trials, Cilengitide showed potential antitumor activity and improved survival in patients with glioblastoma. However, in a recent phase III clinical trial, it failed to improve overall patient survival when combined with the standard of care (temozolomide chemoradiotherapy). Hence, Cilengitide has not been developed further as an anticancer drug (Stupp, Hegi et al. 2014). Unexpectedly, Reynolds *et al.* found evidence *in vitro* and *ex vivo* experiments that low (nanomolar) concentrations of RGD-mimetic  $\alpha\beta3$  inhibitors, including Cilengitide, act as a pro-angiogenic molecule that can promote tumour growth and tumour angiogenesis. The results showed that Cilengitide enhanced VEGF-induced phosphorylation, internalisation, and the accumulation of VEGFR2 in vesicles at the EC periphery as well as the delivery of  $\alpha\beta3$  to FAs at the EC periphery, thereby promoting EC migration (Reynolds, Hart et al. 2009).

#### **1.2.3.2.3.1.1. $\alpha\beta3$ -VEGFR2 complex and NRP1 functions in ECs**

In addition to the studies discussed in the previous sections, which showed the ability of  $\alpha\beta3$  to immunoprecipitate and cross talk with VEGFR2 to promote downstream signalling pathways essential for cellular biological behaviour (Soldi, Mitola et al. 1999), (Mahabeleshwar, Feng et al. 2007), (Dellinger and Brekken 2011), many other studies by numerous groups have shown that  $\alpha\beta3$  can act as a pro-angiogenic molecule through cross talk with VEGFR2. For example, a biochemical interaction was found between ITGB3 and VEGFR2, but not between VEGFR1 or VEGFR3. The cross talk between the two molecules occurs not only in HUVECs but also in proliferating blood vessels (Mahabeleshwar, Chen et al. 2008). Importantly, the complex formation between ITGB3 and VEGFR2 in response to the VEGF stimulation does not require the presence of vitronectin, in contrast to previous

demonstrations (Soldi, Mitola et al. 1999). A study showed that this complex formation can take place in the absence of ECM ligands. Interestingly, this study also showed a ~3 fold decrease in VEGFR2 phosphorylation when the ITGB3 subunit, but not the ITGB1 and ITGA5 subunits, was silenced by siRNA-mediated knockdown in HUVECs, which led to the conclusion that ITGB3 is the major integrin in VEGF-induced angiogenic responses (Mahabeleshwar, Chen et al. 2008). Furthermore, knock-in (DiYF) mice, a mutant ITGB3 that is unable to undergo tyrosine phosphorylation of cytoplasmic domain, disrupted VEGFR2-ITGB3 complex formation and reduced VEGFR2 phosphorylation in response to VEGF stimulation. As a result, cell adhesion, migration, spreading, capillary tube formation of ECs isolated from DiYF mice and vascularization/tumour growth in DiYF mice were impaired (Mahabeleshwar, Feng et al. 2006). In contrast to the phenotypes that emerged in ITGB3 knockout mice (Reynolds, Wyder et al. 2002), (Reynolds, Reynolds et al. 2004), DiYF mice showed normal vascular density, maturation and overall development without haemorrhagic conditions in any organs, indicating that ITGB3 tyrosine phosphorylation is crucial for angiogenesis but not normal vascularization (Mahabeleshwar, Feng et al. 2006). In the following year, the same group supported their ITGB3 knock-in mice findings by showing that the ITGB3 cytoplasmic tyrosine phosphorylation of HUVECs induced by VEGF is directly mediated by downstream tyrosine protein c-Src and that the activation of c-Src is required for the complex formation between ITGB3 and VEGFR2, which then recruits other downstream signalling molecules to promote adhesion, migration, and the initiation of angiogenic programming in ECs (Mahabeleshwar, Feng et al. 2007). Five years later, the same group provided additional evidence of the direct interaction between the ITGB3 cytoplasmic tail and VEGFR2 by identifying the membrane-proximal motif within VEGFR2 (<sup>801</sup>YLSI<sup>804</sup> residues) mediates the binding interaction with the phosphorylated tyrosine<sup>747</sup> located within NpxY motif of ITGB3 cytoplasmic tail. The disruption of tyrosine<sup>747</sup> within the ITGB3 cytoplasmic tail affected the cross talk between ITGB3 and VEGFR2, which suppressed VEGF-induced signalling, endothelial tube formation, and angiogenesis in an aortic ring assay (West, Meller et al. 2012). Another study identified the cytoplasmic regulatory adaptor protein, Sprouty4 (Spry4), which disrupted this required for ITGB3-VEGFR2 interaction (Mahabeleshwar, Feng et al. 2007), thus inhibiting EC adhesion, migration, as well as retinal angiogenesis (Gong, Yang et al. 2013). In addition to evidence that VEGF induces ITGB3-VEGFR2 complex formation, the non-canonical VEGFR2 ligand gremlin was shown to phosphorylate VEGFR2, which resulted in conformational changes in the extracellular and transmembrane regions of VEGFR2 to form a complex with ITGB3

(Ravelli, Mitola et al. 2013). Overall, these studies provided evidence of the essential role of ITGB3 in the activation of VEGFR2 in angiogenesis.

ITGB3-VEGFR2 interactions have also been implicated in functioning as anti-angiogenic signals. This hypothesis emerged in an early study by Reynolds *et al.* (Reynolds, Wyder et al. 2002), who showed that in ECs derived from ITGB3-NULL mice, both VEGF and VEGFR2 were significantly elevated compared to those from WT littermates, indicating that the absence of *Itgb3* gene enhanced tumour growth and angiogenesis (Reynolds, Wyder et al. 2002). Two years later, based on the results of *in vitro* studies, the authors showed that ECs isolated from ITGB3-NULL mice exhibited increases in cell migration and proliferation as well as higher levels of VEGFR2 and ERK1/2 phosphorylation in response to VEGF stimulation compared with WT ECs. Similar results were observed in *ex vivo* aortic ring assays, which showed high number of microvessels sprouts in the rings isolated from ITGB3-NULL mice compared to WT conditions. They concluded that VEGFR2-ERK1/2 signalling in response to VEGF stimuli mediates the elevated tumour growth and angiogenesis seen in ITGB3-NULL mice (Reynolds, Reynolds et al. 2004). In a separate study, the same group revealed that the upregulation of VEGFR2 and VEGF in ITGB3-NULL mice leads to increased VEGF-induced EC permeability. Interestingly, when VEGFR2 was blocked by VEGFR2-antibody in ITGB3-NULL mice, VEGF<sub>164</sub>-induced leakage was abolished. This indicates that the loss of ITGB3 enhances EC permeability through the upregulation of VEGF-VEGFR2-ERK1/2 signalling (Robinson, Reynolds et al. 2004). To determine whether more molecular players are responsible for enhancing angiogenesis in ITGB3-NULL mice, the same group implicated Ras-related C3 botulinum toxin substrate 1 (Rac1), a member of the family of Rho GTPases downstream signalling, in this mechanism. These authors found that Rac1 deletion had no effect on VEGF-mediated angiogenesis *in vivo*, *ex vivo*, or on tumour growth. However, Rac1 enhanced VEGF-mediated angiogenesis and tumour growth in the absence of ITGB3 expression, indicating that the augmentation of angiogenesis signalling and permeability in ITGB3-NULL mice is Rac1-dependent (D'Amico, Robinson et al. 2010). Recently, we found that ITGB3 expression in ECs acted as anti-angiogenic molecule by preventing the extension of microtubules to the peripheral FAs through telophase disk protein (Rcc2)-Annexin A2 (Anxa2) molecules in a Rac1-dependent manner (see the attached published paper for details) (Atkinson, Gontarczyk et al. 2018).

Other studies showed interactions and cross talk between the ITGB3 subunit and NRP1 in ECs (Robinson, Reynolds et al. 2009), (Ellison, Atkinson et al. 2015). Robinson *et al.*

demonstrated a physical interaction between ITGB3 and NRP1 by biochemical immunoprecipitation. Fluorescent confocal microscopy also confirmed the close association between the two molecules in whole cells. However, this association was disrupted when the cytoplasmic tail of ITGB3 was mutated (Robinson, Reynolds et al. 2009). Similar to the upregulation of VEGFR2 seen in ITGB3-NULL mice (Reynolds, Wyder et al. 2002), NRP1 and ERK1/2, which are known downstream targets of VEGF stimulation (Rousseau, Houle et al. 1997), (Takahashi, Ueno et al. 1999), were elevated in ITGB3-NULL ECs compared with WT ECs. Similarly, NRP1-VEGFR2 co-immunoprecipitation was more augmented in ITGB3-NULL ECs than in WT ECs even in the absence of VEGF treatment. Moreover, the same study provided evidence that the VEGF-induced angiogenesis seen in ITGB3-NULL mice is not restricted to the constitutive deletion of the *Itgb3* gene but also occurs in the WT system. Indeed, the knockdown of ITGB3 specifically in WT endothelial cells in an *in vitro* wound closure assay significantly enhanced EC migration, while the deletion of both ITGB3 and NRP1 suppressed the EC migration. Interestingly, when targeting NRP1 in ITGB3-NULL mice, VEGF-induced angiogenesis was significantly inhibited but not in WT mice, indicating that the elevation of angiogenesis that occurs when ITGB3 is absent is dependent on NRP1 (Robinson, Reynolds et al. 2009). This finding was confirmed in two angiogenesis models. *In vivo* sponge implant angiogenesis assays showed that the inhibition of NRP1, using a peptide designed to inhibit NRP1-VEGF binding, reduced VEGF-induced vessel infiltration in subcutaneously implanted sponges in the flanks of ITGB3-NULL mice to a greater extent than in WT mice. This finding was supported by the results of an *ex vivo* aortic ring assay, which showed that the siRNA-mediated knockdown of NRP1 in response to VEGF stimulation did not affect the number of aortic rings sprouting from WT mice, but it significantly suppressed the otherwise enhanced ring sprouting from ITGB3-NULL mice, which indicates that VEGF-driven sprouting is dependent on NRP1 only when ITGB3 is absent. Overall, this study showed that when ITGB3 is expressed normally, it limits the interaction between NRP1 and VEGFR2 and thus NRP1 minimally contributes to VEGF-induced angiogenesis in *in vivo* and *ex-vivo* assays. In contrast, when ITGB3 is absent or depleted, VEGF-induced VEGFR2 phosphorylation, angiogenesis and tumour growth become NRP1-dependent. These findings suggest that by targeting both ITGB3 and NRP1, the efficiency of anti-angiogenic therapy may be significantly increased (Robinson, Reynolds et al. 2009). Because the complete loss of the *Itgb3* gene results in the elevation of angiogenesis (Reynolds, Wyder et al. 2002), (Robinson, Reynolds et al. 2009), the Robinson group moved away from the use of ITGB3-NULL mice. They generated ITGB3-heterozygous

(HET) mice to (hopefully) overcome the developmental upregulation of VEGFR2 in ITGB3-NULL mice, while simultaneously maintaining critical interactions between ITGB3 and VEGFR2 (Ellison, Atkinson et al. 2015). They found that the EC-specific deletion of NRP1 in WT mice had no effect on subcutaneous allograft tumour growth, or on aortic ring sprouting, but both tumour growth and VEGF-induced sprouting were significantly inhibited when endothelial NRP1 was deleted in ITGB3-HET conditions. Similar results were observed when the cytoplasmic tail of NRP1 was missing, suggesting that this region of the molecule plays a role in angiogenesis only when the expression of ITGB3 is reduced (Ellison, Atkinson et al. 2015). As hoped, ITGB3-HET ECs displayed only small increases in expression of VEGFR2. Unlike ITGB3-NULL ECs, VEGF-induced association between NRP1 and VEGFR2 were not enhanced in HET cells. Nonetheless, ITGB3-HET ECs migrated faster than WT ECs, and, in contrast to WT ECs, their migration was dependent on NRP1. Interestingly, in WT ECs, NRP1 immunolocalised with ITGB3 at the end of F-actin fibres, in both VEGF-stimulated and unstimulated conditions. However, in ITGB3-HET ECs, VEGF-stimulation lead to a redistribution of NRP1 away from these sites, suggesting that ITGB3 regulates the retention of the NRP1 within mature FAs following an angiogenic stimulus. This observation was corroborated by the co-localisation of NRP1 and paxillin, a marker of FAs. In WT ECs, NRP1 and paxillin were co-localised in the presence and absence of VEGF; however, in HET ECs, NRP1 was co-localised with paxillin only in the absence of VEGF (Ellison, Atkinson et al. 2015). The authors went on to show that FA disassembly is NRP1 dependent only when ITGB3 expression is suppressed. Overall, the results of this study suggested that reduced levels of ITGB3 promoted VEGF-induced pathological angiogenesis and EC migration through the activation of NRP1 function within FAs (Ellison, Atkinson et al. 2015).

Overall, the results of these previous studies showed that ITGB3 levels play a critical role in VEGF-induced pathological angiogenesis through cross talk with NRP1, raising the possibility of co-targeting the two molecules to increase the effectiveness of ITGB3-directed anti-angiogenic therapy (Robinson, Reynolds et al. 2009), (Ellison, Atkinson et al. 2015). Recently, Jia and Chio *et al.* generated 40 nm silica nanoparticles (NPs) coated with heptapeptide ATWLPPR (ATW peptide) antagonists mixed with cilengitide (RGD peptide) antagonists (ATW/RGD-NPs) and showed their ability to inhibit VEGF-induced VEGFR2 phosphorylation and signalling in human ECs at 0.1nM concentration by co-targeting NRP1 and  $\alpha v\beta 3$ -integrin (Jia, Choi et al. 2018).

It is worth noting that, to date, no studies have addressed the possibility that NRP2 could also cross talk with  $\alpha v\beta 3$ -integrin.

### 1.2.3.2.3.2. $\alpha 5\beta 1$ integrin

In 1985, Pytela *et al.* isolated the ITGA5 subunit in osteosarcoma cells using affinity chromatography. It was identified as a membrane-embedded cell surface glycoprotein of about 140 kDa, which was directly involved in the initial step of cell adhesion to the RGD regions of FN (Pytela, Pierschbacher *et al.* 1985). The endothelial ITGB1 subunit can pair with  $\alpha$  (1 to 9) subunits except the  $\alpha 7$  subunit, which is restricted to skeletal muscle (Velling, Collo *et al.* 1996). However, the ITGA5 subunit can only pair with the  $\beta 1$  subunit (Avraamides, Garmy-Susini *et al.* 2008), indicating that  $\alpha 5\beta 1$  function can be specifically examined by manipulating the ITGA5 subunit.

The  $\alpha 5\beta 1$  integrin plays a crucial role during embryonic development. Unlike the deletion of the gene encoding for ITGAV or ITGB3 subunit, the constitutive deletion of the *Itgb1* gene leads to the loss of 12 members of the integrin family (see **Figure 1.12**). Consequently, ITGB1 knockout mice die *in utero* shortly after embryo implantation because the inner cell mass fails to develop (Fässler and Meyer 1995), (Stephens, Sutherland *et al.* 1995). However, the selective deletion of the ITGB1 subunit in mouse ECs resulted in embryonic lethality between E9.5 and E10.5 because of the reduced amounts of vessel sprouting and branching compared with controls. It was concluded that the vascular ITGB1 subunit is essential for embryonic angiogenesis, and it is indispensable in vasculogenesis (Tanjore, Zeisberg *et al.* 2008). In contrast, ITGA5 knockout mice die *in utero* between E10 and E11 of gestation because of the absence of posterior somites and a general defect in the paraxial mesoderm. These mutant mice also exhibit defects in blood vessel formation, which results in the leakage of a large number of blood cells into the exocoelomic cavity as well as the space between the extra-embryonic mesoderm and endoderm, indicating that ITGA5 expression is required during the embryonic development of early blood vessels (Yang, Rayburn *et al.* 1993). Therefore, it was speculated that amongst integrin knockout mice, ITGA5-deficient animals exhibit the most severe vascular defects (Yang, Rayburn *et al.* 1993), (Bouvard, Brakebusch *et al.* 2001). Similar phenotypes were also observed in FN mutant mice, but they were much more severe than those seen in ITGA5 mutant mice (George, Georges-Labouesse *et al.* 1993). Consistent with these findings, a previous study addressed the role of both ITGA5 and its major ligand, FN, in embryonic development. The results showed that the

ITGA5-NULL embryos exhibit significant decreases in the complexity of blood vessels accompanied by decreased FN assembly and organisation in the basement membrane of ITGA5-NULL ECs compared with WT, ITGB3-NULL and ITGAV-NULL ECs. These findings support a critical role for ITGA5-FN interactions during vascular embryonic development, which are not dependent on the  $\alpha v\beta 3$  integrin (Francis, Goh et al. 2002). Surprisingly, Flier *et al.* reported that endothelial-specific knockout embryos of either ITGA5 or ITGAV alone were viable and had no obvious vascular phenotypic defects. However, FN assembly was defective in ITGA5 (but not ITGAV) knockout endothelial cells *in vitro*, and the fibrillar FN was significantly reduced in ITGA5/ITGAV in double-knockout ECs. Additionally, double-knockout EC-specific embryos developed normally until E11.5, but then extensive defects emerged in the heart and great blood vessels, which resulted in embryonic death at ~E14.5, suggesting genetic interactions between ITGA5 and ITGAV during embryonic vascular developmental and/or compensation between these two integrin subunits (van der Flier, Badu-Nkansah et al. 2010).

Similar to  $\alpha v\beta 3$ ,  $\alpha 5\beta 1$  is poorly expressed on quiescent vascular ECs, but its expression is upregulated during tumour angiogenesis in humans and animals (Kim, Bell et al. 2000), (Avraamides, Garmy-Susini et al. 2008). Kim *et al.* were the first to implicate  $\alpha 5\beta 1$  expression in angiogenesis. They found that the expression of both  $\alpha 5\beta 1$  and its FN ligands were co-ordinately elevated within the same blood vessels in human and mice tumours. Using the chick CAM assay, they also found that the upregulation of  $\alpha 5\beta 1$  and FN were co-localised in pre-existing blood vessels upon stimulation with bFGF, TNF- $\alpha$  and IL-8 angiogenic growth factors, but no change in  $\alpha 5\beta 1$  expression upon VEGF stimulation was detected (Kim, Bell et al. 2000). Interestingly, three different antagonists (antibody, cyclic peptide and non-peptide) of  $\alpha 5\beta 1$  significantly inhibited HUVEC adhesion and migration on FN, but not on collagen. Additionally, the injection of any of these antagonists intravenously into the embryonic chick circulation significantly inhibited bFGF, TNF- $\alpha$  and IL-8, but not VEGF, induced angiogenesis. This initial study demonstrated a central role for  $\alpha 5\beta 1$  binding to FN during angiogenesis (Kim, Bell et al. 2000). In the same year, Kim *et al.* supported their previous findings by confirming that anti- $\alpha 5\beta 1$  antibody significantly inhibited both the adhesion and the migration of HUVEC and DMVECs on FN, whereas anti- $\alpha v\beta 3$  antibody had very little effect on FN. The authors showed that both the anti- $\alpha 5\beta 1$  antibody and the anti- $\alpha v\beta 3$  antibody inhibited HUVEC and DMVEC migration on vitronectin. The adhesion on vitronectin was blocked only by the anti- $\alpha v\beta 3$  antibody, which suggests an additional role

of  $\alpha 5\beta 1$  in affecting  $\alpha \nu\beta 3$ -mediated endothelial migration on vitronectin, but not  $\alpha \nu\beta 3$ -mediated adhesion. As ECs naturally secrete their own FN (i.e. endogenous FN) during angiogenesis, the author found similar effects were detected when treating ECs migrating on vitronectin with function-blocking antibodies directed against the cell-binding domain of FN, suggesting that the ligation of  $\alpha 5\beta 1$  by FN enhances  $\alpha \nu\beta 3$ -dependent migration on vitronectin (Kim, Harris et al. 2000). In two separate studies, Kim *et al.* conducted *in vitro* and *in vivo* chick assays and showed that anti- $\alpha 5\beta 1$  antibody inhibited  $\alpha \nu\beta 3$ -mediated FA assembly and migration on vitronectin by enhancing Protein Kinase A (PKA) (Kim, Harris et al. 2000). They also demonstrated that binding of  $\alpha 5\beta 1$  with FN promotes ECs migration and survival during angiogenesis by suppressing PKA activity, which then blocked apoptosis by suppressing cysteine-aspartic proteases-8 (caspase-8), a central player of programmed cell death, (Kim, Bakre et al. 2002). Another group of studies showed that human ECs in culture secreted soluble VEGFR1, which is known to act as a negative regulator of VEGF-mediated signalling, and that soluble VEGFR1, but not soluble VEGFR2, also functions as an extracellular protein to promote cell adhesion, migration and spreading through binding to the EC  $\alpha 5\beta 1$  integrin, which suggests another role for  $\alpha 5\beta 1$  during angiogenesis in addition to growth factor binding (Orecchia, Lacal et al. 2003). Subsequent studies implicated the upregulation of  $\alpha 5\beta 1$  integrin during tumour angiogenesis with the transcription factor Hox D3, a homeobox-containing transcription factor that converts ECs from the quiescent to the proliferative state, which binds to the ITGA5 subunit promoter and enhances the expression of the endothelial ITGA5 subunit *in vitro* and *in vivo*. The study also showed that Hox D3 binds directly to ITGB3 promoter and that it regulates  $\alpha \nu\beta 3$  integrin by enhancing ITGB3 expression (Boudreau and Varner 2004). Another group of studies showed that ITGA5-NULL embryonic stem (ES) cells resulted in smaller teratocarcinomas with reduced proliferation and blood vessel formation but increased apoptosis compared to WT and ITGA5-heterozygous ( $\alpha 5$ HET) controls, suggesting that  $\alpha 5\beta 1$  integrin plays an essential role in vessel formation both in ES cell cultures and in teratocarcinomas (Taverna and Hynes 2001). Other studies provided strong evidence that antagonising  $\alpha 5\beta 1$  significantly inhibited angiogenesis in *in vivo* mouse models, such as human xenograft tumours, injured corneal and ruptured choroidal angiogenesis assays (Bhaskar, Zhang et al. 2007), (Umeda, Kachi et al. 2006), (Muether, Dell et al. 2007). With regard to cancer, in a large number of studies, the upregulation of  $\alpha 5\beta 1$  integrin was implicated in cancer progression, including colon, breast, ovarian, lung, glioma and melanoma (Schaffner, Ray et al. 2013). Therefore, the antagonists of  $\alpha 5\beta 1$  have been under investigation as clinical agents that suppress human tumour

angiogenesis, such as volociximab (M200) (Figlin, Kondagunta et al. 2006), (Yazji, Bukowski et al. 2007), (Avraamides, Garmy-Susini et al. 2008).

Another group of studies demonstrated the involvement of  $\alpha 5\beta 1$  and  $\alpha v\beta 3$  as well as the FN matrix in adult central nervous system (CNS) angiogenesis (Wang and Milner 2006), (Milner, Hung et al. 2008), (Li, Welser et al. 2010), (Li, Welser-Alves et al. 2012). Wang and Milner conducted *in vitro* studies showing FN was the most effective ECM protein in promoting brain capillary EC survival and proliferation, which was approximately 2-fold greater than any other ECM substrate, mediated through  $\alpha 5\beta 1$  and  $\alpha v\beta 3$  via the activation of the ERK1/2 signalling pathway (Wang and Milner 2006). Using the cerebral hypoxia chamber, a mouse angiogenesis model in which littermates of age 8 to 10 weeks were maintained at either normal oxygen (21%) or hypoxia (8%) for up to 14 days, the Milner group demonstrated that  $\alpha 5\beta 1$  and FN were weakly expressed on cerebral capillaries throughout normoxic CNS development, whereas hypoxia strongly upregulated their expression on capillaries throughout CNS development, in which ITGA5 and FN expressions reached the highest expression at day 4 of hypoxia, then gradually declined to endpoint analyses at 14 days (Milner, Hung et al. 2008). Two years later, Li and Welse showed that both  $\alpha 5\beta 1$  and  $\alpha v\beta 3$  were upregulated and partially co-expressed in the angiogenic brain capillaries during hypoxic conditions compared to normoxic conditions. However, they found that ITGA5 and FN expressions were induced more quickly, peaking at day 4, and then declining compared with ITGB3 and vitronectin expressions, which peaked after day 7. Interestingly, they observed no significant difference in capillary density in the brains of WT and ITGB3-NULL mice, but the EC proliferation in the brains of ITGB3-NULL mice were increased at day 4 of cerebral hypoxia compared with the WT ECs, which correlated with the increase in ITGA5 expression on FN at day 4 of hypoxia. This observation was supported by the results of culturing ITGB3-NULL brain ECs, which exhibited the upregulation of the ITGA5 subunit and increased brain EC proliferation on FN, but not on vitronectin, collagen IV or laminin, compared with WT brain ECs. These findings suggest an important role for  $\alpha 5\beta 1$ , but not  $\alpha v\beta 3$ , in early angiogenic responses, at least in the brain (Li, Welser et al. 2010). Subsequently, the same author generated endothelial-specific knockout mice of ITGA5 ( $\alpha 5$ -EC-KO) and used the same mouse model of cerebral hypoxia to evaluate the function of the ITGA5 subunit in brain ECs. In normoxic conditions, no difference was detected in the density of cerebral blood vessels between WT and  $\alpha 5$ -EC-KO mice. However, in hypoxic conditions, the density of cerebral vessels in  $\alpha 5$ -EC-KO mice was significantly less than in

WT mice after 14 days of hypoxia, indicating that the loss of the endothelial ITGA5 reduced the angiogenic response to cerebral hypoxia. Specifically, the authors found that the proliferation of brain ECs after 4 days of hypoxia was significantly reduced in  $\alpha 5$ -EC-KO compared with WT. However, after 7 days of hypoxia, the number of proliferating brain ECs in  $\alpha 5$ -EC-KO was higher than in WT, indicating that the loss of endothelial ITGA5 delayed the mitogenic response to cerebral hypoxia. It also indicated an important role for the ITGA5 subunit in promoting the proliferation of brain ECs in response to cerebral hypoxia (Li, Welser-Alves et al. 2012).

In addition to hem-angiogenesis, the  $\alpha 5\beta 1$  integrin has been implicated in regulating lymph-angiogenesis (Zhang, Groopman et al. 2005), (Dietrich, Onderka et al. 2007). For example, by stimulating lymphatic hMVECs with VEGF-C<sub>156S</sub>, a mutant form of VEGF-C that binds only to VEGFR3, VEGFR3 phosphorylation and the proliferation of lymphatic ECs on FN were significantly enhanced compared with vitronectin, which showed limited effects. Importantly, immunoprecipitation showed a physical interaction between VEGFR3 and  $\alpha 5\beta 1$ , but not  $\alpha v\beta 3$ , in the presence or absence of VEGF-C<sub>156S</sub>, which suggests the constitutive association between VEGFR3 and  $\alpha 5\beta 1$ . Interestingly, VEGFR3 phosphorylation was significantly inhibited by a specific antibody against  $\alpha 5\beta 1$ , but not anti- $\alpha v\beta 3$ , indicating that FN mediates interactions with  $\alpha 5\beta 1$ , but not with  $\alpha v\beta 3$ , to promote lymphatic ECs proliferation (Zhang, Groopman et al. 2005). Consistent with this finding, Dietrich *et al.* demonstrated that ITGAV and ITGA5 were localised with vitronectin and FN, respectively, in the quiescent lymphatic vessels at the limbal arcade of mice eyes and in the proliferating lymphatic vessels that invaded experimentally inflamed corneas *in vivo*. Additionally, ITGA5 was co-localised with both VEGFR2 and VEGFR3 in the invading lymphatic vessels in the cornea. Immunogold labelling was used to co-localise ITGA5 with ITGAV in the proliferating lymphatic vessels. Interestingly, the anti-ITGA5 antibody significantly inhibited the proliferation of lymphatic vessels *in vivo*, which was slightly greater in combination with an anti-ITGAV antibody, suggesting that the role of ITGA5 is more important than that of ITGAV in pathological lymph-angiogenesis (Dietrich, Onderka et al. 2007). Using JSM8757, an antagonist that selectively inhibits  $\alpha 5\beta 1$  binding to FN, a previous study showed that JSM8757 significantly reduced lymphatic hMVECs proliferation in culture, providing additional evidence for the essential role of  $\alpha 5\beta 1$  in promoting lymphatic ECs proliferation (Okazaki, Ni et al. 2009). The authors supported this observation *in vivo* by using a mouse airway trachea model infected with *Mycoplasma pulmonis* for 14 days and then treated with

the JSM8757 antagonist to investigate the role of  $\alpha 5\beta 1$  in lymph-angiogenesis. The number of lymphatic sprouts as well as ITGA5 immunoreactivity in the lymphatic sprouts was significantly greater in the tracheas of pathogen-infected mice than in the pathogen-free mice. However, JSM8757 significantly reduced these effects, indicating the important role of  $\alpha 5\beta 1$  in lymph-angiogenesis during airway inflammation by promoting lymphatic sprouting and EC proliferation (Okazaki, Ni et al. 2009). Overall, the results of these studies indicate that the  $\alpha 5\beta 1$  integrin regulates several aspects of EC functions through interactions with various molecules during angiogenesis and/or lymph-angiogenesis.

#### **1.2.3.2.4. Integrin trafficking**

In 1989, Bretscher was the first to apply the cell surface receptor labelling technique to follow integrin receptor trafficking. The results showed that FN receptors ( $\alpha 5\beta 1$ ) (Bretscher 1989) and later other integrins, including  $\alpha 3\beta 1$ ,  $\alpha 4\beta 1$  and  $\alpha 6\beta 4$  (Bretscher 1992), were internalised at 37°C from the surface of the tested cells and then returned to the plasma membrane at the leading edges of migrating cells. Importantly, Bretscher also found that  $\alpha 5\beta 1$  and  $\alpha 6\beta 4$  circulated rapidly, whereas  $\alpha 3\beta 1$  and  $\alpha 4\beta 1$  circulate much more slowly, indicating that the rates of integrin trafficking are not the same (Bretscher 1989), (Bretscher 1992). Subsequently, Bretscher described the mechanism by which animal cells migrate by demonstrating that a migrated cell needs to remove its integrins (feet) from the rear of the cell, and these feet can be reused many times by redistributing them in the front of the cell while crawling across a relevant substratum (Bretscher and Aguado-Velasco 1998). A subsequent study on neutrophils demonstrated that the  $\alpha 5\beta 1$  integrin is responsible for the immobilisation of  $Ca^{++}$  on FN and that  $\alpha 5\beta 1$  was internalised from the rear of the cells in vesicles and then recycled back to the vesicles in the leading edges of the cells only when the intracellular  $Ca^{++}$  concentration increases (Pierini, Lawson et al. 2000). Although this mechanism of integrin cycling during cell migration has remained attractive to researchers, the model does not apply to all migrating cells. For example, the shuttling of integrins from the cell rear to the leading edge was not observed in fibroblasts. Instead, fractions of the cytoplasm containing  $\alpha 5\beta 1$  remained attached to the FN substratum to allow the cell body to move forward (Regen and Horwitz 1992), (Palecek, Schmidt et al. 1996), (Laukaitis, Webb et al. 2001). Moreover, the movement of the recycling vesicles from the rear of the cell to its leading edge in chinese hamster ovary (CHO) cells was not observed. Instead,  $\alpha 5\beta 1$  was internalised in vesicles from the cell front to perinuclear region before being shuttled to the

leading edge of the membrane protrusion (Laukaitis, Webb et al. 2001). In a recent review, three directions of integrin trafficking during cell migration were described: from the cell front to the cell rear, from the cell front to the cell front, and from the perinuclear region to the cell rear (Paul, Jacquemet et al. 2015). In recent years, it has become apparent that integrin trafficking also plays a fundamental role in regulating the function, turnover and distribution of integrins in adherent cells during cell adhesion, spreading, migration and cancer invasion. The mechanism of trafficking includes the delivery of newly synthesised integrins as well as the internalisation and recycling of internalised integrins back to the cell surface (Margadant, Monsuur et al. 2011). Most integrins on the cell surface are cleared within 30 minutes, but the degradative turnover of integrins is slow (12–24 hours), which indicates that the majority of internalised integrins are returned to the cell surface (Paul, Jacquemet et al. 2015).

Integrin internalisation can occur through both clathrin-dependent and clathrin-independent (via caveolae or macropinocytosis) mechanisms. Both inactive and active (ligand-bound) integrin heterodimers can promote internalisation, and both can regulate cell migration through the cycles of adhesion assembly and disassembly (turnover) (Valdembri and Serini 2012), (Paul, Jacquemet et al. 2015). The mechanism of integrin internalisation is influenced by two members of the GTPase family: 1) the Rab GTPase, which recruits effector proteins to promote cargo sorting, motor protein binding, tethering, docking and fusion events; 2) the ADP-ribosylation factor (Arf) GTPase, which recruits coat proteins to promote vesicle budding as well as linking to motor cytoskeletal proteins and regulating phospholipid signalling (**Figure 1.17**) (Paul, Jacquemet et al. 2015). Rab and RAF as well as Ran, Ras, and Rho, are five members of the Ras subfamily, all of which are determined by small guanine-nucleotide-binding (G) proteins that act as switches to regulate protein activity or localisation (Gillingham and Munro 2007). Rab GTPase family members are known as central regulators and vesicle transporters of intracellular membrane traffic by shuttling between the cytosol and membranes. Almost 70 members of these small GTPase have been identified in humans (Zhen and Stenmark 2015). Rab GTPase members are localised in different membrane compartments within a cell to ensure that the membrane-bound cargoes are transported to their correct destinations. Similar to other GTPase members, Rab GTPase members are regulated by GEF and GTPase-activating proteins (GAP). The activation of Rab GTPase is mediated by GEFs, which exchange the bound GDP with GTP (to switch on), whereas the deactivation of Rab GTPase is mediated by GAPs, which hydrolyse GTP into GDP (switch

off). When the activation of Rab GTPase occurs, Rab effector proteins are recruited to the Rab GTPase to promote cargo sorting, vesicle motor, vesicle tethering, vesicle docking and vesicle fusion events between donor and acceptor membrane compartments during trafficking (Zhen and Stenmark 2015). In contrast, members of the ARF GTPase family act in the endoplasmic reticulum (ER)-Golgi system, endosomal and lysosomal pathways as well as the secretory membranes and the plasma membrane. In mammals, six conserved members have been identified and classified in three groups based on sequence homology: Class I (ARF1, ARF2 and ARF3), Class II (ARF4 and ARF5) and Class III (ARF6). Class I ARFs are highly conserved, and they are present in all eukaryotic cells (Zhen and Stenmark 2015). Additionally, ARF-like (ARL) proteins and SAR1 proteins are considered members of the ARF GTPase family (Gillingham and Munro 2007). An important feature of ARF regulator proteins, which distinguishes them from other small G proteins, is that they are all modified by myristoylation at the N-terminus, which brings ARF proteins into very close contact with the membrane to initiate biological activity (Donaldson and Jackson 2011). Therefore, in contrast to the Rab effectors that are located distant from membranes, ARF regulators are constrained to localise close to the membrane surface (see **Figure 1.17**) (Gillingham and Munro 2007). Similar to Rab GTPase, ARF GTPase family members are also regulated through a cycle of GTP binding (activation) and GTP hydrolysis (inactivation); however, unlike Rab effectors, no GDP inhibitors have been identified in ARFs. Following the activation of ARFs on the membrane, they recruit large numbers of molecules, including coat proteins, lipid-modifying enzymes, tethers and other effector molecules, which regulate membrane trafficking and organelle structure. For instance, ARF1 recruits the cytosolic coat protein complex I (COPI) to Golgi membranes, where the cargo proteins are then sorted to the COPI-coated vesicles. At the *trans*-Golgi network (TGN), ARF1 regulators subsequently recruit the heterotetrameric clathrin adaptor protein 1 (AP1), AP3 and AP4 as well as other required vesicle coating proteins to the newly formed COPI-coated vesicles for transporting the cargo proteins to the correct destinations (Donaldson and Jackson 2011). Most integrins require adaptor proteins, such as disabled (Dab)-2 and adaptor protein-2 (AP-2), which accumulate at or near FAs shortly before integrin disassembly, to recruit them into clathrin-coated pits where endocytosis occurs (Margadant, Monsuur et al. 2011). Studies showed that silencing of clathrin, Dab-2 or AP-2 reduced the FAs disassembly and cell migration (Ezratty, Bertaux et al. 2009), (Chao and Kunz 2009), (Teckchandani, Toida et al. 2009). It is worth noting that ARF3, ARF4 and ARF5 are also present on Golgi membranes. However,

previous studies focused on ARF1 at the Golgi membrane and on ARF6 at the plasma membrane (Donaldson and Jackson 2011).

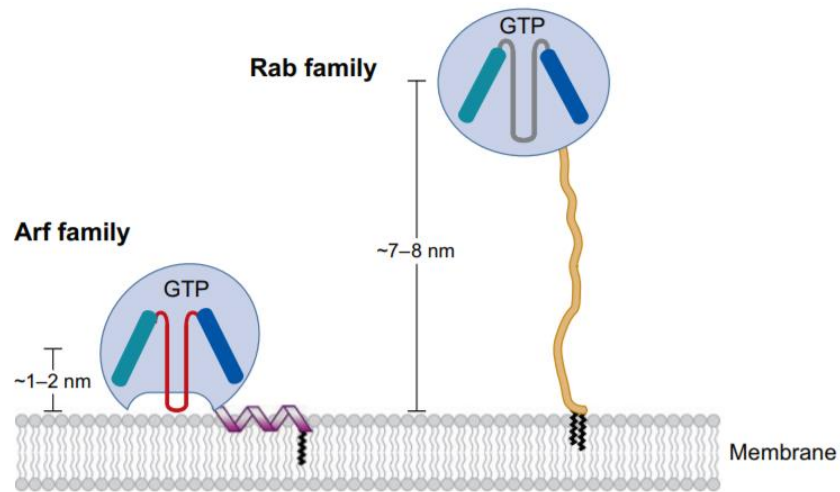


**Figure 1.17 Structure of Arf and Rab G proteins on the plasma membrane.** The schematic illustration shows differences between the structures and functions of the Rab family and the Arf family. Members of the Rab family interact with effector proteins located  $\sim 7\text{--}8$  nm away from the membrane bilayer, which is not the case in Arf family members (Gillingham and Munro 2007).

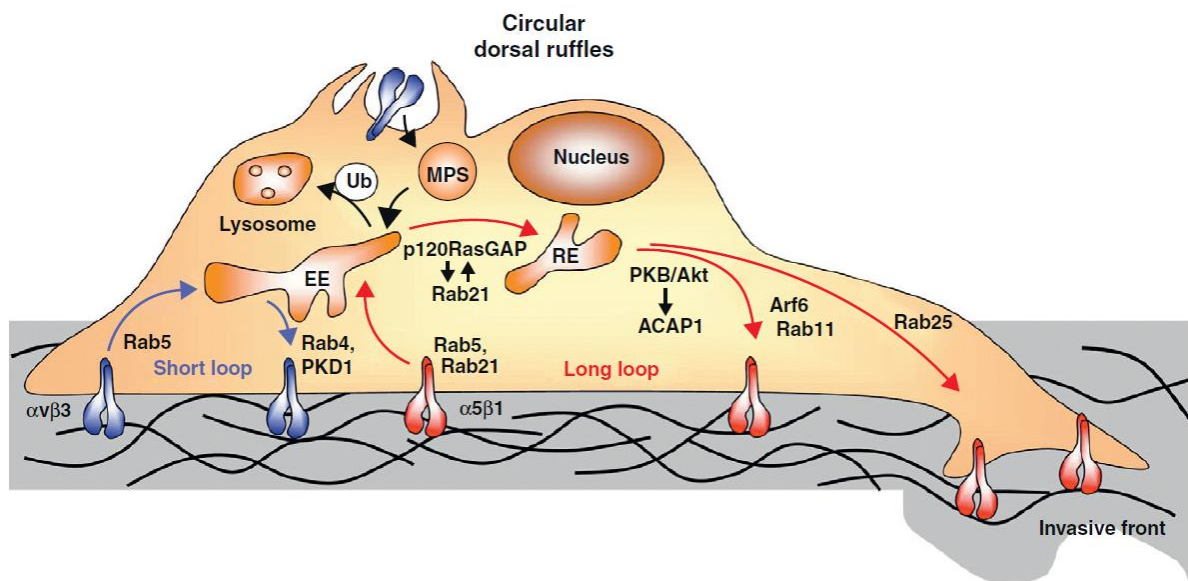
#### 1.2.3.2.4.1. Examples of $\alpha v\beta 3$ and $\alpha 5\beta 1$ trafficking

Following internalisation, the integrins return to the plasma membrane through short-loop recycling in a Rab4- or Rab5-dependent manner or through long-loop recycling in a Rab11-dependent manner (Paul, Jacquemet et al. 2015). For example, Woods *et al.* demonstrated that upon the PDGF stimulation of fibroblasts, the  $\alpha v\beta 3$  integrin was internalised by macropinocytosis from dorsal ruffles by following a rapid recycling route (short-loop recycling) from early endosomes (EE) directly to the plasma membrane through Rab4 and protein kinase D1 (PKD1), in which PKD1 is associated with the cytoplasmic tail of ITGB3 at a vesicular compartment that is downstream of the Rab4-dependent transport step (**Figure 1.18 A**). The study found that a mutant ITGB3 subunit or the suppression of PKD1 inhibited the PDGF-dependent accumulation of PKD1 and  $\alpha v\beta 3$  integrin at intracellular vesicles. Hence, the recycling of  $\alpha v\beta 3$  heterodimer to form new FAs on plasma membrane was blocked during cell spreading (Woods, White et al. 2004). Consistent with this result, another study demonstrated that upon the VEGF stimulation of ECs,  $\alpha v\beta 3$  was internalised to EE and then recycled to the cell surface by short-loop recycling through PKD1 in both Rab4- and Rab5-dependent manners. The results of co-immunoprecipitation and immunofluorescence experiments indicated the direct interaction of PKD1 with  $\alpha v\beta 3$ , but not with  $\alpha 5\beta 1$ . Furthermore, the suppression of PKD1 expression increased the internalisation of  $\alpha v\beta 3$  and reduced recycling to the cell surface, which blocked newly formed FAs and reduced EC migration on vitronectin (Di Blasio, Droetto et al. 2010).

In contrast to  $\alpha v\beta 3$ ,  $\alpha 5\beta 1$  follows a slow recycling (long-loop recycling) mechanism. It travels from EE to the perinuclear recycling compartment (PNRC) through Rab11, Arf6, and Akt before recycling to the plasma membrane. For example, an early study on  $\alpha 5\beta 1$  demonstrated that the formation of initial adhesive complexes occurs in a hierarchical mechanism in which paxillin enters adhesions early at the base of newly forming protrusions and then turns-over rapidly in these regions. When the protrusive activity ceases,  $\alpha$ -actinin begins to appear along the cell border in the membrane protrusions and in fibrous-like structures that slide toward the cell body, but not in the newly forming paxillin adhesions.  $\alpha$ -actinin is followed by co-localisation with ITGA5 to stabilise adhesions and translocate paxillin and  $\alpha$ -actinin-containing cytoskeletal complexes to the cell rear. This study also showed that both ITGA5 and  $\alpha$ -actinin were not observed in the paxillin-rich complexes (Laukaitis, Webb et al. 2001). Shi and Sottile demonstrated that FN matrix turnover occurs through receptor-mediated endocytosis and intracellular degradation undertaken by a process

that involves caveolae-1, the major integral protein components of membrane caveolin (Sottile and Chandler 2005). Subsequently, the same group showed that  $\alpha 5\beta 1$ , but not  $\alpha v\beta 3$ , was co-localised and internalised into FN containing intracellular vesicles during fibronectin turnover, indicating that  $\alpha 5\beta 1$ , but not  $\alpha v\beta 3$ , is important in FN internalisation. Interestingly, by using FN-NULF myofibroblasts, they also showed that  $\alpha 5\beta 1$  internalised in the presence or absence of FN through caveolae-mediated endocytosis (Shi and Sottile 2008). In the following year, three different groups of studies showed that  $\alpha 5\beta 1$  internalisation is clathrin-mediated before entering Rab5 endosomes. Interestingly, the deletion of clathrin or any of its adaptor proteins, Dap2 or AP2, inhibited the FA disassembly, which resulted in increasing the level of  $\alpha 5\beta 1$  on the plasma membrane as well as reducing cell migration (Ezratty, Bertaux et al. 2009), (Chao and Kunz 2009), (Teckchandani, Toida et al. 2009). Another study demonstrated that during the spread of ECs on FN, independently of both VEGF<sub>165</sub> and SEMA-3A receptors, NRP1 did not directly mediate interactions with FN. Instead, through its extracellular domain, NRP1 was required to interact with the active heterodimeric form of  $\alpha 5\beta 1$ -bound FN. Simultaneously, the cytoplasmic domain of NRP1 interacted with the C-terminal SDA sequence of the active ITGA5 subunit, which was mediated by GIPC1/Myo6 to enhance the Rab5/Rab21-dependent endocytosis of active  $\alpha 5\beta 1$ , ensuring the recycling of vesicles containing  $\alpha 5\beta 1$  to new adhesion sites on FN and promoting the fibrillogenic formation required for the adhesion and spread of ECs on FN (**Figure 1.18 B**) (Valdembri, Caswell et al. 2009).

A)



B)

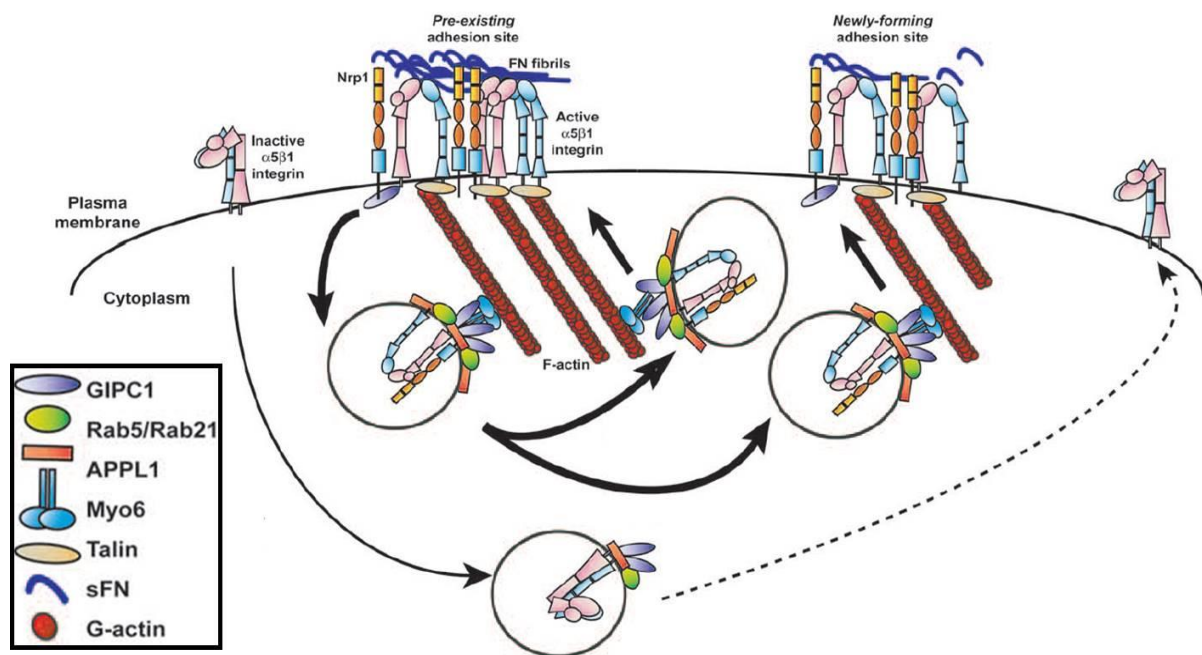


**Figure 1.18 Trafficking mechanisms of  $\alpha\text{v}\beta\text{3}$  and  $\alpha\text{5}\beta\text{1}$  to regulate cell adhesion and migration of adherent cells. A)** The schematic illustration shows the different recycling mechanisms of  $\alpha\text{v}\beta\text{3}$  and  $\alpha\text{5}\beta\text{1}$  in an adherent cell.  $\alpha\text{v}\beta\text{3}$  is internalised through Rab5, while  $\alpha\text{5}\beta\text{1}$  is internalised through both Rab5 and Rab21. Both integrins are then trafficked to early endosome (EE). From EE,  $\alpha\text{v}\beta\text{3}$  follows short-loop recycling in a Rab4-dependent manner, whereas  $\alpha\text{5}\beta\text{1}$  follows long-loop recycling in which  $\alpha\text{5}\beta\text{1}$  first trafficks into recycling endosome (RE) in a Rab11-dependent manner or in a Rab25-dependent manner. Then the repopulation of integrins at the ventral surface occurs to form new FAs during cell migration. Alternatively, integrins may be ubiquitinated (Ub) and then trafficked into late endosome/lysosome for degradation.  $\alpha\text{v}\beta\text{3}$  may also be redistributed to the dorsal ruffles after PDGF stimulation and then trafficked to EE by macropinocytosis (MPS) before recycling at the ventral surface to form new FAs (see text) (Margadant, Monsuur et al. 2011). **B)** The schematic illustration shows the mechanism through which NRP1 regulates the active form of  $\alpha\text{5}\beta\text{1}$  trafficking on FN. During the spread of ECs on FN, the adaptor protein GIPC1 and Myo6 are recruited to the cytoplasmic tail of NRP1, which enhances the binding of the NRP1 cytoplasmic tail to the C-terminal SEA sequence in the ITGA5 subunit of active  $\alpha\text{5}\beta\text{1}$ . It then promotes the Rab5/Rab21-dependent endocytosis of the active  $\alpha\text{5}\beta\text{1}$ . When endocytosis occurs, vesicles carrying  $\alpha\text{5}\beta\text{1}$ -NRP1 undergo trafficking before recycling to form adhesion sites on the plasma membrane. Additionally, the internalised  $\alpha\text{5}\beta\text{1}$ -NRP1 may also be recycled to the same cell-ECM contact adhesion site for support. APPL1 is an adaptor protein that recruits other adaptor proteins essential for vesicles trafficking. Adapted from (Valdembri, Caswell et al. 2009).

### 1.3 Research Aims and Objectives

Previous research conducted in our laboratory showed that angiogenic responses are only sensitive to NRP1 perturbations when  $\beta$ 3-integrin levels are reduced. Because of the structural and functional similarities between NRP1 and NRP2, and because the cellular functions of NRP2 in endothelial cells is less well understood, we felt it was important to investigate a role for this protein during angiogenesis. Therefore, this study was undertaken to:

1. Investigate a potential link between NRP2 and ITGB3 within ECs.
2. Determine if NRP2 depletion affects signalling, migration, proliferation and adhesion on fibronectin in ECs.
3. Identify NRP2 binding partners, using MS, within ECs.
4. Determine whether NRP2 plays a role in angiogenesis *in vivo*.

## Chapter 2: Materials and Methods

---

### 2.1. Chemicals, antibodies, restriction enzymes and VEGF<sub>164</sub>

All chemicals used in this study were purchased from ThermoFisher Scientific (Loughborough, UK) unless otherwise noted. Primary conjugated antibodies, primary antibodies and secondary conjugated antibodies were purchased from suppliers as listed in (Table 2.1), (Table 2.2) and (Table 2.3), respectively. All restriction enzymes and reaction buffers (Table 2.4) were purchased from New England Biolabs (Hitchin, UK).

VEGF<sub>164</sub> was produced by the Robinson lab using the protocol described by Krilleke *et al.* (Krilleke, DeErkenez et al. 2007). Briefly, pPICZαC-VEGF<sub>164</sub> construct (kindly provided by Professor Dave Shema, UCL, London) was transformed into *Pichia pastoris* yeast cells. Then, transformants were subjected to colony blotting for high secreting colonies. The highest secreting yeast transformant of VEGF<sub>164</sub> was cultured in 500 mL of BMGY medium at 30°C until the culture reached an absorbance of 3 at 600nm. Next, yeast pellets were resuspended and grown in 100 mL of BMGY supplemented with 0.01% Antifoam 204 (Sigma-Aldrich, St Louis, US) at 30°C. Cultures were incubated for an additional 36 hours, with methanol added to a final concentration of 1% every 12 hours. Cultures were centrifuged and supernatant was equilibrated (via dialysis) in Ni<sup>2+</sup>-nitrilotriacetic acid chromatography binding buffer (PBS, pH 7.4, with 2.7 mM KCl, 2 mM KH<sub>2</sub>PO<sub>4</sub>, 8 mM Na<sub>2</sub>PO<sub>4</sub>, 300 mM NaCl) and then incubated with Ni<sup>2+</sup>-nitrilotriacetic acid-agarose (Qiagen) for 60 minutes at 4°C. Centrifugation was performed, and the collected beads were washed with the binding buffer. The bound VEGF<sub>164</sub> proteins were eluted in elution buffer and analysed by SDS-PAGE (see subsection 2.9.2 to 2.9.5) and Coomassie blue staining to visualize the amount of VEGF<sub>164</sub> on an SDS-PAGE gel.

**Table 2.1:** List of primary conjugated antibodies

Antigen	Reactivity	Host	Conjugation	Application	Source	Cat. #
CD31	Mouse	Rat (IgG2a, κ)	PE	FC	eBioscience™	12-0311-81
ICAM-2	Mouse	Rat (IgG2a, κ)	Alexa®-488	FC	eBioscience™	53-1021-80
VE-Cadherin	Mouse	Rat (IgG1)	PE	FC	eBioscience™	12-1441-80
ITGA5	Mouse	Hamster (IgG)	PE	FC	eBioscience™	14-0493-81
IgG isotype control	Mouse	Hamster	PE	FC	eBioscience™	12-4888-81
IgG isotype control	Mouse	Rat	PE	FC	eBioscience™	M1-14D12
BS1-lectin	Mouse	—	PE	FC	eBioscience™	L2895

PE: Phycoerythrin; FC: Flow cytometry; ARA: Aortic ring assay.

**Table 2.2:** List of primary antibodies

Antigen	Reactivity	Host	Application	Source	Clone / Cat. #
ICAM-2	Mouse	Rat	ECS	AbD Serotec	#MCA2295EL
VE-Cadherin	Mouse	Rabbit	WB	Abcam	ab33168
LYVE-1	Mouse	Rabbit	WB	Abcam	ab14917
Prox-1	Mouse	Rabbit	WB	Abcam	ab101851
HSC-70	Mouse	Mouse	WB	Santa Cruz Biotechnology	B-6 / sc-7298
GAPDH	Mouse	Mouse	WB	Abcam	ab9484
GAPDH	Mouse	Mouse	WB	Proteintech	60004-1-1g
NRP1	Mouse	Rabbit	WB	Cell Signalling Technology	3725S
NRP2	Mouse	Rabbit	WB, ICC, IP	Cell Signalling Technology	D39A5
NRP2	Mouse	Rabbit	ICC	Abcam	ab155680
NRP2	Mouse	Goat	WB, ICC	R&D	AF567
NRP2	Mouse	Rabbit	WB, ICC	Millipore	AB10522
VEGFR2	Mouse	Rabbit	WB	Cell Signalling Technology	55B11 / #2479
Phospho VEGFR-2 (Y1175)	Mouse	Rabbit	WB	Cell Signalling Technology	19A10 / #2478
ERK1/2 (p44/42 MAPK)	Mouse	Rabbit	WB	Cell Signalling Technology	137F5 / #4695
Phospho ERK1/2	Mouse	Rabbit	WB	Cell Signalling Technology	#9101
ITGB3	Mouse	Rabbit	WB	Cell Signalling Technology	4702S
ITGB1	Mouse	Rabbit	WB	Abcam	ab179471

<b>ITGA5</b>	Mouse	Rabbit	WB	Cell Signalling Technology	4705S
<b>ITGA5</b>	Mouse	Rabbit	ICC	Abcam	ab150361
<b>ITGA6</b>	Mouse	Rabbit	WB	Abcam	ab181551
<b>Paxillin</b>	Mouse	Rabbit	ICC	Abcam	ab32084
<b>Paxillin</b>	Mouse	Rabbit	WB	Cell Signalling Technology	2542S
<b>Phospho Paxillin (Y118)</b>	Mouse	Rabbit	WB	Cell Signalling Technology	2541
<b>Biotin</b>	Mouse	Mouse	IP	Jackson Immunoresearch	3D6.6

ECS: Endothelial cell sorting; WB: Western blot; ICC: Immunocytochemistry; IP: Immunoprecipitation.

**Table 2.3:** List of secondary conjugated antibodies

Host / name	Anti-	Application	Conjugate	Source	Cat. #
<b>Rabbit</b>	Goat	ICC	Alexa®-488	Invitrogen	A-21222
<b>Rabbit</b>	Goat	ICC	Alexa®-594	Invitrogen	A-21223
<b>Donkey</b>	Rabbit	ICC	Alexa®-488	Invitrogen	A-21206
<b>Donkey</b>	Sheep	ICC	Alexa®-633	Invitrogen	A-21100
<b>Sheep</b>	Rat	ECS	Dynabeads	Invitrogen	11035
<b>Goat</b>	Rabbit	WB	HRP	Dako®	P 0448
<b>Rabbit</b>	Mouse	WB	HRP	Dako®	P 0260
<b>Rabbit</b>	Goat	WB	HRP	Dako®	P 0449

HRP: Horseradish peroxidase

**Table 2.4:** List of restriction enzymes and buffers

Enzyme	Cut site	Overhang	Working conc. (U/μL)	Buffer	Plasmid	Cat. #
<b>HpaI</b>	5'...GTT↓AAC...3' 3'...CAA↑TTG...5'	Blunt	0.3	CutSmart	pSico, pSicoR	R0105S
<b>XhoI</b>	5'...C↓TCGAG...3' 3'...GAGCT↑C...5'	5'TCGA	0.4	CutSmart & Buffer 2	pSico, pSicoR	R0146S
<b>SacII</b>	5'...CCGC↓GG...3' 3'...GG↑CGCC...5'	3'GC	0.8	Buffer 2	pSico	R0157S
<b>NotI</b>	5'...GC↓GGCCGC...3' 3'...CGCCGG↑CG...5'	5'GGCC	0.2	Buffer 2	pSico	R0189S
<b>XbaI</b>	5'...T↓CTAGA...3' 3'...AGATC↑T...5'	5'CTAG	0.4	Buffer 2	pSicoR	R0145S

“↓” indicates the cut site; “↑” indicates the cut site in the complementary strand.

## 2.2. Lung microvascular ECs isolation

The Robinson group isolated and immortalised lung ECs as previously described (Reynolds and Hodivala-Dilke 2006) (Robinson, Reynolds et al. 2009). Briefly, following the cervical dislocation and dissection of adult mice under aseptic conditions, the lungs from 3 mice were transferred using a pair of sterile forceps to a 10-cm Petri dish containing fresh Ham's F12 from which any fat, blood clots, and connective tissue were removed. The lungs were then dipped for 2 seconds in a second 10-cm Petri dish containing 70% ethanol (EtOH) before transferring the lungs for extending washing in a third 10-cm Petri dish containing MLEC complete medium [1:1 mix of Ham's F-12:DMEM medium low glucose (Gibco® life technology, Carlsbad, USA), 20% foetal bovine serum (FBS) (Gibco® life technology), 100 units/mL penicillin/streptomycin (P/S) (Gibco® life technology), 2mM glutamax (Gibco® life technology), 50 µg/mL heparin (Sigma-Aldrich), and 25 mg of endothelial mitogen (AbD Serotec, Kidlington, UK)]. Using scalpel blades, the lungs were then minced on an inverted lid of a sterile 10-cm Petri dish for 5 minutes before transferring the paté-like homogenate to a 50-mL centrifuged tube containing filtered sterilised 0.1% collagenase I (Gibco® life technology) to be digested in a 37°C water bath for 1 hour. Following digestion, the collagenase-digested lung solution was transferred to a new sterile 10-cm Petri dish and mixed with 10 mL fresh MLEC medium. Using a 20-mL syringe, the digested lung solution was extracted and separated by mechanical force through a 19.5-gauge needle back into the Petri dish four times before passing the digested lungs through a 70-µm cell strainer into a 50-mL centrifuged tube for centrifuging at 300 g for 5 minutes. The pellet was resuspended carefully in 10 mL fresh MLEC medium and seeded in a T75 flask pre-coated with 0.1% gelatin, 30 µg/mL collagen I, and 10 µg/mL FN at 37°C in a 5% CO<sub>2</sub> incubator. Twenty-four hours later, the cells were washed twice with PBS to remove any red blood cells before performing the first positive sorting of the ECs by magnetic activated cell sorting (MACS) using ICAM-2 as the biomarker for ECs. The cells were incubated with 5 mL PBS containing (1:1000) rat-anti-mouse ICAM-2 antibody for 30 minutes at 4°C. One wash was performed with cold PBS to remove the excess antibody before incubating the ECs bound to ICAM-2 antibody with sheep-anti-rat IgG coated magnetic Dynabeads for another 30 minutes at 4°C. Following three washes with ice-cold PBS to wash off the unbound Dynabeads, the cells were incubated with pre-warmed 0.25% trypsin-EDTA (Invitrogen) for 2–3 minutes at 37°C in a CO<sub>2</sub> incubator to detach the cells. The solution was subsequently neutralised with MLEC medium, transferred to a 15-mL centrifuged tube, and then placed on a magnet. The

supernatant was carefully discarded leaving behind ECs bound to the magnetic, which was then resuspended in fresh, pre-warmed MLEC medium and seeded in a T25 flask pre-coated with 0.1% gelatin, 30 µg/mL collagen I, and 10 µg/mL FN at 37°C in a 5% CO<sub>2</sub> incubator until it reached 90% confluency. The second positive sorting of the ECs was then performed in a similar manner to enhance the purity of the ECs.

### **2.3. Microvascular EC immortalisation**

Prior to immortalisation, a polyoma-middle-T-antigen (PyMT) retrovirus was produced using GgP+E cells. Then the conditioned medium containing a PyMT retrovirus was collected from the cultured packaging GgP+E cells, filtered through a 0.45 µm filter, and preserved at -80°C until needed. For immortalisation, the PyMT retrovirus was thawed and mixed with 8 µg/mL polybrene to enhance the transfection efficiency before transfecting the sorted positive lung ECs with the PyMT conditioned medium at 37°C in a 5% CO<sub>2</sub> incubator for 6 hours. The medium containing the PyMT retrovirus was then replaced by fresh complete MLEC medium and returned to the incubator. Twenty-four hours later, the same transfection procedure was repeated. The cells were maintained for four weeks to ensure their immortalisation, and the MLEC medium was then changed to IMMLEC medium, which is similar except it is supplemented by only 10% FBS and it excludes endothelial mitogen to facilitate the growth and survival of vascular ECs in culture. Flow cytometry for ICAM2, CD31, and VE-Cadherin was performed to ensure endothelial identity. The ECs were then expanded and stored for a long period, as described below.

### **2.4. Freezing and thawing cells**

For cell freezing, confluent ECs grown in a cultural flask were washed with a pre-warmed PBS, trypsinised, counted by a Neubauer counting chamber (Hawksley, Lancing), and centrifuged at 500 g for 4 minutes before resuspending at  $1 \times 10^6$  cells per mL of a pre-chilled medium containing 90% FBS and 10% dimethyl sulfoxide (DMSO) to prevent the formation of ice crystal during freezing. Then 1 mL of cell suspension was aliquoted in cryovials before placing them in a Mr. Frosty freezing container (ThermoFisher Scientific) at -80°C for short-term storage or in a liquid nitrogen DryStore™ for long-term storage. For cell thawing, the 1 mL aliquoted cryovial was thawed in a water bath at 37°C for approximately 20 seconds before transferring the 1 mL cell suspension to an ice-cold centrifuge tube containing 9 mL of IMMLEC media and then centrifuged at 500 g for 4 minutes. The cell pellet was resuspended

with 3 mL of pre-warmed IMMLEC medium and seeded in a T25 flask that was pre-coated with 0.1% gelatin at 37°C in a 5% CO<sub>2</sub> incubator.

## 2.5. Tissue culture

ECs were grown on tissue cultural flasks (T25, T75, or T175) that were pre-coated with 0.1% gelatin for 1 hour at 37°C in a 5% CO<sub>2</sub> incubator. When the cell growth reached a confluency of 90–95%, the ECs were firstly washed once using pre-warmed PBS to remove the excess IMMLEC medium before detaching the adherent ECs using pre-warmed 0.25% trypsin-EDTA for 2–3 minutes at 37°C in a 5% CO<sub>2</sub> incubator. Following trypsinisation, the ECs were neutralised with pre-warmed IMMLEC medium to stop trypsin enzymatic activity. Then, the cell suspension was transferred to a 50-ml centrifuge tube for centrifuging at 500 g for 4 minutes. The cell pellet was gently resuspended in a fresh pre-warmed IMMLEC medium and either split 1:3 or expanded in a new tissue cultural flask that was pre-coated with 0.1% gelatin. It is worth noting that a T175 tissue cultural flask holds up to  $9 \times 10^6$  immortalised ECs, whereas T75 and T25 flasks hold up to  $4 \times 10^6$  and  $1 \times 10^6$  immortalised ECs, respectively. Therefore, in experiments that require more than  $9 \times 10^6$  ECs, as in the case of the cell surface receptors biotinylation assays, we grew ECs in multiple T175 tissue cultural flasks and pooled them before performing the experiment. The EC tissue culture is summarised in **table 2.5**.

**Table 2.5:** Summarisation of EC tissue culture conditions

Tissue Cultural Flask Size	25 cm <sup>2</sup> (T 25)	75 cm <sup>2</sup> (T 75)	175 cm <sup>2</sup> (T 175)
<b>90–95% Confluency</b>	Up to $1 \times 10^6$ ECs	Up to $4 \times 10^6$ ECs	Up to $9 \times 10^6$ ECs
<b>PBS Wash</b>	1 mL	5 mL	10 mL
<b>0.25% Trypsin-EDTA</b>	0.5-1 mL	1.5-2 mL	3-4 mL
<b>Neutralisation</b>	1 mL	4 mL	8 mL
<b>Total Complete Media</b>	3 mL	5 mL	20 mL

## 2.6. Mouse genotyping

### 2.6.1. DNA extraction

The ear of each live mouse was snipped, placed in one well of a 96-well PCR plate (ThermoFisher Scientific), and digested with a 100  $\mu$ L of ear/tail lysis buffer (50mM Tris-HCl pH 8.5, 10mM EDTA pH 8.0, 100mM NaCl, 0.2% SDS) supplemented with 100  $\mu$ g/mL proteinase K and incubated overnight at 56°C in an incubator. To genotype our immortalised lung ECs, the cells were trypsinised and centrifuged as described in **section 2.4**, and then using the ear/tail lysis buffer, the cell pellet was lysed overnight at 56°C. The following day, 100  $\mu$ L of isopropanol was added to the wells to precipitate DNA. The plate was then capped by lids, inverted a few times to mix the isopropanol with the DNA lysate, and then centrifuged at 1400 g for 30 minutes. The supernatant was carefully poured off, and the precipitated DNA pellet was dried in an incubator at 37°C for 2 hours. Next, 200  $\mu$ L of TE buffer (1M Tris-HCL pH 8 and 0.5M EDTA pH 8) was added to the wells and incubated overnight at 37°C to resuspend the DNA pellet. A Veriti™ 96-well thermal cycler PCR machine (ThermoFisher Scientific) was then used to perform the PCR reactions as described below.

#### 2.6.1.1. *Itgb3* knockout genotype

Transgenic mice that expressed a knockout for the  $\beta$ 3-integrin (KO-*Itgb3*) allele were created by substituting a 1.4 kb HindIII fragment of the  $\beta$ 3 gene including exons I and II with a 1.7 kb construct containing a P<sub>gk</sub>-neomycin (neo)-resistance cassette (see chapter 3; **Figure 3.1 A**). The PCR analysis was carried out using the following oligonucleotide primers (Hodivala-Dilke, McHugh et al. 1999):

- Forward primer 1 (**Binds 5' upstream of exon1 or P<sub>gk</sub>-neo**):  
5' – CTTAGACACCTGCTACGGGC – 3'
- Reverse primer 2 (**Binds within P<sub>gk</sub>-neo**):  
5' – CACGAGACTAGTGAGACGTG – 3'
- Reverse primer 3 (**Binds 3' downstream of exon 1**):  
5' – CCTGCCTGAGGCTGAGTG – 3'

In each DNA sample, forward primer 1 was mixed in two separate PCR reactions with reverse primer 2 or reverse primer 3. A typical PCR reaction in each DNA sample consisted

of 0.4  $\mu\text{L}$  of DNA mixed with 10  $\mu\text{L}$  of MegaMix-Blue cocktail, which contains Taq polymerase, reaction buffer, dNTPs, and blue agarose loading dye (Microzone, Haywards Heath, UK), and 0.04  $\mu\text{L}$  of primers 1 and 2 in a final concentration of 0.4  $\mu\text{M}$  or 0.1  $\mu\text{L}$  of primers 1 and 3 in a final concentration of 1  $\mu\text{M}$  in one well of a 96-well PCR plate. Next, the plate was carefully capped with lids and placed in a programmed thermal cycler PCR machine. The PCR reaction programme was started in an initialisation step at 95°C for 15 minutes, followed by 35 amplification cycles repeated in sequential order: denaturation at 95°C for 30 seconds, annealing at 60°C for 45 seconds, and extension at 72°C for 90 seconds. The final cycle was terminated by an elongation step at 72°C for 10 minutes. The amplified products generated by the reactions involving primers 1 and 2 corresponded to the *Itgb3*-NULL allele, whereas the products generated by the reactions involving primers 1 and 3 corresponded to the *Itgb3*-WT allele.

### **2.6.1.2. Pdgfb.CreER genotyping**

Transgenic mice that expressed a tamoxifen-inducible pdgfb-iCreERT2 allele in vascular endothelial cells were created by substituting the exon 1 of the pdgfb gene by the iCreERT2-IRES-EGFP-pA sequence. The DNA extracted from the pdgfb.CreER mice was PCR-analysed using the following oligonucleotide primers (Claxton, Kostourou et al. 2008):

Forward primer: 5' – GCCGCCGGGATCACTCTC – 3'

Reverse primer: 5' – CCAGCCGCCGTCGCAACT – 3'

For each PCR reaction, 0.8  $\mu\text{L}$  of DNA was mixed with 10  $\mu\text{L}$  of MegaMix-Blue cocktail and 0.08  $\mu\text{L}$  of the forward and reverse primers at a final concentration of 0.8  $\mu\text{M}$  in one well of a 96-well PCR plate. The PCR reaction programme was started by an initialisation step at 94°C for 4 minutes, followed by 34 amplification cycles repeated in sequential order: denaturation at 94°C for 30 seconds, annealing at 57.5°C for 45 seconds, and extension at 72°C for 60 seconds. The final cycle was terminated by an elongation step at 72°C for 10 minutes.

## 2.6.2. Agarose gel electrophoresis

### 2.6.2.1. 8% gel preparation

In this procedure, 3.6g of agarose was added to a conical flask containing 150 mL distilled water (dH<sub>2</sub>O), and the conical flask was then placed in a microwave for 2–3 minutes. To reach the final volume of 200 mL, 46 mL of dH<sub>2</sub>O and 4 mL of 50X TAE buffer (0.5 M Tris, 1 M acetic acid, 50 mM EDTA pH 8.0) were added to the conical flask. The gel solution was cooled by running the flask under tap water. Then, 7.5 µL of 10 mg/mL ethidium bromide solution (ThermoFisher Scientific) was added to the gel solution before it was poured into a casting tray (Alpha Laboratories, Eastleigh, UK). A comb was inserted, and the gel solution was left to set for 30 minutes. Next, the casting tray containing the gel was submerged in a running tank containing 1XTAE buffer. The comb was carefully removed from the gel, and the PCR products of each sample as well as 4 µL of HyperLadder™ 1 kB (Bioline, London, UK) were then loaded in gel wells. The DNA separation was carried out at 100 V for 75 minutes, and the DNA bands were imaged under UV transilluminators using a BioDoc-It™ System (UVP-Analytik Jena LLC, Upland, US). In the results of the *Itgb3* genotype analysis, the PCR product bands of 538 base pairs (bp) corresponded to *Itgb3*-NULL allele, while the PCR product bands of 446-bp corresponded to the WT allele. In the results of the *pdgfb.CreER* genotype analysis, the PCR product band of 443-bp was positive, whereas if no PCR product was observed, the animal or cell line was considered to be negative.

## 2.7. Endothelial cells Electroporation (Nucleofection)

EC electroporation was performed as described by the manufacturer's (Lonza, Slough) general protocol with a few changes to obtain high survival rates. DNA plasmid concentration was used between 2 to 15µg per reaction, whereas siRNA was resuspended as described by the manufacturer (Dharmacon, Cambridge) at a concentration of 40µM, and 5.6 µl was used per reaction (for a final mass of 3 µg).

### 2.7.1. General procedure

The ECs were washed with pre-warmed PBS, trypsinised with 0.25% trypsin-EDTA and counted as described in **section 2.4**. Then,  $1 \times 10^6$  ECs per nucleofection were transferred to a 50-ml sterile centrifuged tube (for 10 nucleofections,  $10 \times 10^6$  ECs were collected). Following the centrifugation of ECs at 500 g for 4 minutes, the cell pellet was resuspended at a density

of  $1 \times 10^6$  ECs per 100  $\mu\text{L}$  ( $10 \times 10^6$  ECs per 1 mL) of pre-warmed nucleofection buffer (200 mM Hepes, 137 mM NaCl, 5 mM KCl, 6 mM D-glucose, and 7 mM  $\text{Na}_2\text{HPO}_4$  in nuclease-free water; filter sterilised). Then, 100  $\mu\text{L}$  of the suspended ECs was mixed with siRNA or plasmid in a 1.5-mL sterile centrifuged tube before transferring the mixture to an Amaxa-certified cuvette. Next, the cuvette was placed in the Amaxa™ Nucleofector™ II machine (Lonza, Slough). The voltage programme T-005 was used to nucleofect our immortalised ECs. Following the EC electroporation, the ECs were very gently transferred to a sterile universal tube containing 2 ml of pre-warmed IMMLEC medium and then incubated at  $37^\circ\text{C}$  for 10–15 minutes in a 5%  $\text{CO}_2$  incubator to allow them to recover. Finally, the ECs were seeded very gently in the required sizes of culture dishes.

## **2.8. Reusing cuvettes**

The cuvettes were washed and reused over 30 times without decreasing the efficacy of electroporation. Briefly, the cuvettes were rinsed 7 times with  $\text{dH}_2\text{O}$  to remove any remaining cellular debris. Next, 1 mL of 0.2N HCl was added to each cuvette to denature proteins or nucleic acids and the cuvettes were incubated for 10 minutes at room temperature. Finally, the cuvettes were washed 7 times with 70% EtOH and then left to air-dry in a sterile condition a laminar flow cabinet.

## **2.9. Western blot analysis**

### **2.9.1. Lysate preparation**

The ECs were washed twice with PBS before lysing the cells in high-SDS lysis buffer (3% sodium dodecyl sulphate (SDS), 60mM sucrose, 65mM Tris-HCl PH 7.4). The ECs were then scraped off using a rubber policeman, and the lysates were transferred to a 1.5-mL safe lock Eppendorf tube containing acid-washed glass beads (Sigma-Aldrich). Subsequently, the ECs were homogenised for 2 minutes at 50 Hz using a TissueLyser (QIAGEN, Manchester, UK) followed by centrifugation at 16,000 g for 10–15 minutes at room temperature to dissipate the bubbles generated by the homogenisation process. A BioRad DC™ protein assay (BioRad, Hemel Hempstead, UK) was then used as described by the manufacturer to quantify the protein concentrations in the lysates. Briefly, 5  $\mu\text{l}$  of each protein sample and 5  $\mu\text{l}$  of the previously made standard curves were loaded in triplicate in a 96-well plate. Then, 20  $\mu\text{l}$  of reagent S was mixed with 1 mL of reagent A; 25  $\mu\text{L}$  of the total mixture was then

added to each well containing a protein sample or a standard curve. Next, 200  $\mu\text{L}$  of reagent B was added to each well, and the 96-well plate was incubated for 15 minutes at room temperature. The absorbance was read at 750 nm using a VersaMax™ absorbance microplate reader (Molecular Devices, San Jose, US). The protein concentration of each sample was determined by liner regression analysis and compared to the standard curve..

## 2.9.2. Preparing SDS-PAGE gels

To prepare the SDS-PAGE gels, 4X resolving buffer (also called separating or lower buffer) (1.5M Tris – HCL 0.4% SDS H<sub>2</sub>O to 500 ml pH to 8.8) and 4X stacking buffer (also called upper buffer) (0.5M Tris-HCL 0.4% SDS H<sub>2</sub>O to 500 ml pH to 6.8) were made and then stored at 4°C until needed. The required percentage (usually 8% or 10%) of the SDS-PAGE gels was prepared as shown in **Table 2.6** one day before performing the Western blot analysis. Briefly, the resolving gel was prepared in a 50-mL centrifuged tube (see **table 2.6**). However, ammonium persulfate (APS) 10% and TEMED (Invitrogen) were added just prior to pouring the resolving gel buffer because these two chemicals quickly polymerise acrylamide. The resolving gel buffer was then poured in the spacer between the two glass plates, leaving about 2 cm for the stacking gel buffer. Immediately, 400  $\mu\text{L}$  of isopropanol was added in the spacer to remove any bubbles and then left for 15–20 minutes until the resolving gel was completely polymerised. The isopropanol was carefully poured off, and the remaining isopropanol was then washed off with dH<sub>2</sub>O. Similar to the resolving buffer, APS 10% and TEMED were added just prior to pouring the stacking gel buffer. Immediately after pouring, a 10- or 15-well comb was inserted in the spacer and left for 10–15 minutes until the stacking gel was completely polymerised. The SDS-PAGE gel was then wrapped in moist paper towels and stored overnight at 4°C.

**Table 2.6:** Recipes for preparing the resolving and stacking buffer gels

For Making Lower Gel	7%	7.5%	8%	10%	12%	15%	18%
dH <sub>2</sub> O (mL) *	6.2	6	5.8	5	4.2	3	1.8
Acrylamide (mL)	2.8	3	3.2	4	4.8	6	7.2
Resolving gel buffer (mL)	3	3	3	3	3	3	3
APS% ( $\mu\text{L}$ ) *	72	72	72	72	72	72	72
TEMED ( $\mu\text{L}$ ) *	14	14	14	14	14	14	14

For Making Upper Gel	1 Gel	2 Gel
dH <sub>2</sub> O (mL)	2.43	4.86
Acrylamide (mL)	0.5	1
Stacking gel buffer (mL)	1	2
APS% (μL)	72	144
TEMED (μL)	7	14

\* Abbreviations: Distal water (dH<sub>2</sub>O); Ammonium persulfate (APS); Tetramethylethylenediamine (TEMED)

### 2.9.3. Electrophoretic separation of proteins and transferring proteins to a membrane

The following day, 20–40 μg protein from each sample was transferred to 1.5-Eppendorf tubes and mixed with 4X NuPAGE™ LDS sample buffer (Invitrogen) and 10X NuPAGE™ sample reducing (Invitrogen), at a final 1X concentration of each. Then, the protein samples were heated on a dry block thermostat (Grant instrument Ltd, Shepreth, UK) at 95°C for 5 minutes. Next, following the removal of the comb, the gel was clamped into the apparatus, and the tank blotting chamber (BIO RAD) was filled with 1X running buffer. The samples and molecular mass protein markers were then carefully loaded into the wells using gel-loading pipette tips (Star Lab, Hamburg, Germany). The separation of proteins by electrophoresis was performed at 100 V for 2 hours. The separated proteins were transferred onto a 0.45 μm Amersham Protran® nitrocellulose membrane (GE Healthcare, Amersham) using an Xcell surelock blot module (Invitrogen) at 35 V for 160 minutes. The transferred proteins on the nitrocellulose membrane were then stained with 0.1% Ponceau S stain in 5% acetic acid for 3 minutes at room temperature, followed by two washes with dH<sub>2</sub>O to remove the excess Ponceau S stain. Next, the membrane was cut into strips according to the size of the proteins of interest.

### 2.9.4. Primary/secondary antibody incubation and chemiluminescence detection

The membrane was blocked with 5% milk powder/PBS plus 0.1% Tween-20 (ThermoFisher Scientific) for 30 minutes on a rotatest shaker (Luckham LTD, burgess hill, UK) at room temperature, followed by three washes with 0.1% Tween-20 in PBS (PBS/T). The membrane strips (blots) were incubated overnight with diluted primary antibodies (1:1000) (see **Table**

**2.2)** in 5% bovine serum albumin (BSA) in PBS/T on a rotatest shaker at 4°C. Next, the blots were washed three times with PBS/T for 5 minutes each and incubated with horseradish peroxidase (HRP)-conjugated secondary antibodies (see **Table 2.3**) for 2 hours on a rotatest shaker at room temperature in a dark room. Following three washes with PBS/T for 5 minutes each on a rotatest shaker, the blots were incubated with Pierce™ ECL substrate (ThermoFisher Scientific) for 3 minutes at room temperature in a dark room. Finally, a Fujifilm LAS-3000 darkroom (Fujifilm UK Ltd, Bedford, UK) was used to image the chemiluminescence.

### **2.9.5. Western blot analysis**

The density of Western blot bands were measured by Image J™ software, and the signal of each protein was normalised to the loading control (HSC-70 or GAPDH) of the same sample. In the signalling assay, the phosphorylation of VEGFR2 and ERK1/2 were normalised to the total levels of VEGFR2 and ERK1/2 in the same sample, respectively.

### **2.10. Signalling assays**

To analyse the effects of NRP2 depletion on VEGFR2, ERK1/2, NRP1, and ITGB3 expression in our immortalised murine lung ECs, cells were first subjected to electroporation with control-siRNA (Ctrl-siRNA) and NRP2-siRNA (see chapter 3; **Figure 3.2 C-D** for specific information on siRNAs used) as described in **section 2.7**. Following EC nucleofection,  $5 \times 10^5$  ECs were seeded in 6-cm culture dishes pre-coated with 10 µg/mL FN in PBS for 48 hours at 37°C in a 5% CO<sub>2</sub> incubator. Then, the ECs were washed twice with pre-warmed PBS to remove any excess complete medium and replaced by pre-warmed serum-free OptiMEM® for 3 hours to starve the cells. Following EC starvation, OptiMEM® medium was replaced by fresh pre-warmed OptiMEM® medium supplemented by 30 ng/mL VEGF<sub>164</sub> and then incubated sequentially for 5, 15, 30, 45, or 60 minutes at 37°C in a 5% CO<sub>2</sub> incubator. To stop the VEGF stimulation, the dishes were quickly placed on ice, which was followed by two cold PBS washes. The ECs were then subjected to lysing, protein quantification, and protein expression analysis as described in **section 2.7**.

## **2.11. EC detachment assay**

### **2.11.1. Trypsin**

ECs were seeded in five 10-cm dishes pre-coated overnight with 10 µg/ml FN for 24 hours at 37°C in a 5% CO<sub>2</sub> incubator. After washing the adherent cells twice with PBS, the cells adhered in dish 1 were scraped off using a rubber policeman and then lysed with SDS lysis buffer. The ECs adhered in dish 2 were trypsinised, neutralised with pre-warmed IMMLEC medium and centrifuged at 500 g for 4 minutes. The cell pellets were subjected to two PBS washes and two centrifugations at 500 g for 4 minutes to remove the excess remaining medium before lysing the cell pellets with high SDS lysis buffer. The ECs adhered in dishes 3, 4, and 5 were trypsinised, centrifuged at 500 g for 4 minutes, and then resuspended gently in pre-warmed IMMLEC medium. The suspended cells from dishes 3, 4 and 5 were then placed in a CO<sub>2</sub> incubator at 37°C for 1, 2, or 3 hours, respectively. The suspended cells were subjected to centrifugation, PBS washes, and lysing with high-SDS lysis buffer as described for dish 2. The supernatant proteins from the lysed ECs in the five 10-cm dishes were quantified by DC™ protein assay so that equivalent protein masses (20 µg) from each sample could be subjected to Western blot analysis to examine the enzymatic effect of trypsin cleavage on the cell surface receptor proteins, including NRP1, NRP2, ITGA5, ITGA6, and ITGB3.

### **2.11.2. Other cell detachment reagents**

Using the same protocol as described in **subsection 2.11.1**, Gibco TrypLE (kindly provided by Dr Samuel Fountain, UEA, Norwich, UK), Dispase (kindly provided by Dr Ernst Pöschl, UEA, Norwich, UK), sodium saline buffer (1.35M potassium chloride and 0.15M sodium citrate), and different concentrations of EDTA (5mM, 10mM and 15mM) were also used to examine their detaching effect capabilities on our immortalised ECs.

## **2.12. Adhesion assay**

ECs were subjected to electroporation with either Ctrl-siRNA or NRP2-siRNA, as described in **section 2.7**. Following EC nucleofection,  $1 \times 10^6$  of ECs were seeded in 10-cm dishes pre-coated with 0.1% gelatin for 48 hours at 37°C in a 5% CO<sub>2</sub> incubator. One day before the experiment, the 96-well plates were coated overnight with 10 µg/ml FN at 4°C. The adherent cells were washed twice with PBS, trypsinised, and centrifuged at 500 g for 4 minutes. The

cell pellets were then resuspended in pre-warmed serum-free OptiMEM<sup>®</sup>, and the cells were incubated in a suspension state at 37°C for 1 hour to allow cell surface receptor proteins cleaved by trypsin to be re-express on the plasma membrane. Simultaneously, the FN coating solution was removed from the pre-coated 96-well plates and blocked with 5% BSA for 1 hour at room temperature. Wells were then washed once with PBS before seeding  $40 \times 10^3$  cells per condition in eight wells of a 96-well plate. After seeding, the plates were incubated for 15 minutes, 30 minutes, or 3 hours at 37°C in a 5% CO<sub>2</sub> incubator. The 3-hours plate was used as a control for the total number of seeded cells in each condition, while the 15 and 30 minutes plates were used to examine the effect of NRP2 depletion on EC adhesion on FN. After the desired incubation time, wells were subjected to three washes with PBS + 1mM MgCl<sub>2</sub> + 1mM CaCl<sub>2</sub> before fixing the cells with 4% paraformaldehyde (PFA) for 10 minutes at room temperature. The cells were then stained with methylene blue for 30 minutes at room temperature. After the removal of the methylene blue stain, the plates were gently submerged, all at once, in a bucket of dH<sub>2</sub>O until the blue stain disappeared from the negative control (i.e., the cells seeded on BSA only). After the removal of any excess dH<sub>2</sub>O from the wells, the plates were air-dried for 30 minutes at room temperature. The dye from the stained adhered ECs was extracted by a destain solution (50% ethanol and 50% 0.1M HCL) for 10 minutes at room temperature before the absorbance of each well was read at 630 nm.

To analyse the results of the adhesion assay, the relative number of the adhered cells at 15 minutes or 30 minutes in each well was normalised to the relative number of the total cells seeded in the 3-hours plates.

### **2.13. Random migration assay**

One day before the experiment was performed, 10-cm dishes were coated overnight with 10 µg/ml FN at 4°C. The ECs were subjected to electroporation with siRNA (Ctrl-siRNA or NRP2-siRNA), as described in the ECs electroporation (see **section 2.7**), and  $1 \times 10^6$  cells were seeded in 10-cm dishes pre-coated with 10 µg/ml FN for 48 hours at 37°C in a 5% CO<sub>2</sub> incubator. Twenty-four hours before the cells were trypsinised, a 24-well plate was coated overnight with 10 µg/ml FN at 4°C. Next, the ECs were trypsinised, resuspended in serum-free OptiMEM<sup>®</sup>, and seeded at a concentration of  $7 \times 10^4$  cells from each condition in triplicate wells on a 24-well plate pre-coated with 10 µg/ml FN for 3 hours at 37°C in a 5% CO<sub>2</sub> incubator to starve and allow the cells to adhere in the wells. Following starvation, the medium in half of the plate was replaced by only fresh serum-free OptiMEM<sup>®</sup> plus 2% FBS,

while the medium in the other half of the plate was replaced by fresh serum-free OptiMEM<sup>®</sup> plus 2% FBS supplemented by 30 ng/mL VEGF<sub>164</sub>. Fixed images of multiple fields/well in each condition were taken every 10 minutes for 15 hours at 37°C and 5% CO<sub>2</sub> using an inverted Axiovert (Carl Zeiss Ltd, Cambridge, UK) microscope with one-phase contrast.

To analyse the results of random migration assays, individual cells in different fields/well in the same condition were manually tracked using the ImageJ<sup>™</sup> cell tracking plugin, and the migration speed of each individual cell was calculated in µm/hour.

## **2.14. Wound healing migration assay**

ECs were nucleofected with siRNA (Ctrl-siRNA or NRP2-siRNA), seeded in 10-cm dishes pre-coated with FN as described in the random migration assay and incubated for 24 hours at 37°C in a 5% CO<sub>2</sub> incubator. On day of nucleofection, 6-well plates were coated overnight with 10 µg/ml FN at 4°C. Twenty-four hours post nucleofection, the ECs were trypsinised, resuspended in IMMLEC medium, and seeded at a high density of 5×10<sup>5</sup> cells of each condition in quadruple wells of the 6-well plates. Then, the plates were incubated for another 24 hours at 37°C in a 5% CO<sub>2</sub> incubator. Forty-eight hours post nucleofection, IMMLEC medium was replaced by serum-free OptiMEM<sup>®</sup> for 3 hours to starve the cells. Following starvation, manual scratching of the confluent monolayer of ECs using a P200 pipette tip was performed. The serum-free OptiMEM<sup>®</sup> containing debris caused by scratching in two wells of each condition was replaced by only fresh serum-free OptiMEM<sup>®</sup> plus 2% FBS, while the serum-free OptiMEM<sup>®</sup> in the other two wells of each condition was replaced by fresh serum-free OptiMEM<sup>®</sup> plus 2% FBS supplemented by 30 ng/mL VEGF<sub>164</sub>. Using an axiovert 40/cfl inverted microscope (Carl Zeiss Ltd), phase contrast images of scratches were captured on the day of scratching (time 0), and the plates were then incubated at 37°C in a 5% CO<sub>2</sub> incubator. Then, phase contrast images of the same scratches were captured every 24 hours. Most wounds closed between 48–72 hours post scratching.

To analyse the wound healing assay, the closure distance of each captured wound was calculated by normalising the closure distance after 24 hours or 48 hours to the starting wound at time 0.

## 2.15. Proliferation assays

### 2.15.1. WST-1

ECs were treated with siRNAs and seeded in 10-cm dishes for 48 hours at 37°C in a CO<sub>2</sub> incubator. Twenty-four hours before the cells were trypsinised, 96-well plates were coated overnight with 10 µg/ml FN at 4°C. Following trypsinisation, 7,000 cells from each condition were seeded in a final volume of 100 µl of culture medium in two 96-wells plates. One plate was left for 4 hours (this plate served as a control for the total number of seeded cells in each condition). The second plate was left for 24 hours. At the end of each incubation period, 10 µl of WST-1 was added to each well and the plates were left for an additional 2 hours, then the absorbance of each well was measured at 450 nm.

To analyse the results of the WST-1 proliferation assay, the absorbance of each well at 24 hours was normalised to the absorbance at 4 hours.

### 2.15.2. BrdU

ECs were treated with siRNA and seeded in 10-cm dishes pre-coated with 0.1% gelatin for 30 hours at 37°C in a 5% CO<sub>2</sub> incubator. One day before the cells were trypsinised, 4 acid-washed/oven-sterilised glass coverslips were transferred into each well of a 6-well plate. Then, the coverslips were coated with 10 µg/ml FN at 4°C. Thirty hours post nucleofection, the cells were trypsinised and centrifuged at 500 g for 4 minutes. The cell pellets were resuspended in pre-warmed serum-free OptiMEM<sup>®</sup> and seeded onto the coverslips for 4 hours to allow the cells to adhere. In the meantime, 10 µM BrdU 5-bromo-2'-deoxyuridine (Abcam) labelling solution was made in a IMMLEC medium and filtered sterilised through a 0.2-µm filter. Next, the serum-free OptiMEM<sup>®</sup> was replaced by the 10 µM BrdU labelling solution and the cells were incubated for another 12 hours at 37°C in a 5% CO<sub>2</sub> incubator. Thereafter, the BrdU labelling solution was removed and two washes with PBS (15 seconds each) were performed. An additional three PBS washes at 2 minutes each were carried out before the cells were fixed with 4% PFA for 10 minutes at room temperature. For staining, the coverslips were incubated with 1N HCL for 30 minutes at room temperature to hydrolyse the DNA. Then, the cells were permeabilised with PBS + 0.25% Triton X-100 for 10 minutes at room temperature. Following permeabilization, the coverslips were blocked in Dako<sup>®</sup> Protein Block Serum-Free for 30 minutes at room temperature. The coverslips were washed once

with PBS before incubation in a 60  $\mu$ L volume of 1:20 sheep anti-BrdU overnight at 4°C in a humidified chamber. The following day, unbound primary antibody was washed off three times with PBS before the coverslips were incubated with donkey anti-sheep IgG antibody conjugated to Alexa 633 for 45 minutes at room temperature in a humidified chamber. Unbound secondary antibody was then washed off three times with PBS. The coverslips were individually dipped three times in a pocket of dH<sub>2</sub>O to remove the excess salt and then left to dry for 5 minutes at room temperature in a dark room. Next, the coverslips were mounted with ProLong™ Gold Antifade Mountant with DAPI (ThermoFisher Scientific) to stain the nucleus in blue and then cured in a dark room at room temperature. The coverslips were then sealed by nail varnish.

For BrdU proliferation assay analysis, the percentage of cells in S-phase of the cell cycle was determined by dividing the number of the BrdU-labelled cells by the total number of cells (as determined by DAPI staining) on the coverslip.

## **2.16. Protein and FA turnover assay**

In this assay,  $1 \times 10^6$  ECs were double nucleofected with Ctrl-siRNA or NRP2-siRNA and GFP-paxillin constructs (3  $\mu$ g) or ITGA5-GFP constructs (tested 3–8 $\mu$ g) (both kindly provided by Dr Maddy Parsons, King's College, London) and seeded in 10-cm dishes pre-coated with 10  $\mu$ g/ml FN for 24 hours at 37°C in a 5% CO<sub>2</sub> incubator. After 24 hours, the cells were washed with PBS, trypsinised, counted, and seeded at a low density of  $4 \times 10^4$  cells per condition on acid-washed/oven-sterilised glass coverslips (2 per well in a 6-well plate) pre-coated with 10  $\mu$ g/ml FN for another 24 hours at 37°C in a 5% CO<sub>2</sub> incubator. Forty-eight hours post nucleofection, one coverslip at a time was washed once with pre-warmed PBS, fixed carefully in a Ludin chamber (Life Imaging Services GmbH, Basel, Switzerland), and live-imaged in OptiMEM® phenol-red free medium supplemented with 2% FBS and P/S at 37°C and 5% CO<sub>2</sub> using an inverted Axiovert (Carl Zeiss Ltd) microscope in which an individual cell was captured every one minute for 30 minutes.

The focal adhesion assembly and disassembly speeds were analysed by manually tracking the number of selected GFP-paxillin-positive focal adhesions using the Image J™ MTrackJ plugin software.

## 2.17. Immunocytochemistry

ECs were treated with siRNA (Ctrl-siRNA or NRP2-siRNA) and seeded on 10-cm dishes pre-coated with 10 µg/ml FN at 37°C for 36 hours in a 5% CO<sub>2</sub> incubator. The following day, acid-washed/oven-sterilised glass coverslips were placed into each well of a 6-well plate (4 per well) and coated overnight with 10 µg/ml FN at 4°C. Thirty-six hours post nucleofection, the cells were washed with pre-warmed PBS, trypsinised, counted, and seeded at low density on the aforementioned coverslips for 12 hours. The cells grown on the coverslips were carefully washed twice with pre-warmed PBS before performing a fixation step with 4% PFA for 10 minutes at room temperature. This step was followed by cell permeabilization with 0.25% Triton X-100 in PBS for 10 minutes at room temperature. Next, the permeabilised cells were blocked by with 5% BSA + 1% goat/donkey serum (depending on the secondary antibody used) in PBS in a 6-well plate at room temperature for 30 minutes. The ECs were then incubated overnight in a humidified chamber at 4°C with 60 µL of the required primary antibodies in PBS: anti-ITGA5 at 1:250; anti-NRP2 (various dilutions tested: 1:100, 1:150 and 1:200). Two washes with PBS were performed to remove the unreacted primary antibody, followed by incubation with fluorescently labelled secondary antibodies in PBS at 1:500 for 1 hour at room temperature in a dark room. Next, three washes with PBS were performed followed by one wash with dH<sub>2</sub>O before drying the coverslips for 5 minutes at room temperature in a dark room. The coverslips then were mounted with ProLong™ Gold Antifade Mountant with DAPI. The coverslips were then cured overnight at room temperature in a dark room. Finally, the coverslips were sealed with nail varnish around their edge and allowed to dry for 1 hour at room temperature. At this stage, the coverslips were either stored at 4°C or imaged directly using an Axioplan Epifluorescent microscope (Carl Zeiss Ltd) and the AxioCam MRm camera (Carl Zeiss Ltd).

ITGA5 was analysed by measuring the length of ITGA5 in both siRNA-treated conditions using the ImageJ™ software plugin (simple neurite tracer).

## 2.18. Immunoprecipitation

One day before the experiment was performed, 10-cm dishes were coated overnight with 10 µg/ml FN at 4°C. The ECs were washed with pre-warmed PBS, detached with 0.25% trypsin-EDTA, neutralised with IMMLEC, and then counted and nucleofected as described in **section 2.7** by either Ctrl-siRNA or NRP2-siRNA and seeded at a density of  $2 \times 10^6$  cells per 10-cm

dish that had been pre-coated with 10 µg/ml at 37°C in a 5% CO<sub>2</sub> incubator. Forty-eight hours later, the ECs were placed on ice, washed twice with cold PBS, and then lysed in a cold lysis buffer [25mM Tris-HCl (pH 7.6), 100mM NaCl, 0.15% Tween-20, 5% glycerol, 0.5mM ethylene glycol tetra acetic acid (EGTA), and Halt<sup>®</sup> Protease and Phosphatase inhibitor cocktail (1:100)] using a rubber policeman. The lysates were transferred to correspondingly labelled 1.5-mL Eppendorf tubes, incubated for 20 minutes on ice, and then centrifuged at 15,000 g for 20 minutes at 4°C. The amount of protein per lysate was quantified using the DC<sup>™</sup> protein assay as described in **section 2.9.1**. Protein-G Dynabeads<sup>®</sup> (Invitrogen) were washed once with 200 µL of 0.02% Tween<sup>®</sup>-20/PBS and then coupled to the antibody of interest (NRP2 or biotin) in a tube rotator for 10 minutes at room temperature. Next, the tubes were placed in the magnet, the supernatant was removed, and the coupled Dynabeads-antibody complex was washed once with 200 µL of 0.02% Tween<sup>®</sup>-20/PBS. The tubes were placed back in the magnet, and the supernatant was discarded before the coupled Dynabeads-antibody complex was immunoprecipitated with an amount equivalent to 1,200 µg of total protein from each sample overnight in a tube rotator at 4°C. The following day, the immunoprecipitated samples were washed three times with 200 µL of the lysis buffer, once with 100 µL of PBS, and then transferred to new 1.5-mL Eppendorf tubes to avoid the co-elution of proteins bound to the tube wall. The tubes were placed in the magnet, and the supernatant was discarded. To detect the NRP2 co-associated proteins, the immunoprecipitated Dynabeads complex was eluted with 1X NuPAGE<sup>®</sup> sample buffer in H<sub>2</sub>O in a total volume of 20 µL, heated at 95°C for 5 minutes, and separated by SDS-PAGE. The proteins were transferred to nitrocellulose, probed with anti-ITGA5, and detected by chemiluminescence as described in the **subsection 2.9.3 to 2.9.5**. For silver staining or mass spectrometry, the immunoprecipitated Dynabeads complex was eluted in 20 µL of high-SDS lysis buffer.

### **2.18.1. Silver staining**

The silver staining assay was performed to confirm the efficiency of NRP2 coimmunoprecipitation. Briefly, from 20 µL of the eluted Dynabeads complex, 5 µL was mixed with 1X NuPAGE<sup>®</sup> sample buffer, heated at 95°C for 5 minutes and then separated by SDS-PAGE. The remaining 15 µL drawn from each coimmunoprecipitated sample were stored at -20°C for the mass spectrometry. The SDS-PAGE gel was silver stained as described by the manufacturer using Pierce<sup>™</sup> Silver Stain (ThermoFisher Scientific). The

efficiency of NRP2 coimmunoprecipitation was confirmed by comparing the immunoprecipitated samples to 1  $\mu$ l of total cell lysate (TCL). The SDS-PAGE gel was placed in a single clean tray, washed twice at 5 minutes each in ultrapure water and then fixed twice at 15 minutes each in a 30% ethanol: 10% acetic acid solution. Following fixation, the SDS-PAGE gel was subjected to a series of washes: two washes at 5 minutes each in 10% ethanol; two washes in ultrapure water; one wash for 1 minute in a sanitiser working solution; and two washes in ultrapure water. The SDS-PAGE gel was then stained for 30 minutes in a stain working solution followed by washing twice in ultrapure water at 20 seconds each. Next, the stain was developed in a developer working solution until the bands on the gel appeared (2–3 minutes). When the density of the bands reached the required degree, the SDS-PAGE gel was treated with 5% acetic acid for 10 minutes to stop the development of the bands.

### **2.18.2. Mass spectrometry**

After confirming the efficiency of the coimmunoprecipitation samples in the silver staining experiment, 15  $\mu$ L of the remaining coimmunoprecipitation samples were sent to the Fingerprints Proteomics Facility (Dundee University, Dundee, UK), which carried out label-free quantitative mass spectrometry and peptide identification using the MaxQuant software based on the Andromeda peptide database as described by (Schiller, Friedel et al. 2011). Each sample was analysed in three technical repeats using a mass spectrometer machine. Non-statistical analysis was performed to visually represent the data with no assumption about the number of repeat. The Log 2 of peptides detected more in the immunoprecipitated Ctrl-siRNA samples than that in NRP2-depleted samples were considered as specific binding partner proteins with NRP2, whereas those detected more in the NRP2-depleted samples than that in Ctrl-siRNA were considered as non-specific binding partners with NRP2.

### **2.19. Flow cytometry (FC)**

ECs were trypsinised, counted, nucleofected with either Ctrl-siRNA or NRP2-siRNA, and seeded in 10-cm dishes that had been pre-coated with 10  $\mu$ g/ml FN for 48 hours at 37°C in a 5% CO<sub>2</sub> incubator. Untreated ECs were also seeded in 10-cm dishes that had been pre-coated with 10  $\mu$ g/ml FN and incubated for 48 hours at 37°C in a 5% CO<sub>2</sub> incubator. For the flow cytometric analysis, the ECs were detached using a pre-warmed sodium saline buffer (1.35M potassium chloride and 0.15M sodium citrate) for 4–5 minutes at 37°C in a 5% CO<sub>2</sub>

incubator. They were then neutralised with IMMLEC medium and centrifuged at 500 g for 4 minutes. Next, a  $1 \times 10^6$  EC pellet from each condition (Ctrl-siRNA, NRP2-siRNA, and untreated ECs) was resuspended in 1 mL of fluorescence activated cell sorting (FACS) buffer (1% FBS in PBS + 1mM  $\text{CaCl}_2$  + 1mM  $\text{MgCl}_2$ ), transferred to an Eppendorf tube, and then centrifuged at 270 g for 4 minutes at 4°C. The supernatant was then removed. A second wash with 1 mL FACS buffer and centrifugation at 270 g for 4 minutes at 4°C were performed before transferring 100  $\mu\text{L}$  (i.e.,  $1 \times 10^5$  ECs) from each condition to new Eppendorf tubes. Next, the ECs in each Eppendorf tube were incubated for 30 minutes at 4°C with the following labelling antibodies (used at 1:200): PE-anti-mouse CD49e (ITGA5); Arm. hamster IgG isoform control. The tubes were centrifuged at 270 g for 4 minutes at 4°C. The pellet in each tube was then washed and centrifuged twice at 4°C with 500  $\mu\text{L}$  FACS. The cell pellet in each tube was then resuspended in 300  $\mu\text{L}$  of cold FACS buffer and transferred to a flow cytometric tube (Sarstedt Ltd, Leicester, UK). Finally, the cell surface receptor proteins were measured using CytoFLEX flow cytometry (Beckman Coulter, Brea, USA) and analysed using FlowJo software<sup>TM</sup> (FlowJo LLC, Ashland, Oregon).

## **2.20. Subcellular protein fractionation assay**

ECs were treated with Ctrl- or NRP2-siRNA as described in **section 2.7**. Then, the nucleofected ECs were seeded in two 10-cm dishes that had been pre-coated with 10  $\mu\text{g}/\text{ml}$  FN per condition at a density of  $2 \times 10^6$ /dish for 24 hours at 37°C in a 5%  $\text{CO}_2$  incubator. The cells from each condition were trypsinised, counted, and seeded in a T75 flask that had been pre-coated with 10  $\mu\text{g}/\text{ml}$  FN at a density of  $3 \times 10^6$ /flask for 24 hours at 37°C in a 5%  $\text{CO}_2$  incubator. The cells were detached with sodium saline buffer, transferred to 50-mL centrifuged tubes, centrifuged at 500 g for 4 minutes, washed once with PBS, and then transferred to 1.5-mL centrifuged tubes. The supernatants were carefully discarded, and the obtained pellets were subjected to the cellular protein fractionation assay as described by the manufacturer (ThermoFisher Scientific) to sequentially extract proteins located in five different cellular compartments: the cytoplasm, cellular membranes, soluble nucleus, chromatin-bound nucleus, and cytoskeleton. The sequential extraction of the proteins was based on different extraction buffers and different centrifugation speeds. Briefly, ice-cold cytoplasmic extraction buffer (CEB) was added to the cell pellet of each siRNA-treated EC (Ctrl-siRNA and NRP2-siRNA), incubated at 4°C for 10 minutes, and centrifuged at 500 g for 5 minutes. The supernatant (cytoplasmic extract) was immediately transferred to a new

1.5-mL centrifuged tube on ice. Then, ice-cold membrane extraction buffer (MEB) was added to the cell pellet, which was incubated at 4°C for 10 minutes and centrifuged at 3,000 g for 5 minutes. The supernatant (membrane extract) was immediately transferred to a new 1.5-mL centrifuged tube on ice. Then, ice-cold nuclear extraction buffer (NEB) was added to the cell pellet, incubated at 4°C for 10 minutes, and centrifuged at 5,000 g for 5 minutes. The supernatant (soluble nuclear extract) was immediately transferred to a new 1.5-mL centrifuged tube on ice. Then, NEB at room temperature was added to the cell pellet, incubated at room temperature for 15 minutes, and centrifuged at 16,000 g for 5 minutes. The supernatant (chromatin-bound nuclear extract) was immediately transferred to a new 1.5-mL centrifuged tube on ice. Next, pellet extraction buffer (PEB) at room temperature was added to the cell pellet, incubated at room temperature for 15 minutes, centrifuged at 16,000 g for 5 minutes. The supernatant (cytoskeletal extract) was immediately transferred to a new 1.5-mL centrifuged tube. Finally, the extracted proteins from the five cellular compartments were separated by SDS-PAGE, and then a Western blot analysis was performed as described in the **subsection 2.9.3 to 2.9.5**.

The analysis was performed by normalising the total level of ITGA5 in each compartment to the total level of the control protein for that compartment: ERK1/2 for cytoplasmic extract; VEGFR2 for cellular membrane extract; vimentin for cytoskeletal extract.

## **2.21. Protein stability assay**

ECs were treated with either Ctrl- or NRP2-siRNA as described in **section 2.7** and seeded in a T75 flask that had been pre-coated with 10 µg/ml FN per condition at a density of  $4 \times 10^6$ /flask for 24 hours at 37°C in a 5% CO<sub>2</sub> incubator. The cells were trypsinised, counted, centrifuged, resuspended in serum-free OptiMEM<sup>®</sup>, and seeded per condition at a density of  $2 \times 10^6$  cells in two 10-cm dishes that had been pre-coated with 10 µg/ml FN for 12 hours at 37°C in a 5% CO<sub>2</sub> incubator. Then, 10 µg/ml of cycloheximide (Cell Signalling Technology) was added to one dish per condition for eight hours as described by (Sampieri, Nuttall et al. 2008); the second dish was left untreated as the control. Following lysing the cells with high-SDS lysis buffer, the amount of protein per lysate was quantified by the DC<sup>TM</sup> protein assay, separated by SDS-PAGE, and subjected to a Western blot analysis as described in the **subsection 2.9.3 to 2.9.5** to determine NRP2 and ITGA5 stability.

Using the ImageJ™ software, the ITGA5 densitometry in the samples treated with cycloheximide was compared to that in the untreated samples.

## 2.22. Protein cell surface internalisation assay

ECs were treated with either Ctrl-siRNA or NRP2-siRNA, as described in the nucleofection protocol (see **section 2.7**), and seeded at a density of  $2 \times 10^6$  cells per 10-cm dish (total of 12 dishes), which had been pre-coated with 10  $\mu\text{g/ml}$  FN, for 48 hours at 37°C in a 5% CO<sub>2</sub> incubator (see chapter 5; **Figure 5.6 A**). The cells were washed with pre-warmed PBS to remove excess IMMLEC medium and then starved in pre-warmed serum-free OptiMEM® for 3 hours at 37°C in a 5% CO<sub>2</sub> incubator. Following starvation, the dishes were placed on ice for 5 minutes, followed by two washes with ice-cold Soerensen buffer (SBS) 7.8 pH (14.7mM KH<sub>2</sub>PO<sub>4</sub>, 2mM Na<sub>2</sub>HPO<sub>4</sub>, and 120mM Sorbitol pH 7.8) (Remacle, Murphy et al. 2003). Next, the EC cell surface proteins were labelled with 0.3 mg/ml of EZ-Link Sulfo-NHS-SS-Biotin (ThermoFisher Scientific) in SBS 7.8 pH for 30 minutes at 4°C. Then, SBS containing biotin solution was poured off, and the unreacted biotin was quenched with 100mM glycine for 10 minutes at 4°C. Another two washes with ice-cold SBS pH 7.8 were conducted to remove excess glycine solution. Next, one dish per siRNA-treated cells (i.e., a dish from Ctrl-siRNA and NRP2-siRNA) was incubated in pre-warmed serum-free OptiMEM® for 2, 4, 10, and 20 minutes (total of 8 dishes) at 37°C in a 5% CO<sub>2</sub> incubator. Simultaneously, two dishes per siRNA-treated ECs (total of 4 dishes) were maintained at 4°C for use as positive/negative (+/- Mesna) controls (see below). The incubation step was performed to allow the labelled cell surface proteins to internalise inside the cells at different time points. After each incubation time, the dishes were immediately placed on ice to stop the internalisation of the cell surface proteins, which was followed by two washes with ice-cold SBS pH 8.2. Next, all 10 dishes were incubated with 100mM Mesna (2-mercaptoethane sulfonate Na) (Sigma-Aldrich) to strip the biotin from the cell surfaces in SBS pH 8.2 or Tris base buffer (50mM Tris-HCl, pH 8.6; 100mM NaCl) for 75 minutes at 4°C, with the exception of two (- Mesna) control dishes (a dish from each siRNA-treated EC) were immediately lysed in lysis buffer (25mM Tris-HCl, pH 7.4, 100mM NaCl, 2mM MgCl<sub>2</sub>, 1mM Na<sub>3</sub>VO<sub>4</sub>, 0.5 mM EGTA, 1% Triton X-100, 5% glycerol, and protease inhibitors) and then transferred to 1.5-mL tubes on ice. The (- Mesna) controls were used to determine the total biotin-labelled cell surface proteins on the EC plasma membranes. The (+ Mesna) controls were used to determine the efficacy of biotin removal from the surface of the EC

cells. Following the biotin stripping step, the Mesna solution was poured off, and the excess Mesna was quenched with 100mM iodoacetamide (Sigma-Aldrich) for 10 minutes at 4°C. The ECs in all dishes were washed twice with SBS pH 8.2 and then lysed. The lysates were transferred to 1.5-mL tubes on ice. Then, the lysates were cleared by centrifugation at 12,000 g for 20 minutes at 4°C. The supernatant proteins were placed in clean 1.5-mL tubes and quantified using a DC™ protein assay in the **subsection 2.9.1**. The equivalent protein concentration in each sample was immunoprecipitated with Dynabeads-coupled to mouse anti-biotin antibody overnight at 4°C as described in the immunoprecipitation assay (see **section 2.18**). The immunoprecipitated biotin-labelled proteins were separated by SDS-PAGE and then subjected to a Western blot analysis.

The densitometry analysis of the ITGA5 bands was measured using Image J™ software. The level of the internalised ITGA5 at each time of incubation was normalised to the (- Mesna) control, that is, the total ITGA5 on the plasma membrane.

### **2.23. Protein cell surface recycling assay**

ECs were treated with siRNA (Ctrl-siRNA or NRP2-siRNA) and seeded at a density of  $2 \times 10^6$  cells per 10-cm dish (total of 20 dishes) pre-coated with 10 µg/ml FN for 48 hours at 37°C in a 5% CO<sub>2</sub> incubator (see chapter 5; **Figure 5.7 A**). EC starvation, cell surface protein labelling, and biotin quenching were all performed in the same manner as the internalisation assay (see **section 2.22**). Following another two washes with ice-cold SBS pH 7.8 to remove any excess of glycine solution, eight dishes per siRNA-treated ECs (total of 16 dishes) were incubated in pre-warmed serum-free OptiMEM® for 20 minutes at 37°C in a 5% CO<sub>2</sub> incubator to allow all biotin-labelled cell surface proteins to internalise in the ECs. Two dishes per siRNA-treated ECs (total of 4 dishes) were maintained at 4°C for use as positive and negative controls. The rest of dishes were immediately transferred to ice to stop the internalisation process, which was followed by two washes with ice-cold SBS pH 8.2. Any un-internalised biotin-labelled proteins were then stripped off by treatment with 100mM Mesna in Tris buffer for 75 minutes at 4°C. Next, two dishes for each subsequent time point (i.e., two dishes of Ctrl-siRNA-treated cells and two dishes of NRP2-siRNA-treated cells per condition) were incubated in pre-warmed serum-free OptiMEM® for 2, 4, 10, and 20 minutes (total of 8 dishes per siRNA treatment) at 37°C in a 5% CO<sub>2</sub> incubator. This incubation step was performed to allow recycling of the already internalised biotin-labelled proteins back to the plasma membranes. After each incubation time, the dishes were immediately placed on

ice to stop the recycling process, which was followed by two washes with ice-cold SBS pH 8.2. One dish from each condition was subjected to Mesna incubation for 75 minutes at 4°C to strip off the recycled biotin-labelled proteins. The second dish was left at 4°C with no Mesna treatment. After the biotin was stripped, the Mesna solution was poured off, and the excess Mesna was quenched with 100mM Iodoacetamide for 10 minutes at 4°C. The cell lysing, biotin immunoprecipitation, protein separation by SDS-PAGE, and Western blot analysis for ITGA5 were performed in the same manner as the internalisation assay (see **section 2.22**).

The densitometry analysis of the ITGA5 bands was measured using ImageJ™ software. The level of the recycled ITGA5 in the EC plasma membranes was determined by normalising the amount of ITGA5 in each siRNA-treated cell to the total amount of ITGA5 on the EC plasma membranes of the Mesna-untreated cells in the same period of incubation.

## **2.24. Building shRNA constructs**

### **2.24.1. Target sequence selection**

Based on the criteria of the PSICOLIGOMAKER1.5 programme, which were established by Ventura *et al.* (Ventura, Meissner *et al.* 2004), our target sequences and the shRNA oligonucleotides (Oligo) were selected and designed, respectively. Briefly, the mouse NRP2 gene sequence (ENSMUSG00000025969) was first downloaded from the Ensemble Genomes Database Project browser, which was established by Hubbard *et al.* (Hubbard, Barker *et al.* 2002). The sequence was then pasted in the sequence window displayed in the PSICOLIGOMAKER1.5 programme, and a cut-off value (from -2 to 9) was selected before clicking “search”. Based on the criteria established by Reynolds *et al.* (Reynolds, Leake *et al.* 2004), all potential 19 oligomers (19-mers) were then listed in the right window in addition to a score equal or higher than the cut-off value. Reynolds *et al.* demonstrated that 19-mers with a value higher than 6 exhibited an approximately 90% chance of silencing of the target messenger RNA (mRNA). Because no target sequence higher than 7 were listed by the programme, only the target sequences containing 19-mers with a score of 7 were selected.

### 2.24.2. Oligomer design

Using the PSICOLIGOMAKER1.5 programme, the selected target sequences were simply pasted in the left “target” window, where both the forward (sense) and reverse (antisense) oligos (in the 5' to 3' orientation) were generated by applying the following formulas:

**Sense:** 5'-T-(complement sequence of 19-mers)-TTCAAGAGA-(reverse complement sequence of 19-mers)-TTTTTTC-3'

**Antisense:** 5'-TCGAGAAAAAA-(complement sequence of 19-mers)-TCTCTTGAA-(reverse complement sequence of 19-mers)-A-3'

Following the design of the oligos, 5'phosphorylated oligos were ordered (Invitrogen) and resuspended accordingly in nuclease-free water (ThermoFisher Scientific) for 30 minutes at room temperature to a final concentration of 100µM. The oligos were then stored at -80°C until they were needed.

### 2.24.3. Vector digestion and extraction

The pSico vector (Plasmid for Stabile Interference Condition) and the pSico reverse vector (pSicoR), which are based on the pLL3.7 lentiviral vector developed by Rubinson *et al.* (Rubinson, Dillon et al. 2003), were ordered from Addgene (Cambridge, US). The pSico or the pSicoR vector was then digested with HpaI and XhoI restriction enzymes on a heat block at 37°C for 1 hour. The reaction for each digested plasmid was prepared as follows: 10 µg of vector; 1 µl of XhoI; 3 µl of HpaI; 5 µl of CutSmart Buffer (New England Biolabs, Hitchin, UK) and nuclease-free water to a total volume of 50 µL. Next, the digested vectors were mixed with 6X gel loading dye (New England Biolabs) before being separated in 1% agarose gel at 100 V for 90 minutes. Under a long-wave UV light, the DNA bands were cut using a scalpel, and the gel blocks were transferred to 1.5-mL tubes. Using the QIAquick Gel Extraction Kit (QIAGEN), the digested vectors were extracted and then eluted in 30 µL of elution buffer (EB) as described by the manufacturer. Vector concentrations were quantified using a NanoDrop ND-1000 UV/Vis spectrophotometer (NanoDrop Technologies Inc, Wilmington, US).

### 2.24.4. Oligo annealing

Following resuspension, the oligos were annealed as suggested by Ventura *et al.* (Ventura, Meissner et al. 2004). Briefly, the annealing reaction for each target sequence was first

prepared in one well of a 96-well PCR plate in a total volume reaction of 50  $\mu\text{L}$  as follows: 23  $\mu\text{L}$  of nuclease-free water; 1  $\mu\text{L}$  of sense oligo; 1  $\mu\text{L}$  of antisense oligo; and 25  $\mu\text{L}$  of 2X annealing buffer (200mM potassium acetate, 60mM HEPES-KOH pH 7.4, and 4mM magnesium acetate). Next, the PCR plate was placed in a programmed thermal cycler PCR machine in which the annealing reaction started with a denaturation step at 95°C for 4 minutes, followed by annealing step at 70°C for 10 minutes, and finally a slow cooling step at 4°C.

#### **2.24.5. Vector-oligo (pconstruct) ligation**

The ligation of each annealed oligo to the digested vector (pSico or pSicoR) was performed in a well of a 96-well PCR plate in a total volume reaction of 10  $\mu\text{L}$  ligation reaction, as suggested by Ventura *et al.* (Ventura, Meissner et al. 2004). Briefly, 1  $\mu\text{L}$  of each annealed oligo was first diluted in 19  $\mu\text{L}$  of nuclease-free water. Next, 1  $\mu\text{L}$  of the diluted oligo was mixed with the following: 100 ng of digested vector; 1  $\mu\text{L}$  of 10X ligation buffer; 1  $\mu\text{L}$  of T4 DNA ligase (New England Biolabs, Hitchin); and nuclease-free water to a total reaction of 10  $\mu\text{L}$ . The ligation was performed overnight at 16°C.

#### **2.24.6. Bacterial transformation and colony selection**

One Shot Stb13 chemically competent *E. coli* (Invitrogen) was used. The ligated plasmid was transferred to *E. coli* as described by the manufacturer. Briefly, 1  $\mu\text{L}$  from pSico or pSicoR plasmid was transferred to a vial of *E. coli* bacteria, thawed on ice for 30 minutes, heat-shocked for 45 seconds at 42°C, and then placed on ice for 2 minutes before 250  $\mu\text{L}$  of pre-warmed SOC medium was added to each bacterial vial. The vials were incubated in an Innova™ 4330 incubator shaker (New Brunswick Scientific, Cambridge, UK) for 1 hour. Next, 100  $\mu\text{L}$  of the transformation from each bacterial vial was spread on 1.5% agar containing 100  $\mu\text{g}/\text{ml}$  ampicillin, and the plates were incubated overnight at 37°C in an inverted manner. Using one sterile pipette tip per bacterial colony, 6–10 colonies were randomly selected and grown in 25-mL tubes containing 2 mL of sterile lysogeny broth (LB) medium supplemented by 100  $\mu\text{g}/\text{mL}$  ampicillin in an Innova™ 4330 incubator shaker overnight at 37°C.

### **2.24.7. Plasmid miniprep**

Using EZNA<sup>®</sup> Plasmid DNA Mini kit (Omega Bio-Tek, Norcross, US), plasmid DNA was isolated as described by the manufacturer at room temperature. Briefly, 1 mL of overnight-cultured bacteria from each selected colony was centrifuged at 10,000 g for 1 minute. The generated pellet was then resuspended in 250  $\mu$ L of buffer containing RNase. This step was followed by the addition of 250  $\mu$ L SDS-based lysis buffer for 2–3 minutes and then 350  $\mu$ L of a precipitation buffer. A centrifugation step at a maximum speed ( $> 13,000$  g) for 10 minutes was then performed to generate a compact white pellet. The supernatant was carefully passed through a HiBind<sup>®</sup> DNA Mini collection column tube by centrifugation at maximum speed for 1 minute, followed by the addition of 350  $\mu$ L of a high salt washing buffer containing isopropanol to the DNA collected in the column tube and centrifugation at maximum speed for 1 minute. The collected DNA was then washed twice with 700  $\mu$ L DNA washing buffer containing 100% EtOH, followed by centrifugation at a maximum speed and a drying step. The collected DNA was then eluted in a new 0.5-mL centrifuge tube with 30–50  $\mu$ L of an EB pre-heated at 70°C. Then, the plasmid concentration was quantified using a NanoDdrop spectrophotometer.

### **2.24.8. Plasmid digestion and positive clone detection**

The collected pSico or pSicoR plasmid from the plasmid miniprep was subjected to a digestion test with restriction enzymes to detect the plasmids containing the target sequences (i.e., positive clones). Briefly, 1,000 ng/ $\mu$ l of pSico and pSicoR plasmid was digested with SacII-NotI and XhoI-XbaI (New England Biolabs), respectively, in 10X buffer-2 (New England Biolabs) and nuclease-free water in a total volume of 20  $\mu$ L for 1 hour on a heat block at 37°C. The activity of the restriction enzymes in buffer-2 was used as suggested by the manufacture as follows: Not I (50%); SacII (100%); XhoI (100%); and XbaI (100%). Next, the digested plasmids were mixed with 6X gel loading dye before being separated in 2% agarose gel at 100 V for 90 minutes. The digested pSico plasmid released 701-bp (positive cloning) and 646-bp (negative cloning), whereas the digested pSicoR released 374-bp (positive cloning) and 319-bp (negative cloning) DNA fragments.

### **2.24.9. Sequencing and plasmid maxiprep**

The positive clones were sent to Source BioScience Ltd (Cambridge) to carry out Sanger sequencing using the following primers (Ventura, Meissner et al. 2004):

**pSico:** 5'-CAAACACAGTGCACACCACGC-3'

**pSicoR:** 5'-TGCAGGGGAAAGAATAGTAGAC-3'

Next, the verified positive clone sequence was subjected to EZNA® FastFilter Plasmid DNA Maxi Kit (Omega Bio-Tek) to generate high-copy plasmids (yield of 1.5 to 3 mg) as described by the manufacturer. Briefly, 100 mL of overnight cultural bacteria was centrifuged at 4,000 g for 10 minutes. Similar to the plasmid miniprep, the generated pellet was resuspended with a 10 mL buffer containing DNase followed by addition of 10 mL lysis buffer. Next, 5 mL of neutralisation buffer was added and gently inverted for 2 minutes. When flocculent white precipitates were formed, 8.3 mL of binding buffer was added and gently inverted 4 times. Then, the lysates were transferred to the lysate clearance filter syringe provided in the kit. The cleared lysate was expelled through a filter into a 50-mL centrifuge tube by gently inserting a plunger into the barrel. The cleared supernatant was passed through a HiBind® DNA Maxi Column into a 50-mL tube and then centrifuged at 4,000 g for 3 minutes. As in the plasmid mini prep, the collected plasmid was washed once with a 10 mL high salt buffer containing isopropanol and twice with a 10 mL DNA washing buffer containing EtOH. Finally, the DNA was then then eluted with 1 mL of EB.

### **2.24.10. Lentivirus production**

Lentivirus was generated by co-transfecting HEK293 using the ViraPower™ Packaging Mix (a mixture of the optimised pLP1, pLP2, and pLP/VSVG plasmids in TE buffer, pH 8.0) (Invitrogen) as described by the manufacturer. Briefly, the HEK293 cells were seeded at a density of  $5 \times 10^6$  cells per 10-cm dish in high-glucose DMEM medium (10% FBS, 2mM GlutaMAX™) overnight at 37°C in a 5% CO<sub>2</sub> incubator. On the following day, 9 µg of ViraPower™ Packaging Mix was mixed gently with 3 µg of each positive clone plasmid (pSico or pSicoR) DNA in a sterile 5-mL tube containing 1.5 mL serum-free OptiMEM® medium (no P/S). Additionally, 36 µg of Lipofectamine™ 2000 (Invitrogen) was gently mixed with 1.5 mL serum-free OptiMEM® medium in a separate sterile 5-mL tube for 5 minutes at room temperature. Next, the solutions in the two tubes were combined and incubated for another 20 minutes at room temperature to allow the plasmid construct-Lipofectamine™ 2000 complex to form. During the incubation step, high-glucose DMEM medium was removed from the 90–95% confluent overnight-cultured HEK293 and replaced by 5 mL serum-free OptiMEM® medium in each dish of cells. After 20-minutes incubation, the plasmid construct-Lipofectamine™ 2000 complex was added in drops to each dish of

cells, rocked back and forth gently, and incubated overnight at 37°C in a 5% CO<sub>2</sub> incubator. On the following day, the medium containing the plasmid-Lipofectimin™ 2000 complex was replaced by fresh 10 mL serum-free OptiMEM® medium and the dishes placed back in the incubator for another 48 hours before harvesting.

#### **2.24.11. Concentrating lentivirus**

The lentiviruses were harvested by filtering the cultured medium containing the supernatant virus through a 0.45 µm polyether sulfone filter (Sigma-Aldrich) into a sterile 15-mL tube. One volume of the Lenti-X concentrator (Takara Bio Inc, Mountain View, US) was added to 3 volumes of the clarified supernatant, gently mixed by inversion, and the tubes incubated overnight at 4°C. Next, the mixture was centrifuged at 1,500 g for 45 minutes at 4°C. The supernatant was carefully and safely discarded, and the generated white pellet was then resuspended in 1/10 of the original volume by serum-free OptiMEM® medium. Immediately, the lentivirus was tittered or stored at -80°C in single-use aliquots.

#### **2.24.12. Lentivirus titering**

Lentivirus titre estimation by transduction is a titering technique based on the serial dilution of the concentrated virus. This technique was used as previously described (Wollebo, Woldemichael et al. 2013). HEK293 cells were washed with PBS, trypsinised, counted and centrifuged as described above (see **section 2.4**). Then, the cell pellet was resuspended in a high-glucose DMEM medium, seeded at a density of  $2 \times 10^4$  cells per well of a 6-well plate that had been pre-coated with 0.1% gelatin and incubated overnight at 37°C in a 5% CO<sub>2</sub> incubator. On the following day, the cells in each well were washed once with PBS and then incubated with 2 mL of high-glucose DMEM medium containing 8 µg/mL polybrene plus a serial dilution of the concentrated virus in each well of the 6-well plate for 48 hours at 37°C in a 5% CO<sub>2</sub> incubator. The serial dilutions used for titering each concentrated lentivirus were 1, 2, 4, 8, 32, and 64 µL. For the lentiviral titering and estimating the equivalent amount of each lentivirus needed for experimental use, the cells were imaged in a Zeiss axiovert 40/cfl inverted microscope and a green channel, and the percentage of GFP-expressing cells was calculated for each lentiviral prepared at all the dilutions described above.

## **2.24.13. Plasmid transfection and infection**

### **2.24.13.1. Immortalised mLMCEs transfection with shRNAs constructs**

The mLMCEs were nucleofected with pSicoR constructs as described in the nucleofection protocol (see **section 2.7**) and seeded in 6-well plates that had been pre-coated with 0.1% gelatin for 48 hours at 37°C in a 5% CO<sub>2</sub> incubator. The cells were lysed with high-SDS lysis buffer, and the lysates were quantified by the DC™ protein assay, separated by SDS-PAGE, and then subjected to Western blot analysis, as described in **the subsection 2.9.3 to 2.9.5**, to determine NRP2 silencing compared to the control conditions.

### **2.24.13.2. Primary lung ECs infection with lentivirus**

Lung ECs were isolated from pdgfb-iCreER mice as described in **section 2.6.1.2**. One day before the ECs were trypsinised, a 6-well plate was coated with 0.1% gelatin + 10 µg/mL FN + 10 µg/mL collagen overnight at 4°C. The primary lung ECs were washed with PBS, trypsinised, counted, and seeded at a density of 2x10<sup>6</sup> cells in MLEC medium per well of the pre-coated 6-well plate at 37°C in a 5% CO<sub>2</sub> incubator. Twenty-four hours later, the MLEC medium was replaced by 2 mL of fresh MLEC medium (no P/S). Then, the ECs in each well were infected with the generated conditional lentiviruses carrying pSico shRNA constructs supplemented with 8 µg/mL of polybrene overnight at 37°C in a 5% CO<sub>2</sub> incubator. The following day, the MLEC medium containing lentivirus in each well was replaced by 2 mL of fresh MLEC medium and placed back in the incubator. Forty-eight hours later, the ECs were checked for GFP signals using a Zeiss axiovert 40/cfl inverted microscope and a green channel. The ECs then received 2 mL of fresh MLEC medium supplemented by 1 µM of 4-hydroxytamoxifen (OHT) to activate shRNA expression and then placed back in the incubator. Ninety-six hours later, the ECs were lysed with a high-SDS lysis buffer. The lysates were quantified by the DC™ protein assay, separated by SDS-PAGE, and then subjected to Western blot analysis as described in **the subsection 2.9.3 to 2.9.5** to determine NRP2 silencing compared to the control condition.

## **2.25. *ex vivo* aortic ring assay**

Thoracic aorta isolation and infection with lentivirus were performed as described by Baker *et al.* (Baker, Robinson *et al.* 2012). Briefly, thoracic aortas were isolated from 6- to 8-week old pdgfb-iCreERT2 mice and transferred to a 10-cm dish containing serum-free OptiMEM®

medium supplemented by P/S inside a sterile culture hood. Using a Stemi SV 11 Stereomicroscopes (Carl Zeiss Ltd) inside a laminar flow cabinet (Labcaire Systems Ltd, Clevedon, UK), the thoracic aortas were carefully cleaned of any surrounding fat and connective tissues. Using a rounded scalpel, the aortas were then cut into rings approximately 0.5 mm in width. Then, 20–25 aortic rings from different pooled mice were infected by the generated pSico lentivirus in each well of a 24-well plate in 1 mL serum-free OptiMEM<sup>®</sup> medium overnight at 37°C in a CO<sub>2</sub> incubator. The following day, a sterile collagen embedding solution in water [1.2 mg/mL collagen I (Millipore, Watford, UK), 1X DMEM medium, and 1N sodium hydroxide (NaOH)] was prepared and mixed in a 50-mL tube on ice before adding 50 µL of the embedding solution to each well of a 96-well plate on ice. Using a dissection microscope inside a laminar flow hood, each aortic ring was embedded (lumen facing upright) in each well of the 96-well plate for 1 hour at 37°C in a 5% CO<sub>2</sub> incubator to allow collagen polymerisation to occur. Next, the embedded rings were fed with 50 µL of serum-free OptiMEM<sup>®</sup> medium + 2.5% FBS + 1 µM OHT supplemented or not with 30 ng/mL VEGF every three days. Six days later, the serum-free OptiMEM<sup>®</sup> growth medium was removed carefully, and the intact embedded rings were fixed with 4% PFA for 10 minutes and then permeabilised with 0.25% Triton-X100/PBS for 30 minutes at room temperature. Two washes at 15 minutes each with PBLEC solution (1× PBS + 1mM CaCl<sub>2</sub> + 1mM MgCl<sub>2</sub>, 0.1mM MnCl<sub>2</sub> and 1% Tween-20) were performed in a dark room before the blocking step was performed using 2% BSA in PBLEC for 30 minutes at room temperature. Next, the aortic rings were stained overnight with 50 µL FITC-conjugated BS-1 lectin (1:500) in PBLEC at 4°C in a dark room followed by three washes at 15 minutes each with 0.1% Triton/PBS. Finally, the micro vessels sprouting from the rings were counted using a Zeiss axiovert 40/cfl inverted microscope and a green channel.

## **2.26. Graphics and statistical significance analysis**

The graphic illustrations and the analyses to determine statistical significance were generated using the GraphPad Prism 6 software and Student's t-tests, respectively. The bar charts show the standard error of the mean (+SEM). The asterisks indicate the statistical significance of P values: P > 0.05 = nsd (not significantly different), \* P < 0.05, \*\* P < 0.01, \*\*\* P < 0.001 and \*\*\*\* P < 0.0001.

## Chapter 3: An introduction to investigating potential links between ITGB3 and NRP2

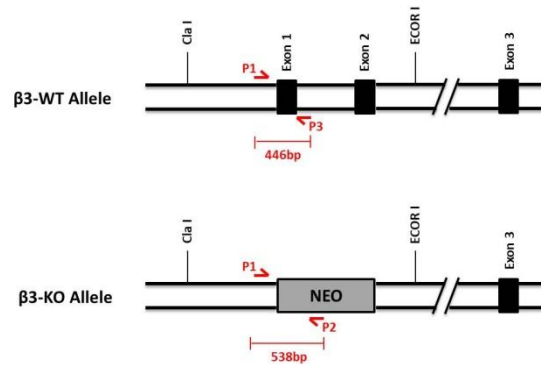
---

It was previously shown that NRP1 in ECs affects VEGF-stimulated responses (migration, signaling and tumor growth/angiogenesis) in a ITGB3 dependent manner (Ellison, Atkinson et al. 2015). Because NRP1 and NRP2 share a similar domain structure, and an overall 44% amino acid homology (Zachary 2014), we thought it is possible that NRP2 function is similarly regulated by ITGB3 levels, or that NRP2 may compensate for the loss of NRP1 in NRP1-depleted cells. To investigate this, we isolated lung microvascular endothelial cells (mLMECs) from both wild-type (WT) and  $\beta$ 3HET mice and immortalised them with PyMT by retroviral transduction, as described in chapter 2; **section 2.2 and 2.3**. We employed polyoma-middle-T-antigen immortalised ECs because: (1) they are easy and cost-effective to maintain in culture; (2) they allow us to reduce the number of experimental animals required for large biochemical studies, thus adhering to 3R principles (Russell, Burch et al. 1959), (Tannenbaum and Bennett 2015), (Carter and Shieh 2015); and (3) we and others have shown they present good models to study angiogenesis (Dong, Bernasconi et al. 1997), (Reynolds and Hodivala-Dilke 2006), (Robinson, Reynolds et al. 2009), (Burek, Salvador et al. 2012), (Ni, Kumar et al. 2014), (Steri, Ellison et al. 2014), (Ellison, Atkinson et al. 2015)

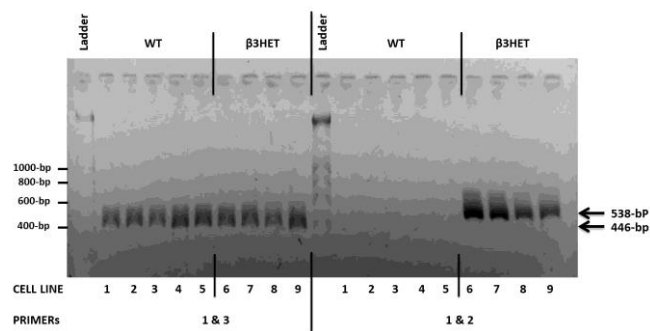
### 3.1. Examining ITGB3 levels across a panel of polyomavirus middle-T-antigen immortalized ECs.

DNA was extracted from multiple immortalized lines, as described in the previous chapter, and analysed by PCR to confirm their genetic status as either WT or  $\beta$ 3HET cells (**Figure 3.1 A-B**). We confirmed the endothelial cell identity of each clone by examining the expression of VE-Cadherin, an EC marker (Sivarapatna, Ghaedi et al. 2015), (Ikuno, Masumoto et al. 2017). We also quantified ITGB3 expression in each cell line (**Figure 3.1 C-D**) and confirmed that  $\beta$ 3HET ECs expressed approximately 50% less ITGB3 compared to their WT counterpart ECs (**Figure 3.1 E**). It is worth noting, however, the level of ITGB3 expression varied across the independent lines. It will become clear in the subsequent chapter why this is important.

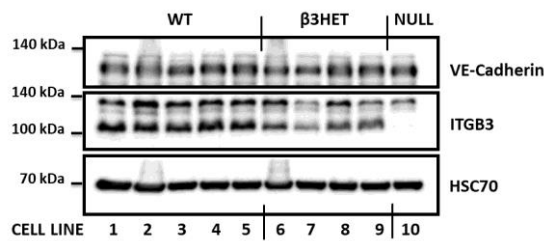
A)



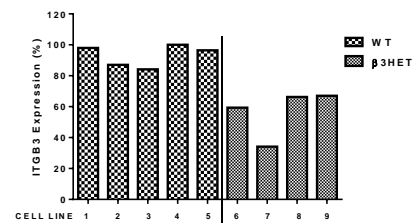
B)



C)



D)



E)

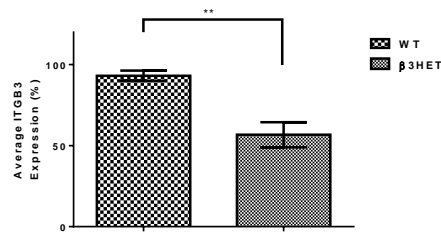


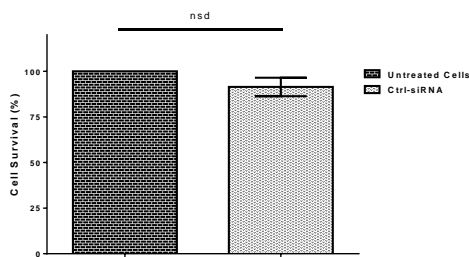
**Figure 3.1 β3-integrin genotyping and expression level analyses of immortalised EC lines.** PyMT mLMCEs were seeded in 10-cm dishes pre-coated with gelatin and incubated overnight at 37°C in a CO<sub>2</sub> incubator. After trypsinization, cells from each line were split into two tubes, and centrifuged twice at 500 g for 4 minutes. For each cell line, the pellet in

tube #1 was subjected to DNA extraction and PCR-based genotyping, whereas the cell pellet in tube #2 was subjected to protein extraction and Western blot analyses. **A)** Schematic diagram of the ITGB3 (WT) and (HET) loci, showing where PCR genotyping primers align. P1 and P3 amplify a wild-type product of 446-bp, whilst P1 and P2 amplify a knockout product of 538-bp. **B)** Agarose gel of P1/P3 and P1/P2 primer products from 9 different immortalised EC lines. Lines 1-5 show only a P1/P3 product, and are therefore wild-type (WT) for the ITGB3 locus, whilst lines 6-9 show both a P1/P3 product, and a P1/P2 product, and are therefore heterozygous ( $\beta$ 3HET) for the ITGB3 locus. **C)** Western blot analysis of VE-Cadherin and ITGB3 expression in the same clones shown in **B)**. HSC70 was used as a loading control. Because the antibody used for detection of ITGB3 recognises a non-specific band at approximately (135kDa), a  $\beta$ 3-knockout (NULL) lysate was included as a control (cell line #10). **D)** ImageJ<sup>TM</sup> densitometric quantification of the blot shown in C). Levels of ITGB3 were normalised against HSC70, and are shown relative to those in cell line #1. **E)** Average expression of ITGB3 in WT versus HET ECs (pooled data from panel D). The asterisks indicate statistical significance: \*\*  $P < 0.01$ . Unpaired two-tailed t-test

### 3.2. Analysis of NRP2 knockdown efficiency in immortalised ECs.

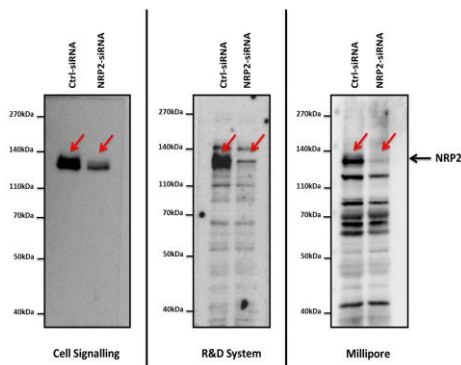
To evaluate the potential roles of NRP2 in microvascular ECs, we first needed to identify: 1) optimised conditions for efficient knockdown of NRP2 in PyMT mLMECs; 2) NRP2 specific antibodies; 3) short interference RNAs (siRNA) that were specific to NRP2, but showed no cross-reactivity to the closely related transmembrane glycoprotein NRP1. Delivering siRNA into eukaryotic cells to knockdown specific genes of interest can be accomplished via viral vectors (transduction), or via non-viral vectors (transfection), including both physical and chemical delivery systems (Biçeroglu and Memis 2005). Historically, the Robinson lab has only achieved efficient siRNA mediated knockdown in PyMT mLMECs by electroporation (e.g. nucleofection via Amaxa Nucleofector II<sup>TM</sup>). Electroporation is defined as an electrical field applied to target cells to increase the permeability of the plasma membrane by producing very small pores through which DNA/RNA sequences, drug, or chemicals may enter (Sharma, Khajuria et al. 2004). Aside from being the only tested method that works in these cells, electroporation is fast to deliver, highly efficient, and cheap. However, electroporation can irreversibly damage cell membranes, resulting in large numbers of dead cells. Therefore, we tested multiple conditions (not shown) and settled on those that gave us between 90-95% overall cell survival (**Figure 3.2 A**). Four different mouse-specific NRP2-siRNAs were then purchased from Dharmacon (Cat# D-040423-01, 02, 03 and 04). At this stage, we randomly chose one of the four siRNA constructs, (NRP2-siRNA 01), and then tested three commercially available NRP2 antibodies (Cell Signalling Technology Cat#D39A5, R&D System Cat#AF2215 and Milipore Cat#AB10522), to determine which would be the best to carry forward in future analyses (**Figure 3.2 B**). After establishing these two parameters, we tested four different NRP2-siRNAs against a non-targeting control siRNA (Ctrl-siRNA), NRP2-siRNAs 03 and 04 showed a 90% suppression of NRP2 expression and NRP1 level remain unchanged (**Figure 3.2 C-D**). Finally, we wanted to know how long the NRP2 knockdown will last for future studies (**Figure 3.2 E**), and we determined that NRP2 knockdown lasted for at least 72 hours from the day of nucleofection.

**A)**

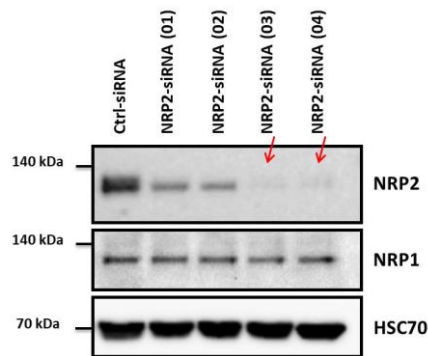


Cell Line	Condition	ug/ml	Survival Rate (%)
Cell Line (1)	No Electroporation	1506.417	100
	Ctrl-siRNA	1190.338	79.01783
Cell Line (2)	No Electroporation	1562.265	100
	Ctrl-siRNA	1545.216	98.9087
Cell Line (3)	No Electroporation	1398.445	100
	Ctrl-siRNA	1223.847	87.51485
Cell Line (4)	No Electroporation	1461.935	100
	Ctrl-siRNA	1467.03	100.3485

**B)**



**C)**



**D)**



**E)**

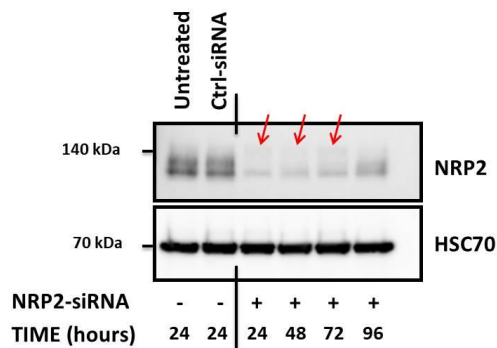


**Figure 3.2 Establishing optimised NRP2 knockdown and Western blotting conditions.** **A)**  $1 \times 10^6$  cells from four different WT ECs were immediately seeded on 10-cm dishes pre-coated with gelatin (No nucleofection), or nucleofected with a non-targeting siRNA (Ctrl-siRNA) for 48 hours at 37°C in a CO<sub>2</sub> incubator. Each plate of cells was lysed with the same volume (150µl) of lysis buffer. Lysates were then analysed by BioRad DC protein assay. For each cell line, the “cell survival rate” was estimated by dividing the total amount of protein in Ctrl-siRNA sample by the amount of protein in no electroporation sample. The bar chart shows the mean percentage of surviving cells; n=4, and (mean +SEM),  $P=0.14$ . **B)**  $1 \times 10^6$  ECs were nucleofected with either Ctrl-siRNA or NRP2-siRNA (#01) and seeded on 10-cm dishes pre-coated with gelatin for 48 hours at 37°C in a CO<sub>2</sub> incubator. The cells were lysed and the lysates were subjected to the DC protein assay. The lysates were analysed by Western blots to determine the best NRP2 antibody to be used in future studies. The antibody from Cell Signalling appeared to be the most specific (less background). **C)**  $1 \times 10^6$  ECs were nucleofected with either Ctrl-siRNA or with one of four different NRP2-specific siRNAs (01, 02, 03 or 04) and seeded on 10-cm dishes pre-coated with gelatin for 48 hours at 37°C in a CO<sub>2</sub> incubator. The cells were lysed and the lysates were subjected to the DC protein assay before being analysed by Western blot using the Cell Signalling antibody shown in B). HSC70 was used as a loading control. **D)** Quantification of NRP2 knockdown was analysed by ImageJ™ densitometric analysis of the blot in D). Relative levels of NRP2 expression were normalised to HSC70 levels and plotted relative to the Ctrl-siRNA. **E)**  $1 \times 10^6$  ECs were nucleofected with either Ctrl-siRNA or NRP2-siRNA (04) and seeded on 10-cm dishes pre-coated with gelatin for the indicated time at 37°C for 24, 48, 72 and 96 hours in a CO<sub>2</sub> incubator. After lysing the cells, the lysates were subjected to the DC protein assay before being analysed by Western blot using the Cell Signalling antibody shown in B).

### 3.3. Discussion

NRPs are single transmembrane receptor proteins that are expressed in a variety of cells including nerve cells, ECs, immune cells, epithelial cells, osteoblasts and tumour cells (Zachary 2014), (Bielenberg, Hida et al. 2004). They carry out versatile multi-functional roles depending on the type of cells that express them (Neufeld, Cohen et al. 2002), (Parker, Guo et al. 2012), (Prud'homme and Glinka 2012), (Li, Parker et al. 2014), (Guo and Vander Kooi 2015). In ECs, NRPs function as co-receptors with many cell-surface growth-factor receptors, including VEGFR, TGF- $\beta$ 1R, hepatocyte growth factor receptor (HGFR), FGFR, PGF-BR and PDGFR. They enhance the binding and activation of these growth factor signalling pathways (Parker, Guo et al. 2012). NRPs can also function independently of the growth-factor receptors by regulating the function of integrins, thus influencing cell adhesion, migration and permeability during angiogenesis, under both physiological and pathological conditions (Fukasawa, Matsushita et al. 2007), (Valdembri, Caswell et al. 2009), (Ellison, Atkinson et al. 2015).

Many previous studies have shown that NRP2 is overexpressed in cancer, and its upregulation is linked to cancer progression (Fakhari, Pullirsch et al. 2002), (Kawakami, Tokunaga et al. 2002), (Bielenberg, Hida et al. 2004), (Tomizawa, Sekido et al. 2001), (Kawakami, Tokunaga et al. 2002), (Lantuéjoul, Constantin et al. 2003), (Vales, Kondo et al. 2007), (Bachelder, Crago et al. 2001), (Fukahi, Fukasawa et al. 2004). Interestingly, Favier *et al.* showed that the overexpression of NRP2 in hMVECs increased cell survival induced by VEGF<sub>165</sub> and that NRP2 knockdown significantly inhibited VEGF<sub>165</sub>-induced migration (Favier, Alam et al. 2006). These findings supported the suggestion that NRP2 knockdown may help in cancer therapy. Hence, it is important to understand NRP2 biology.

Regarding the role of NRP2 in the embryo, a previous study on embryonic vascular development in chicks showed that NRP2 was expressed in the blood islands of 24-hour-old embryos (Herzog, Kalcheim et al. 2001). Subsequent studies showed that mice lacking the *NRP2* gene and containing only one functional *NRP1* allele exhibited more severe defects in vascular development than those reported in mice lacking both *NRP1* alleles and an intact *NRP2* gene (Takashima, Kitakaze et al. 2002). The results of these studies indicated the contributory role of NRP2 in the early development of embryonic vessels. Another study found that NRP2, similar to NRP1, bound to VEGF<sub>165</sub> with high affinity in HUVEC, suggesting that NRP2 has a role in cardiovascular biology through binding to VEGFR2

(Gluzman-Poltorak, Cohen et al. 2000). This finding was supported by Favier *et al.*, who showed that NRP2 immunoprecipitated with VEGFR2, and the stimulation of cells with VEGF<sub>165</sub> increased the association between NRP2 and VEGFR2, indicating that NRP2 binds to VEGFR2 in both a ligand-dependent and ligand-independent manner (Favier, Alam et al. 2006). The author also showed that VEGFR2 phosphorylation was increased when the cells were transfected with human pCDNA hygro-NRP-2 and stimulated by VEGF<sub>165</sub> compared to low VEGFR2 phosphorylation in the absence of NRP2 (Favier, Alam et al. 2006). Additionally, Kärpänen *et al.* found NRP2 expression in human lymphatic dermal microvascular ECs was higher than in human blood dermal microvascular ECs, indicating that NRP2 must play roles in both types of ECs (Kärpänen, Heckman et al. 2006). Furthermore, the results of subsequent studies revealed that both NRP1 and NRP2 are expressed in normal blood and lymphatic endothelial cells, and both play essential roles in forming blood and lymphatic vasculatures (Jurisic, Maby-El Hajjami et al. 2012), (Bouvrée, Brunet et al. 2012), (Mucka, Levonyak et al. 2016).

Most previous studies on NRPs were focused on NRP1 (Zachary 2014), (Wittmann, Grubinger et al. 2015). With regard to NRP2, only two studies addressed the roles of NRP2 in regulating the function of integrins, one in breast cancer and one in renal cell carcinoma (Goel, Pursell et al. 2012), (Cao, Hoepfner et al. 2013). Goel *et al.*'s study led to the discovery of a potential mechanism whereby NRP2 regulates  $\alpha 6\beta 1$  signalling to promote the association of  $\alpha 6\beta 1$  with the extracellular matrix (laminin) and to form stable FAs at the leading edge, which is required in the spreading of breast cancer cells (Goel, Pursell et al. 2012). Cao *et al.*'s study revealed a unique pathological mechanism through which the NRP2 expressed on these RCC cancer cells functioned as adhesion molecules to *trans*-bind with the ITGA5 subunit expressed on the surface of the ECs to promote vascular adhesion, extravasation and tumour metastasis (Cao, Hoepfner et al. 2013). To the best of our knowledge, no previous study has addressed the possibility that NRP2 could cross-talk with the integrins within ECs.

The Robinson laboratory previously showed that NRP1 expression in ECs affected VEGF<sub>164</sub>-stimulated responses (migration, signalling and tumour growth/angiogenesis) in an ITGB3 dependent manner (Ellison, Atkinson et al. 2015). Because NRP2 shares a very similar domain structure and overall ~44% of the amino acid level with NRP1 (Zachary 2014) (see chapter 1; **Figure 1.9 A**), we aimed to answer the following question: Does NRP2 also regulate the ITGB3 subunit function in ECs?

The Robinson group and others have shown that polyoma-middle-T-antigen immortalised ECs provide a good model for studying angiogenesis (Dong, Bernasconi et al. 1997), (Reynolds and Hodivala-Dilke 2006), (Robinson, Reynolds et al. 2009), (Burek, Salvador et al. 2012), (Ni, Kumar et al. 2014), (Steri, Ellison et al. 2014), (Ellison, Atkinson et al. 2015). Furthermore, immortalised ECs offer at least three advantages: they are easy, cost-effective and adhere to 3R principles (Russell, Burch et al. 1959), (Tannenbaum and Bennett 2015), (Carter and Shieh 2015). Therefore, we employed the polyoma-middle-T-antigen to immortalise different clones of WT ECs and  $\beta$ 3HET ECs, confirming that each clone expressed VE-cadherin (an EC marker) and showing that  $\beta$ 3HET ECs expressed approximately 50% less ITGB3 compared to WT ECs (see **Figure 3.1 E**). Historically, the Robinson laboratory has only achieved efficient siRNA mediated knockdown in PyMT mLMECs by electroporation using the Amaxa Nucleofector II<sup>TM</sup>. Under the right nucleofection conditions, we were successful in achieving overall cell survival rate of 90–95% (see **Figure 3.2 A**). We also tested three commercially available anti-NRP2 antibodies and showed that the monoclonal antibody produced by Cell Signalling Technology<sup>®</sup> was more specific to NRP2 than the polyclonal antibodies produced by the R&D system and Merck Millipore (see **Figure 3.2 B**). Finally, we tested four different NRP2-siRNAs and identified two specific and effective NRP2-siRNAs (03 and 04), which produced ~90%-suppression of NRP2 expression (see **Figure 3.2 C-D**), which lasted for 72 hours from the day of nucleofection (see **Figure 3.2 E**).

### 3.4. Conclusion

In this chapter, we have shown that:

- **The immortalized PyMT mLMECs are expressing VE-Cadherin, a specific marker of microvascular ECs.**
- **Nucleofection of PyMT mLMECs gave us between 90-95% overall cell survival.**
- **NRP2 antibody from Cell Signalling Technology is best to use for Western blot.**
- **NRP2-siRNAs 03 and 04 produce an approximate 90% suppression of NRP2 expression that last for 72 hours.**
- **NRP1 levels are not affected by NRP2 knockdown.**

## Chapter 4: Investigating the roles of NRP2 in ECs

---

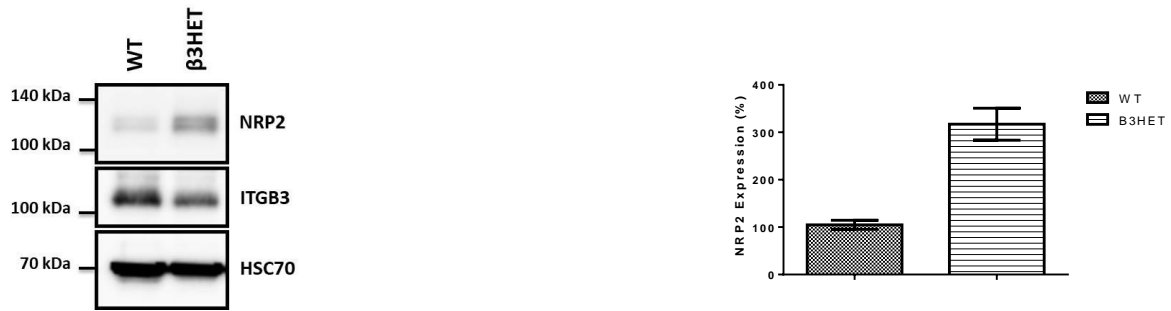
### 4.1. Upregulation of NRP2 in $\beta$ 3HET cells; ITGB3 depletion upregulates the expression of NRP2, similar to what was previously reported with NRP1.

As described earlier, NRP1 and NRP2 share a similarity in many aspects: 1) they have a similar domain structure and overall 44% amino acid homology (Zachary 2014); 2) both can form a complex with the same receptors, including VEGFRs (Soker, Miao et al. 2002), (Favier, Alam et al. 2006), and Plexins (Raper 2000) to transduce signalling through binding with the same ligands, including VEGFs (Gluzman-Poltorak, Cohen et al. 2000), (Soker, Miao et al. 2002) and Semaphorins (Chen, Bagri et al. 2000); 3) both have been shown to immunoprecipitate with ITGA5 integrin subunit in different cell types, and to regulate ITGA5 function (Valdembri, Caswell et al. 2009), (Cao, Hoepfner et al. 2013). Despite these similarities, most studies have focused on the biological functions of NRP1, including studies from our own lab. In fact, it is these very similarities that led us to investigate whether NRP2 has a role to play in regulating endothelial cell behaviour.

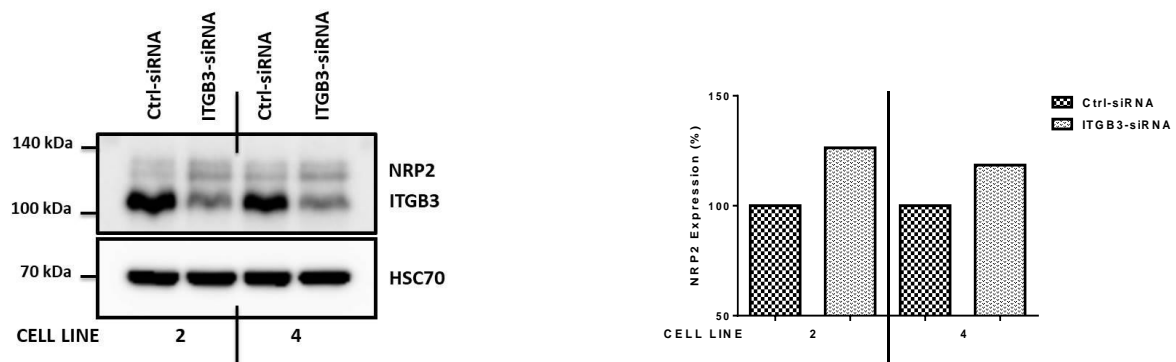
The Robinson lab previously showed that NRP1 expression is up-regulated in  $\beta$ 3HET ECs compared to WT ECs. Moreover, NRP1 seems to only play a role in angiogenic processes, at least post developmentally, when ITGB3 expression is reduced (Ellison, Atkinson et al. 2015). Given the similarities noted above, and the possibility that NRP2 might play a functionally redundant role to NRP1 in ECs, we decided to ask whether NRP2 expression and/or function is linked to ITGB3 expression in these cells. We first performed a Western blot on protein lysates from WT cell line #4 (see **Figure 3.1 C-D**), which (of the lines employed) has the highest expression of ITGB3, and  $\beta$ 3HET cell line #7 (see **Figure 3.1 C-D**), which has the lowest expression of ITGB3. Like NRP1, NRP2 expression was elevated in  $\beta$ 3HET cells (**Figure 4.1 A**). We also noted increased NRP2 expression upon siRNA-mediated ITGB3 knockdown in two different WT ECs (cell lines #2 and #4) (**Figure 4.1 B**), suggesting the increased expression of NRP2 in  $\beta$ 3HET cells is not a response to long-term depletion of ITGB3. We were intrigued by this result, and decided to explore whether NRP2 has a role to play in VEGF-induced endothelial angiogenic responses and if so, whether that

role is linked to ITGB3. Again, given the similarities between NRP1 and NRP2, we thought it was important to demonstrate that (1) our NRP2 siRNA was having no effect on NRP1 in VEGF<sub>164</sub>-induced stimulation and (2) that VEGF stimulation itself did not alter NRP2 expression. To this end, we knocked-down NRP2 in both WT ECs and  $\beta$ 3HET ECs in the presence or absence of VEGF<sub>164</sub> stimulation. As noted above, both NRP1 and NRP2 were elevated in  $\beta$ 3HET ECs compared to WT. Furthermore, NRP2 knockdown had no effect on NRP1 expression, and VEGF<sub>164</sub>-stimulation did not affect NRP1 or NRP2 expression when ITGB3 is expressed normally or reduced, at least over this short time course of VEGF treatment (**Figure 4.1 C**).

A)



B)



C)

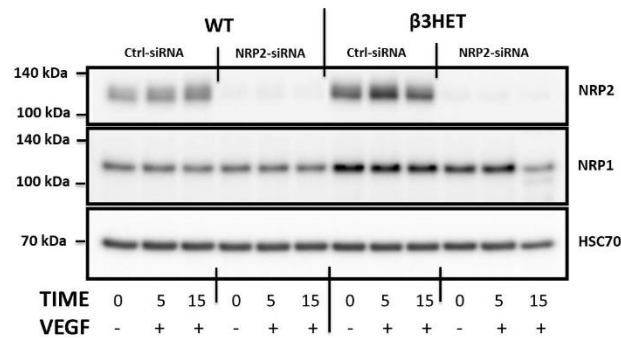


**Figure 4.1 Upregulation of NRP2 expression in β3HET ECs.** **A)** WT or β3HET ECs were seeded on 10-cm dishes pre-coated with 10 μg/ml FN and incubated at 37 °C in CO<sub>2</sub> overnight. Each plate of cells was washed twice with PBS before the cells were lysed. Following a protein quantification analysis using the BioRad DC protein assay, the samples were subjected to a Western blot to analyse NRP2 expression in the WT and β3HET ECs (left); NRP2 was quantified by ImageJ™ densitometry software (right). The bar charts of means (+SEM) are representative of three repeats. The asterisks indicate statistical significance: \*\*\*\* P<0.0001. **B)** Two different WT ECs were either nucleofected with Ctrl-siRNA or ITGB3-siRNA and seeded on 10-cm dishes pre-coated with 10 μg/ml FN and incubated for 48 hours at 37 °C in CO<sub>2</sub> incubator. The cells were lysed and the proteins were quantified in the same manner. The samples were then subjected to a Western blot to analyse NRP2 expression in the two genotype ECs (left); NRP2 was quantified by ImageJ™ densitometry software (right). **C)** 1x10<sup>6</sup> cells from both WT and HET ECs were nucleofected with either Ctrl-siRNA or NRP2-siRNA and then seeded on 6-cm dishes pre-coated with 10 μg/ml FN and incubated in CO<sub>2</sub> at 37 °C for 48 hours. Following two washes with PBS and starving ECs in pre-warmed serum-free OptiMEM® for 3 hours, one dish from each condition was left unstimulated, while the rest were stimulated with 30 ng/ml VEGF<sub>164</sub> for 5 or 15 minutes. All dishes, including those left unstimulated, were immediately placed on ice to stop the stimulation process. The cells were lysed and the proteins were quantified in the same manner. The samples were then subjected to a Western blot to analyse NRP1 and NRP2 expression.

## **4.2. There is no link between NRP2 and ITGB3 in response to VEGF<sub>164</sub> stimulation, but NRP2 depletion marginally impairs VEGFR2/ERK phosphorylation in response to VEGF-stimulation.**

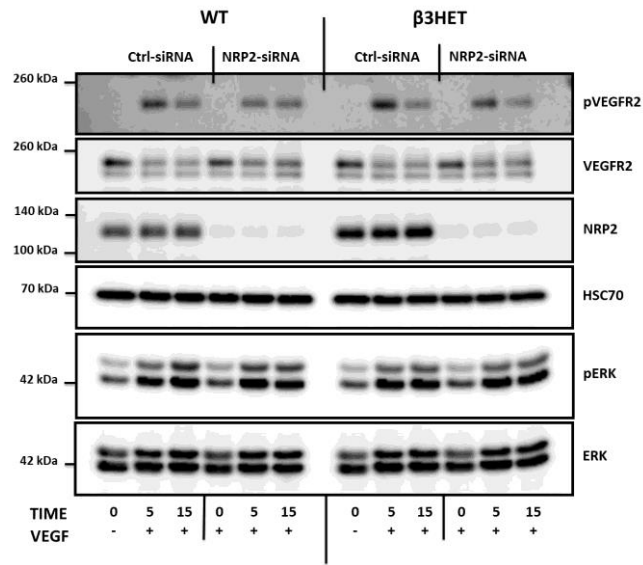
VEGFR signalling is regulated, to some extent, through interaction with NRPs (Álvarez-Aznar, Muhl et al. 2017). In the endothelium, VEGF-A, a major angiogenic factor (Neufeld, Cohen et al. 1999), binds to NRPs (Neufeld, Cohen et al. 2002) and forms a complex with VEGFR2 that leads to optimal binding of VEGF-A to its receptor and results in enhanced VEGFR2 phosphorylation, intracellular signalling and cell migration (Whitaker, Limberg et al. 2001), (Soker, Miao et al. 2002), (Favier, Alam et al. 2006). Therefore, we next investigated whether NRP2 modulates, in mMLECs, VEGF-induced activation of VEGFR2, as well as downstream signalling through ERK1/2 (Vellon, Menendez et al. 2006), (Koch and Claesson-Welsh 2012), (Tan, Popel et al. 2013), (Almalki and Agrawal 2017), (Park-Windhol, Ng et al. 2017).

Because VEGFR2 signalling is also regulated by the ITGB3 subunit (Ravelli, Mitola et al. 2013), (Somanath, Malinin et al. 2009), (Reynolds, Wyder et al. 2002), we decided to investigate whether the VEGFR2-NRP2 interaction is dependent on ITGB3 expression in response to VEGF<sub>164</sub>. As mentioned earlier, because ITGB3 levels varied somewhat across cell lines in both WT and  $\beta$ 3HET ECs (see **Figure 3.1 C-D**), we performed signalling assays with multiple lines of both genotypes; to minimize any potential cell line specific effects. Then, the phosphorylation difference of both VEGFR2 (pVEGFR2) and ERK1/2 (pERK) in Ctrl-siRNA versus NRP2-siRNA in WT ECs was compared to the phosphorylation in Ctrl-siRNA versus NRP2-siRNA in  $\beta$ 3HET ECs (**Figure 4.2 A-B**). For signal quantification, the phosphorylation level of each protein was normalized to total levels for that protein. As previously reported (Ellison, Atkinson et al. 2015), the phosphorylation patterns of ERK and VEGFR2 were slightly greater but not significantly in  $\beta$ 3HET compared to WT ECs. However, densitometric analysis indicated no significant changes in the overall pERK and pVEGFR2 levels when comparing WT to  $\beta$ 3HET ECs following NRP2 silencing, suggesting no link between ITGB3 and NRP2-dependent VEGF-induced signalling. Nevertheless, NRP2 knockdown did marginally attenuate the expression of pERK at 15 minutes and pVEGFR2 expression at 5 and 15 minutes in ECs of both genotypes, though statistical significance was not achieved in either case (see **Figure 4.2 A-B**).

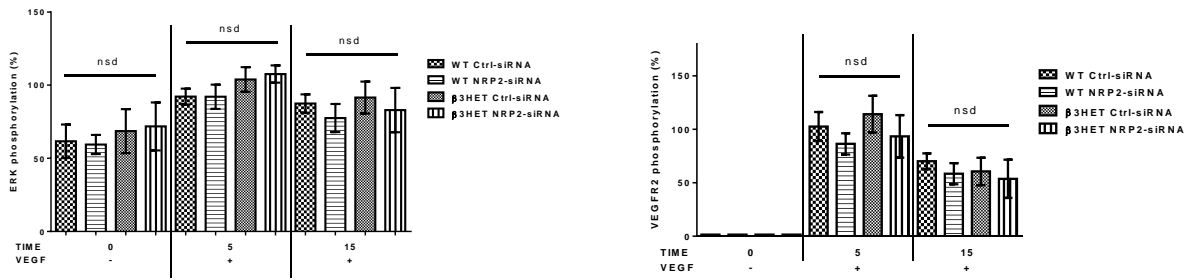
To further examine the marginal reduction of pERK and pVEGFR2 upon NRP2 depletion seen in **Figure 4.2 A-B**, we looked at the effect of NRP2 knockdown on VEGFR2 and ERK phosphorylation in different WT ECs, again, to minimize any potential cell-line specific responses, in longer VEGF-induced stimulation (60 minutes) (**Figure 4.2 C-D**). ERK phosphorylation in NRP2-siRNA treated cells was again marginally impaired at 15 and 30 minutes compared to Ctrl-siRNA treated cells, whereas VEGFR2 phosphorylation in NRP2-siRNA treated cells was also marginally reduced at 5, 15 and 30 minutes compared to Ctrl-siRNA treated cells (see **Figure 4.2 C-D**). This suggests that NRP2 may regulate VEGF-VEGFR2 signalling.

Previous reports showed that NRP2 can regulate VEGF-induced signalling in lymphatic human microvascular ECs cells (Favier, Alam et al. 2006), and human lymphatic ECs (Caunt, Mak et al. 2008). In our mMLECs, however, we observed only marginal attenuation of ERK and VEGFR2 phosphorylation.

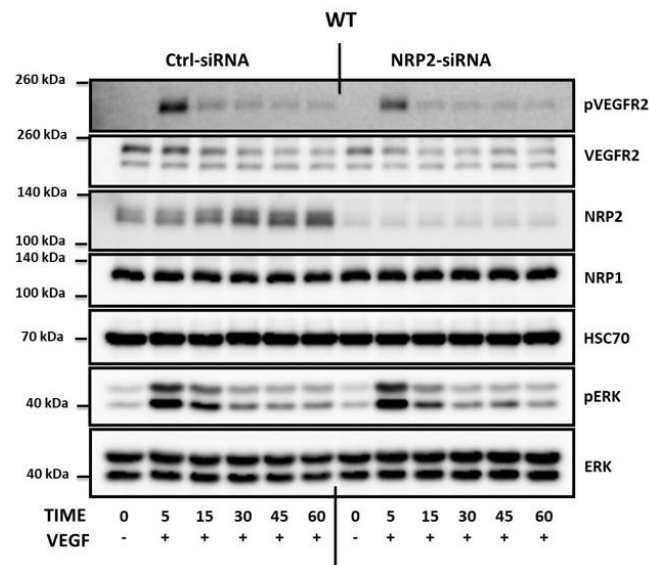
A)



B)



C)



D)

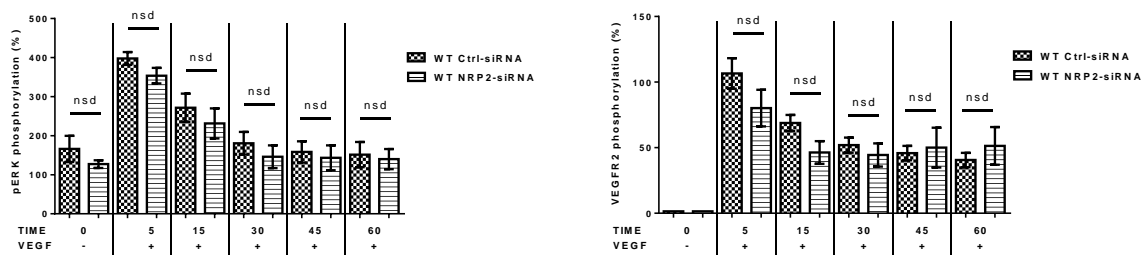


**Figure 4.2 NRP2 silencing attenuates VEGFR2 phosphorylation in response to VEGF<sub>164</sub>.** **A)** ECs from both genotype cells were nucleofected with either Ctrl-siRNA or NRP2-siRNA, and then seeded at a density of  $5 \times 10^5$  cells in 6-cm dishes pre-coated with 10  $\mu\text{g/ml}$  FN and then incubated in CO<sub>2</sub> for 48 hours at 37°C. Following two washes with PBS, the cells were starved in serum-free OptiMEM<sup>®</sup> for 3 hours. 30 ng/mL VEGF<sub>164</sub> was added to dishes with respect to the indicated time at 15 and 5 minutes. All dishes, including unstimulated one, immediately placed on ice to stop stimulation process. After lysing the cells from both genotype ECs and quantifying the concentration of proteins, the lysates were analysed by Western blots to examine any differences in the phosphorylation expression of both VEGFR2 and ERK1/2 in the two genotype ECs. The blot is representative of six independent experiments. **B)** The phosphorylation expression of ERK1/2 and VEGFR2 were quantified using ImageJ densitometry software<sup>™</sup>. The bar charts are representative of six experiments. The results of the densitometry analysis are shown in bar charts of mean (+SEM);  $P > 0.05$ . **C)** As in A) but this time after the starvation step, the cells were stimulated with 30 ng/mL VEGF<sub>164</sub> was added to dishes with respect to the indicated time at 60, 45, 30, 15 and 5 minutes. All dishes, including unstimulated one, immediately placed on ice to stop stimulation process. After lysing the cells from both genotype ECs and quantifying the concentration of proteins, the lysates were analysed by Western blots. **D)** The phosphorylation expression of VEGFR2 and ERK1/2 were quantified using ImageJ densitometry software<sup>™</sup>. The bar charts are representative of six independent experiments. The results of the densitometry analysis are shown in bar charts of mean (+SEM). The asterisks indicate statistical significance:  $P > 0.05$ . Unpaired two-tailed t-test.

### **4.3. NRP2-depletion reduces random migration in ECs, but the effects are not linked to ITGB3.**

A previous study on NRP2-dependent migration showed that monoclonal antibodies that specifically bind to the coagulation V/VII factor (b1-b2) domains of NRP2 (the two domains that are essential for optimal binding of both VEGF-C and VEGF<sub>165</sub>) inhibited the migration of human lymphatic ECs (LECs) in the presence of VEGFC but not VEGF<sub>165</sub> (Caunt, Mak et al. 2008). Another study showed that knocking down NRP2 in HMVEC inhibited VEGF<sub>165</sub>-induced migration (Favier, Alam et al. 2006). In contrast to Favier et al.'s study, NRP2 knockdown resulted in increasing the migration of HUVECs (German, Mammoto et al. 2014).

Previous studies in our lab demonstrated that NRP1 plays a role in mLMEC migration only in  $\beta$ 3HET ECs (Ellison, Atkinson et al. 2015). These studies showed NRP1-dependent effects on cell migration only when ITGB3 levels were reduced. This was shown in both cell random motility (CRM) assays and wound healing (WH) assays. Therefore, we decided to test the effects of NRP2-depletion in both WT and  $\beta$ 3HET ECs in the presence or absence of VEGF<sub>164</sub>. Forty-eight hours after Ctrl-siRNA or NRP2-siRNA treatment, cells were seeded on FN matrix, with or without VEGF stimulation. Fixed images from multiple wells of each condition were taken every 10 minutes for 15 hours, creating short videos. Individual cells were then tracked manually to measure random cell migration speed. This type of experiment was repeated four-independent times, on four different cell lines from each genotype; the results were pooled in a single graph (**Figure 4.3**). As previously reported (Ellison, Atkinson et al. 2015),  $\beta$ 3HET ECs migrated faster than WT ECs. Unlike NRP1, however, NRP2 depletion significantly reduced migration speed independently of ITGB3 levels; the percent reduction in migration speed when comparing NRP2-siRNA to Ctrl-siRNA treated cells was roughly similar in both unstimulated (76% in WT cells, 68% in  $\beta$ 3HET cells) and VEGF-stimulated (73% in WT cells, 74% in  $\beta$ 3HET cells) conditions. However, in contrast to the studies published previously in the lab (Ellison, Atkinson et al. 2015), we were not able to demonstrate a VEGF-induced increase in cell migration speed. One possible explanation for this discrepancy is differences in batches of serum used. It is possible that the serum used in the migration studies presented here contained inhibitory factors, such as Sempahorins, that might, in the long term, negate the effects of VEGF (Vadasz, Haj et al. 2012), (Silverio, Prota et al. 2015), (Nakayama, Bruneau et al. 2015). For example, both SEMA-3A and SEMA-3F

can act as competitors of VEGF binding to NRP1-VEGFR2 complex and subsequently inhibit VEGF-induced EC migration (Miao, Soker et al. 1999), (Kessler, Shraga-Heled et al. 2004).

We also attempted to perform WH assays, but in my hands these assays were very inconsistent, and we were not able to derive any concrete conclusions. Possible explanations for this are: 1) the width of the manual scratches were always uneven. This resulted in unreliable read outs because the speed of the migrated cells increases just before the wound closure of the two borders (Kramer, Walzl et al. 2013); 2) some detached cells, which were generated by manual scratches, remained attached to the monolayer cells at the border of the scratch, even after washing the cell debris with PBS. These cells were eventually reattached to the plate, moved to the wound closure area, and then migrated independently of the connecting population, which led to unreliable closure and difficult interpretation (Ascione, Vasaturo et al. 2016); 3) the scratching caused cell damage at the border of the closure area, which affected the motion of other cells, forcing them to migrate around the obstacle to reach the wound closure area (Ashby and Zijlstra 2012); 4) the scratching to generate a wound area caused scrapping off the FN from the pre-coated plates so that read-outs generated were FN independent (Kam, Guess et al. 2008).

Because the CRM assay provides a statistically robust measure of cell motility (Decaestecker, Debeir et al. 2007), (Terry, Bonnomet et al. 2009), (Caserta, Campello et al. 2013), and is considered “a gold standard” in cell migration studies (Ascione, Vasaturo et al. 2016), we conclude that NRP2 plays a role in EC migration on FN, but this role is independent of ITGB3. For this reason, we decided to re-focus our attention on NRP2’s role in regulating angiogenic processes, irrespective of a link to ITGB3.

Unlike NRP1 (Ellison, Atkinson et al. 2015), we have not seen any link between NRP2 and ITGB3, at least with respect to EC migration (see **Figure 4.3**) or VEGF-induced signalling (see **4.2 A-B**). The expression data presented at the beginning of this chapter (see **Figure 4.1**) suggests a regulatory crosstalk between NRP2 and ITGB3, but the detail of that crosstalk is currently unclear. As mentioned above, we were unable to observe a VEGF-induced increase in EC migration in our studies, so we cannot establish a firm connection between NRP2’s role in VEGF-induced signalling and migration, though undoubtedly the two are linked (Lake, Vassy et al. 2006), (Pan, Chanthery et al. 2007), (Hsieh, Ying et al. 2008), (Lamy, Lachambre et al. 2010), (Herzog, Pellet-Many et al. 2011), (Chu, Ramakrishnan et al. 2013), (Lamy, Ouanouki et al. 2014), (Xu, Wang et al. 2018). We therefore decided to pursue

further NRP2's involvement in regulating EC migration, independently of VEGF-stimulation, as well as independently of ITGB3 expression (the remainder of this chapter, and chapter 5). In chapter 6, we will come back to examining NRP2's role in mediating VEGF-induced events; in the final results chapter we will present work in which we attempted to develop and test NRP2-shRNA constructs for use in *ex vivo* aortic ring studies.

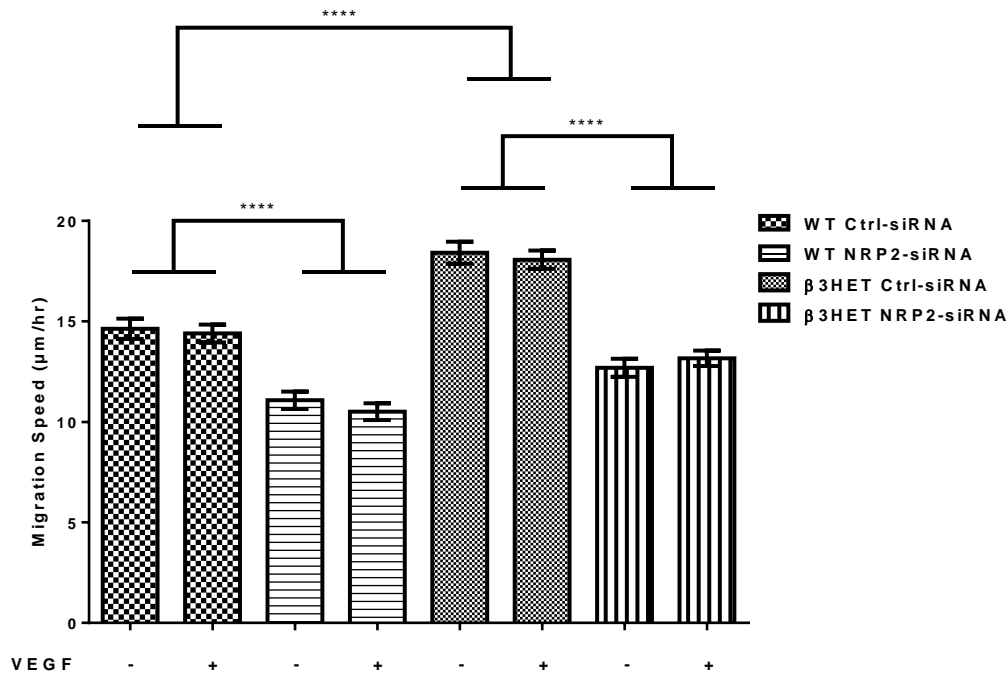


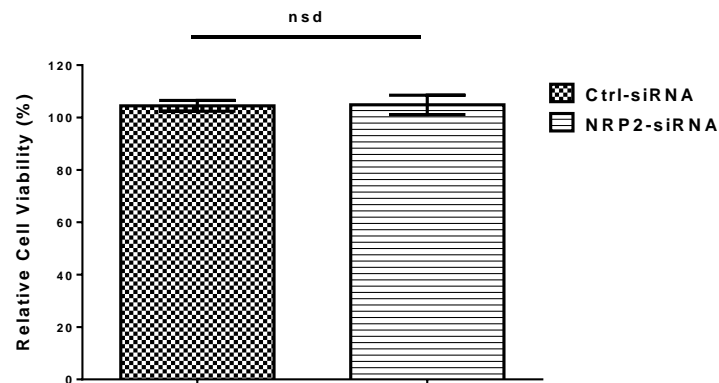
**Figure 4.3 NRP2-siRNA significantly reduces ECs migration in both WT and β3HET ECs.** ECs from WT and β3HET were nucleofected with either Ctrl-siRNA or NRP2-siRNA;  $1 \times 10^6$  cells were seeded in 10-cm dishes pre-coated with 10 µg/ml FN and incubated at 37 °C in CO<sub>2</sub> for 48 hours. The ECs from each condition were subjected to trypsin, re-suspended in serum-free OptiMEM<sup>®</sup> and seeded at a low density of  $7 \times 10^5$  cells in triplicate wells of a 24-well plate pre-coated with 10 µg/ml FN for 3 hours at 37 °C to starve and to allow the cells to adhere in the wells. In half of the plate, the medium was replaced by fresh serum-free OptiMEM<sup>®</sup> plus (2% FBS). The medium in the second half was replaced by fresh serum-free OptiMEM<sup>®</sup> plus (2% FBS) supplemented by 30 ng/mL VEGF<sub>164</sub>. Fixed images of multiple field/well of each condition were taken every 10 minutes for 15 hours at 37 °C and 5% CO<sub>2</sub> using an inverted Axiovert (Zeiss) microscope in one-phase contrast. Cells were manually tracked using ImageJ<sup>™</sup> Plugin Manual Tracking, and the migration speed of an individual cell was measured in µm/hours: **A)** Chart bar shows the cell migration speed over 15 hours. The asterisks indicate statistical significance: \*\*\*\* P<0.0001. Unpaired two-tailed t-test

#### **4.4. NRP2 does not regulate EC proliferation.**

Endothelial cell proliferation, as well as cell migration, plays an important role in angiogenic process (Jain 2003), (Suzuki, Montagne et al. 2007), (Contois, Akalu et al. 2009), (Carmeliet and Jain 2011), (Park-Windhol, Ng et al. 2017). Therefore, we decided to investigate whether proliferation was affected by NRP2 knockdown in our cells. First, we employed WST-1 assays to assess cell viability. When the tetrazolium WST-1 is added to cells, it is cleaved to formazan dyes by mitochondrion oxidoreductase enzymes (dehydrogenase) present in “viable” cells; the absorbance of formazan can be measured spectrophotometrically, and OD readings correlated to cell viability. When comparing Ctrl-siRNA to NRP2-siRNA treated ECs, we did not see any differences (**Figure 4.4 A**). We then turned to a more direct measurement of proliferation by assaying BrdU incorporation. BrdU is a thymidine analogue that is incorporated into replicating DNA during the S phase of the cell cycle. When counting the percentage of BrdU positive cells, no difference in relative rates of proliferation were noted when comparing Ctrl-siRNA to NRP2-siRNA treated ECs (**Figure 4.4 B**).

A number of studies have suggested NRP2 does not play a role in cell proliferation. This includes studies in human microvascular ECs (Favier, Alam et al. 2006), human lymphatic ECs (Caunt, Mak et al. 2008), human breast cancer cells (Goel, Pursell et al. 2012), and human renal cell carcinoma cells (Cao, Hoepfner et al. 2013). Our data suggest this is also true in mMLECs.

A)



B)

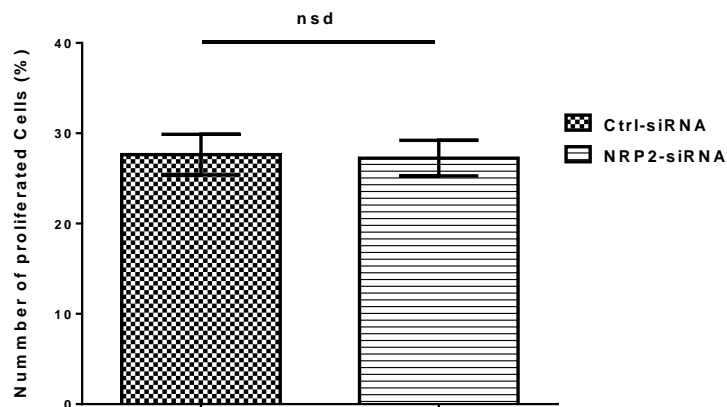


**Figure 4.4 NRP2 doesn't regulate mouse microvascular ECs proliferation.** ECs were nucleofected with either Ctrl-siRNA or NRP2-siRNA and seeded on 10-cm pre-coated with 10  $\mu\text{g/ml}$  FN at 37°C. **A)** 48 hours later, 7,000 cells were seeded into two 96-well plates pre-coated with 10 $\mu\text{g/ml}$  FN; one plate was incubated for 4 hours, and the second plate was incubated for 24 hours. 10  $\mu\text{l}$  of WST-1 was added to each well and then incubated for 2 hours before the absorbance was read at 450 nm versus 650 nm using a multi-well spectrophotometer (ELISA reader). The relative number of metabolically active cells was analysed by normalizing the absorbance of cells proliferated after 24 hours of incubation to the absorbance of total cells seeded for 4 hours (n= 40). **B)** After 30 hours of incubation, the cells were trypsinised, re-suspended in pre-warmed serum-free OptiMEM<sup>®</sup> and seeded on acid-washed/oven-sterilised glass coverslips at a density of  $1 \times 10^4$  cells in a well of a 6-well plate, in which each well held 4 coverslips, for 4 hours to allow cells to adhere. The serum-free OptiMEM<sup>®</sup> was then replaced by 10  $\mu\text{M}$  BrdU in complete culture medium; the cells were then incubated for 12 hours at 37°C. Following two washes with PBS, the cells were fixed with 4% PFA for 10 minutes before hydrolysing the DNA with 1M HCL for 30 minutes at room temperature. The cells were then permeabilised with PBS 0.25% Triton X-100 for 10 minutes at room temperature prior to blocking with Dako<sup>®</sup> Protein Block Serum-Free for 30 minutes. After two washes with PBS, the cells were incubated with anti-BrdU at 4°C overnight in a humidified chamber. Following two washes with PBS, the cells were incubated with secondary antibody for 45 minutes in a humidified chamber at room temperature. After two washes with PBS, the coverslips were mounted and sealed. The percentage of the number of proliferated cells was determined by dividing the number of the BrdU-labelled (divided) cells by the number of Dapi-labelled cells; (n = 19 field of view, containing on average 50 cells per field); nsd means not significantly different. Unpaired two-tailed t-test.

#### **4.5. NRP2 is Trypsin sensitive; and siRNA-mediated depletion of NRP2 reduces the relative number of ECs adhered on Fibronectin.**

Cell adhesion is a fundamental step required for cells to migrate through binding of integrins expressed on the cell surface with ECM ligands. Binding is initiated through the formation of nascent adhesions which can either regress, or mature into larger adhesions, called FAs, through the recruitment of more integrins to these sites. This results in linking the clustered integrins to actin filaments with the help of intracellular adaptor/signalling proteins such as paxillin, talin, vinculin, etc. . . (see chapter 1; **Figure 1.16**) (Nagano, Hoshino et al. 2012), (Small, Rottner et al. 1998), (Knight, Laukaitis et al. 2000), (Webb, Parsons et al. 2002), (Li, Guan et al. 2005). Alteration of integrins, or any of the intracellular adaptor proteins, will result in disruption of cellular adhesion and, subsequently, migration.

A variety of studies have linked NRP1 to a number of integrins (Ellison, Atkinson et al. 2015), (Valdembri, Caswell et al. 2009), (Hirota, Clements et al. 2015), (Maric, Annis et al. 2015), (Wu, Chen et al. 2014), (Kim, Jung et al. 2017), (Fukasawa, Matsushita et al. 2007), (Ruffini, Graziani et al. 2015), while only two studies, so far, have reported a physical interaction between NRP2 and integrins. One study showed that NRP2 expressed in human breast carcinoma cells is located in FAs through interactions with the integrin ITGA6, and this interaction is necessary for FA formation on laminin. The same study also reported that shRNA-depletion of NRP2 impaired adhesion of these cancer cells to laminin matrices (Goel, Pursell et al. 2012). A second study showed that NRP2 in human renal cell carcinoma functions as an adhesion molecule through *trans*-binding with ITGA5 expressed on HUVEC (Cao, Hoepfner et al. 2013).

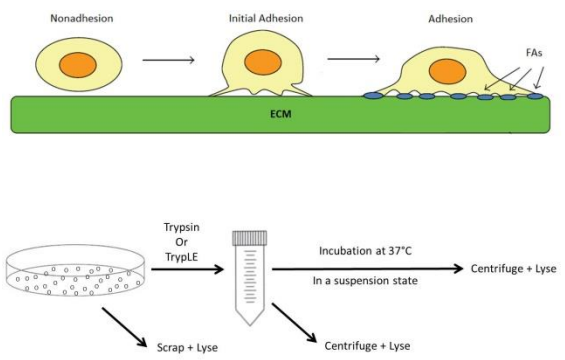
Because adhesion of cells to the ECM is a key regulator of cell migration, we sought to determine whether the significant migration reduction observed in NRP2-siRNA treated ECs (see **Figure 4.3**) was the consequence of attenuated cell adhesion to FN. For this, we decided to examine whether NRP2 is required for the initial attachment of ECs to FN, employing a previously published technique (Vlodavsky, Lui et al. 1980), (Vlodavsky and Gospodarowicz 1981), (Valdembri, Caswell et al. 2009), (Goel, Pursell et al. 2013) in which cells were detached with Trypsin and then seeded onto FN-coated substratum for short (15 and 30 minutes) periods of time. However, a previous study reported that NRP2 expressed in human breast carcinoma cells is Trypsin sensitive (Cao, Hoepfner et al. 2013); this means cleavage of NRP2 by Trypsin might generate inaccurate read outs of adhesion. Therefore, we wanted

to test whether NRP2 expressed in mMLECs is Trypsin sensitive. ECs were seeded into two 10-cm dishes overnight; ECs in the first dish were trypsinized, centrifuged and then lysed, while ECs in the second dish were lysed directly, without Trypsin treatment. We then assayed for NRP2 expression by Western blot. We observed a sharp reduction in the total level of NRP2 after Trypsin treatment (**Figure 4.5 B-C** lane 2). For this reason, we decided to test different cell-dissociation reagents that have been reported to be less aggressive than Trypsin when it comes to cleaving cell surface proteins. We tested Dispase, which was originally used for separating epidermis from dermis and epithelial cells from substratum in culture by cleaving FN and Type IV collagen (Stenn, Link et al. 1989), (Chen, Tredget et al. 2009) (kindly provided by Dr Ernst Pöschl, UEA, Norwich, UK), as well as different concentrations of EDTA (5mmol, 10mmol and 15mmol); none of these treatments were able to detach mMLECs from their substrata. We also tested TrypLE, another enzymatic reagent, which, according to the manufacturer (ThermoFisher Scientific) is superior to Trypsin in protecting cell surface proteins. Similar to Trypsin treatment, NRP2 was also cleaved by TrypLE (**Figure 4.5 B-C** lane 3). Due to this limitation, we decided to try NRP2 recovery after detaching ECs with either Trypsin or TrypLE by incubating the detached cells in suspension for 1 hour before lysing the cell pellets and performing Western blots (**Figure 4.5 A**). By comparing NRP2 levels in cells treated with Trypsin (Lane 2) or TrypLE (Lane 3) to the NRP2 levels in the untreated cells (Lane 1), it was clear that NRP2 is sensitive to both Trypsin and TrypLE, though NRP2 seems to be slightly less sensitive to Trypsin. Interestingly, incubating cells treated with both Trypsin and TrypLE for 1 hour at 37°C in suspension allowed cells to recover NRP2 expression (**Figure 4.5 B-C** lanes 4 and 5). Since Trypsin showed less cleavage effect on NRP2 than TrypLE, we decided to continue with Trypsin and increased the incubation time in suspension to 3 hours, hoping to fully recover NRP2 expression levels (**Figure 4.5 D**). We also examined Trypsin's effect on other molecules we were interested in, or have been shown previously to interact with NRP2, including ITGA5, ITGA6, ITGB3 and NRP1 (Goel, Pursell et al. 2012), (Cao, Hoepfner et al. 2013). Unlike NRP2, NRP1 was not sensitive to Trypsin treatment (see **Figure 4.5 D**). In contrast to previous reports, ITGA5 was not cleaved from the cell surface with Trypsin (Cao, Hoepfner et al. 2013), though we did note a slightly truncation of the molecule, suggesting, perhaps, cleavage of a small extracellular fragment. ITGB3 was not sensitive to Trypsin treatment. However, after one hour of incubation in suspension, both ITGA5 and ITGB3 levels decrease, presumably through intracellular degradation. Like NRP2, ITGA6 was Trypsin sensitive. Finally, we tested citric saline buffer, which is most often used to detach

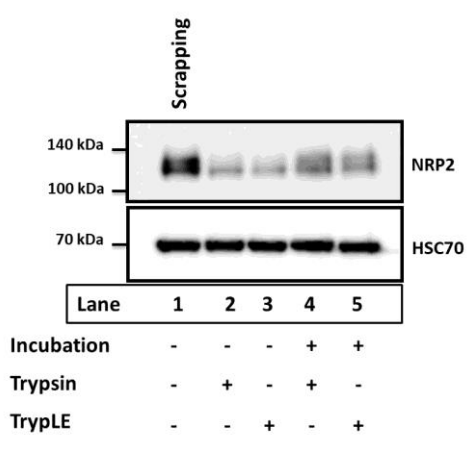
cells for flow cytometry analyses (Chang, Thalhoffer et al. 2007), (Rauch, Müschenborn et al. 2007), (Gaur, Showalter et al. 2009). When we used citric saline buffer to detach cells, all proteins we examined remained intact (**Figure 4.5 E**). However, in this buffer, cells detach as a sheet of attached cells, rather than individual cells, which made counting cells before seeding into downstream studies impossible.

Given these experimental limitations, we decided to explore the role of NRP2 in mediating cell adhesion using Trypsin as a detaching agent, and then incubating ECs in suspension for 1 hour, which elicits 50-60% recovery of NRP2 expression (see **Figure 4.5 C**), whereas ITGB3 and ITGA5 (in spite of the slight truncation of ITGA5), are still expressed at relatively high levels. Following this treatment regime,  $1 \times 10^4$  cells from each condition were seeded in 96-well plates pre-coated with FN for 15 or 30 minutes. The relative number of adhered cells in NRP2-siRNA conditions compared to Ctrl-siRNA conditions was then measured using a colorimetric assay (Goel, Pursell et al. 2012). Under these conditions, NRP2 knockdown resulted in a significant reduction in the number of ECs adhered to FN compared to Ctrl-siRNA treated ECs (**Figure 4.5 F**).

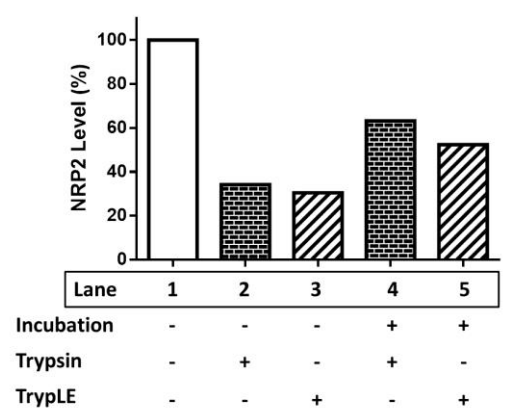
**A)**



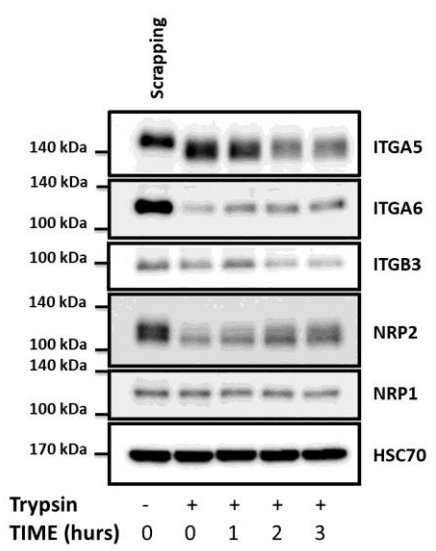
**B)**



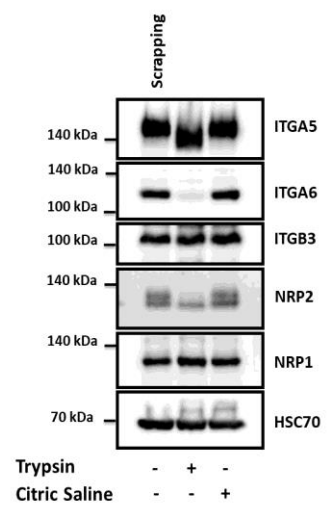
**C)**



**D)**



**E)**



**F)**

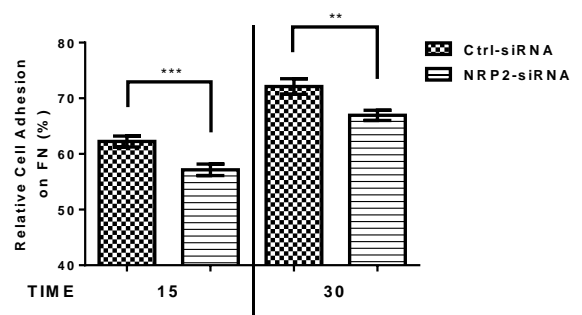


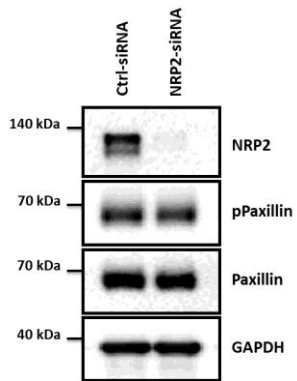
**Figure 4.5 NRP2 is Trypsin sensitive, and siRNA-mediated depletion of NRP2 reduces the relative number of microvascular ECs adhered on FN.** **A)** Cell surface proteins recovery assay schematic (adapted from (Nagano, Hoshino et al. 2012)) :**B)** The comparison of Trypsin and TrypLE for the cleavage effect on NRP2 before and after incubation for 1 hour in a suspension state. NRP2 level was analysed by Western Blot; **C)** Quantification of NRP2 was analysed by ImageJ™ densitometric analysis of the blot in **B)**; Relative levels of NRP2 expression were normalised to HSC70 levels. **D)** The cleavage effect of trypsin on other proteins, including NRP1, NRP2, ITGA5, ITGB3 and ITGA6 before and after 1, 2 and 3 hours of incubation at 37°C in a suspension state. **E)** Comparison of the cleavage effect of Trypsin and citric saline buffer on the same proteins of interest in which ECs were seeded in three 10-cm dishes overnight at 37°C. Two dishes were treated with either Trypsin or citric saline buffer to detach cells; the third dish was lysed directly by scrapping off cells using a rubber policeman. The cells treated with the detaching reagents were then centrifuged and lysed. The proteins level in lysates were analysed by western blot. **F)**  $1 \times 10^6$  ECs were nucleofected with either Ctrl-siRNA or NRP2-siRNA and seeded in pre-coated 10-cm dishes for 48 hours at 37°C in a CO<sub>2</sub> incubator. The cells were trypsinised, centrifuged at 500 g and then re-suspended in serum-free OptiMEM® in a suspension state for 1 hour at 37°C in a CO<sub>2</sub> incubator;  $40 \times 10^5$  cells were seeded per well in 96-well plates pre-coated with 10 µg/ml FN and incubated for short (15 and 30 minutes) adhesion. The non-adhered cells were gently washed off with PBS, and the adhered cells were fixed with 4% PFA for 10 minutes at room temperature. The cells were stained by methylene blue for 30 minutes. Then the plates were submerged in water to remove the excess stain and then left to dry for 30 minutes. Destain solution was added to each well for 10 minutes before the absorbance was read at 630 nm using a multi-well spectrophotometer (ELISA reader). The relative number of adhered cells in each condition was analysed by normalizing the absorbance of cells adhered for 15 and 30 minutes to the absorbance of total cells seeded for 4 hours (n= 24). The chart bar of mean (+SEM) shows the cell adhesion assay. It is representative of three experiments. The asterisks indicate statistical significance: \*\* P<0.01, \*\*\* P<0.001. Unpaired two-tailed t-test.

## 4.6. NRP2 knockdown slows the rate of focal adhesion turnover

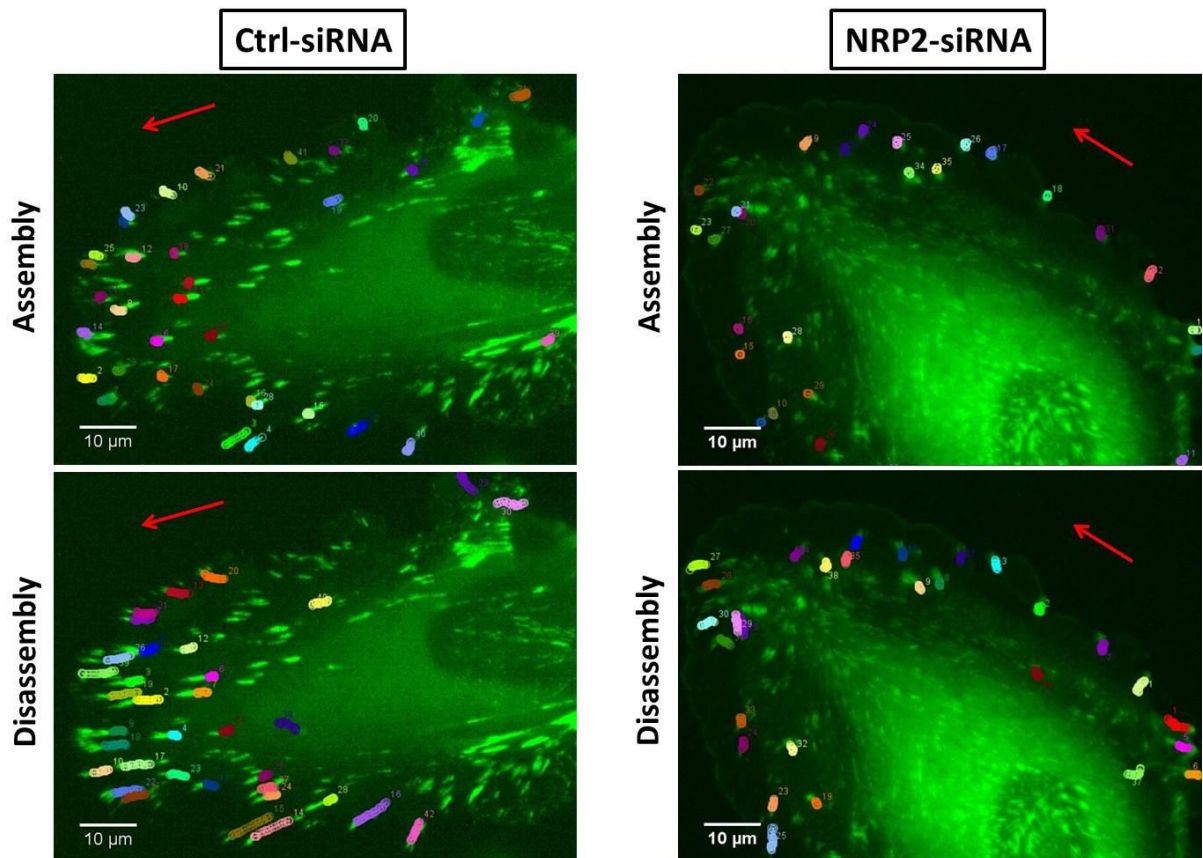
Cell migration requires the coordination of a complex integrated process involving the integrins, signalling/adaptor molecules and actin-binding proteins, which are activated temporally and spatially at different locations in the cell to achieve the correct balance in the assembly and disassembly of adhesions during cell migration (Webb, Parsons et al. 2002). The attachment of clustered integrins to ECM results in stabilizing the formation of FAs, which in turn leads to cell spreading at the leading edge whereas the reduction of integrin attachment to ECM results in destabilization of FAs, which in turn leads to a spherical, non-adherent cell phenotype (Webb, Parsons et al. 2002).

We monitored the kinetics of FA turnover in live mMLECs migrating on FN-coated coverslips following transfection with paxillin-GFP (Webb, Parsons et al. 2002). Paxillin is a required FA adapter protein that promotes FA turnover during cell migration (Zaidel-Bar, Milo et al. 2007), (Pasapera, Schneider et al. 2010) and it can control cell migration depending on its location within the cell. At the leading edge it can initiate, with other adaptor proteins, adhesions and stabilise FAs (Nayal, Webb et al. 2006). At the trailing edge it disperses to destabilize FAs for the rear of the cell to move forward (Nishiya, Kiosses et al. 2005). However, a previous study in HUVEC suggested cross-talk between NRP2 and paxillin. This was shown by siRNA depletion of paxillin in HUVEC, which led to 50% reduction of NRP2 expression at both RNA and protein level (German, Mammoto et al. 2014). Therefore, before using paxillin as a biomarker for FAs, we wanted to examine whether siRNA-mediated knockdown of NRP2 changes the expression or activation of paxillin in our ECs. We noted no change in either parameter when comparing NRP2 knockdown to control knockdown (**Figure 4.6 A**). We therefore proceeded to track FAs in live cells on an inverted Axiovert (Zeiss) microscope. Cells were double transfected with (paxillin-GFP) plus either NRP2-siRNA or Ctrl-siRNA and imaged every minute for 30 minutes. After defining the direction of migration, the assembly and disassembly speeds of single FAs were manually tracked using ImageJ™ software (**Figure 4.6 B**). As expected, FA disassembly was faster than the assembly of FAs; siRNA-mediated knockdown of NRP2 significantly reduced both the assembly and disassembly of FAs compared to that in control cells (**Figure 4.6 C**).

A)



B)



C)

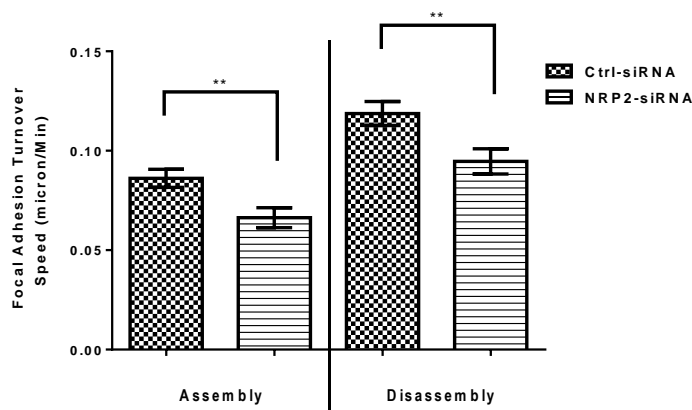


**Figure 4.6 NRP2 regulate FAs turnover.** **A)**  $1 \times 10^6$  ECs were nucleofected with either Ctrl-siRNA or NRP2-siRNA and seeded in 10-cm dishes pre-coated with  $10 \mu\text{g/ml}$  FN for 48 hours at  $37^\circ\text{C}$  in a  $\text{CO}_2$  incubator. Following two washes with PBS, the cell lysates were subjected to a DC protein assay. From each sample,  $20 \mu\text{g/ml}$  were analysed by Western blot to examine the expression of both paxillin and phospho-paxillin using ImageJ™ densitometry software. GAPDH was used as a loading control. **B)**  $1 \times 10^6$  ECs were double nucleofected with paxillin-GFP construct plus either Ctrl-siRNA or NRP2-siRNA. The cells were then seeded in 10-cm dishes pre-coated with  $10 \mu\text{g/ml}$  FN overnight at  $37^\circ\text{C}$  in a  $\text{CO}_2$  incubator. The following day,  $4 \times 10^4$  cells per condition were seeded on three coverslips pre-coated with  $10 \mu\text{g/ml}$  FN. 24 hours later, individual cells were then imaged every minute for 30 minutes, using an inverted fluorescence microscope. Each FA turnover was analysed by tracking the front of FA (assembly) and the back of FA (disassembly) using the ImageJ™ MTrackJ plugin. One representative cell per condition is shown here; the arrows indicate the direction of cells movement. **C)** The bar chart shows the speed of FAs (assembly and disassembly) in microns/minute of mean (+SEM); in each bar chart,  $n > 100$  FAs. The asterisks indicate statistical significance: \*\*  $P < 0.01$ . Unpaired two-tailed t-test.

## 4.7. Identifying the potential NRP2 binding partners using Mass Spectrometry (MS).

So far, we have shown that NRP2 plays an essential role in FN-dependent migration, adhesion and FA turnover in mLMECs. Though we were mainly interested in the potential interactions between NRP2 and integrins that might be responsible for these findings, due to the large number of proteins involved in FA formation and turnover, we decided to take an unbiased approach to identifying NRP2's binding partners by using mass spectrometry. We transfected three different WT EC lines (Cell Lines 2, 3 and 4) (see **Figure 3.1 C-D**) with either NRP2-siRNA or Ctrl-siRNA and incubated them for 48 hours at 37°C. NRP2 was then immunoprecipitated and NRP2-associated proteins were re-suspended in 20 µl lysis buffer. NRP2 knockdown was confirmed by Western blotting (**Figure 4.7 A**). The efficiency of the IPs was confirmed in two ways: (1) before sending the samples for MS analysis, 5 µl of each sample was subjected to SDS-PAGE separation followed by Silver Staining (**Figure 4.7 B**) to determine sample complexity (we hypothesised that anything immunoprecipitated by anti-NRP2 antibody in NRP2-siRNA treated cells would be non-specific, and that the sample would be less complex), whereas 1 µg of total cell lysate was used as a measure of the overall immunoprecipitation (IP) efficiency; (2) Ctrl-siRNA and NRP2-siRNA samples from two cell lines were sent off for MS analyses, while samples from the third cell line were stored at -20°C for further verification of the (MS) analysis (explained later in **section 2.9**). Peptides in each sample were detected using Label-Free quantitative (LFQ) mass spectrometry, as three technical repeats, and analysed by Andromeda software integrated in MaxQuant software. Each dot in **Figure 4.7 C** represents a single hit protein, which is the average Log<sub>2</sub> of three LFQs derived from (Ctrl-siRNA) minus (NRP2-siRNA) in each cell line (one cell line plotted on the x-axis, the other plotted on the y-axis). A large number of proteins (1,154 hits) were detected in MS. To narrow our focus, we considered proteins detected more in NRP2-siRNA IP samples than Ctrl-siRNA as non-specific binding. To further clarify: the single dot at the (0,0) point contains (507 hits) detected more in (NRP2-siRNA samples) than (Ctrl-siRNA samples) in both cell lines, whereas (195 hits), blotted in the x-axis, and (365 hits), plotted in the y-axis, were detected more in Ctrl-siRNA samples than NRP2-siRNA samples in cell line clones (#1) and (#2), respectively. It is worth pointing out that some of the hits detected in only one cell line are probably true NRP2 binding partner proteins (such as ITGB3, ITGA6, ITGA3 and others), but we decided to focus only on those proteins (87 hits) detected more in (Ctrl-siRNA samples) than (NRP2-siRNA samples) in **both** cell lines (**Table 4.1**).

Among these hits, four microvascular ECs specific markers were identified as NRP2 binding partners: Pecam1, Mcam, Endoglin and Plasmalemma vesicle-associated protein (PLVAP) (Adams and Alitalo 2007) (Keuschnigg, Tvorogov et al. 2012) (Herrnberger, Ebner et al. 2012) (Keuschnigg, Karinen et al. 2013) (Park, Sorenson et al. 2015) (see **Figure 4.7 C**). Interestingly, three fibronectin receptors were identified in both cell lines: ITGA5, ITGAV and ITGB1 (see **Figure 4.7 C**). NRP1, which shares similar domain structure with NRP2, was not detected at all, suggesting that the anti-NRP2 antibody is specific, and that NRP2 does not physically interact with NRP1.

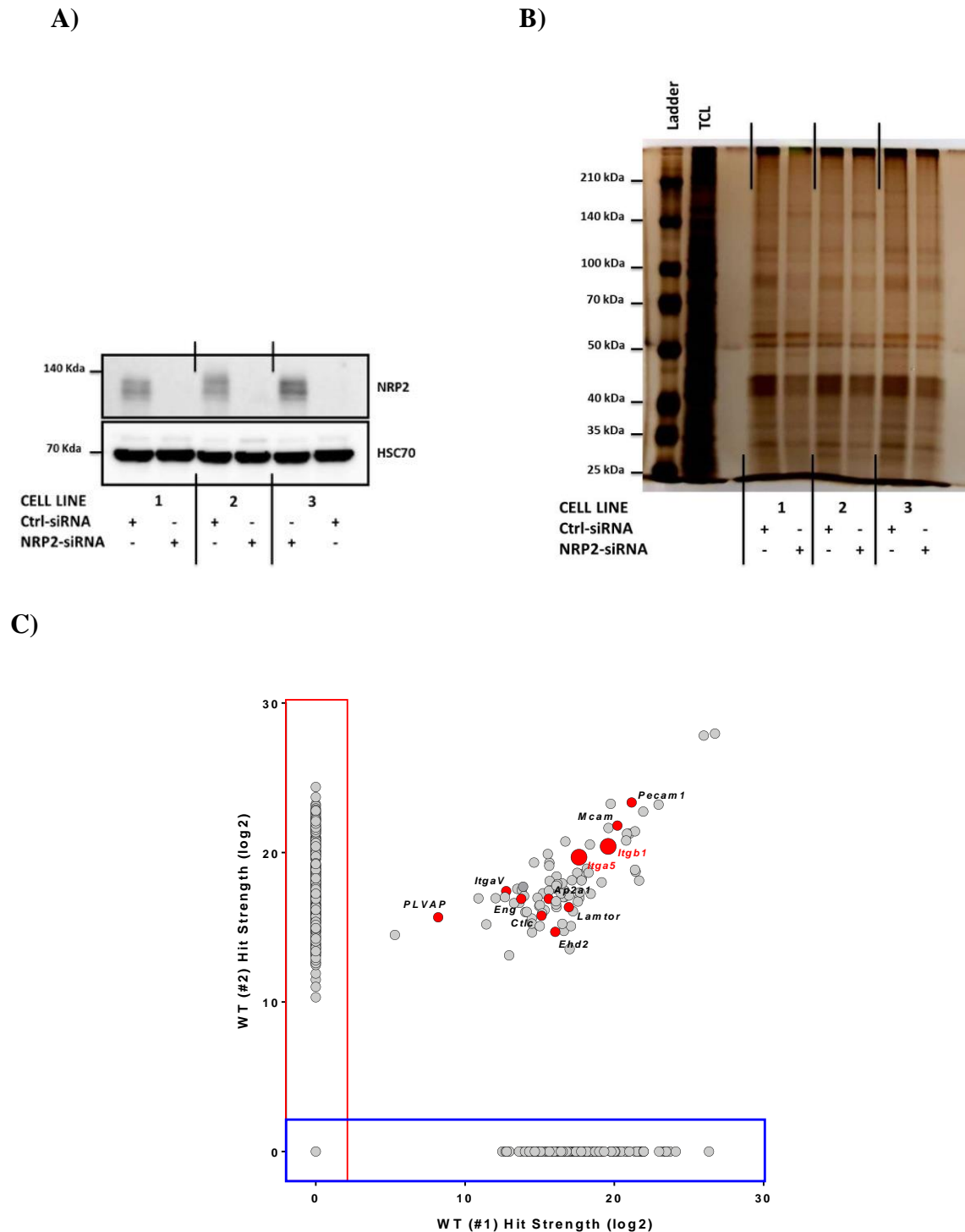


**Figure 4.7 Mass Spectrophotometry to identify NRP2's binding partners.**  $1 \times 10^6$  cells were nucleofected with either Ctrl-siRNA or NRP2-siRNA and seeded in 10-cm dishes pre-coated with  $10 \mu\text{g/ml}$  FN and incubated at  $37^\circ\text{C}$  in a  $\text{CO}_2$  incubator. 48 hours later, the ECs were washed twice with PBS before the cells were lysed with (25 mM Tris-HCl, pH 7.4, 100 mM NaCl, 2 mM MgCl<sub>2</sub>, 1 mM Na<sub>3</sub>VO<sub>4</sub>, 0.5 mM EGTA, 1% Triton X-100, 5% glycerol, cocktail protease inhibitors) and then transferred to 1.5-ml centrifuged tubes on ice. The tubes were centrifuged at 12,000 g for 20 minutes, and the lysates were then analysed by DC proteins assay. **A)** 20  $\mu\text{g}$  of total cell lysates (TCL) from the three cell line clones were subjected to a Western blot analysis of NRP2 knockdown. **B)** 1,200  $\mu\text{g}$  from all three cell line clones were subjected to NRP2 immunoprecipitation in a total volume of 1 ml of lysis buffer for overnight incubation with magnetic Dynabeads Protein G coupled with NRP2 antibody. After resuspending the NRP2-associated proteins in 20  $\mu\text{l}$  of lysis buffer, 5  $\mu\text{l}$  from each clone (cell line clone #1 and #2) was subjected to SDS-PAGE separation and silver staining, whereas 1  $\mu\text{g}$  of TCL was used as a measure of the overall IP efficiency. **C)** 86 hits of 1,166 proteins were detected as NRP2 binding partner proteins, including ITGA5, ITGAV, ITGB1, Mcam and Pecam1.

**Table (4.1):** Label-Free quantitative (LFQ) mass spectrometry results of NRP2 immunoprecipitation in two mLMEC clones.

Gene names	Protein names	Log2 of three (LFQ) derived from (Ctrl-siRNA) minus (NRP2-siRNA)	
		mLMECs (1)	mLMECs (2)
<i>Shank3</i>	SH3 and multiple ankyrin repeat domains protein 3	17.82211	18.26145
<i>Itgav</i>	<b>Integrin alpha-V;Integrin alpha-V heavy chain;Integrin alpha-V light chain</b>	12.75036	17.41807
<i>Eif3k</i>	Eukaryotic translation initiation factor 3 subunit K	16.67751	17.44238
<i>Ldlr</i>	Low-density lipoprotein receptor	16.65608	17.01857
<i>Ubp2</i>	Ubiquitin-associated protein 2	15.22819	17.27588
<i>Tfpi</i>	Tissue factor pathway inhibitor	15.94133	17.69823
<i>Lgals8</i>	<b>Galectin-8</b>	14.48788	14.66178
<i>Ywhag</i>	14-3-3 protein gamma;14-3-3 protein gamma, N-terminally processed	11.42696	15.19255
<i>Pecam1</i>	<b>Platelet endothelial cell adhesion molecule</b>	21.15972	23.34476
<i>Actb;Actg1</i>	<b>Actin, cytoplasmic 1;Actin, cytoplasmic 1, N-terminally processed</b>	26.74492	27.96095
<i>Anxa1</i>	<b>Annexin;Annexin A1</b>	14.97204	16.4172
<i>Ddx3x;DIPas1</i>	ATP-dependent RNA helicase DDX3X;Putative ATP-dependent RNA helicase P110	16.1337	18.40222
<i>Eif4e2</i>	Eukaryotic translation initiation factor 4E type 2	14.8525	16.96642
<i>Cope</i>	<b>Coatomer subunit epsilon (COP-I)</b>	12.94733	13.11721
<i>Fmr1</i>	Fragile X mental retardation protein 1 homolog	12.05212	16.94615
<i>Sipa1</i>	Signal-induced proliferation-associated protein 1	16.50711	17.93118
<i>Ctnnb1</i>	<b>Catenin beta-1</b>	14.04132	16.01054
<i>Cald1</i>	Caldesmon	15.64976	19.31011
<i>Eps15</i>	Epidermal growth factor receptor substrate 15	13.49852	17.56639
<i>Eng</i>	<b>Endoglin</b>	13.63594	16.6332
<i>Ahnak2</i>	AHNAK nucleoprotein 2	15.62247	17.44713
<i>Plvap</i>	<b>Plasmalemma vesicle-associated protein</b>	8.196397	15.66909
<i>Sdcbp</i>	<b>Syntenin-1</b>	16.56674	17.01283
<i>Myadm</i>	Myeloid-associated differentiation marker	14.62495	19.32868
<i>H2-D1;H-2D;H2-L</i>	H-2 class I histocompatibility antigen, D-B alpha chain;H-2 class I histocompatibility antigen, L-D alpha chain	13.2829	16.61588
<i>Tuba1b;Tuba4a</i>	Tubulin alpha-1B chain;Tubulin alpha-4A chain	17.77056	18.55225
<i>Itgb1</i>	<b>Integrin beta-1</b>	19.58851	20.40907

<i>Itga5</i>	<b>Integrin alpha-5;Integrin alpha-5 heavy chain;Integrin alpha-5 light chain</b>	17.63318	19.69024
<i>Rpl7</i>	<b>60S ribosomal protein L7</b>	22.96149	23.20262
<i>Ap2a1</i>	<b>AP-2 complex subunit alpha-1</b>	15.59941	16.89696
<i>Slc2a1</i>	Solute carrier family 2, facilitated glucose transporter member 1	17.6579	16.96909
<i>Rpl13a</i>	<b>60S ribosomal protein L13a</b>	19.60422	21.64278
<i>Cttna1</i>	<b>Catenin alpha-1</b>	14.46956	15.58295
<i>Pabpc1</i>	Polyadenylate-binding protein;Polyadenylate-binding protein 1	21.00949	21.25427
<i>Kras;Hras</i>	GTPase KRas;GTPase KRas, N-terminally processed;GTPase HRas;GTPase HRas, N-terminally processed	15.3272	16.14503
<i>Rpl18</i>	<b>60S ribosomal protein L18</b>	21.38325	21.41876
<i>Sep-02</i>	Septin-2	18.15594	18.91559
<i>Pura</i>	Transcriptional activator protein Pur-alpha	18.42197	17.23809
<i>Capza2</i>	<b>F-actin-capping protein subunit alpha-2</b>	21.93517	22.74181
<i>Rpl9</i>	<b>60S ribosomal protein L9</b>	20.84547	21.25882
<i>Atp6v0d1</i>	V-type proton ATPase subunit d 1	10.89936	16.93522
<i>Entpd1</i>	Ectonucleoside triphosphate diphosphohydrolase 1	15.66521	18.09918
<i>Acot8</i>	Acyl-coenzyme A thioesterase 8	15.01396	16.4817
<i>Eif4a1;Eif4a2</i>	Eukaryotic initiation factor 4A-I;Eukaryotic initiation factor 4A-II;Eukaryotic initiation factor 4A-II, N-terminally processed	13.80137	17.49214
<i>Actr1a</i>	<b>Alpha-centractin (Arp1)</b>	15.16257	15.92509
<i>Rpl37a</i>	<b>60S ribosomal protein L37a</b>	21.42535	18.72089
<i>Rps24</i>	<b>40S ribosomal protein S24</b>	16.96428	17.11952
<i>Rps26</i>	<b>40S ribosomal protein S26</b>	21.66345	18.11942
<i>Actg1</i>	<b>Actin, cytoplasmic 2;Actin, cytoplasmic 2, N-terminally processed</b>	21.38089	18.84251
<i>Rala</i>	Ras-related protein Ral-A	17.51902	18.64505
<i>Rpl22</i>	<b>60S ribosomal protein L22</b>	20.79656	20.80591
<i>Actc1;Acta2;Actg2;Acta1</i>	<b>Actin, alpha cardiac muscle 1;Actin, aortic smooth muscle;Actin, gamma-enteric smooth muscle;Actin, alpha skeletal muscle</b>	16.71621	20.74104
<i>Ywhah</i>	14-3-3 protein eta	16.12161	16.34551
<i>Cct2</i>	<b>T-complex protein 1 subunit beta (TCP1)</b>	17.23135	16.06967
<i>Tubb5;Tubb2b;Tubb2a;Tubb3</i>	<b>Tubulin beta-5 chain;Tubulin beta-2B chain;Tubulin beta-2A chain;Tubulin beta-3 chain</b>	16.61827	14.75881
<i>Rsu1</i>	Ras suppressor protein 1	13.95432	17.09032
<i>Scamp1</i>	<b>Secretory carrier-associated membrane protein 1</b>	14.12918	16.03603

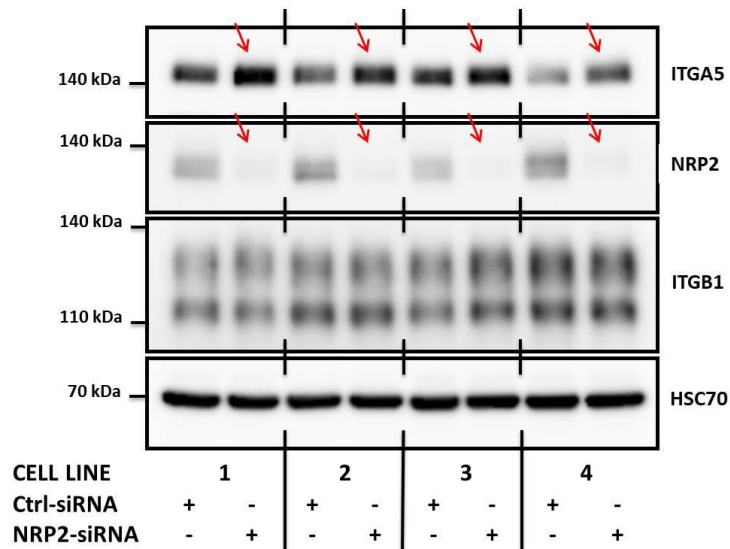
<i>Lrrc59</i>	Leucine-rich repeat-containing protein 59	17.09987	15.07779
<i>Tmod3</i>	<b>Tropomodulin-3</b>	19.75966	23.26303
<i>Pdia6</i>	Protein disulfide-isomerase A6	12.67655	17.01683
<i>Vat1</i>	Synaptic vesicle membrane protein VAT-1 homolog	14.4797	15.24995
<i>Eif3f</i>	Eukaryotic translation initiation factor 3 subunit F	16.42773	17.25752
<i>Btf3</i>	Transcription factor BTF3	17.55739	16.72103
<i>Scamp3;Tu52</i>	<b>Secretory carrier-associated membrane protein 3</b>	16.18946	17.89125
<i>Ddx1</i>	ATP-dependent RNA helicase DDX1	17.0069	13.54432
<i>Igf2bp2</i>	Insulin-like growth factor 2 mRNA-binding protein 2	16.95587	16.34851
<i>Cltc</i>	<b>Clathrin heavy chain;Clathrin heavy chain 1</b>	15.11689	15.77486
<i>Fxr2</i>	Fragile X mental retardation syndrome-related protein 2	17.69423	17.33225
<i>Rpl35</i>	<b>60S ribosomal protein L35</b>	18.36439	20.53602
<i>Actb12</i>	<b>Beta-actin-like protein 2</b>	25.99547	27.82845
<i>Ehd2</i>	<b>EH domain-containing protein 2 (EHD2)</b>	16.04132	14.69171
<i>Rtn4</i>	Reticulon;Reticulon-4	18.27337	18.64878
<i>Add3</i>	<b>Gamma-adducin</b>	15.54402	19.90345
<i>Fbxo30</i>	F-box only protein 30	15.00358	15.07755
<i>Tollip</i>	Toll-interacting protein	5.29768	14.48283
<i>Add2</i>	<b>Beta-adducin</b>	13.89125	17.71187
<i>Ralb</i>	Ras-related protein Ral-B	17.80305	18.1332
<i>Mcam</i>	<b>Cell surface glycoprotein MUC18</b>	20.20144	21.8063
<i>Myct1</i>	<b>Myc target protein 1</b>	13.76763	16.90254
<i>Pcd10</i>	Programmed cell death protein 10	17.15686	18.14309
<i>Rps5</i>	<b>40S ribosomal protein S5;40S ribosomal protein S5, N-terminally processed</b>	19.15041	18.0047
<i>Lamtor1</i>	<b>Ragulator complex protein LAMTOR1</b>	16.09562	16.52925
<i>Napa</i>	<b>Alpha-soluble NSF attachment protein</b>	14.9917	15.09713
<i>Lsm12</i>	Protein LSM12 homolog	16.51124	15.23132
<i>Plac8</i>	Placenta-specific gene 8 protein	15.63915	19.11841
<i>Flii</i>	<b>Protein flightless-1 homolog (flightless I actin binding protein)</b>	16.09678	16.73463
<i>Twf2</i>	<b>Twinfilin-2 (Twinfilin actin binding protein 2)</b>	16.10847	17.78743

#### **4.8. siRNA-mediated knockdown of NRP2 upregulates ITGA5 expression.**

As mentioned previously, some of the MS hits that were only detected in one cell line are likely true hits, but were set-aside (these might be followed up in future studies) to help focus the studies. ITGB3 happens to be one of these hits, suggesting a link between NRP2 and ITGB3, but, as we have shown, this potential link does not seem to play a role in EC migration (see **Figure 4.3**). Therefore, we focused our attention on the other integrin subunits that were identified in both cell lines. We decided to ignore (at least at this stage) ITGAV subunit because it would be an ITGB3 binding partner (ITGB5 might also be an ITGAV binding partner, but this subunit was not detected in the MS). Therefore, we were left with ITGA5 and ITGB1 subunits which dimerise to form the fibronectin receptor ( $\alpha5\beta1$ ).

Given that  $\alpha5\beta1$  heterodimer is known to be the predominant receptor in ECs mediating adhesion to FN (Serini, Valdembri et al. 2006), (Hynes 2007), (Valdembri, Caswell et al. 2009), (Mana, Clapero et al. 2016), we wondered if the reduction in FN-dependent cell migration, adhesion and FA turnover was due to the disruption of the  $\alpha5\beta1$  heterodimerization in mLMECs. Therefore, we decided to examine whether NRP2 knockdown regulates the expression level of either subunit. Interestingly, the siRNA-mediated silencing of NRP2 resulted in the upregulation of ITGA5 subunit expression in four different ECs clones, whereas the expression of the ITGB1 subunit did not change (**Figure 4.8 A-B**).

**A)**



**B)**



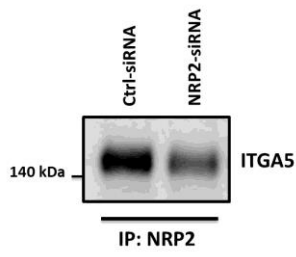
**Figure 4.8 siRNA-mediated silencing of NRP2 upregulates ITGA5 expression, but not ITGB1.**  $1 \times 10^6$  cells from four different EC clones were nucleofected with either Ctrl-siRNA or NRP2-siRNA and seeded in 10-cm dishes pre-coated with 10  $\mu$ g/ml FN and incubated at 37°C in a CO<sub>2</sub> incubator. The ECs were then washed twice with PBS before lysing the cells. Protein quantification was analysed using DC protein assay, and an equivalent concentration of 20  $\mu$ g from each sample was subjected to Western blot analysis to determine **A)** the total expression of both ITGA5 and ITGB1 subunits. **B)** The bar charts of means (+SEM) show the levels of the ITGA5 and ITGB1 subunits normalised against HSC70 using ImageJ™ densitometric quantification. The asterisks indicate statistical significance: \* P<0.05; nsd means not significantly different. Unpaired two-tailed t-test.

#### **4.9. ITGA5 subunit interacts with NRP2.**

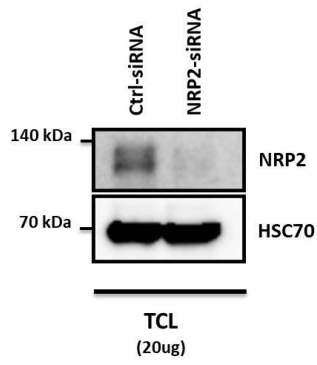
A previous study has shown that NRP2 can form a complex with ITGA5 when NRP2 is co-immunoprecipitated from a co-culture of renal cell carcinoma and HUVECs (Cao, Hoepfner et al. 2013). Another study has shown that NRP1 co-immunoprecipitated with ITGA5 in HUVEC (Valdembri, Caswell et al. 2009). Our MS analyses suggest NRP2 can form a complex with ITGA5 in mLMECs.

To further validate our MS results, samples from the third cell line (as mentioned above) were subjected to Western blot analyses (**Figure 4.9 A**). We confirmed ITGA5 was co-immunoprecipitated with NRP2; however, some ITGA5 was also co-immunoprecipitated with NRP2 in NRP2-depleted cell lysates (see **Figure 4.9 A**), which is likely due to incomplete silencing of NRP2. To explore this, we decided to further verify the interaction between NRP2 and ITGA5 by reducing the incubation time of NRP2 co-immunoprecipitation to 1 hour and compare it to overnight incubation, which was our standard immunoprecipitation incubation period used in the MS studies (**Figure 4.9 C**). In this experiment NRP2 was also immunoprecipitated from 1200 µg of total cell lysate but this time non-specific IgG was used as a negative control. We also included an additional control in which 600 µg from each (Ctrl-siRNA sample) and (NRP2-siRNA sample) (see **Figure 4.9 C** Lane 5) were equally mixed to investigate whether the amount of the co-immunoprecipitated ITGA5 would increase. Interestingly, ITGA5 was co-immunoprecipitated with NRP2 in both the short and overnight incubations (see **Figure 4.9 C**). Finally, we also demonstrated the interaction between the two proteins by immunoprecipitating with anti-ITGA5 and probing for NRP2 (**Figure 4.9 E**). We concluded from these studies that there is a physical interaction between ITGA5 and NRP2.

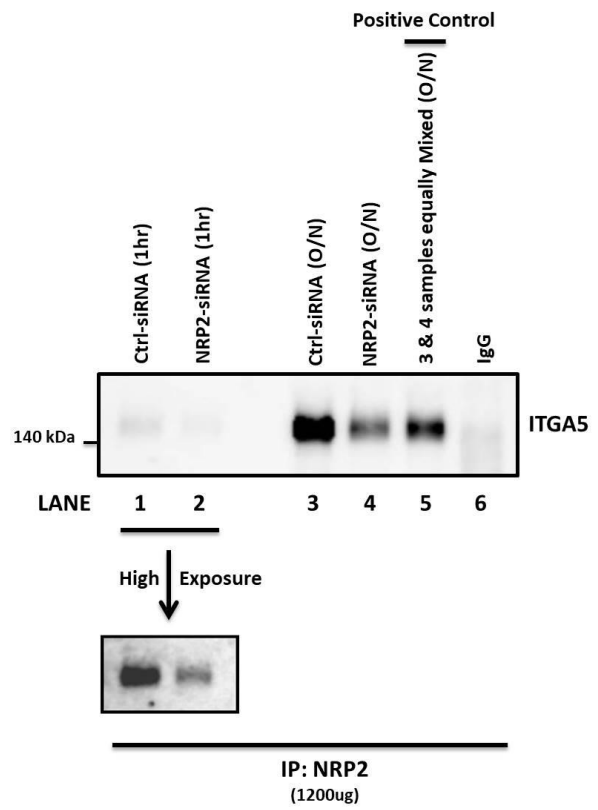
**A)**



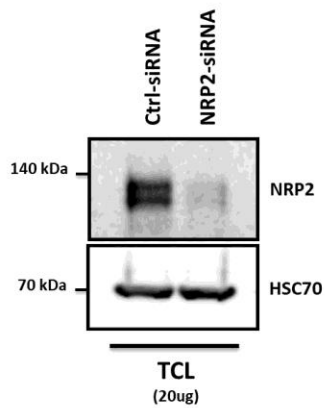
**B)**



**C)**



D)



E)

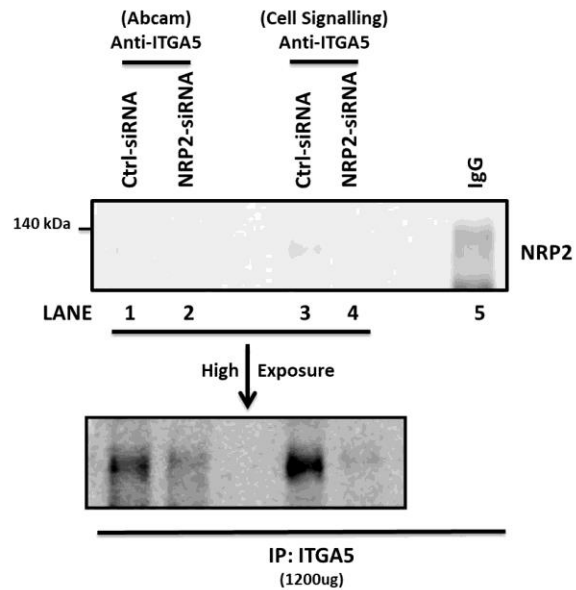


**Figure 4.9 ITGA5 is a partner binding with NRP2.** A) Ctrl-siRNA and NRP2-siRNA from cell line clone #3 were subjected to Western blot analysis to verify the direct physical interaction between NRP2 and ITGA5. **B-E)**  $1 \times 10^6$  cells were nucleofected with either Ctrl-siRNA or NRP2-siRNA and seeded in 10-cm dishes pre-coated with 10  $\mu\text{g/ml}$  FN and incubated at 37  $^\circ\text{C}$  for 48 hours. The cells then were lysed on ice, and the lysates were subjected to DC protein quantification assay. **B & D)** 20  $\mu\text{g}$  of total cell lysate was subjected to Western blot analysis to determine the efficiency of NRP2 silencing. **B-C)** NRP2 was immunoprecipitated from 1,200  $\mu\text{g}$  of total protein concentration for a short period immunoprecipitation (1 hour) or overnight immunoprecipitation at 4  $^\circ\text{C}$  before subjecting the sample to Western blot analysis to determine **B)** the efficiency of NRP2 knockdown and **C)** the presence of ITGA5 in the NRP2 IPed samples. IgG was used as a negative control, whereas (Lane 5), which is a mixture of (Lane 3) 600  $\mu\text{g}$  from Ctrl-siRNA plus (Lane 4) 600  $\mu\text{g}$  from NRP2-siRNA, was used as a positive control. **D-E)** ITGA5 was immunoprecipitated from 1,200  $\mu\text{g}$  of total protein concentration using two different anti-ITGA5 antibodies overnight before subjecting the samples to Western blot analysis to determine **D)** the efficiency of NRP2 knock down and **E)** the presence of NRP2 in the ITGA5 IPed samples. IgG was used as a negative control.

## 4.10. Discussion

Integrins are the main heterodimeric transmembrane receptor proteins that transduce signalling bi-directionally by connecting the ECM deposition proteins to the actin cytoskeleton by recruiting intracellular adaptor proteins to the cytoplasmic tails of the activated integrins (Menter and DuBois 2012), (Hu and Luo 2013), (Tabatabai and Weller 2013). Integrins regulate many cellular processes, including cell adhesion, proliferation, migration, differentiation, survival, apoptosis, the shapes of certain types of cells, ECM protein assembly, cytoskeleton organisation and angiogenesis under physiological and pathological conditions (Bökel and Brown 2002) (Srichai and Zent 2010), (Pan, Zhao et al. 2016), (Jia, Choi et al. 2018). With respect to angiogenesis, integrins modulate the behaviour of many cell types, including ECs, perivascular cells, fibroblasts and BMDC (Desgrosellier and Cheresh 2010).

The major integrins in ECs are  $\alpha\beta3$ ,  $\alpha5\beta1$ ,  $\alpha\beta5$  and  $\alpha6\beta4$  (Somanath, Ciocea et al. 2009). During angiogenesis, integrins enhance the signal transduction of VEGFs through interactions with VEGFRs and NRPs (Menter and DuBois 2012), (Goel and Mercurio 2012), (Seguin, Desgrosellier et al. 2015). Many studies have shown that  $\alpha\beta3$  “cross talked” with VEGFR2 (Soldi, Mitola et al. 1999), (Mahabeleshwar, Feng et al. 2006), (Mahabeleshwar, Chen et al. 2008), (Mahabeleshwar, Feng et al. 2007), (Dellinger and Brekken 2011), (West, Meller et al. 2012). (Gong, Yang et al. 2013), (Ravelli, Mitola et al. 2013), (Reynolds, Wyder et al. 2002), (Reynolds, Reynolds et al. 2004), (Robinson, Reynolds et al. 2004), (D'Amico, Robinson et al. 2010), (Masson-Gadais, Houle et al. 2003) (see chapter 1; **subsection 1.2.3.2.3.1.1**), while others showed “cross-talk” between  $\alpha\beta3$  and NRP1 (Robinson, Reynolds et al. 2009), (Ellison, Atkinson et al. 2015). The expression of  $\alpha\beta3$  is upregulated in sprouting capillaries under physiological and pathological conditions, whereas its expression is rarely detected in quiescent capillaries (Hodivala-Dilke, Reynolds et al. 2003), (Somanath, Malinin et al. 2009). In ECs, ITGAV subunits can pair with the  $\beta1$ ,  $\beta3$ ,  $\beta5$  and  $\beta8$  subunits, whereas the ITGB3 subunit only pairs with the ITGAV subunit, which means that the investigation of the functions of endothelial  $\alpha\beta3$  in ECs can be conducted best by manipulating the ITGB3 subunit (Hynes 2002).

Reynolds *et al.* showed that the genetic depletion of the ITGB3 subunit resulted in the upregulation of VEGF, VEGFR2, and ERK1/2 phosphorylation in ECs, indicating that the absence of the *Itgb3* gene increased VEGF-induced angiogenesis, which resulted in excessive

vasculature and enhanced tumour growth (Reynolds, Wyder et al. 2002), (Reynolds, Reynolds et al. 2004). Robinson *et al.* found that the complete loss of *Itgb3* gene enhanced ECs permeability through the upregulation of VEGF-VEGFR2-ERK1/2 signalling (Robinson, Reynolds et al. 2004). In another study, Robinson found that NRP1 and ERK1/2 were also elevated in ITGB3-NULL ECs. He also showed that NRP1-VEGFR2 co-immunoprecipitation was augmented in ITGB3-NULL ECs compared with WT ECs even in the absence of VEGF treatment. Furthermore, NRP1 knockdown reduced the phosphorylation of VEGFR2 and ERK1/2 in the ECs of both WT and ITGB3-NULL ECs. In *in vivo* and *ex vivo* assays, Robinson showed that targeting NRP1 in ITGB3-NULL mice significantly inhibited VEGF-induced angiogenesis to a greater extent than that in WT, indicating that the elevation of angiogenesis in the absence of the *Itgb3* gene is dependent on NRP1 expression (Robinson, Reynolds et al. 2009). This study showed that when ITGB3 subunit is expressed normally, through its cytoplasmic tail, it limits the interaction between NRP1 and VEGFR2. Hence, NRP1 becomes less substantial through its contribution to VEGF-induced signalling, migration, vessel infiltration and sprouting angiogenesis. However, when the *Itgb3* gene is absent or siRNA-depleted, VEGF induces VEGFR2 phosphorylation, angiogenesis and tumour growth, become NRP1-dependent (Robinson, Reynolds et al. 2009).

Because the complete loss of the *Itgb3* gene resulted in the elevation of angiogenesis and targeting NRP1 only inhibited the otherwise enhance angiogenesis (Reynolds, Wyder et al. 2002), (Reynolds, Reynolds et al. 2004), (Robinson, Reynolds et al. 2004), (Robinson, Reynolds et al. 2009), the Robinson group ceased using ITGB3-NULL mice and instead generated  $\beta$ 3HET mice to overcome the developmental upregulation of the VEGFR2, ERK1/2 and NRP1 expressions that arose in ITGB3-NULL mice, while maintaining the 50% expression of ITGB3, which is critical for full VEGFR2 function (Ellison, Atkinson et al. 2015). Unlike ITGB3-NULL ECs, VEGFR2 expression was not significantly increased in  $\beta$ 3HET ECs. Additionally, the VEGF-induced association between NRP1 and VEGFR2 was, unlike NULL cells, unchanged. Importantly, though,  $\beta$ 3HET ECs migrated faster than WT ECs, and, like NULL ECs, retained sensitivity to NRP1 perturbations, unlike their WT counterparts (Ellison, Atkinson et al. 2015).

As mentioned previously, because of the structural and the functional similarity between NRP1 and NRP2 (see chapter 1; **subsection 1.2.3.1.4.2**), and because no study has addressed the interaction between NRP2 and integrins within ECs, we investigated the potential link between the ITGB3 subunit and NRP2 in mLMECs. Similar to NRP1 (Ellison, Atkinson et

al. 2015), we found that NRP2 expression was upregulated in  $\beta$ 3HET ECs compared to WT ECs. Additionally, the upregulation of NRP2 expression was also observed in ITGB3-siRNA-depleted WT ECs, indicating that the upregulation of NRP2 expression is not a response to a long-term depletion of the *Itgb3* gene, as it can be replicated by ITGB3-siRNA knockdown (see **Figure 4.1 A-B**). Furthermore, we showed that NRP2 knockdown did not change NRP1 expression in the presence or absence of VEGF<sub>164</sub> (see **Figure 4.1 C**). This result suggests that NRP1 does not compensate the loss of NRP2 expression in ECs in short-term depletion.

It was previously shown by Robinson *et al.* that inhibiting NRP1 function with a peptide minimally reduced VEGF-induced angiogenesis in WT mice (Robinson, Reynolds *et al.* 2009). However, this effect was exacerbated in ITGB3-NUL mice, indicating that ITGB3 limits the participation of NRP1 in VEGF-driven angiogenesis when ITGB3 is expressed normally (Robinson, Reynolds *et al.* 2009). Additionally, the authors also showed that NRP1 knockdown significantly reduced VEGFR2 and ERK1/2 phosphorylation in WT and ITGB3-NUL ECs (Robinson, Reynolds *et al.* 2009), which supported the finding of other studies that NRP1 expression in ECs acted as co-receptor molecule with VEGFR2 to enhance VEGF-induced downstream signalling (Prahst, Héroult *et al.* 2008), (Fuh, Garcia *et al.* 2000), (Gluzman-Poltorak, Cohen *et al.* 2001), (Kärpänen, Heckman *et al.* 2006), (Xu, Yuan *et al.* 2010), (Ballmer-Hofer, Andersson *et al.* 2011), (Fearnley, Smith *et al.* 2016), (Fuh, Garcia *et al.* 2000), (Herzog, Pellet-Many *et al.* 2011), (Tiwari, Jung *et al.* 2012). Similarly, this effect was also exacerbated in ITGB3-NUL mice compared to WT mice (Robinson, Reynolds *et al.* 2009). Furthermore, Pan *et al.* found some evidence of the same effect by showing that blocking the extracellular domains (b1/b2) of NRP1 with the function-blocking antibodies directed against NRP1 marginally, but not significantly, reduced VEGFR2 and ERK1/2 phosphorylation levels (Pan, Chantry *et al.* 2007). A subsequent study showed that VEGFR2 phosphorylation was not significantly altered by deleting the NRP1 cytoplasmic tail in either WT or  $\beta$ 3HET ECs, suggesting that the cytoplasmic tail of NRP1 is not required for VEGFR2 phosphorylation in mLMECs. In contrast to VEGFR2 phosphorylation, ERK1/2 phosphorylation was sensitive to the deletion of the NRP1 cytoplasmic tail (Ellison, Atkinson *et al.* 2015). Unlike the NRP1 knockdown (Robinson, Reynolds *et al.* 2009), our findings showed that NRP2 knockdown produced no significant changes in the overall VEGFR2 and ERK phosphorylation when comparing WT and  $\beta$ 3HET ECs (see **Figure 4.2**), thus

suggesting the absence of a link between ITGB3 and NRP2-dependent VEGF-induced signalling.

Regarding migration, Pan *et al.* showed that the inhibition of the NRP1 function by blocking its extracellular domain had no effect on the HUVEC migration on FN in the absence of VEGF. However, the inhibition of the NRP1 function in the presence of VEGF significantly reduced VEGF-induced EC migration, in an *in vitro* endothelial bead sprouting angiogenesis assay, and in an *in vivo* corneal pocket neovasciogenesis assay (Pan, Chanthery *et al.* 2007). Robinson *et al.* showed that both ITGB3-NULL ECs and the siRNA-depletion of ITGB3 expression in WT ECs significantly enhanced ECs migration, whereas targeting both ITGB3 and NRP1 suppressed the enhancement of EC migration (Robinson, Reynolds *et al.* 2009). A subsequent study showed that the deletion of the cytoplasmic tail of NRP1 did not affect WT mLMECs migration on FN in the presence or absence of VEGF<sub>164</sub> stimulation (Ellison, Atkinson *et al.* 2015). However,  $\beta$ 3HET EC migration was significantly reduced when the cytoplasmic tail of NRP1 was deleted, indicating that NRP1 regulates mLMECs migration only when ITGB3 expression is reduced (Ellison, Atkinson *et al.* 2015). Our finding showed that NRP2 knockdown significantly reduced mLMECs migration on FN in both WT and  $\beta$ 3HET ECs (see **Figure 4.3**). The effects of reduction in both cell types upon NRP2 knockdown were similar, suggesting that NRP2 regulates ECs migration on FN independently of ITGB3.

The upregulation of NRP2 expression we observed when ITGB3 expression was reduced (see **Figure 4.1**) suggests an, as yet, unclear cross-talk mechanism between NRP2 and ITGB3, which needs further investigation. However, because we did not observe any link between NRP2 and ITGB3 in VEGF-VEGFR2-ERK1/2 signalling (see **Figure 4.2**) or EC migration (see **Figure 4.3**), we decided to take the effect of NRP2 knockdown in ECs to the next step and investigate how NRP2 regulates EC migration independently of both VEGF-stimulation and ITGB3. Therefore, we first investigated whether NRP2 knockdown affected mLMEC proliferation. In two different proliferation assays, we found that NRP2 knockdown did not affect mLMECs proliferation on FN (see **Figure 4.4**). This finding supported previous findings that suggested that NRP2 does not play a role in the proliferation of lymphatic ECs (Favier, Alam *et al.* 2006), (Caunt, Mak *et al.* 2008) and cancer cells (Goel, Pursell *et al.* 2012), (Cao, Hoepfner *et al.* 2013).

Because cell adhesion is a key regulator during cell migration (Nagano, Hoshino et al. 2012), (Small, Rottner et al. 1998), (Knight, Laukaitis et al. 2000), (Webb, Parsons et al. 2002), (Li, Guan et al. 2005), we asked whether the reduction of the EC migration upon NRP2 knockdown was the result of the attenuation of EC adhesion on the FN substratum. Interestingly, we found that NRP2-siRNA-treated mLMECs adhered to the FN substratum more slowly than the Ctrl-siRNA-treated cells, suggesting that NRP2 plays an essential role in the adhesion of mLMECs to FN (see **Figure 4.5**).

The FA intracellular adapter protein paxillin is essential during cell migration (Zaidel-Bar, Milo et al. 2007), (Pasapera, Schneider et al. 2010). Using a transwell chamber coated with 1% gelatin and Matrigel to study cell migration and invasion, respectively, German *et al.* showed that paxillin or NRP2 knockdown in the presence of growth factors, including bFGF, VEGF, IGF, EGF and 5% serum, exhibited ~2 or ~1.5 fold increases, respectively, in HUVEC migration and invasion compared to siRNA-treated cells. Additionally, paxillin knockdown exhibited a 50% decrease in NRP2 at both protein and mRNA levels in cultured HUVEC. The overexpression of NRP2 prevented the augmentation of HUVEC migration and invasion in paxillin-depleted HUVEC, suggesting that paxillin controls angiogenesis by altering NRP2 expression (German, Mammoto et al. 2014). Because integrins accumulate at the lamellum to form stable FAs that act as “hand grips” in connecting the ECM to the intracellular cytoskeleton during the cell migration process (Small, Rottner et al. 1998), (Webb, Parsons et al. 2002), (Li, Guan et al. 2005), and the disruption of integrin attachment to the ECM substratum or any of the FAs intracellular adaptor proteins, such as paxillin (see chapter 1; **Figure 1.16**), affects cellular adhesion and migration, we sought to determine whether NRP2 expression contributed to the assembly and disassembly of FAs. Therefore, before using paxillin as a marker of FAs, we first sought to determine whether NRP2 knockdown in mLMECs changed the expression of paxillin on the FN substratum in the absence of VEGF<sub>164</sub> stimulation. We found that both the total and phosphorylation protein levels of paxillin were unchanged in NRP2-siRNA-treated cells compared to siRNA-Ctrl-treated cells (see **Figure 4.6 A**). Interestingly, consistent with the attenuation we observed in mLMEC migration and adhesion upon NRP2 knockdown, we found that the NRP2-siRNA-treated cells exhibited reduced assembly and disassembly (turnover) of FAs on FN (see **Figure 4.6 B-C**).

We next employed NRP2 co-immunoprecipitation followed by silver staining to confirm the uniform efficiency of the immunoprecipitation between the samples, and we used MS to

identify potential binding partners of NRP2 (see **Figure 4.7**). Interestingly, the MS analysis did not show NRP1 as a binding partner of NRP2, which supported our findings (see **Figure 3.2 C** and **4.1 C**), which showed that NRP1 did not compensate the loss of NRP2 expression. Our MS analysis identified three FN receptors: ITGA5, ITGAV and ITGB1 (see **Figure 4.7 C**). With respect to the ITGAV subunit, it is a binding partner of both ITGB3 and ITGB5. However, because we showed the absence of a link between ITGB3 and NRP2 in EC migration, and the MS analysis showed that ITGB5 was not a binding partner, we were left with the ITGA5 and ITGB1 subunits, the main FN receptor ( $\alpha 5\beta 1$ ) in ECs to mediate the adhesion to FN (Serini, Valdembri et al. 2006), (Hynes 2007), (Valdembri, Caswell et al. 2009), (Mana, Clapero et al. 2016). Therefore, we first examined the effects of NRP2 knockdown on the total expression of the ITGA5 and ITGB1 subunits. The Western blot analysis of four different clones of WT mLMECs revealed that the NRP2-siRNA-depleted ECs exhibited the upregulation of the ITGA5 subunit, whereas the ITGB1 subunit was unchanged (see **Figure 4.8**). This potential cross-talk between the NRP2 and ITGA5 subunits led us to examine the direct interaction between these two molecules before proceeding further. Interestingly, the co-immunoprecipitation experiment revealed that both molecules co-immunoprecipitated with one another, indicating a physical interaction between ITGA5 and NRP2 in mLMECs (see **Figure 4.9**).

## **4.11. Conclusion**

In this chapter, we have shown that:

- **NRP2 expression, similar to NRP1, is upregulated in  $\beta 3$ HET ECs compared to WT ECs, and that upregulation of NRP2 is not a response to long-term depletion of ITGB3.**
- **NRP2 knockdown modestly attenuates ERK and VEGFR2 phosphorylation, but this is independent of ITGB3 expression.**
- **NRP2 knockdown significantly reduces mLMEC random migrations, and, this too is not linked to ITGB3.**
- **NRP2 does not regulate ECs proliferation.**
- **NRP2 knockdown reduced the relative number of mLMECs adhered to FN matrix.**

- **NRP2 knockdown slows the rate of FA turnover.**
- **siRNA-mediated knockdown of NRP2 upregulates ITGA5 subunit expression, but not ITGB1 subunit expression.**
- **MS analysis identified the major FN receptors  $\alpha 5\beta 1$  as NRP2 binding partners. Importantly, NRP2 is not a binding partner with NRP1.**

## Chapter 5: Investigating how NRP2 regulates ITGA5 function in mouse lung endothelial cells

---

In the previous chapter, we reported that siRNA-mediated knockdown of NRP2 resulted in a significant reduction in migration, adhesion, FA turnover and the upregulation of ITGA5 levels. In this chapter, we attempt to understand how NRP2 regulates ITGA5 function.

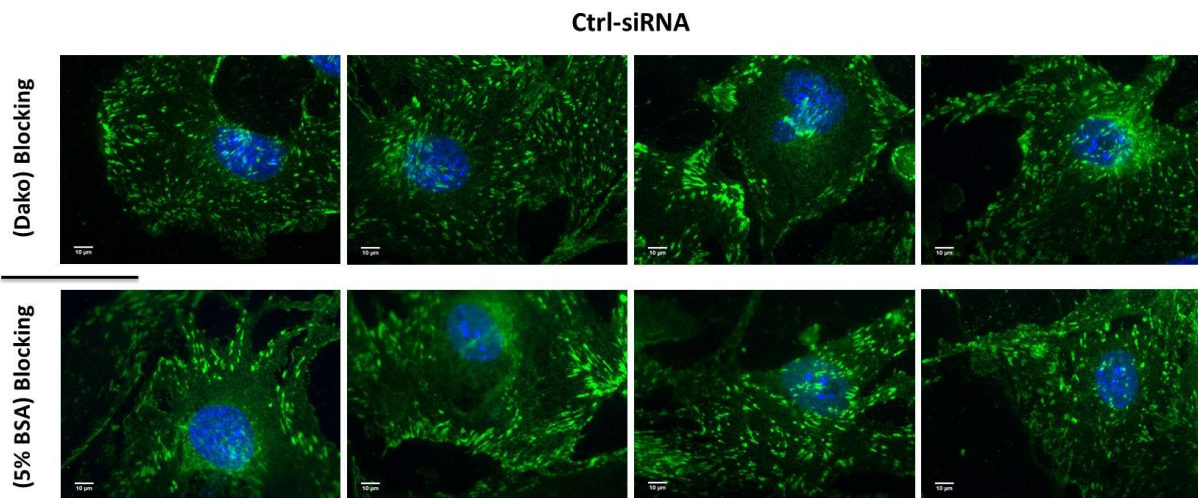
### 5.1. NRP2 knockdown disrupts the structural formation of ITGA5 on FN; and attempting to localise NRP2 with ITGA5 in mLMECs.

The interaction of cells with ECM during cell migration has been described as developing in three stages: 1) focal contacts, which represent the short-lived structural interactions of cells with ECM through  $\alpha\beta3$  integrins; 2) FAs, which are contacts developed from the clustering of both  $\alpha\beta3$  and  $\alpha5\beta1$  integrins to form a stable adhesion contact with ECM; 3) fibrillar adhesions, which are developed exclusively (on fibronectin) when  $\alpha5\beta1$  integrins translocate from FAs along the ECM fibronectin contact (Zaidel-Bar, Ballestrem et al. 2003), (Pankov, Cukierman et al. 2000), (McCleverty, Lin et al. 2007). A previous study showed NRP1 (structurally related to NRP2) in HUAEC promotes cell adhesion to FN. It does not directly interact with FN, but instead its cytoplasmic SEA motif first binds to the adaptor protein (GIPC1), which in turn binds to the ITGA5 subunit through its C-terminal SDA sequence; however, this interaction which stimulates  $\alpha5\beta1$  integrin endocytosis and trafficking appears to be specific for active  $\alpha5\beta1$  heterodimers. Subsequently, NRP1 guides and promotes the internalisation of active  $\alpha5\beta1$  heterodimers to intracellular vesicles, which are then rapidly trafficked and, finally, recycled back to the plasm membrane (Valdembri, Caswell et al. 2009).

NRP2 and NRP1 have a similar domain structure (Zachary 2014). However, no previous study has addressed a potential biological interaction between NRP2 and ITGA5 in ECs. Therefore, we decided to investigate further whether the observed physical interaction between NRP2 and ITGA5 (see **Figure 4.9**) influences ITGA5 biology. Given their similar domain structure, and given the upregulation of ITGA5 upon NRP2 knockdown (see **Figure 4.8 A-B**), we sought to determine whether NRP2 co-localises with ITGA5 in ECs, and whether NRP2 regulates ITGA5 trafficking in ECs.

To carry out this investigation, we first tried to visualise ITGA5 movement in living cells by transfecting cells with GFP-labelled ITGA5. However, the signal of the ITGA5-GFP construct (kindly provided by Dr. Maddy Parsons) was too weak to visualise, at least in our hands, using the equipment available to us. Therefore, we visualised endogenous ITGA5 in fixed cells treated with Ctrl-siRNA or NRP2-siRNA. Twenty-four hours post siRNA treatment, cells were seeded overnight on coverslips pre-coated with FN. The cells were fixed, permeabilised, blocked and immuno-labelled for both ITGA5 and NRP2. Whilst ITGA5 was readily detected, we were unable to convince ourselves that NRP2 signals were specific. Three different anti-NRP2 antibodies (Abcam 155680, Cell Signalling 3366S and Millipore AB10522) (see **Figure 3.2 B**) were tested using different dilutions of these antibodies as well as different blocking solutions (BSA or Dako<sup>®</sup> Protein Block Serum-Free). However, no difference in the intensity of NRP2 staining was detected when comparing the NRP2-depleted cells to control cells. We therefore examined ITGA5 localisation in isolation. Interestingly, compared to control cells, NRP2-siRNA treated ECs exhibited a significant disruption of ITGA5 organisation, which appeared in elongated fibrillar structures (**Figure 5.1**). Using ImageJ<sup>™</sup> software, we measured the overall length of these ITGA5 containing structures in both NRP2-depleted and control cells and noted a significant increase in NRP2-siRNA treated cells (**Figure 5.2**).

A)



B)

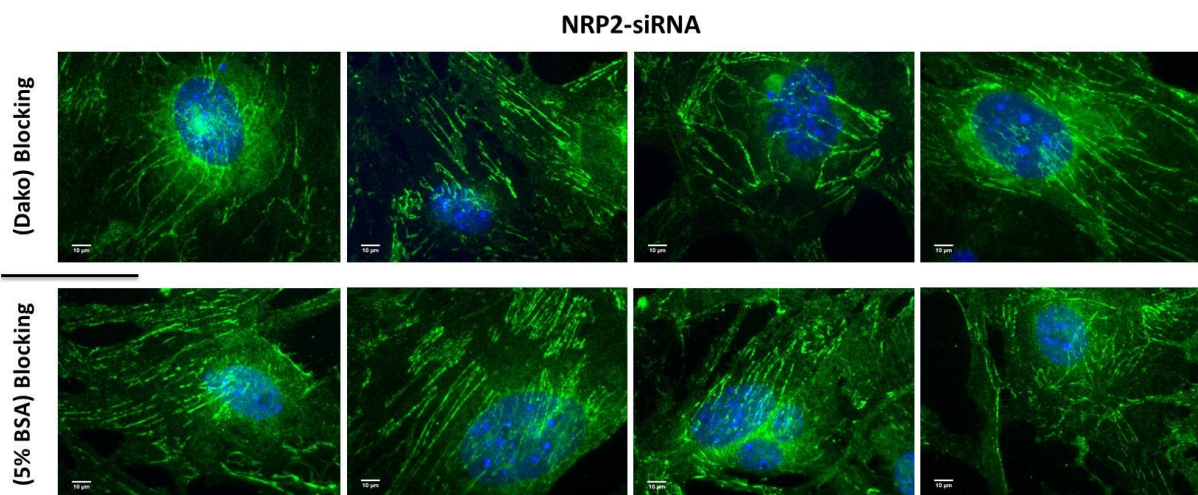
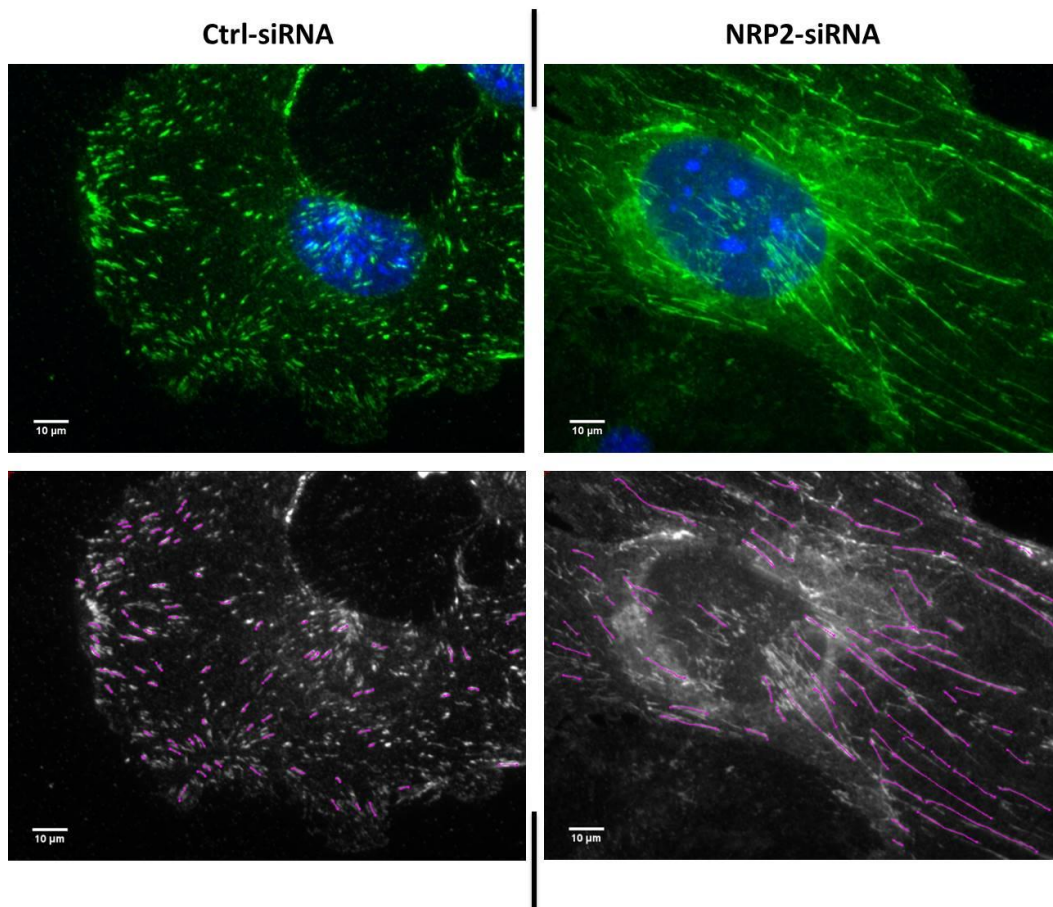


**Figure 5.1 NRP2 knockdown disrupts the structural formation of ITGA5 subunit on FN.** ECs were nucleofected with either Ctrl-siRNA or NRP2-siRNA and seeded on 10-cm dishes pre-coated with 10  $\mu\text{g/ml}$  FN and incubated at 37  $^{\circ}\text{C}$  in  $\text{CO}_2$  incubator. Thirty-six hours later, the cells were trypsinised and seeded at low density on coverslips pre-coated with 10  $\mu\text{g/ml}$  FN and incubated at 37  $^{\circ}\text{C}$  in  $\text{CO}_2$  incubator for 12 hours. The cells were fixed and permeabilised before blocking with either 5% BSA or Dako Protein Block Serum-Free. ECs were then incubated with rabbit anti-ITGA5 primary antibody overnight in a humidified chamber at 4  $^{\circ}\text{C}$ . Following two washes to remove the unreacted primary antibody, the cells were incubated with donkey anti-rabbit Alexa 488 secondary antibody. The coverslips were mounted with Prolong Gold with Dapi to stain the nucleus in blue, whereas ITGA5 was stained green. **A)** Representative ECs treated with Ctrl-siRNA. **B)** Representative NRP2-depleted ECs. Scale bar is shown as 10  $\mu\text{m}$ .

A)



B)

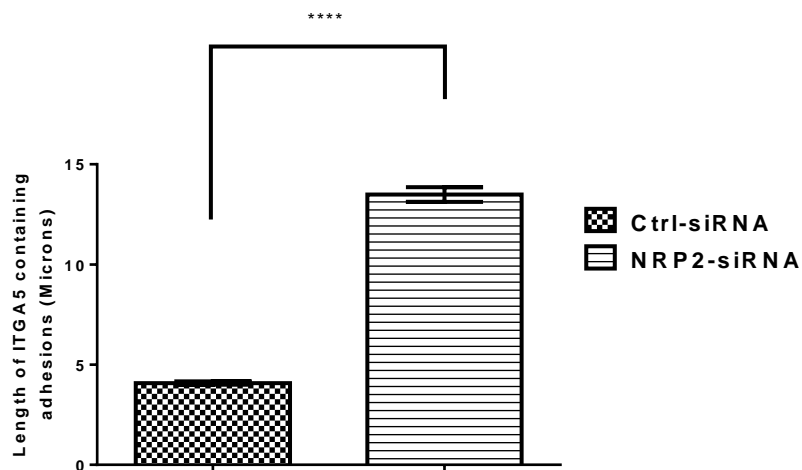


**Figure 5.2 Measuring the elongated shape of the ITGA5 formed in the NRP2-depleted ECs compared to control cells.** A) A representative EC (Top) treated with either Ctrl-siRNA or NRP2-siRNA. ImageJ™ software Plugin-(simple neurite tracer) was used to measure the length of ITGA5 in both siRNA-nucleofected conditions. B) The bar chart shows the average length of ITGA5 in both siRNA-nucleofected conditions; n>490, and (mean +SEM). Asterisks indicate statistical significance: \*\*\*\* P<0.0001

## **5.2. Subcellular protein fractionation revealed NRP2 is localized in cellular membranes.**

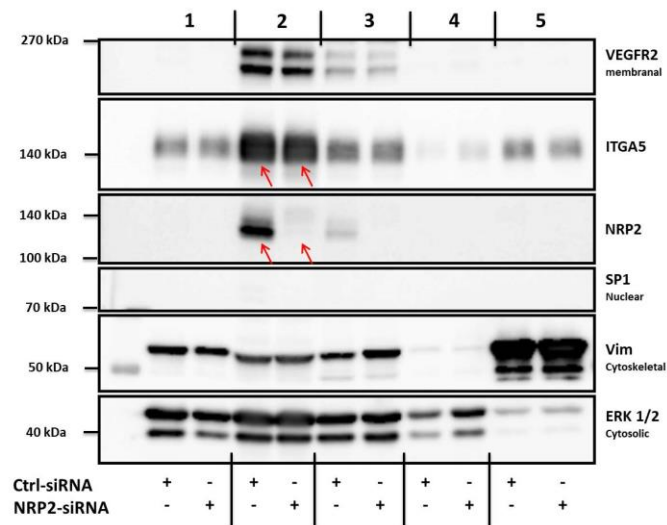
Since the late 1980s (Bretscher 1989), (Szeczek and Juliano 1990), it has been known that integrin heterodimers are internalised from the plasma membrane, trafficked into endosomal compartments, and recycled back to the cell surface (Ramsay, Keppler et al. 2007).

Because we were not able to visualise NRP2 in our mLMECs (see above), we decided to examine NRP2's subcellular localisation biochemically. To this end, we employed a subcellular protein fractionation kit, which allows the extraction of subcellular proteins from five different cellular compartments sequentially (i.e., cytoplasm, cellular membranes, soluble nucleus, chromatin-bound nucleus and cytoskeleton) based on the addition of different extraction buffers for each compartment and different centrifugation speeds to separate the proteins residing in these different compartments from the same starting material. We reasoned that if NRP2 regulates ITGA5 trafficking, which may be the reason for the disruption of ITGA5 organisation in NRP2-depleted cells, as shown in **Figure 5.1** and **5.2**, this assay might yield a general idea of which compartments display changes in ITGA5 or NRP2 cellular distribution. Prior to describing the findings from these studies, it is worth noting the following: 1) because of the sequential extraction of cellular compartments from the same cell pellet, there is some inevitable carry over between extraction steps (i.e. the method is not perfect in definitively isolating each examined compartment); 2) the membrane extraction buffer extracts proteins that reside in the plasma membrane, mitochondrial membrane, and ER and Golgi membranes; in other words, these distinct, and important, locations cannot be distinguished from one another using this method.

Nonetheless, we explored the distribution of both NRP2 and ITGA5 in siRNA-treated cells using this method. Interestingly, NRP2 seemed to reside only in the cellular membrane compartments in Ctrl-siRNA treated cells (**Figure 5.3 A**). In contrast, although ITGA5 was detected in all subcellular compartments (noting the limitations mentioned above), most was localised in cellular membranes. Taken together, this suggests that ITGA5 and NRP2 normally co-localise in cellular membranes. Upon NRP2 knockdown, only small changes were observed in ITGA5 localisation: we noted increased levels of ITGA5 in the cytoplasm and in cellular membranes, and a reduction in the cytoskeleton compartment (**Figure 5.3 B**).

Given the noted changes in ITGA5 expression and organisation upon NRP2-depletion e.g. upregulation of total cellular expression (see **Figure 4.8 A-B**), changes in what look to be fibrillar adhesions (see **Figure 5.1 and 5.2**), and potential changes in subcellular distribution (see **Figure 5.3**), coupled with observed physical interactions between NRP2 and ITGA5 (see **Figure 4.9**), we decided to further explore whether NRP2 regulates ITGA5 trafficking.

A)



B)

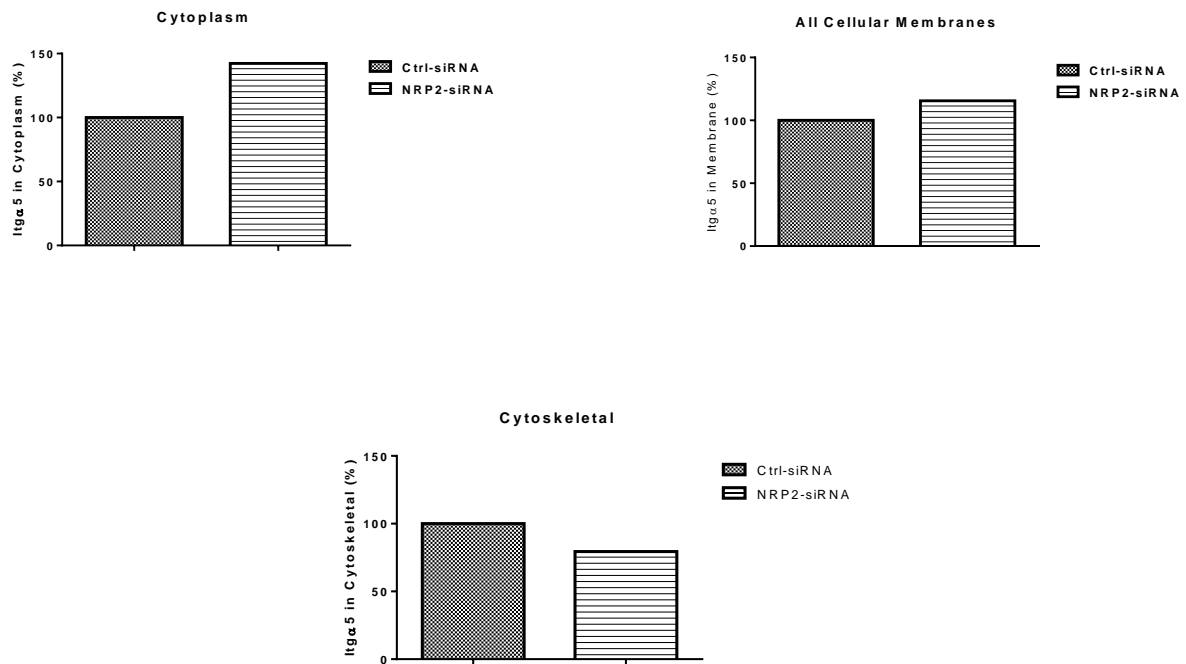


**Figure 5.3 NRP2 resides only in the cellular membranes in which only the compartment NRP2 was localised with ITGA5.** A)  $4 \times 10^6$  ECs were nucleofected with either Ctrl-siRNA or NRP2-siRNA and seeded in a T75 flask pre-coated with 10  $\mu\text{g/ml}$  FN and incubated at 37 °C in CO<sub>2</sub>. Twenty-four hours later, the cells were trypsinised and  $3 \times 10^6$  cells from each siRNA-nucleofected condition were seeded in a new T75 flask pre-coated with 10  $\mu\text{g/ml}$  FN and incubated at 37 °C in CO<sub>2</sub> incubator. After another 24 hours, the cells were detached with sodium saline buffer and then transferred to tubes that were centrifuged at 500 g for 4 minutes to obtain a visible pellet from each siRNA-nucleofected condition. The pellets were then subjected to the cellular fractionation assay to extract proteins from five subcellular compartments sequentially (i.e., cytoplasm, cellular membranes, soluble nucleus, chromatin-bound nucleus and finally cytoskeleton) based on different extraction buffers and different centrifugation speeds. B) Fractionated samples were then subjected to Western blot analysis, and the blot was quantified by ImageJ™ densitometric analysis. The controls were (1) cytoplasmic extract; (2) all cellular membranes extracts; (3) soluble nuclear extracts; (4) chromatin-bound extracts; (5) cytoskeletal extracts. ITGA5 level in each compartment was normalised to the control detected in that compartment. The bar charts represent the ITGA5 levels in different compartments normalised to the indicated protein control of that compartment.

### **5.3. NRP2 seems to regulate ITGA5 turnover**

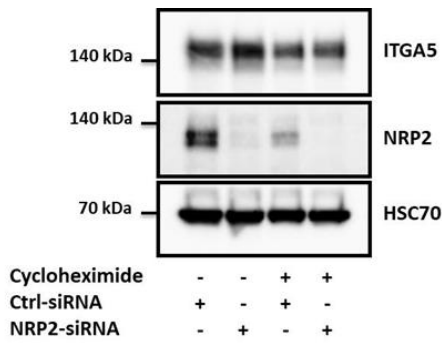
Seven different large ribosomal 60S subunits (Rpl3a, Rpl7, Rpl8, Rpl9, Rpl22, Rpl35 and Rpl37a) and three different small ribosomal 40S subunits (Rps5, Rps24 and Rps26) were detected as partner proteins of NRP2 in MS (see **Table 4.1**). These interactions, in addition to the upregulation of ITGA5 in the cytoplasm upon NRP2 knockdown in the fractionation study (see **Figure 5.3 B**), suggested that NRP2 may regulate the translation of ITGA5. Therefore, we decided to examine this potential mechanism by treating cells with cycloheximide, which inhibits protein synthesis by binding to the E-site of the large ribosomal 60S subunit and subsequently blocking translational elongation (Schneider-Poetsch, Ju et al. 2010), (Klinge, Voigts-Hoffmann et al. 2011).

ECs were transfected with either Ctrl-siRNA or NRP2-siRNA and treated with 10 µg/ml of cycloheximide for eight hours as described previously (Sampieri, Nuttall et al. 2008). The lysates then were subjected to a Western blot to analyse the half-life of ITGA5 (**Figure 5.4 A-B**). Cycloheximide successfully inhibited the synthesis of both ITGA5 and NRP2 compared to the untreated ECs (levels of both were decreased after cycloheximide treatment). However, after cycloheximide treatment, there was no significant difference in the level of ITGA5 in the NRP2-depleted ECs compared to the Ctrl-siRNA treated ECs; the normally increased expression of ITGA5 observed upon NRP2 knockdown was gone. This suggested to us that either NRP2 regulates ITGA5 translation, or ITGA5 is turned-over faster in the absence of NRP2.

### **5.4. NRP2 knockdown does not change ITGA5 levels on the cell surface**

Integrins are the main ECM receptors, and the number of these receptors expressed on the plasma membrane is believed to be proportional to the efficacy of the spreading and adhesion of cells on ECM (Ginsberg, Partridge et al. 2005), (Serini, Valdembri et al. 2006). Because we also detected a slight increase in ITGA5 level in the NRP2-depleted membrane extracted proteins, which could be any of the cellular membranes, we decided to start with the plasma membrane and examine the expression of ITGA5 on the cell surface using flow cytometry. However, no significant difference was observed in the amount of total ITGA5 on the plasma membrane compared to the Ctrl-siRNA treated cells (**Figure 5.5**).

A)



B)

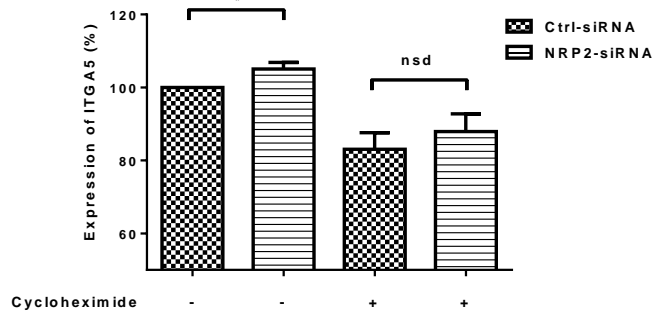


**Figure 5.4 NRP2 regulates ITGA5's turnover.**  $4 \times 10^6$  ECs were nucleofected with either Ctrl-siRNA or NRP2-siRNA, seeded in a T75 flask pre-coated with  $10 \mu\text{g/ml}$  FN and then incubated at  $37^\circ\text{C}$  in  $\text{CO}_2$ . Twenty-four hours later, the cells were trypsinised and seeded at a density of  $3 \times 10^6$  cells serum-free OptiMEM<sup>®</sup> in new T75 flasks pre-coated with  $10 \mu\text{g/ml}$  FN to starve the cells for 12 hours. Then  $10 \mu\text{g/ml}$  of cycloheximide was added to half of the dishes for eight hours. Following lysing, the cells were subjected to DC protein quantification assay. **A)** The lysates were subjected to a Western blot to examine the levels of ITGA5 and NRP2 with or without the cycloheximide treatment. **B)** The graph shows the level of ITGA5 analysed by ImageJ<sup>™</sup> densitometric quantification;  $n = 4$ , and (mean +SEM). The asterisks indicate statistical significance:  $* = 0.029$ ; nsd means not significantly different. Unpaired two-tailed t-test.

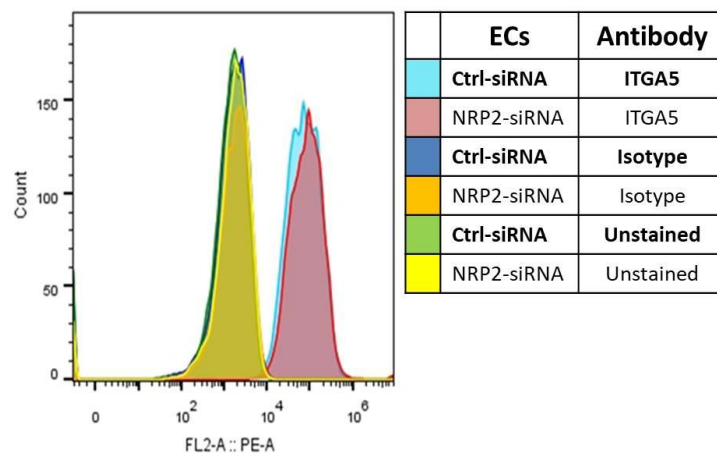


**Figure 5.5 NRP2 does not change the amount of ITGA5 on the plasma membrane.** The nucleofected ECs with either Ctrl-siRNA or NRP2-siRNA were seeded in 10-cm dishes pre-coated with  $10 \mu\text{g/ml}$  FN and incubated at  $37^\circ\text{C}$  in  $\text{CO}_2$ . After 48 hours, the cells were detached with sodium saline buffer, centrifuged, and resuspended in FACS buffer.  $1 \times 10^5$  ECs from each siRNA-nucleofected condition were untreated with antibody, labelled with ITGA5 BE-conjugated antibody or labelled with isotype BE-conjugated antibody control in a dark room. Flowing two washes with FACS to remove the unbound conjugated antibodies, the cells were subjected to flow cytometry to measure ITGA5 expression on the plasma membrane. The histogram was generated using FlowJo<sup>™</sup> software to analyse the expression on ITGA5 in NRP2-depleted ECs compared to the Ctrl-siRNA-transfected ECs.

## 5.5. NRP2 does not regulate the total ITGA5 subunit internalization.

Dynamic membrane trafficking (i.e., endocytosis and recycling) regulates integrin-ECM adhesion turnover and the assembly of actin cytoskeleton during cell migration (Huttenlocher and Horwitz 2011), (De Franceschi, Hamidi et al. 2015), (Ata and Antonescu 2017). In general, integrins are internalised from the plasma membrane at the base of the protrusion and retracting edge, trafficked into endosomal compartments, and then recycled back to the cell surface at the leading edge to form new adhesions. The disassembly of FAs at the cell posterior and the polymerisation of actin cytoskeletal within the lamellipodium then allows for retracting the rear of the migrating cell (Caswell and Norman 2006), (Caswell and Norman 2008), (Chao and Kunz 2009), (Ata and Antonescu 2017).

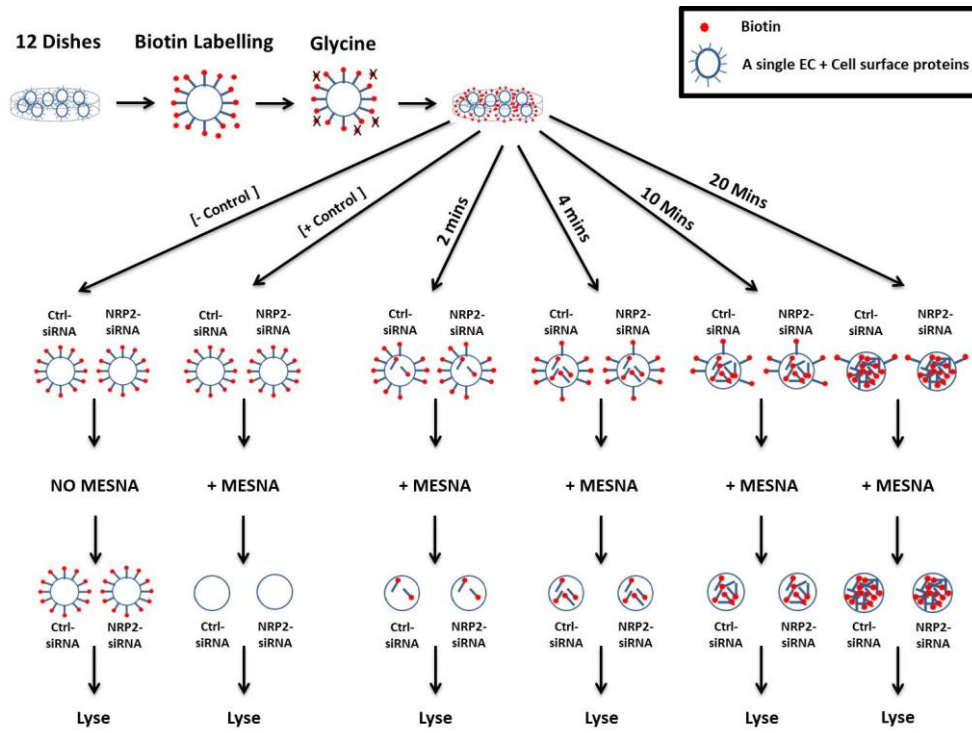
Activated integrins can be internalised through clathrin-dependent endocytosis (Ramsay, Keppler et al. 2007), (Ezratty, Bertaux et al. 2009), clathrin-independent endocytosis (Bridgewater, Norman et al. 2012), (Lakshminarayan, Wunder et al. 2014) or circular dorsal ruffles during phagocytosis (Gu, Noss et al. 2011) and then recycled back to the plasma membrane in a Ras-related family proteins (Rab)-dependent fashion (see chapter 1; **subsection 1.2.3.2.4**) (Roberts, Barry et al. 2001), (Powelka, Sun et al. 2004), (Yoon, Shin et al. 2005), (Caswell, Vadrevu et al. 2009), (Morgan, Byron et al. 2009). For example, the active  $\alpha 5 \beta 1$ -NRP1 interaction forms a complex with the GIPC1 adaptor protein, which then regulates the endocytosis of this integrin through the Rab5 pathway (Valdembri, Caswell et al. 2009) (see chapter 1; **Figure 1.18 B**). The non-ECM-engaged integrin can also be endocytosed through the clathrin-independent pathway or the caveolin-dependent pathway (Fabbri, Di Meglio et al. 2005), (Echarri and Pozo 2006). However, several lines of evidence support the idea that inactive integrins can also be endocytosed by a clathrin-adaptor mechanism (Teckchandani, Toida et al. 2009). For example, a quantitative proteomic analysis showed that depletion of the endocytic Dab2 adaptor protein in human immortalised HeLa cells slowed the endocytosis of ITGA1, ITGA2, ITGA3 and ITGB1 (but not ITGA5 or ITGAV) that were not attached to the cytoskeleton whether they were bound to ECM or not. Moreover, the same study showed that ITGA5 and ITGB1 were more dependent on AP-2 complex adaptor, or clathrin-dependent endocytosis, than on Dab2, suggesting that clathrin and the AP-2 complex adaptor regulate freely diffusing ITGA5 and ITGB1 endocytosis (Teckchandani, Toida et al. 2009). Interestingly, other studies reported that AP-2 complex (Chao and Kunz 2009) and clathrin (Ezratty, Bertaux et al. 2009) were involved in FA disassembly and regulated  $\alpha 5 \beta 1$  integrin endocytosis in a clathrin-dependent fashion (Ezratty,

Bertaux et al. 2009). MS results (shown in **Table 4.1**) identified NRP2 interactions with the clathrin-dependent endocytosis protein clathrin heavy chain and its classical AP-2 complex adaptor proteins, which bind to the cytoplasmic tail of cell surface proteins and recruit clathrin to form clathrin-coated pits (Chao and Kunz 2009), (Ezratty, Bertaux et al. 2009), (Ezratty, Bertaux et al. 2009). We therefore decided to study the endo-exocytosis of ITGA5 in NRP2-depleted cells.

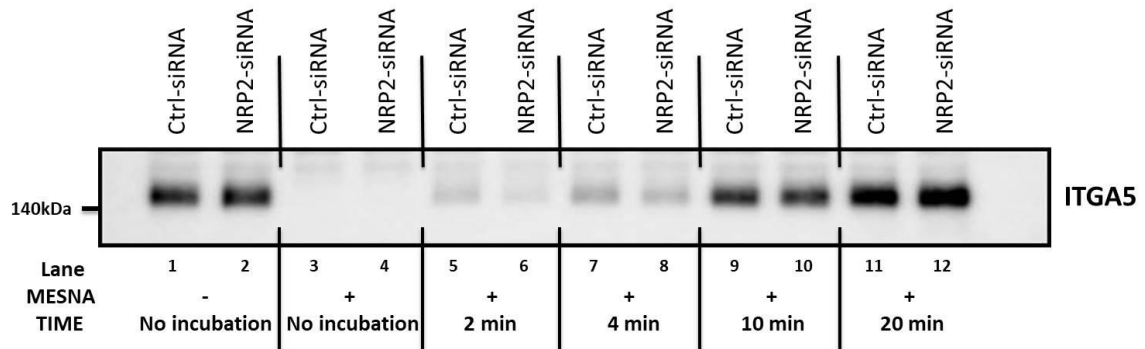
To this end, we used cell surface biotinylation assays in which cell surface proteins are first labelled with biotin and then incubated for different times at 37°C to allow the biotin-labelled proteins to internalise before remaining biotin is stripped off the cell surfaces using a membrane-impermeable reducing agent. The lysates were then subjected to immunoprecipitation for biotin before analysing the amount of the internalised protein of interest by Western blot. However, the Robinson lab previously failed to strip off the remaining biotin using two different membrane-impermeable reducing agents (Mesna and TCEP) from mLMECs (Ellison, Atkinson et al. 2015). Therefore, we first optimised the protocol by testing different concentrations of reducing agents, times of incubation and lysis buffers. After performing multiple rounds of troubleshooting, we successfully achieved the complete stripping of biotin from the cell surfaces of immortalised ECs using both reducing agents (Mesna and TCEP). In short, we found that dissolving the reducing reagents in Tris buffer (Valdembri, Caswell et al. 2009) while increasing both their concentration and the incubation period, resulted in enhancing the biotin stripping efficacy compared to dissolving the reducing agents in SBS (Remacle, Murphy et al. 2003).

Given this success, we conducted a cell surface biotinylation assay to investigate the internalisation of ITGA5 in NRP2-depleted ECs compared to Ctrl-siRNA treated cells at different incubation times. A schematic representation of the internalisation assay is shown in **Figure 5.6 A**. No change was detected in the amount of the internalised ITGA5 in the NRP2-depleted ECs compared to control cells (**Figure 5.6 B-D**). This result suggests that NRP2 does not regulate internalisation of total ITGA5. Similarly, Serini's group (Valdembri, Caswell et al. 2009) reported that human NRP1 does not regulate total ITGA5 internalisation in HUVECs. However, because they were using human cells, Valdembri *et al.* were able to examine active  $\alpha 5\beta 1$  internalisation using the SNAKA51 antibody. They found that NRP1 regulates the internalisation of the active  $\alpha 5\beta 1$ . Because no commercially available antibody detects mouse active  $\alpha 5\beta 1$ , we are unable to comment further.

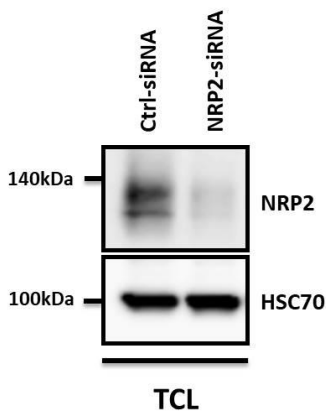
A)



B)



C)



D)

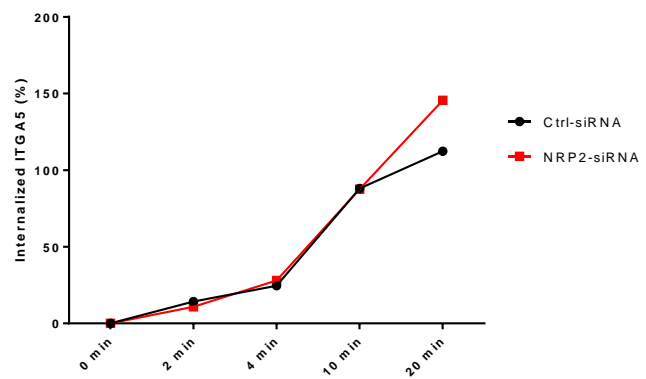


**Figure 5.6 NRP2 doesn't regulate the total ITGA5 internalization.**  $2 \times 10^6$  of ECs nucleofected with either Ctrl-siRNA or NRP2-siRNA were seeded in each 10-cm dish (12 dishes in total) that were pre-coated with  $10 \mu\text{g/ml}$  FN for 48 hours and

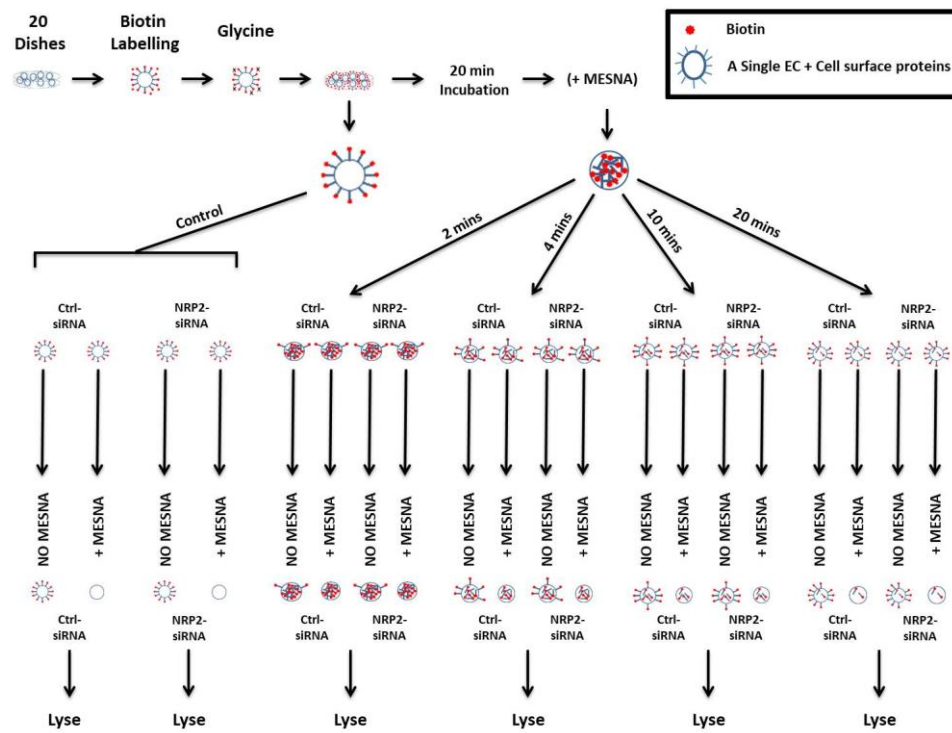
incubated at 37 °C in a CO<sub>2</sub> incubator. The cells were starved in a serum-free OptiMEM<sup>®</sup> for three hours before placing all the dishes on ice. **A)** Internalisation assay schematic, in which all steps were performed at 4 °C unless otherwise indicated. EC surface proteins were labelled with biotin before quenching the non-reacted biotin with glycine. The plates were incubated in a pre-warmed serum-free OptiMEM<sup>®</sup> for different times at 37 °C to allow the cell surface biotin-labelled proteins to internalise, whereas (-/+ control dishes were left at 4 °C. Then the incubated plates were immediately placed on ice to stop the internalisation process. The remaining biotin on the cell surfaces in the incubated plates, including the (+) control plates, was stripped off by Mesna before quenching the Mesna with iodoacetamide. The cells in all the plates were lysed at the same time. The lysates were subjected to a DC protein assay and then immunoprecipitated for biotin. **B)** Western blot of biotin-pulldowns shows the internalisation level of ITGA5 over the indicated time. **C)** Western blot shows the efficiency of NRP2 knockdown. The blot in B) was quantified by a densitometric analysis. **D)** The graph shows the internalisation of ITGA5 in percentages at different times normalised to their total level (in cells not incubated and not stripped off). The data are representative of two independent experiments.

## **5.6. NRP2 knockdown supresses ITGA5 subunit recycling.**

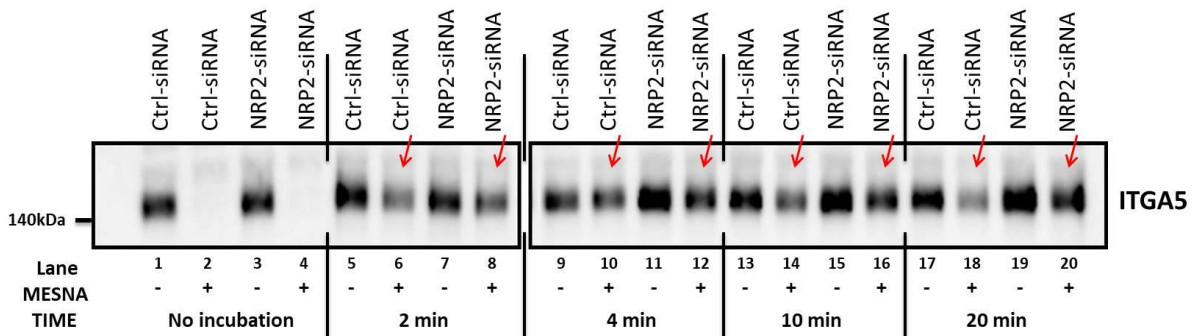
Because NRP2 did not regulate the internalisation of ITGA5 (see **Figure 5.6**), but the MS data analysis identified an interaction between NRP2 and other trafficking and recycling molecules (see **Table 4.1**), including Lamtor1, Scamp1, Scamp3, COPI,  $\alpha$ -SNAP and Annexin-A1, we conducted a recycling assay to investigate whether NRP2 regulates ITGA5 recycling to the plasma membrane.

A recycling assay was performed in a manner that was similar to the internalisation assay but with eight more plates than were used in the internalisation assay. The schematic representation of the recycling assay is shown in **Figure 5.7 A**. In this assay, the biotin-labelled cell surface proteins were allowed to internalise before stripping off the remaining biotin from the cell surfaces. The cells then were incubated at different time points before stripping off or not the recycled biotin-labelled proteins. The level of biotinylated ITGA5 was then compared between these two samples. Comparing Ctrl-siRNA cells to NRP2-depleted cells, we found that ITGA5 is recycled to the plasma membrane more slowly in the latter (**Figure 5.7 B-D**).

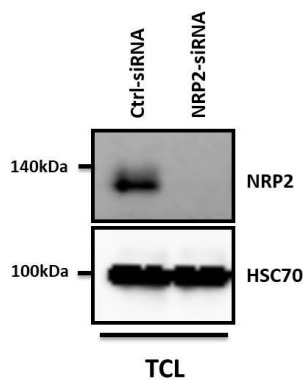
A)



B)



C)



D)

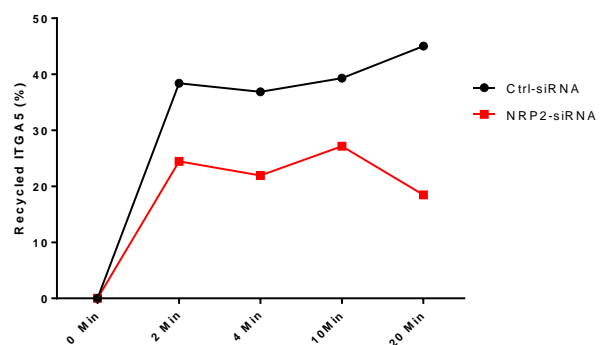


**Figure 5.7 NRP2 knockdown suppresses total ITGA5 Recycling.**  $2 \times 10^6$  of ECs nucleofected with either Ctrl-siRNA or NRP2-siRNA were seeded in each 10-cm dish (20 dishes in total) that were pre-coated with  $10 \mu\text{g/ml}$  FN and incubated for 48 hours at  $37^\circ\text{C}$  in  $\text{CO}_2$ . **A)** Recycling assay schematic, in which all steps were performed at  $4^\circ\text{C}$  unless otherwise indicated. Following cell starvation and biotinylation, the cells in two plates from each siRNA-nucleofected condition (Lanes

1 to 4) were kept at 4 °C, and the rest were incubated in pre-warmed serum-free Opti-MEM® for 20 minutes at 37 °C in a CO<sub>2</sub> incubator to allow the biotin-labelled cell surface proteins to internalise. Then incubated plates were immediately placed on ice to stop the internalisation process. The un-internalised biotin-labelled proteins were stripped off by Mesna. Two plates from each condition (Lanes 5 to 20) were incubated for different periods at 37 °C in a CO<sub>2</sub> incubator to allow the internalised biotin-labelled proteins to recycle to the cell surfaces. Then the plates were immediately placed on ice to stop the recycling process. One plate from each condition (Lanes 5 to 20) was kept at 4 °C, and the rest were subjected to Mesna to strip off the recycled biotin-labelled proteins. The cells in all the plates (Lane 1 to 20) were lysed at the same time. The lysates were subjected to the DC protein assay and then immunoprecipitated for biotin. **B)** Western blot of biotin-pulldowns shows the level of ITGA5 inside the cells (i.e. the ITGA5-biotin labelled that didn't recycle back to the cell surface) over the indicated periods. **C)** Western blot shows the efficiency of NRP2 knockdown. The blot in B) was quantified by a densitometric analysis. **D)** The graph shows the percentage of the recycled ITGA5 in which the amount of ITGA5 in each siRNA-nucleofected condition was normalised to the total amount of ITGA5 on the surface of the untreated cells with Mesna in the same period of incubation. For example, lane 18 was normalised to lane 17, and lane 20 was normalised to lane 19. The control lanes (1 to 4) were used to show the efficiency of stripping biotin from the plasma membranes by Mesna. The data are representative of two independent experiments.

## 5.7. Discussion

Laukaikis *et al.* showed that the initial adhesive complex formation of a migrated cell begins when paxillin enters nascent adhesions and turns-over rapidly at the adhesion regions in the newly forming protrusion at the leading edge (Laukaitis, Webb *et al.* 2001). This process is followed by the appearance of  $\alpha$ -actinin along the cell border in the membrane protrusion and in the fibrous-like structure that slides toward the cell body. Subsequently, the ITGA5 subunit appears to stabilise the FAs as well as to translocate paxillin and  $\alpha$ -actinin-containing cytoskeletal complexes to the cell rear (Laukaitis, Webb *et al.* 2001). With respect to the function of NRP in this context, Goel *et al.* showed that NRP2 co-localised with the ITGA6 subunit at the leading edge of laminin-dependent matrices and regulated  $\alpha 6\beta 1$  signalling to promote the robust association between  $\alpha 6\beta 1$  and laminin required for the spread of breast cancer cells during the migration process (Goel, Pursell *et al.* 2012). In the following year, Cao *et al.* showed that NRP2 expressed on renal cell carcinoma promoted vascular adhesion, extravasation and tumour metastasis via *trans*-binding with the ITGA5 subunit expressed on ECs (Cao, Hoepfner *et al.* 2013). Furthermore, Valdembri *et al.* showed that NRP1 promoted HUVEC adhesion to FN matrices via its cytoplasmic tail, which binds to the active ITGA5 subunit mediated by the GIPCI/Myo6 complex to ensure the recycling of vesicles containing active  $\alpha 5\beta 1$  to the new adhesion sites required for the spread of ECs on FN matrixes (Valdembri, Caswell *et al.* 2009). Based on the findings of these studies and our findings that NRP2 was a binding partner with the ITGA5 subunit in ECs (see **Figure 4.7 C** and **Figure 4.9**) and that NRP2 knockdown upregulated the expression of the ITGA5 subunit (see **Figure 4.8**), we investigated the mechanism by which NRP2 regulates the ITGA5 subunit in mLMECs, which could explain our finding of the significant reduction in migration (see **Figure 4.3**), adhesion (see **Figure 4.5 F**) and FA turnover (see **Figure 4.6 B-C**) upon NRP2 knockdown.

We first attempted to visualise the effect of NRP2 knockdown on the movement of the ITGA5 subunit in living mLMECs. However, the ITGA5-GFP construct signal after cell nucleofection was too weak to track using the available inverted Axiovert microscope. Alternatively, we investigated this effect on fixed cells. Unfortunately, by using three different commercial anti-NRP2 antibodies, we were unable to confirm that these antibodies worked in immunocytochemistry (ICC). Therefore, we were not able to co-localise the two molecules in this context. However, by examining the effect of NRP2 knockdown on ITGA5 organisation in fixed mLMECs, we showed that NRP2-siRNA-treated ECs exhibited a

significant disruption of ITGA5 organisation on FN matrices, which appeared in elongated fibrillar structures, compared to the Ctrl-siRNA-treated cells (see **Figure 5.1 and 5.2**). Because we were unable to localise NRP2 in fixed cells, we then used the subcellular protein fractionation kit to study the distribution of the two molecules in different cellular compartments. Interestingly, NRP2 was localised only in the cellular membrane compartments, and a majority of ITGA5 was localised in the same compartments, which suggested that the two molecules were co-localised in the cellular membranes. Overall, the localisation of NRP2 on the cellular membranes and the biochemical interaction between NRP2 and ITGA5 subunit, as well as the upregulation of ITGA5, the disruption of ITGA5 organisation in FN, and the potential changes in ITGA5 levels in the subcellular compartments upon NRP2 knockdown led us to investigate the possibility that NRP2 could regulate ITGA5 turnover/trafficking. Additionally, the detection of small and large ribosomal subunits as a binding partner of NRP2 in MS (see **Table 4.1**) suggested that NRP2 may also regulate the transcription of ITGA5 expression. To investigate these two possibilities, we first employed cycloheximide to inhibit protein synthesis in NRP2-depleted cells and in Ctrl-siRNA treated cells. Interestingly, compared to the cycloheximide-untreated cells, the upregulation of ITGA5 level in the NRP2-depleted cells was absent. This finding suggests that the ITGA5 subunit was degraded faster in the NRP2-depleted cells and that simultaneously, the translation of ITGA5 was increased to compensate the degraded ITGA5. Because the number of integrins expressed on the plasma membrane is believed to be proportional to cell adhesion on ECM (Ginsberg, Partridge et al. 2005), (Serini, Valdembri et al. 2006), we also examined whether NRP2 knockdown would change ITGA5 expression on the plasma membranes using flow cytometry. However, the NRP2 knockdown exhibited no difference in the total ITGA5 level on the cell surface compared to the control conditions, which supported our suggestion that the rate of ITGA5 translation is also rapid in the NRP2-depleted cells to compensate for increased degradation of ITGA5.

In general, it has been shown that activated integrins are endocytosed from the plasma membrane through different mechanisms: clathrin-dependent endocytosis (Ramsay, Keppler et al. 2007), (Ezratty, Bertaux et al. 2009), clathrin-independent endocytosis (Bridgewater, Norman et al. 2012), (Lakshminarayan, Wunder et al. 2014) or circular dorsal ruffles during phagocytosis (Gu, Noss et al. 2011). With respect to clathrin-dependent endocytosis, most integrins recruit endocytic adaptor proteins, such as Dab-2 and AP-2 complex adaptor proteins, at or near FAs shortly before the integrins disassemble to form the clathrin-coated

pits required for integrin endocytosis (Margadant, Monsuur et al. 2011). Previous studies showed that the silencing of clathrin, Dab-2, or AP-2 complex adaptor resulted in reductions in FA disassembly and cell migration (Ezratty, Bertaux et al. 2009), (Chao and Kunz 2009), (Teckchandani, Toida et al. 2009) (see chapter 1; **subsection 1.2.3.2.4**). With respect to  $\alpha 5\beta 1$ , Teckandani *et al.* suggested that both ITGB1 and ITGA5 endocytosis were regulated by clathrin and AP-2 complex adaptor complex (Teckchandani, Toida et al. 2009). In agreement with Teckandani, two studies published in the same year showed that clathrin (Ezratty, Bertaux et al. 2009) and AP-2 adaptor complex (Chao and Kunz 2009) were involved in the induction of FA disassembly and in  $\alpha 5\beta 1$  endocytosis in a clathrin-dependent manner (Ezratty, Bertaux et al. 2009). Interestingly, the clathrin heavy chain and its classical AP-2 complex adaptor proteins were identified in MS results (see **Table 4.1**) as NRP2 binding partners.

The MS analysis also identified ITGA5, ITGB1 and ITGAV but not ITGB3 or ITGB5, which are binding partners of ITGAV, which suggested that, similar to NRP1 (Valdembri, Caswell et al. 2009), NRP2 may also regulate the trafficking of active  $\alpha 5\beta 1$  during the cell migration on FN matrices. Additionally, this suggestion was supported by the identification of EH domain-containing protein 2 (EHD2) as a binding partner protein in MS, which is functionally localised to the neck of the invaginated caveolae to form oligomeric rings around lipid membranes to limit the scission and subsequent endocytosis of these membrane pits (Morén, Shah et al. 2012), (Stoeber, Stoeck et al. 2012), (Mohan, Morén et al. 2015), (Hoernke, Mohan et al. 2017). In addition to EHD2, other molecules involved in the endocytosis and trafficking processes were also identified in the MS analysis, including the regulator complex protein LAMTOR1 (Lamtor1) (Mu, Wang et al. 2017), (Malek, Guillaumot et al. 2012), the secretory carrier-associated membrane protein 1 (Scamp1) (Lam, Siu et al. 2007), (Cai, Jia et al. 2011), (Zhang and Castle 2011), (Vadakekolathu, Al-Juboori et al. 2018), the secretory carrier-associated membrane protein 3 (Scamp3) (Falguières, Castle et al. 2012), (Naboulsi, Bracht et al. 2016), the epsilon-coatomer subunit (COPI) (Lippincott-Schwartz, Roberts et al. 2000), (Ward, Polishchuk et al. 2001), (Wang, Wang et al. 2010) (Benyair, Ogen-Shtern et al. 2015), the alpha-soluble NSF attachment protein ( $\alpha$ -SNAP) (Stenbeck 1998), (Shah, Colbert et al. 2015) and Annexin-A1 (Lizarbe, Barrasa et al. 2013) as well as other cytoskeletal binding proteins, such as  $\beta$ -actin and  $\gamma$ -actin, T-complex protein 1 subunit beta (TCP1) (Llorca, McCormack et al. 1999), (Gómez-Puertas, Martín-Benito et al. 2004),  $\alpha$ -catenin 1 and  $\beta$ -catenin 1 (Peng, Maiers et al. 2012), (Choi, Estarás et

al. 2013), alpha-actinin (Arp1) (Holleran, Tokito et al. 1996), (Cheong, Feng et al. 2014)  $\beta$  and  $\gamma$ -adducin (Yang, Sui et al. 2018), F-actin-capping protein subunit alpha-2 and tropomodulin-3 (Almenar-Queralt, Gregorio et al. 1999), (Fischer, Fritz-Six et al. 2003) (see **Table 4.1**).

Using the cell-surface biotinylation assay, Valdembri *et al.* showed that human NRP1 did not regulate total  $\alpha 5\beta 1$  endocytosis. However, they found that the NRP1-GIPC1-Myo6 complex was bound to active  $\alpha 5\beta 1$ , thus regulating the endocytosis of the active  $\alpha 5\beta 1$  via the Rab5-dependent pathway in HUVECs (see chapter 1; **Figure 1.18 B**) (Valdembri, Caswell et al. 2009). Using the same technique, we found that mouse NRP2, similar to human NRP1 (Valdembri, Caswell et al. 2009), did not regulate total  $\alpha 5\beta 1$  endocytosis. Recently, Lilja *et al.* showed that the silencing of SHANK3 significantly increased the active ITGB1 levels on the cell surface without affecting the total ITGB1 expression on the cell surface (Lilja, Zacharchenko et al. 2017). Interestingly, the MS analysis showed that SHANK3 was a potential binding partner of NRP2; however, we could not investigate this possibility because there is no commercially available antibody against mouse active ITGA5.

Based on this finding, as well as the identification of other trafficking, recycling and cytoskeletal adaptor molecules as binding partner adaptor proteins in the MS analysis, we sought to investigate the possibility that NRP2 regulates ITGA5 recycling. Interestingly, the cell-surface biotinylation assay showed that total ITGA5 in NRP2-depleted ECs was recycled to the cell surface slower than the total ITGA5 in the Ctrl-siRNA-treated cells, indicating that NRP2 expression regulates the total ITGA5 subunit recycling in mLMECs.

## 5.8. Conclusion

In this chapter, we have shown that:

- **NRP2 knockdown disrupts the structural formation of ITGA5 subunit on FN matrix.**
- **NRP2 is mainly localized in cellular membranes; and ITGA5 is also highly expressed in the cellular membranes compartments.**
- **NRP2 regulates ITGA5 subunit turnover.**
- **NRP2 does not regulate total ITGA5 subunit internalisation.**
- **NRP2 knockdown attenuates total ITGA5 subunit recycling.**

## Chapter 6: Investigating NRP2 silencing effect in the angiogenesis *ex vivo* aortic ring model

---

As mentioned in chapter 3, previous studies showed that NRP2 regulates VEGF-induced signalling (Favier, Alam et al. 2006) (Caunt, Mak et al. 2008) and angiogenesis (Dallas, Gray et al. 2008), (German, Mammoto et al. 2014). However, because when we knocked down NRP2 levels, we only detected marginal reductions in VEGFR2 and ERK phosphorylation (see **Figure 4.2**), and no VEGF-induced alterations in cell migration (see **Figure 4.3**), we decided to investigate the biological function of endothelial NRP2 in VEGF-induced sprouting by using a Cre-loxP model; a model that would allow us to control NRP2 gene activity in a time and tissue-specific manner (Feil, Valtcheva et al. 2009). We wanted to import NRP2 floxed mice, but because of the health status of the facility from which the mice were available, we were not allowed to import them into our animal research unit before the end of this project. Alternatively, we therefore decided to generate Cre-induced lentiviral-mediated shRNAs. By transfecting these into aortic rings derived from animals carrying an endothelial, and Tamoxifen-inducible, Cre recombinase, we endeavoured to stably silence NRP2 expression specifically in endothelial cells to study the effects on *ex vivo* angiogenesis.

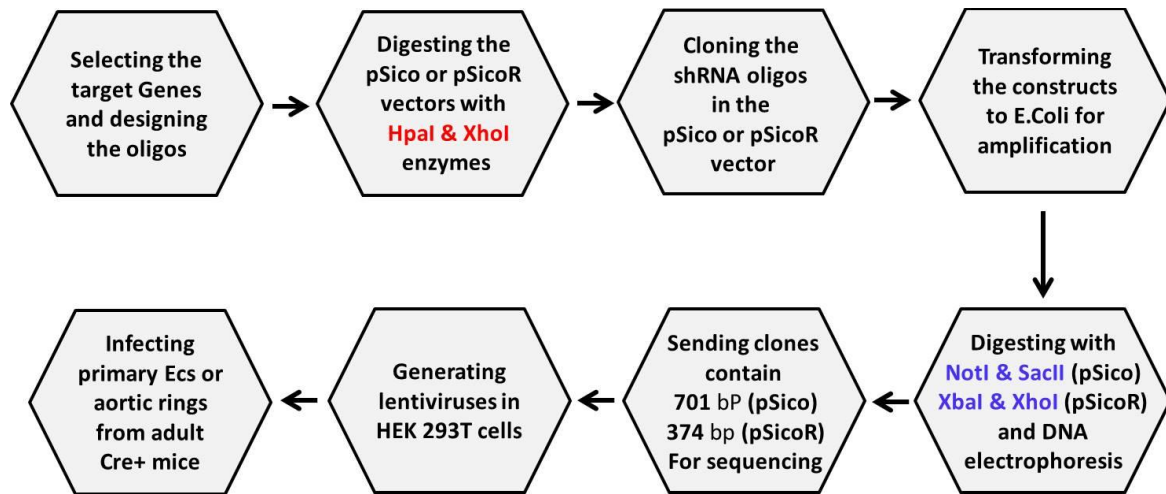
The *ex vivo* aortic ring assay has been documented to provide a complete picture of angiogenic processes including: cellular proliferation, migration, tube formation, microvessel branching, perivascular recruitment and remodelling (Baker, Robinson et al. 2012). Therefore, it has become widely used as an angiogenesis model to investigate the effect of silencing a certain gene in the formation of microvessel sprouts in response to angiogenic stimuli (Nicosia 2009), (Yang and Proweller 2011), (Han, Yang et al. 2012), (Yakkundi, Bennett et al. 2015), (Ellison, Atkinson et al. 2015), (Mukai, Muramatsu et al. 2016). However, the aorta explants are composed of ECs as well as other cells including pericytes, fibroblasts, macrophages and dendritic cells (Nicosia 2009). In order to silence NRP2 specifically in aortic ECs but not in other cells, we opted for the Plasmid for Stable Interference Condition system which has been widely used for conditional cell-type-specific gene-silencing based on the Cre-loxP system (Ventura, Meissner et al. 2004), (Susanto, Lin et al. 2008), (D'Amico, Robinson et al. 2010), (Heitz, Johansson et al. 2014), (Jung, Lee et al. 2016). This was done by cloning different oligonucleotides coding for NRP2-shRNA into the

pSico vector to generate lentiviruses carrying these pSico-shRNA constructs to silence endothelial NRP2 expression conditionally in aortic rings derived from a tamoxifen inducible (iCreER<sup>T2</sup>) system under the transcriptional control of endothelial-specific promoter (pdgfb) (Claxton, Kostourou et al. 2008).

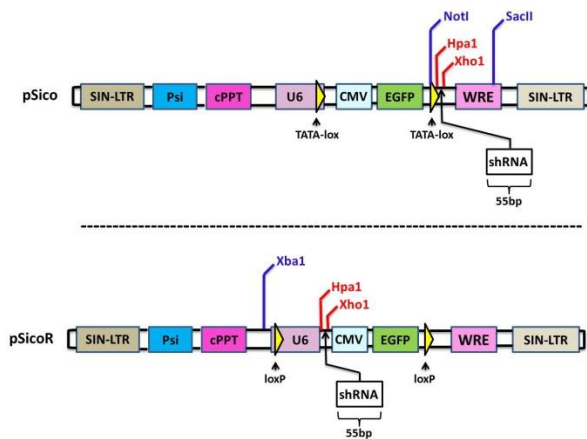
### **6.1. Selection of NRP2 targeting sequences, designing the short hairpin RNA (shRNA) oligonucleotides, and generating conditional lentiviral vectors.**

A schematic diagram showing an overview of the whole process used to generate lentiviruses for conditional silencing of NRP2 (**Figure 6.1 A**) using pSico (for conditional activation) and pSicoR (for conditional inactivation) vectors (**Figure 6.1 B**). We used PSICOLIGOMAKER1.5, a programme established by Tyler Jacks's lab at MIT (Ventura, Meissner et al. 2004), to choose targeting sequences most likely to elicit efficient NRP2 silencing. Because NRP2 is composed of five extracellular domains (Pellet-Many, Frankel et al. 2008), we selected three target sequences from different domains (**Figure 6.1 C**). We also included the NRP2-siRNA (#3) sequence GCUAUGACAUGGAGUAUCA that we used in previous chapters because it showed 90% knockdown in transient assays (see chapter 3; **Figure 3.2 C-D**) and it conforms to PSICOLIGOMAKER1.5 rules for a fourth target sequence (**Table 6.1**). Then, we used the same programme to design both the sense and anti-sense shRNA oligonucleotides for cloning into pSico and pSicoR (**Table 6.2**). By using the Web Surfaces for RNA Secondary Structure Prediction (Reuter and Mathews 2010), we also checked the percentage probability of the designed shRNAs to form the hairpin structures required for efficient silencing (**Figure 6.2**). The NRP2-shRNAs were cloned in both vectors at HpaI-XhoI sites and the vectors were then digested with restriction enzymes (NotI & SacII for pSico; XbaI & XhoI for pSicoR) as shown in **Figure 6.1 B**. Positive clones released a larger DNA sequence than the fragment released by empty vector: 701-bp vs 646-bp for pSico (**Figure 6.3 A**), and 375-bp vs 319-bp for pSicoR (**Figure 6.3 B**). The positive clones were Sanger sequenced by Source BioScience Ltd to confirm the correct cloned sequences. Finally, the pSico conditional lentivirus vectors were generated as described in the Virapower Lentiviral Expression System User Manual (Invitrogen).

A)



B)



C)

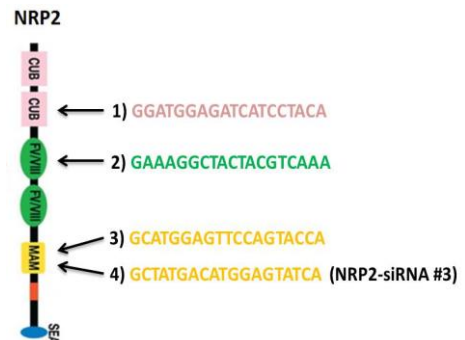


**Figure 6.1 Selection of NRP2 targets and cloning the shRNA oligonucleotides in conditional vectors.** A) A schematic representation of generating a conditional lentiviral vectors. B) A schematic representation showing the sites of cloning the designed 55 shRNA oligonucleotides in the pSico or pSicoR vectors. Following digestion of the pSico or pSicoR vectors with HpaI and XhoI restriction enzymes, the designed shRNAs were annealed at HpaI-XhoI sites. After cloning the shRNA in the pSico vector, the two sites NotI and SacII were digested with their restriction enzymes and released 701-bp positive fragment compared to 646-bp negative cloning, whereas the shRNA cloned in the pSicoR were digested with the HpaI nad XhoI restriction enzymes and released 374-bp positive fragments compared to 315-bp negative fragments. C) A schematic representation showing the four selected NRP2 sequences and their target domains. Adapted from (Ventura, Meissner et al. 2004)

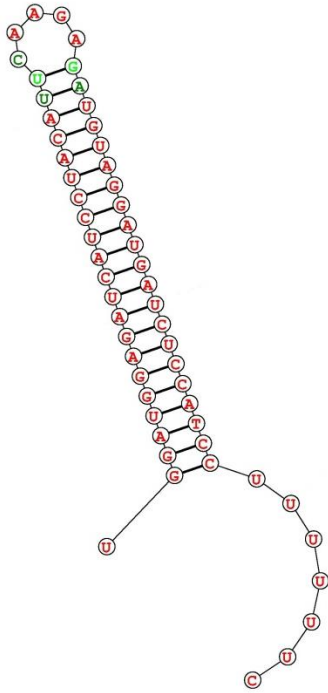
**Table 6.1:** Selecting four different NRP2 targeting sequences starting with (G) and indicating the position, length, score, exon number and the targeting domain of each target.

Target	Position	Sequence	Length	Score	Exon	Domain
1	1071	<u>GGATGGAGATCATCCTACA</u>	19	7	4	CUP (a2)
2	1588	<u>GAAAGGCTACTACGTCAA</u>	19	7	7	FV/VIII (a1)
3	2691	<u>GCATGGAGTTCCAGTACCA</u>	19	7	13	MAM (1)
4	2837	<u>GCTATGACATGGAGTATCA</u>	19	7	13	MAM (2) = NRP2-siRNA #3

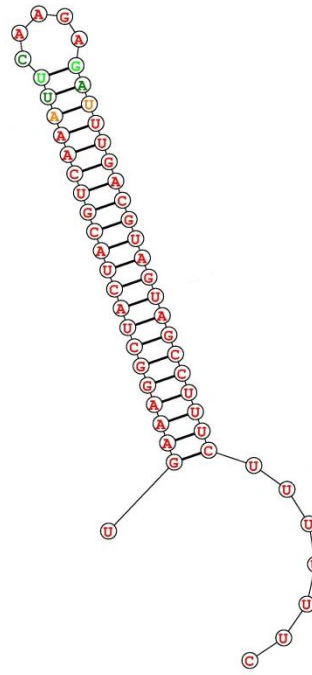
**Table 6.2:** Designing NRP2-shRNA (sense & anti-sense) oligonucleotides containing hairpin sequences.

Target	NRP2-shRNA	
1	Sense	5'- <u>TGGATGGAGATCATCCTACA</u> TTCAAGAGATGTAGGATGATCTCCATCCTTTTTTC
	Anti-sense	5'-TCGAGAAAAA <u>GGATGGAGATCATCCTACA</u> TCTCTTGAATGTAGGATGATCTCCATCCA
2	Sense	5'- <u>TGAAAGGCTACTACGTCAA</u> TTCAAGAGATTTGACGTAGTAGCCTTTCTTTTTTC
	Anti-sense	5'-TCGAGAAAAA <u>GAAAGGCTACTACGTCAA</u> TCTCTTGAATTTGACGTAGTAGCCTTTCA
3	Sense	5'- <u>TGCATGGAGTTCCAGTACCA</u> TTCAAGAGATGGTACTGGAACCTCCATGCTTTTTTC
	Anti-sense	5'-TCGAGAAAAA <u>GCATGGAGTTCCAGTACCA</u> TCTCTTGAATGGTACTGGAACCTCCATGCA
4	Sense	5'- <u>TGCTATGACATGGAGTATCA</u> TTCAAGAGATGATACTCCATGTCATAGCTTTTTTC
	Anti-sense	5'-TCGAGAAAAA <u>GCTATGACATGGAGTATCA</u> TCTCTTGAATGATACTCCATGTCATAGCA

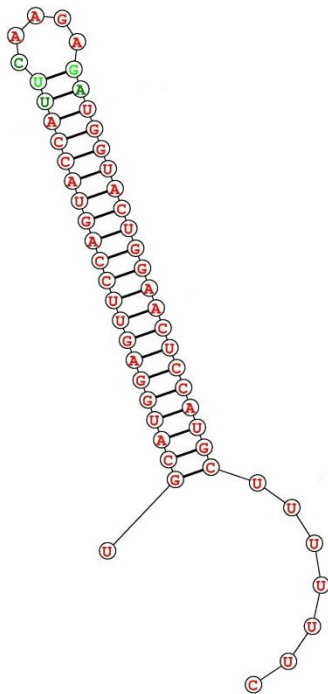
1) CUP (a2)



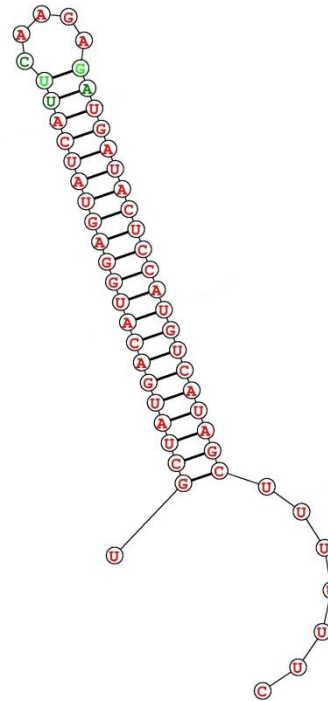
2) FV/VIII (a1)



3) MAM1



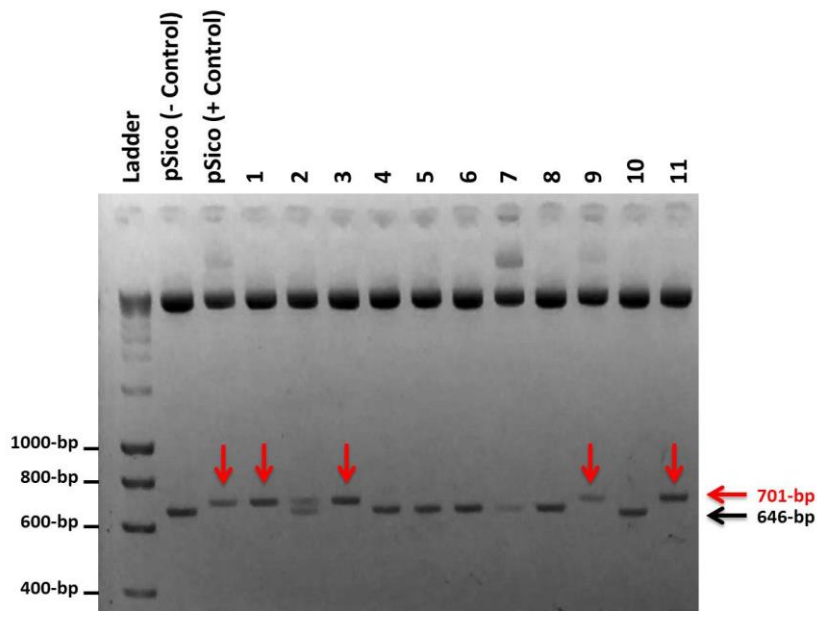
4) MAM2 = NRP2-siRNA (#3)



Probability >= 99%  
 99% > Probability >= 95%  
 95% > Probability >= 90%  
 90% > Probability >= 80%  
 80% > Probability >= 70%  
 70% > Probability >= 60%  
 60% > Probability >= 50%  
 50% > Probability

**Figure 6.2** The percentage prediction formation of the short hairpin structures of the four designed shRNAs oligonucleotides targeting different domains of NRP2. The Web Surfaces for RNA Secondary Structure Prediction (Reuter and Mathews 2010) was used to predict the percentage formation of the short hairpin RNA structure of four designed oligonucleotides that target different domains of NRP2 gene.

A)



B)

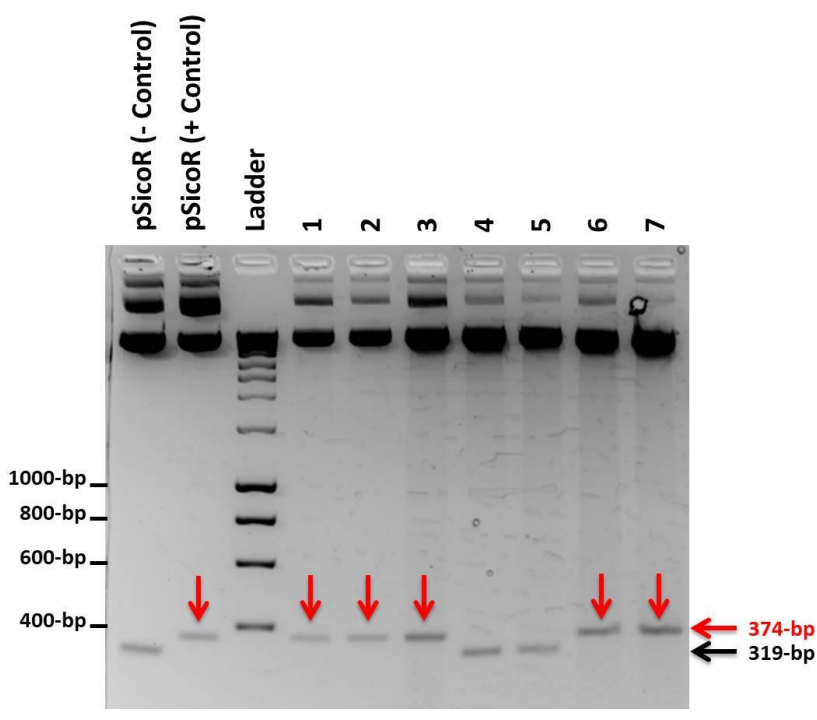


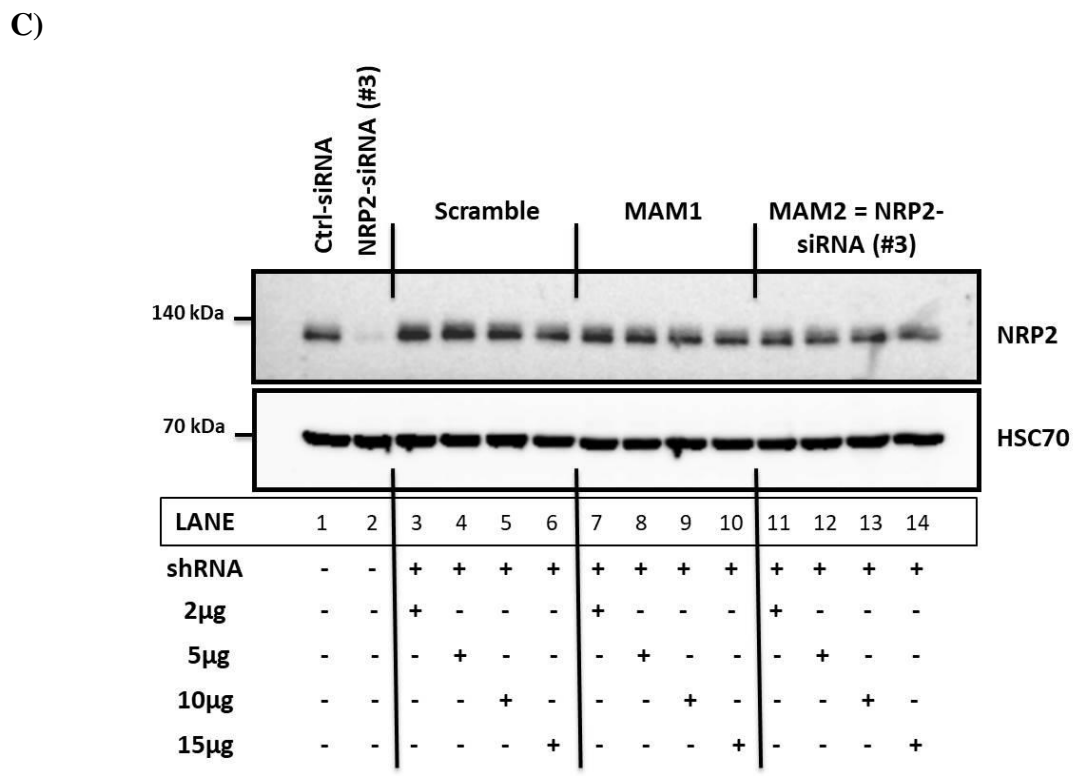
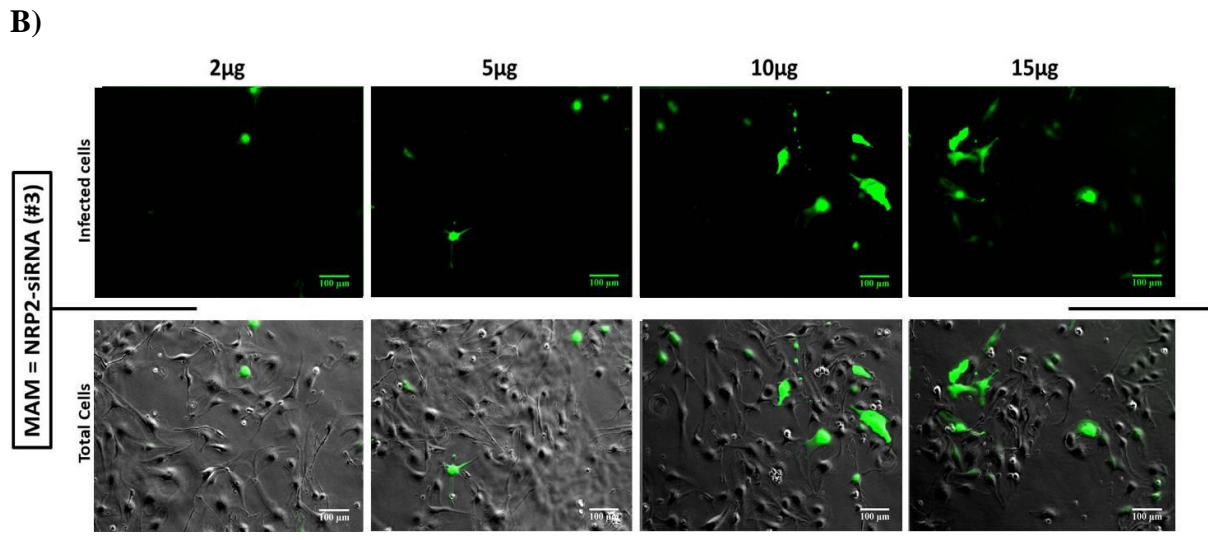
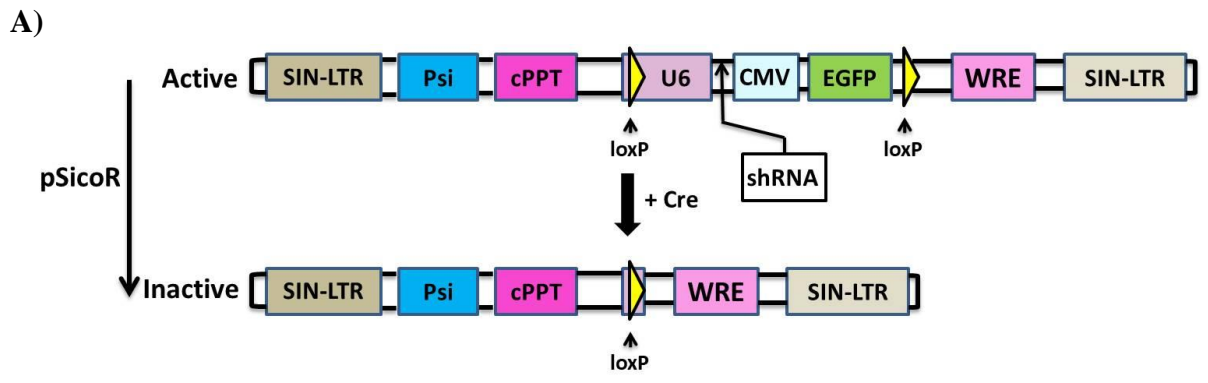
**Figure 6.3 pSico and pSicoR constructs digestions with restriction enzymes to detect the positive cloned shRNAs.** Following inserting the designed shRNA in either pSico or pSicoR plasmids and then transforming the vectors into *E.coli* for amplification, numbers of selected colonies were grown in LB media before purifying the plasmid DNA using plasmid DNA mini kit (OMEGA). **A)** pSico vectors carrying the designed shRNAs were digested with NotI & SacII and released 701-bp (positive cloning) and 646-bp (Negative cloning), whereas **B)** pSicoR vectors were digested with XbaI & XhoI and released 374-bp (positive cloning) and 319-bp (negative cloning). Note that the red arrows are all the potential positive cloning samples that were then sent to the Source BioScience Ltd to confirm the correct cloned shRNAs sequences.

## 6.2. Inefficient mLMECs uptake of pSicoR constructs introduced by electroporation.

pSicoR constructs allow for constitutive expression of the target shRNAs with no need for Tamoxifen. In fact, the addition of Tamoxifen will turn off the shRNAs expression by activating the Cre-loxP recombination which will, in turn, result in the excision of the target shRNAs (**Figure 6.4 A**).

We showed that electroporation is a fairly efficient technique in delivering the paxillin-GFP constructs in mLMECs (see **figure 4.6**); therefore we decided to nucleofect our mLMECs with different amounts of the pSicoR constructs to examine their ability to silence NRP2. Forty-eight hours post nucleofection, the cells were checked for the intensity of the GFP expression (**Figure 6.4 B**), which reflects the efficacy of the shRNAs expression, before subjecting the lysed cells to Western blot and evaluating NRP2 knockdown. Unexpectedly, silencing NRP2 expression by NRP2-siRNA #3 (lane 2) showed 90% knockdown, whereas the shRNA (lane 11-14), which targets the same sequence as the siRNA, showed only 20% knockdown when it was compared to the scramble-shRNA condition (**Figure 6.4 C-D**).

Two possibilities may explain the low number of cells transfected with pSicoR constructs compared with siRNA induced knockdown in **Figure 6.4 B**: 1) electroporation does not allow complete uptake of pSicoR constructs by mLMECs. The pSicoR construct is relatively large (7,271-bp) compared to NRP2-siRNA #3 (19-bp); 2) in this experiment, the nucleofected cells were seeded in complete IMMLEC medium, which contains phenol red. Previous studies indicated that phenol red can mimic the action of estrogen (Berthois, Katzenellenbogen et al. 1986), (Węsierska-Gądek, Schreiner et al. 2007). This may mean that even though Tamoxifen was not added, phenol red was able to bind to the estrogen receptor and thus turn off the shRNA by activating the Cre-loxP system leading to the excision of the cloned shRNA (see **Figure 6.4 A**). Another way to get better uptake of the pSicoR plasmid would be to treat mLMECs with lentiviral particles, but the Robinson lab has previously found these viral particles to be rather inefficient in these immortalised cells.



D)

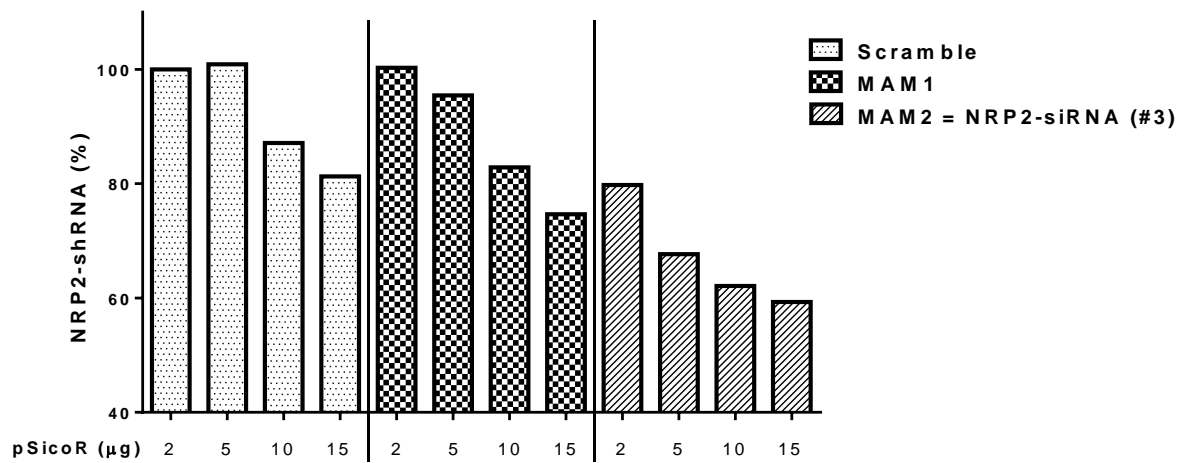


**Figure 6.4 Inefficient uptake of pSicoR constructs by electroporation.** **A)** A schematic representation showing the active pSicoR and its inactivation. **B)** mLMCEs were nucleofected with Ctrl-siRNA, NRP2-siRNA or different amount of pSicoR constructs and seeded on 6-well plates coated with 0.1% gelatin in a CO<sub>2</sub> incubator. 48 hours later, only the cells that nucleofected with the constructs were fluorescence imaged as shown in B, and the cells were lysed. **C)** The lysates were protein quantified before being subjected to Western blot to check NRP2 knockdown. **D)** ImageJ<sup>TM</sup> densitometric quantification of the blot shown in C).

### **6.3. Infecting primary ECs with pSico lentiviruses induced marginal NRP2 knockdown.**

Because mLMECs do not uptake plasmids by lentiviral particles, we decided to infect primary ECs with lentivirus containing our pSico constructs. The lung ECs were isolated (as described in chapter 2; **section 2.2**) from the lungs of *pdgfb-Cre* mice. ECs were then infected with the four conditional lentiviruses that carry the pSico shRNA constructs to test their efficacy in silencing NRP2 (**Figure 6.5 A**). Four days after adding Tamoxifen, which mediates the inducible loxP-specific recombination event by sequestering the bound HSP90 and translocating the active iCreER from the cytoplasm to the nucleus (Claxton, Kostourou et al. 2008), the ECs were lysed and subjected to Western blot analysis. Comparing the NRP2 knockdown induced by the four shRNA constructs with the scrambled sample, the shRNA constructs that target FV/VIII and MAM domains of NRP2 seemed to be somewhat promising, eliciting knockdowns ranging from 25% – 40%. The NRP2-shRNA targeting CUP (a2) domain showed no effect (**Figure 6.5 B-C**). Therefore, the three somewhat promising shRNA lentiviruses were taken forward to study NRP2 silencing in the *ex vivo* aortic ring angiogenesis assay.

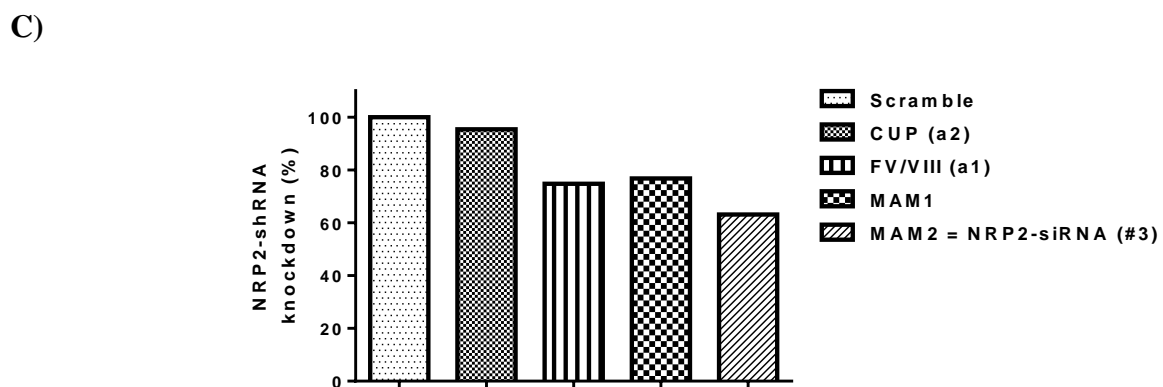
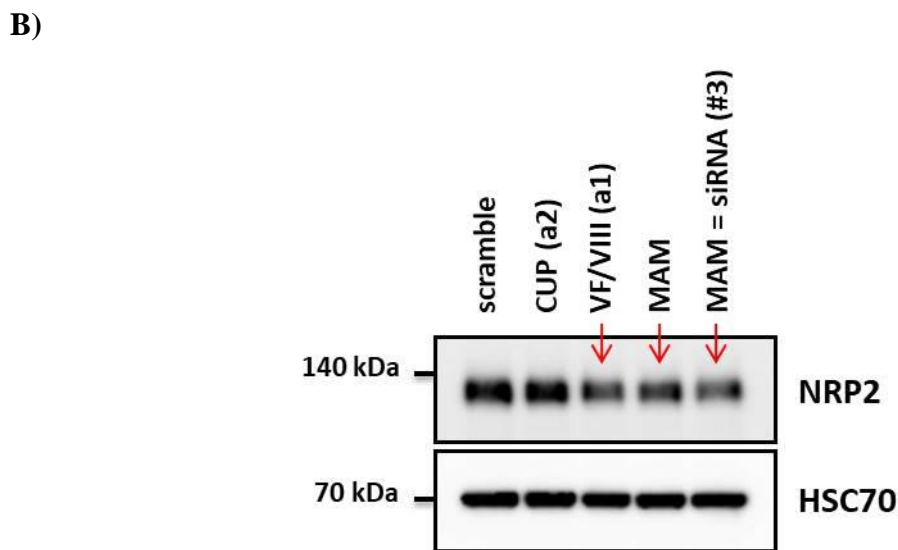
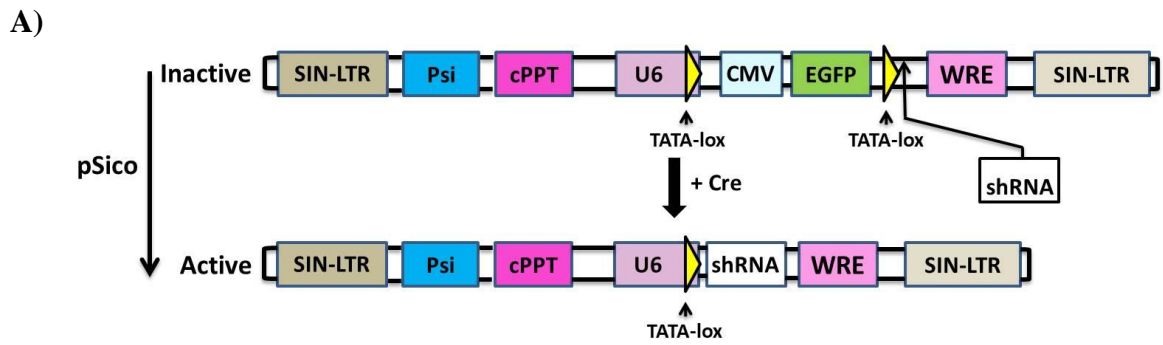


**Figure 6.5 Testing pSico lentivirus of primary ECs.** **A)** A schematic representation of the pSico constructs activation. **B)** Following the isolation of the lung primary ECs from pdgfb-iCreER mice, the cells were infected with pSico lentivirus targeting different domain in NRP2 gene. The cells were lysed and subjected to Western blot to evaluate NRP2 expression. Scramble-shRNA was used as a negative control, whereas the NRP2-shRNA targeting the same sequence as NRP2-siRNA #3 was used as a positive control. **C)** ImageJ™ densitometric quantification of the blot shown in B).

#### **6.4. Infecting aortic rings with the pSico lentivirus provided inconclusive results.**

To analyse the role of NRP2 in VEGF-induced neovascularisation responses, we used the aortic ring assay in which thoracic aortic rings from pdgfb-iCreER mice were infected with lentiviruses carrying pSico shRNAs constructs. These were a scrambled control shRNA, a VEGFR2 shRNA, or one of the shRNAs targeting NRP2 (see **Table 6.1**). These rings were embedded in collagen matrix in the presence of VEGF plus Tamoxifen to induce shRNA expression. Quantification of the number of endothelial microvessel sprouts after 6 days of treatment indicated that: 1) VEGF induced-sprouting was achieved (no VEGF showed very little sprouting, **Figure 6.6** Lane 1-2). 2) VEGFR2-shRNA stopped VEGF-induced sprouting (positive control, **Figure 6.6** Lane 3-4); 3) The NRP2-shRNAs did not significantly alter the microvessel sprouting compared to the scrambled shRNA condition (**Figure 6.6** Lane 5-7), though there seemed to be a trend of reduced sprouting effect similar to NRP2 silencing trend seen in **Figure 6.5 B-C**. However, because the slight (insufficient) NRP2 knockdown introduced by pSicoR, which was tested on mLMECs, (see **Figure 6.4 B-C**) and pSico, which was tested on primary ECs, (see **Figure 6.5 B-C**), the NRP2 role in VEGF-induced neovascularisation remained inconclusive.

To overcome this problem in the future we would need to generate Tamoxifen-dependent (inducible) NRP2 knockout mice. This will allow studying the role of NRP2 in VEGF-induced neovascularisation responses and other *in vivo* studies without needing lentivirus.

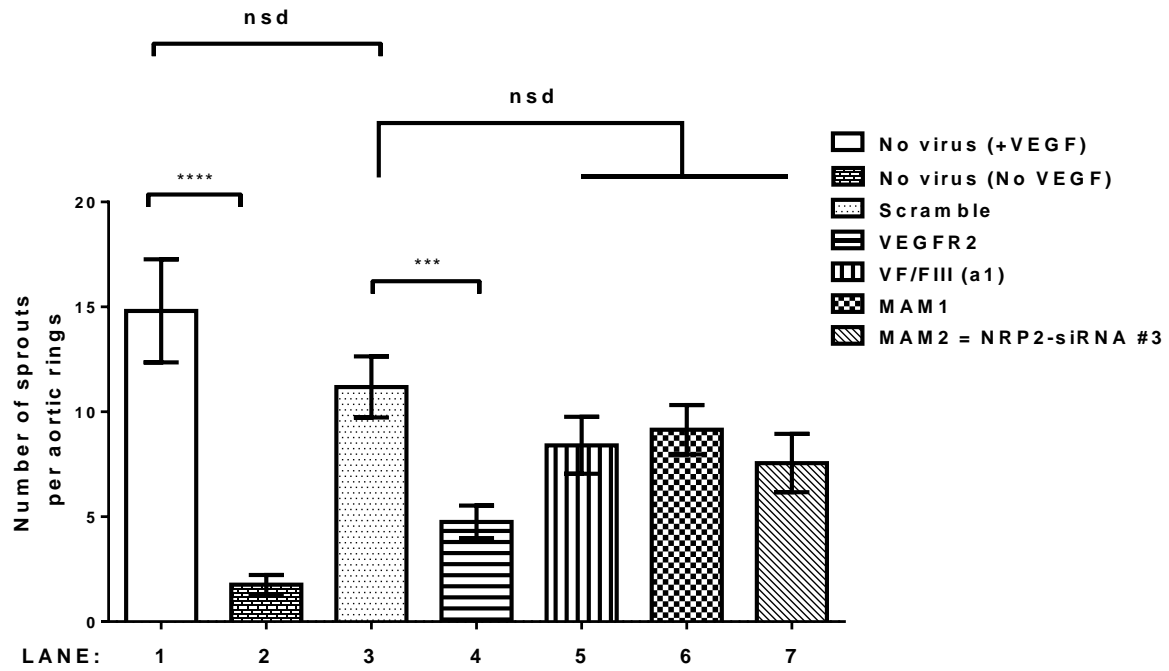


**Figure 6.6 Infecting aortic rings with the pSico lentivirus provided inconclusive results.** Thoracic aortae were isolated from pdgfb-iCreER mice, cut into rings, before transfecting 20–25 rings with the indicated lentivirus (Lane 3-7) in serum-free OptiMEM® in a 24-well plate overnight. No lentivirus transfection controls were included (Lane 1-2). The rings were then impeded in collagen type-1 supplemented with 30ng/mL VEGF plus 1  $\mu$ M OHT for 6 days. Following fixation with 4% PFA, the rings were stained with FITC-conjugated BS1-Lectin overnight. The endothelial Microvessel sprouting of aortic rings were then counted. The bar chart shows the total number of sprouts per aortic ring (mean  $\pm$ SEM from 3 independent experiments;  $n \geq 25$  rings per condition). Asterisks indicate statistical significance: \*\*\*,  $P < 0.001$ ; \*\*\*\*,  $P < 0.0001$ ; nsd = not significantly different. Unpaired two-tailed t-test.

## 6.5. Discussion

In 1982, the aortic ring assay was first described by Nicosia *et al.* as a model for studying angiogenesis *in vitro* that produces microvessels in 3-dimensional matrix in a less complex setting than the live animal models, such as the rabbit ear chamber, the rat cornea, the dorsal air sac of the rat, and the chorioallantoic membrane of the chick embryo, which provides invaluable information on the growth of blood vessels (Nicosia, Tchao et al. 1982), (Nicosia 2009). Briefly, in response to angiogenic stimuli, the aortic ring in culture is composed of a mixed population of cells that appear at different time points. After two days in culture, fibroblasts and macrophages, which originate in the aortic ring adventitia, are the first cells that migrate beyond the aortic ring. After three days, endothelial tip cells start to appear and migrate without dividing, whereas the trailing endothelial cells actively proliferate to extend filopodia-like processes that elongate and develop a vessel with a visible lumen surrounded by pericytes and dendritic cells. After one week of spouting and branching, the vessels stop growing. Subsequently, they regress and eventually dissociate from the aortic ring (Nicosia 2009). Because this model provides a complete view of angiogenic processes and has many other advantages, including reproducibility, cost effectiveness, ease of use, and bridging the gap between *in vitro* and *in vivo* angiogenesis assays, it has become a widely used model in studying angiogenesis (Nicosia 2009), (Baker, Robinson et al. 2012).

Because the purpose of our study was to investigate the role of NRP2 in ECs in a VEGF-induced aortic ring micro vessel sprouting model, and that previous studies showed that NRP2 was also expressed on the surfaces of fibroblast (Zimmermann-Geller, Köppert et al. 2016) and dendritic cells (Curreli, Arany et al. 2007), (Rey-Gallardo, Escribano et al. 2010) we therefore used pSico, a widely used technique for silencing a gene of interest in time- and tissue-specific contexts. We selected NRP2 target sequences, designed shRNA oligonucleotides, cloned the selected oligonucleotides coding for NRP2-shRNA in both pSico and pSicoR vectors, and generated lentiviral vector-mediated NRP2-shRNA.

To investigate the ability of the selected target to silence NRP2, we first tested different concentrations of the pSicoR constructs in silencing of NRP2 expression on mLMECs by electroporation. However, all pSicoR constructs exhibited a low number of transfected cells, and thus failed to induce NRP2 knockdown compared to NRP2-siRNA, which showed a knockdown of 90% (see **Figure 6.4 C** lane 1-2). We reasoned that this failure was due to either the large size of pSicoR (7,271-bp) constructs compared to NRP2-siRNA (19-bp) or

the presence of phenol red in the IMMLEC cultural medium. As mentioned earlier, the Robinson group previously found that the transfection of lentiviral particles was inefficient in mLMECs, we tested the selected NRP2 target sequences in primary ECs isolated from pdgfb-iCreER mice. Unfortunately, by infecting the generated lentiviral vector-mediated NRP2-shRNA in primary ECs, the NRP2-shRNA constructs that targeted the CUP domain failed to induce NRP2 knockdown. In contrast, the constructs that targeted the FV/VIII and MAM domains of NRP2 induced low knockdowns ranging from 25–40% (see **Figure 6.5**). Though it could be argued that this low knockdown was insufficient, we used these NRP2-shRNA lentiviruses to study the biological function of NRP2 in VEGF-induced aortic ring microvessel sprouting. The quantification analysis showed that the NRP2-shRNA lentiviruses induced a slight, but insignificant, reduction in the number of endothelial microvessel sprouts compared to the scrambled-shRNA lentiviruses (see **Figure 6.6**). This trend suggested that NRP2 may regulate VEGF-induced angiogenesis in ECs. However, because we did not achieve sufficient NRP2 silencing by using the pSico technique, we need to generate a tamoxifen-dependent (inducible) NRP2 knockout mouse model. This model would allow the study of the role of NRP2 in VEGF-induced neovascularisation responses and other *in vivo* studies without the need for the lentivirus.

## **6.6. Conclusion**

In this chapter, we generated conditional lentiviral vectors-mediated NRP2-shRNA to investigate the biological function of endothelial NRP2 in VEGF-induced sprouting by using a Cre-loxP model and showed that:

- **mLMECs do not uptake pSicoR constructs efficiently by electroporation.**
- **Infecting primary ECs isolated from PDGFB-iCreER mice with pSico lentiviruses carrying NRP2-shRNA induced only marginal NRP2 knockdown.**
- **Infecting aortic rings isolated from PDGFB-iCreER mice with pSico lentiviruses carrying NRP2-shRNA did not significantly alter the microvessel sprouting, thus providing inconclusive results as to the angiogenic role of EC NRP2 *in vivo*.**

## Chapter 7: Summary and Conclusion

---

### 7.1. Novelty and Significance

Does this thesis contribute to the field of angiogenesis?

Several studies have reported the upregulation of NRP2 levels in cancers, including prostate cancer, bladder cancer, breast cancer, lung cancer, liver cancer, pancreatic cancer, colorectal cancer and oral cancer. They found that NRP2 expression was consistently correlated with cancer progression and aggressiveness, suggesting that NRP2 may serve as a potential target in treating cancers (see **subsection 1.2.3.1.4.2.2.1.**). Favier *et al.* imitated this upregulation of NRP2 observed in cancer cells by overexpressing NRP2 in hMVECs and found that cell survival in these ECs was significantly increased with VEGF-A- or VEGF-C-induced stimulation, whereas NRP2 knockdown significantly inhibited both VEGF-A- or VEGF-C-induced migration. Therefore, Favier suggested that NRP2 is an interesting pharmacological target. Additionally, Favier pointed out that it is important to understand the cross-talk between NRP2 and other receptors (mainly VEGF, integrins and plexins) in ECs to understand the mechanisms underlying angiogenesis and lymph-angiogenesis, which would help in designing new drugs to better control these phenomena in autoimmune diseases and tumour development (Favier, Alam et al. 2006). In 2014, in an interview, Ian Zachary said, “*the cellular function of NRP2 is less well studied than for NRP1, and it is unclear what its primary functions are in endothelial, lymphatic or cancer cells*” (Zachary 2014). My study is the first to investigate the biological function underlying the interaction between integrins and NRP2 within ECs.

### 7.2. Summary of the Findings and discussion

Previous research conducted in our laboratory showed that NRP1 expression is upregulated in  $\beta$ 3HET ECs, and that migration is only sensitive to NRP1 perturbations when ITGB3 levels are reduced (Ellison, Atkinson et al. 2015). We began this project by investigating the potential interaction between the ITGB3 subunit and NRP2 in mLMECs. We found that similar to NRP1, NRP2 expression was upregulated in  $\beta$ 3HET ECs (see **Figure 4.1 A**). Additionally, we showed that the upregulation of NRP2 was not a response to the long-term

depletion of ITGB3 (see **Figure 4.1 B**). Based on these findings, we carried out signalling and migration studies, and we investigated the potential cross-talk between the two molecules. However, whilst NRP2 silencing modestly reduced VEGFR2 and ERK1/2 phosphorylation, it did so in both WT and  $\beta$ 3HET ECs (see **Figure 4.2 A-B**), which suggested the absence of a link between NRP2 and ITGB3 in VEGF-induced signalling. NRP2 knockdown significantly reduced EC migration on FN matrices, but this effect was also independent of ITGB3 expression (see **Figure 4.3**).

The adhesion of ECs to ECM deposition is a requisite stage in EC migration, proliferation and invasion during angiogenesis (Somanath, Razorenova et al. 2006), (Matsunaga, Iyoda et al. 2014). This process is mainly mediated through integrins that connect the ECM to the actin filaments, which is mediated by more than 150 intracellular adaptor molecules (Somanath, Razorenova et al. 2006), (Reinhart-King 2008). Mechanistically, these adaptor molecules bind to the cytoplasmic tail of integrins and recruit other integrins to cluster at the sites of adhesion to assemble stable FA complexes, which act as hand grips to tether the cell fronts during migration (Small, Rottner et al. 1998), (Webb, Parsons et al. 2002), (Li, Guan et al. 2005), (Valdembri and Serini 2012), (De Pascalis and Etienne-Manneville 2017). Therefore, we sought to determine whether the significant reduction in EC migration on FN upon NRP2 silencing was the result of the disruption of EC adhesion on FN. Our findings (see **Figure 4.5 F**) suggest that EC adhesion on FN substratum is also dependent on NRP2 expression. This finding led us to further investigate whether NRP2 expression regulated the formation of FAs. By using paxillin as a marker of FAs, we showed that NRP2 silencing significantly reduced both the assembly and disassembly of FAs on FN substratum (see **Figure 4.6**). Our findings are the first to show that EC migration is dependent on NRP2 expression by regulating FA turnover.

To understand the molecular mechanism underlying the effects of NRP2 silencing on EC migration, adhesion and FA turnover on FN matrixes, we employed MS analysis to identify the potential binding partners of NRP2, which could help us to understand the mechanism of this regulation. We were able to identify translational, endocytic, trafficking and cytoskeletal proteins as binding partner proteins of NRP2 (see **Table 4.1**). Importantly, the ITGA5 and ITGB1 subunits, which are the main FN receptors in ECs (Serini, Valdembri et al. 2006), (Hynes 2007), (Valdembri, Caswell et al. 2009), (Mana, Clapero et al. 2016), were among the binding partner proteins of NRP2. We showed that the siRNA-depletion of NRP2 significantly upregulated ITGA5 subunit expression (see **Figure 4.8**), which suggests that

NRP2 may regulate the biological function of the endothelial ITGA5 subunit. Importantly, we showed that NRP2-depleted ECs exhibited a significant disruption of ITGA5 organisation on FN, ITGA5 appearing as elongated fibrillar structures after NRP2 silencing (see **Figure 5.1 and 5.2**). Using the subcellular fractionation kit, we localised NRP2 specifically in the cellular membrane compartments (see **Figure 5.3**). This finding and the upregulation of ITGA5 levels upon NRP2 knockdown as well as the identification of translational, endocytic, trafficking and cytoskeletal proteins as binding partner proteins of NRP2 led us to investigate the possibility that NRP2 regulates the translation and/or turnover of the ITGA5 subunit. The data we obtained following the inhibition of protein synthesis using cycloheximide reagent (see **Figure 5.4**) suggested that ITGA5 was degraded faster when NRP2 expression was absent, whereas the translation of ITGA5 was simultaneously increased to (possibly) compensate for increased ITGA5 degradation. By using flow cytometry and a cell-surface biotinylation assay to determine whether these effects would change the total cellular membrane level of ITGA5 subunit or ITGA5 endocytosis, respectively, we found that NRP2 knockdown changed neither the cellular membrane level (see **Figure 5.5**) nor endocytosis (see **Figure 5.6**) of the “total” ITGA5 subunit. However, these data are inconclusive because we cannot comment on the “active” ITGA5 subunit. Interestingly, by investigating ITGA5 recycling, we showed that the total ITGA5 in the NRP2-depleted cells was recycled to the cell surface more slowly than that in the Ctrl-siRNA-treated cells (see **Figure 5.7**), indicating that NRP2 regulates the ITGA5 subunit recycling in mLMECs (**Figure 7.1**).

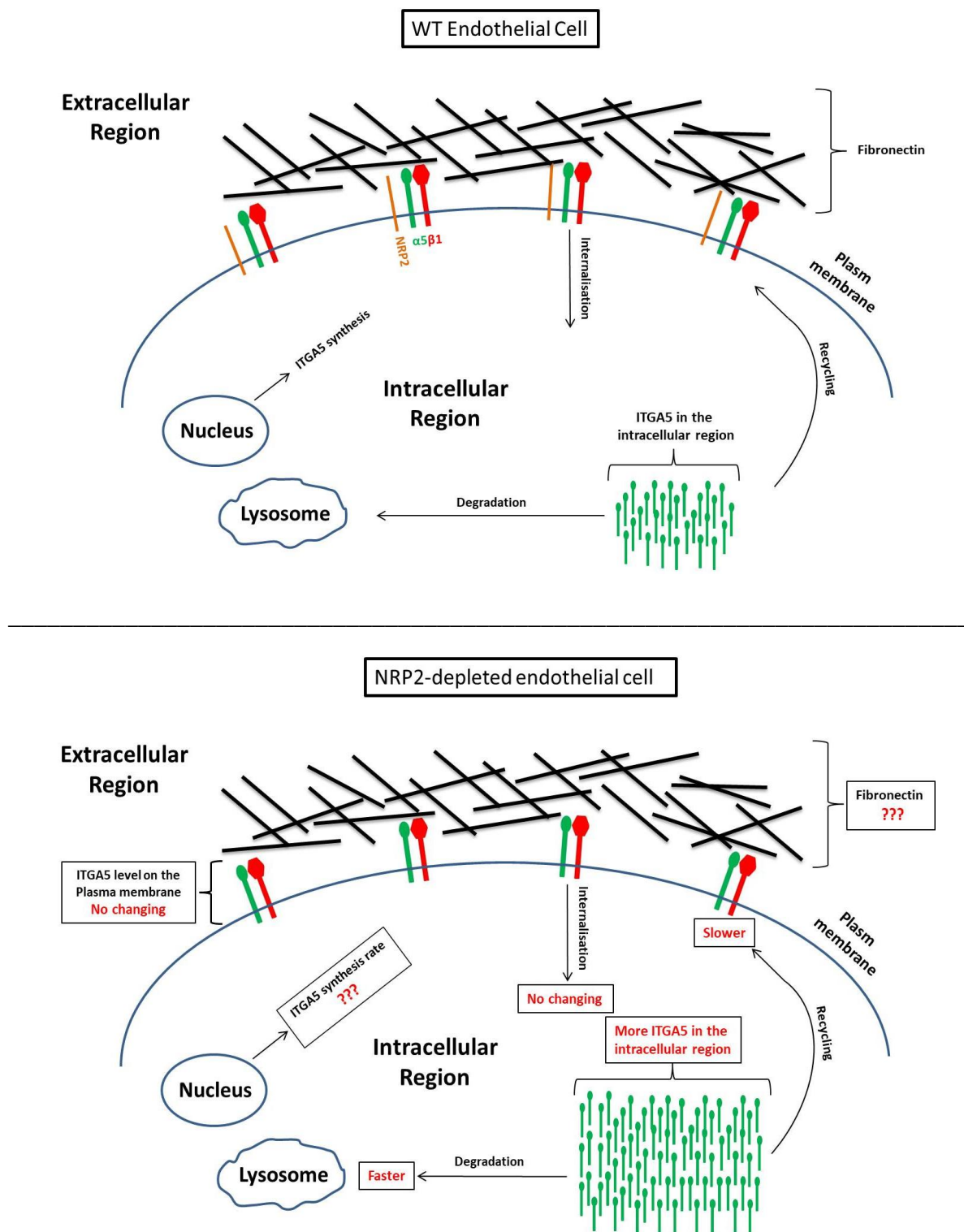


**Figure 7.6 Model mechanism.** Schematic representation of how neuropilin-2 (NRP2) regulates integrin- $\alpha 5$  (ITGA5) in microvascular endothelial cells (ECs). Microvascular ECs migration, adhesion and FAs turnover were significantly reduced when NRP2 expression was knocked down (not drawn). The structural organisation of endothelial ITGA5 on fibronectin (FN) were disrupted in NRP2-depleted ECs (not drawn), whereas the effect of NRP2 silencing on FN organisation (FN fibrillogenesis) is still unknown (??). The total level of the ITGA5 subunit was upregulated in the intracellular region when NRP2 expression was silenced, whereas the total level of ITGA5 on the plasma membrane and the rate of ITGA5 endocytosis in NRP2-depleted ECs remained unchanged in these two parameters compared to that in the WT ECs. However, the recycling rate of “total” ITGA5 to the plasma membrane became slower in the NRP2-depleted ECs compared to the WT ECs. The blocking of protein synthesis by the cycloheximide reagent suggests that ITGA5 degradation is faster when NRP2 expression is knocked down, but whether NRP2 controls the translational rate of ITGA5 expression or not is still unknown (??).

### 7.3. Final Conclusion

Overall, we highlight two main findings of this thesis that will contribute to the field of angiogenesis:

- EC migration is dependent on NRP2 expression by regulating EC adhesion and FA turnover on FN.
- NRP2 expression regulates the biological function of the ITGA5 subunit within ECs.

### 7.4. Priority future work

The data presented in this thesis suggested that NRP2 controls microvascular EC migration, adhesion and FA turnover by regulating ITGA5 biological function. At this time, we want to answer two questions to understand the molecular mechanism through which NRP2 regulates the biological function of ITGA5 in ECs. First, does NRP2 regulate FN organisation (i.e. FN fibrillogenesis)? Second, does NRP2 control ITGA5 protein synthesis in ECs? These questions must be answered to validate the findings reported in this thesis before its publication (see **Figure 7.1**).

First, as shown in **Figure 5.1** and **Figure 5.2**, compared to the control condition, the NRP2 siRNA-depleted ECs exhibited a significant disruption of ITGA5 organisation on FN. Based on the prior knowledge that ECM remodelling involves numerous cellular processes, including cell signalling, proliferation, migration, differentiation, survival, morphogenesis, angiogenesis etc. (Iivanainen, Kähäri et al. 2003) (Theocharis, Skandalis et al. 2016) (Hellewell, Rosini et al. 2017), and because  $\alpha 5\beta 1$  integrin is the main FN receptor in ECs to mediate the cell adhesion (Serini, Valdembri et al. 2006) (Hynes 2007) (Valdembri, Caswell et al. 2009) (Mana, Clapero et al. 2016), it is possible that the elongated structure of ITGA5 observed in the NRP2 siRNA-depleted ECs could be the result of the disruption of FN assembly formation during ECs migration, which then caused the disruption of ITGA5 organisation.

To investigate whether NRP2-siRNA silencing regulates ECs-derived FN organisation, we will follow the protocol of a recent study in which a rapid method was described for detaching the cells adhered on cultured plates by using ammonium hydroxide, while the cell-derived ECM will remain intact for use in further experiments (Hellewell, Rosini et al. 2017). In the experiment, WT and NRP2-siRNA ECs will be seeded on uncoated acid-washed/oven-sterilised glass coverslips in two wells of a 6-well plate for 48 hours at 37 °C in a 5% CO<sub>2</sub>

incubator to achieve NRP2-siRNA knockdown and to allow the ECs enough time to deposit their own ECMs, including FN. Forty-eight hours post-nucleofection, the ECs from both conditions will be detached by 20 mM ammonium hydroxide. The intact EC-derived FN on the coverslips will be subjected to fluorescence microscopy using a mouse anti-FN antibody to investigate whether NRP2 knockdown would change the FN fibrillogenesis compared to the control condition. Additionally, we will determine whether the NRP2-depleted ECs seeded on the WT EC-derived FN exhibits the same significant disruption of ITGA5 organisation shown in **Figure 5.1** and **Figure 5.2**. This will be done by performing the same protocol described above. However, after detaching the ECs from both conditions using 20 mM ammonium hydroxide, the WT ECs will be seeded on the coverslips containing the ECs-derived FN from both conditions for 24 hours at 37 °C in a 5% CO<sub>2</sub> incubator. The ECs then will be sequentially fixed with 4% PFA, permeabilised with PBS 0.25% Triton X-100, and blocked with 5% BSA before the cells are subjected to immuno-labelling for ITGA5 to examine the organisation of ITGA5 in the NRP2-depleted ECs compared with the WT ECs.

Second, Dutta *et al.* described a molecular mechanism by which NRP2 expression in PC3 prostate cancer cells controlled the synthesis of the vesicle trafficking protein WDFY1 (Dutta, Roy et al. 2016). These authors showed that NRP2 knockdown increased the transcriptional activity of WDFY1 in both mRNA and protein levels by shifting the localisation of the transcriptional repressor protein FAC1 from the nucleus to the cytosol. In the absence of NRP2 expression, this translocation resulted in the reduction of the repressor protein FAC1 binding to WDFY1 in the nucleus, which caused the continual synthesis of WDFY1 (Dutta, Roy et al. 2016). The results of treating the ECs with cycloheximide (see **Figure 5.4**) suggested that the ITGA5 subunit degraded faster in the NRP2-depleted ECs. Simultaneously, the translation of ITGA5 in these depleted cells increased to compensate for the fast degradation of ITGA5, thus maintaining the total level of ITGA5 on the plasma membrane similar to that in the control condition (see **Figure 7.1**). Importantly, cycloheximide assay is not an assay that allows measuring the rate of protein synthesis. In fact, cycloheximide reagent binds to the E-site of the large ribosomal 60S subunit and subsequently inhibit protein synthesis by blocking the translational elongation (Schneider-Poetsch, Ju et al. 2010), (Klinge, Voigts-Hoffmann et al. 2011). This assay allowed us to measure the half-life of the remaining ITGA5 in NRP2-depleted cells compare to that in the cycloheximide-untreated cells.

As we mentioned previously, MS analysis identified numbers of the large 60S and small 40S ribosomal subunits as partner proteins of NRP2 and because NRP2 knockdown increases the protein level of ITGA5 subunit (see **Figure 4.8**), it is possible that NRP2 may use a mechanism similar to that described by Dutta *et al.* to regulate ITGA5 synthesis in ECs. To investigate this hypothesis, we need to use an assay that measures the translational rate of ITGA5 (i.e. how fast is ITGA5 is synthesised) in NRP2-depleted cells compare to control condition. This will be done by using polysome profiling assay which measures the association between mRNA and ribosomes by separating the mRNA-ribosome complex in five layers of sucrose gradients (10%, 20%, 30%, 40% and 50%) using ultracentrifugation and RTqPCR analysis.

## **7.5. Other future work**

In this thesis, there were research limitations and number of results need to be also considered in the future. First, our findings showed that similar to NRP1 (Ellison, Atkinson et al. 2015), NRP2 expression was upregulated in  $\beta$ 3HET ECs, which is not a response to the long-term depletion of the *Itgb3* gene because it can be replicated by ITGB3-siRNA knockdown. We therefore suggest that a mechanism for cross-talk exists between the NRP2 and ITGB3 subunits in ECs. However, we did not observe a link between the two molecules in EC migration or in VEGF-induced signalling. Thus, further investigation is required to understand the mechanism of the cross-talk between NRP2 and ITGB3 within ECs. Second, we successfully showed that EC migration on FN is dependent on NRP2 in a VEGF-independent manner. However, we were not able to demonstrate a VEGF-induced increase in the speed of cell migration using the time-lapse CRM assay. Thus, we could not comment on the role of NRP2 in VEGF-induced EC migration. Favier *et al.* previously showed that human NRP2 interacted with VEGFR2 and enhanced its phosphorylation threshold as induced by VEGF<sub>165</sub> (Favier, Alam et al. 2006). These authors also showed that NRP2 knockdown inhibited VEGF<sub>165</sub>-induced migration using the BD BioCoat angiogenesis system-endothelial cell migration, a version of the transwell migration assay that facilitates investigation of the effects on endothelial cell invasion, migration, and tube formation (Favier, Alam et al. 2006). Therefore, we suggest using this system or another *in vitro* 3D migration assay (Kramer, Walzl et al. 2013) to investigate the role of NRP2 in VEGF-induced EC migration. Third, similar to others (Cao, Hoepfner et al. 2013), we showed that NRP2 is trypsin sensitive. To overcome this limitation, we tested different cell-dissociation

reagents and buffers that were reported to be less aggressive in cleaving cell surface proteins, including dispase, TrypLE, citric saline buffer and EDTA. However, these reagents and buffers either failed to detach our mLMECs (dispase and EDTA), were more aggressive than trypsin (TrypLE), or it was impossible to count cells after cell-dissociation (citric saline buffer). Therefore, we recovered NRP2 expression in a suspension state before seeding the cells. Because the citric saline buffer successfully detached mLMECs without affecting the cell-surface receptors, we suggest that this buffer should be developed by including other chemicals such as chelators to help detach the cells singly rather than in sheets of attached cells. Fourth, using the MS analysis, we were able to identify 87 binding partner proteins of NRP2. For example, the ITGAV subunit and four EC specific markers were identified: Pecam1, Mcam, endoglin and PLVAP. Furthermore, other translational, endocytic, trafficking, and cytoskeletal proteins were also identified as binding partners of NRP2. These proteins require further research to better understand the cellular mechanisms that are regulated by NRP2 expression in ECs. Fifth, because our attempts to visualise the movement of ITGA5 in living cells using the ITGA5-GFP constructs as well as the localising of NRP2 and ITGA5 in fixed cells were unsuccessful, these experiments remain a priority for better understanding their functions in living ECs. To localise or visualise the movement of ITGA5 and NRP2 separately in living cells, we suggest using the fluorescent labelling technique and generating new tagged ITGA5 and NRP2 constructs, whereas biomolecular fluorescence complementation (BiFC) could be used to validate NRP2-ITGA5 interaction in living cells. The BiFC technique is based on genetically attaching nonfluorescent, unfolded and complementary fragments of differently coloured fluorescent proteins (FP) to NRP2 and ITGA5. When NRP2-ITGA5 interacts with a living cell, the fluorescent fragments are attracted, and they generate fluorescent signals that can be detected using an inverted fluorescent microscope. Furthermore, this technique utilises the visualisation and analysis of the intensity and the distribution of the interaction between the two molecules in living cells (Zal 2008). Sixth, we showed that NRP2 did not regulate total ITGA5 internalisation similar to human NRP1 in HUVECs (Valdembri, Caswell et al. 2009). However, by using the available SNAKA51 antibody, Valdembri *et al.* showed that human NRP1 regulated active  $\alpha 5\beta 1$  internalisation in HUVECs. As previously mentioned, because no commercially available antibody detects mouse active  $\alpha 5\beta 1$ , it remains a priority for us to investigate whether NRP2 regulates active  $\alpha 5\beta 1$  internalisation in mouse ECs. A recent study showed that the silencing of SHANK3 significantly increased the active ITGB1 levels on the cell surface without affecting the total ITGB1 expression on the cell surface (Lilja, Zacharchenko

et al. 2017). Because SHANK3 is one of the 87 binding partner proteins of NRP2, it would be interesting to investigate whether the silencing of SHANK3 changes the active ITGA5 or NRP2 levels on the plasma membrane. Seventh, because the applications of the pSico and pSicoR techniques were unsuccessful in our study of NRP2 in VEGF-induced *ex vivo* angiogenesis, we strongly suggest that NRP2 knockout mice should be ordered, which we have already done. When these mice arrive in the laboratory, we will generate an EC-specific, tamoxifen-dependent (inducible) NRP2 knockout mice model. This model can (and will) be intercrossed with ITGA5 floxed mice, so that we can better investigate both the *in vivo* role of NRP2, and interactions between the two molecules.

## **Publication:**

Samuel J Atkinson, Aleksander M Gontarczyk, Abdullah AA Alghamdi, Tim S Ellison, Robert T Johnson, Wesley J Fowler, Benjamin M Kirkup, Bernardo C Silva, Bronwen E Harry, Jochen G Schneider, Katherine N Weilbaecher, Mette M Mogensen, Mark D Bass, Maddy Parsons , Dylan R Edwards & Stephen D Robinson. *The  $\beta$ 3-integrin endothelial adhesion regulates microtubule-dependent cell migration*. Submitted to EMBO reports

## Abbreviations:

<b>ITGA5</b>	Integrin- $\alpha$ 5
<b>ITGAV</b>	Integrin- $\alpha$ v
<b>ITGA6</b>	Integrin- $\alpha$ 6
<b>ITGB1</b>	Integrin- $\beta$ 1
<b>ITGB3</b>	Integrin- $\beta$ 3
<b>ITGB5</b>	Integrin- $\beta$ 5
<b><math>\alpha</math>v<math>\beta</math>3</b>	alpha-v-beta-3-integrin
<b><math>\alpha</math>5<math>\beta</math>1</b>	alpha-5-beta-1-integrin
<b>Nuropilin 1</b>	NRP1
<b>Nuropilin 2</b>	NRP2
<b>HSC70</b>	Heat shock cognate 70 kDa protein 8
<b>GAPDH</b>	Glyceraldehyde 3-phosphate dehydrogenase
<b>ECs</b>	Endothelial cells
<b>ECM</b>	Extracellular matrix
<b>HUAECs</b>	Human umbilical artery endothelial cells
<b>HUVECs</b>	Human umbilical vein endothelial cells
<b>HDMECs</b>	Human dermal microvascular endothelial cells
<b>HLDMVECs</b>	Human lymphatic dermal microvascular endothelial cells
<b>HBDMVECs</b>	Human blood dermal microvascular endothelial cells
<b>PAE</b>	Porcine aortic endothelial cell
<b>HEK293</b>	Human embryonic kidney 293 cells expressing the SV40 large T antigen
<b>EPCs</b>	Endothelial progenitor cells
<b>SMCs</b>	Smooth muscle cells
<b>BMDCs</b>	bone marrow-derived dendritic cells
<b>vSMCs</b>	Vascular smooth muscle cells
<b>TSAd</b>	Nuclear factor of activated T-cells
<b>BM</b>	Basement membrane
<b>OPP</b>	Oxygen partial pressure
<b>VE-cadherin</b>	Vascular endothelial cadherin
<b>JAM-A</b>	Junctional adhesion molecules A
<b>MCAM</b>	Melanoma cell-associated molecules
<b>ICAM</b>	Intercellular adhesion molecule
<b>VCAM 1</b>	Vascular cell adhesion molecule 1
<b>PECAM</b>	Platelet endothelial cell adhesion molecule
<b>CD99</b>	Cluster of differentiation 99
<b>TJ</b>	Tight junctions
<b>GJ</b>	Gap junctions
<b>AJ</b>	Adhesion junctions
<b>HSPGs</b>	Heparan sulphate proteoglycans
<b>FN</b>	fibronectin
<b>MMPs</b>	matrix metalloproteases
<b>NSCLC</b>	nonsmall cell lung carcinoma
<b>HCC</b>	Hepatocellular carcinoma
<b>OSCC</b>	Oral squamous cell carcinoma
<b>RCC</b>	Renal cancer cell carcinoma

<b>VEGFs</b>	Vascular endothelial growth factors
<b>CHO</b>	Chinese hamster ovary cells
<b>VEGF-A or VEGF</b>	Vascular endothelial growth factor A
<b>VEGF-B or VRF</b>	Vascular endothelial growth factor B
<b>VEGF-C</b>	Vascular endothelial growth factor C
<b>VEGF-D</b>	Vascular endothelial growth factor D
<b>VEGF-E</b>	Vascular endothelial growth factor E
<b>VEGF-F</b>	Vascular endothelial growth factor F
<b>VEGFR</b>	Vascular endothelial growth factor receptor
<b>VEGFR1 or flt-1</b>	Vascular endothelial growth factor receptor 1
<b>VEGFR2 or flk-1</b>	Vascular endothelial growth factor receptor 2
<b>VEGFR3 or flt-4</b>	Vascular endothelial growth factor receptor 3
<b>FGFR1</b>	Fibroblast growth factor receptors
<b>PDGFR</b>	Platelet-derived growth factor receptor
<b>TGFR-<math>\beta</math>1</b>	transforming growth factor- $\beta$ 1
<b>HGFR</b>	Hepatocyte growth factor receptor
<b>FGFR</b>	Fibroblast growth factor receptor
<b>PGF-B</b>	Placental growth factor-B receptor
<b>IGF-1R</b>	Insulin-like growth factor-1 receptor
<b>PAR-1</b>	Protease-activated receptors-1
<b>GPCR</b>	G protein coupled receptor
<b>CXCR4</b>	Chemokine receptor 4
<b>RTKs</b>	Receptor tyrosine kinases
<b>ANG-1</b>	Angiotensin 1
<b>ANG-2</b>	Angiotensin 2
<b>GRB2</b>	growth factor receptor-bound protein 2
<b>HIF-2<math>\alpha</math></b>	Hypoxia-inducible factor-2 $\alpha$
<b>PlGF, PLGF, PGF</b>	Placental growth factor
<b>TGF-<math>\beta</math>1</b>	Transforming growth factor- $\beta$ 1
<b>GEF</b>	Guanine nucleotide-exchange factors
<b>PDGF-B</b>	Platelet-derived growth factor B
<b>PDGF-BB</b>	Platelet derived growth factor-BB
<b>FGF</b>	Fibroblast growth factor
<b>FGF-1</b>	Fibroblast growth factor-1
<b>bFGF</b>	Basic fibroblast growth factor
<b>EGF</b>	Epidermal growth factor
<b>bEGF</b>	Basic epidermal growth factor
<b>TNF<math>\alpha</math></b>	Tumour necrosis factor alpha
<b>DLL4</b>	Delta like ligand 4
<b>TIMPs</b>	Tissue inhibitors of metalloproteinases
<b>PAI-1</b>	Plasminogen activator inhibitor-1
<b>Rac1</b>	Ras-related C3 botulinum toxin substrate 1
<b>NO</b>	Nitric oxide
<b>eNOS</b>	Endothelial nitric oxide synthase
<b>Akt or PKB</b>	Protein kinase B
<b>ERK1/2</b>	Extracellular-signal-regulated kinase
<b>PLC<math>\gamma</math></b>	Phospholipase C $\gamma$
<b>PKC</b>	Protein kinase C

<b>WDFY1</b>	WD Repeat and FYVE domain containing 1
<b>LAMP2</b>	Lysosome-associated membrane protein 2
<b>Spry4</b>	Sprouty4
<b>Tyr</b>	Tyrosine
<b>VRAP</b>	VEGF receptor associated protein (VRAP)
<b>PI 3-kinase</b>	Phosphatidylinositol 3-kinase
<b>FAs</b>	Focal adhesions
<b>FAK</b>	Focal adhesion kinase
<b>SOS</b>	Nucleotide-exchange factor Son of sevenless
<b>SHC</b>	Src homology collagen homology
<b>ER</b>	Endoplasmic reticulum
<b>PIP2</b>	Phospholipid phosphatidylinositol (4, 5)-bisphosphate
<b>PIP3</b>	Phosphatidylinositol-3,4,5-trisphosphate
<b>IP3</b>	Inositol 1,3,5-triphosphate
<b>DAG</b>	Diacylglycerol
<b>PAK2</b>	p21-activated protein kinase-2
<b>MAPK</b>	Mitogen activated protein kinase
<b>CDC42</b>	cell division cycle 42
<b>p38-MAPK</b>	P38 mitogen-activated protein kinases
<b>MAPKAPK2</b>	MAPK-activated protein kinase 2
<b>HSP27</b>	Heat shock protein 27
<b>ILK</b>	Integrin linked kinase
<b>PDK-1</b>	Phosphoinositide-dependent kinase-1
<b>PDK-2</b>	Phosphoinositide-dependent kinase-2
<b>FOXO1</b>	Forkhead box protein O1
<b>GSK-3<math>\beta</math></b>	Glycogen synthase kinase 3 beta
<b>Anxa2</b>	Annexin A2
<b>Sema-3</b>	Semaphorin 3
<b>C-terminal</b>	Carboxyl-terminal domain
<b>N-terminus</b>	amino-terminus
<b>CUB doamin</b>	Complement C1r/C1s, <u>U</u> egf, <u>B</u> mp1 domain
<b>MAM domain</b>	<u>M</u> eprin, <u>A</u> -5 protein domain, and a receptor protein-tyrosine phosphatase <u><math>\mu</math></u> domain
<b>V/VIII domain</b>	Coagulation factor V/VIII homology domain
<b>TMD</b>	Transmembrane domain
<b>FAT</b>	focal adhesion targeting domain
<b>PTB</b>	phosphotyrosine binding domain
<b>PHD2</b>	Prolyl hydroxylase domain 2
<b>GAG</b>	Glycosaminoglycan
<b>GIPC</b>	RGS-GAIP interacting protein C-terminus
<b>NIP-1</b>	neuropilin-interacting protein-1
<b>GIK</b>	GlyIsoLys
<b>sNRP1</b>	Soluble NRP1
<b>sNRP2</b>	Soluble NRP2
<b>sFN</b>	Soluble FN
<b>F-actin</b>	Filamentous actin
<b>TURBT</b>	Transurethral resection
<b>RCT</b>	Radio-chemotherapy

<b>ZEB-1</b>	Zinc finger E-box-binding homeobox-1
<b>RGD</b>	Arginine-glycine-aspartic acid tripeptide
<b>LDV</b>	Leucine-aspartic acid-valine
<b>Src</b>	Src family kinase
<b>PP2A</b>	Protein phosphatase 2A
<b>Dok1</b>	Docking protein 1
<b>RIAM</b>	Rap1-GTP-interacting adaptor molecule
<b>P38 or p38 MAPK</b>	P38 mitogen-activated protein kinases
<b>SAPK2/p38</b>	Stress-activated protein kinase-2/p38
<b>Rac1</b>	Ras-related C3 botulinum toxin substrate 1
<b>Rcc2</b>	Telophase disk protein
<b>β3HET</b>	ITGB3-heterozyous
<b>α5HET</b>	ITGA5-heterozyous
<b>-NULL mice</b>	Knockout mice
<b>-EC-KO</b>	Endothelial-specific knockout mice
<b>CNS</b>	Central nervous system
<b>Arf</b>	ADP-ribosylation factor GTPase
<b>GAP</b>	GTPase-activating proteins
<b>ARL</b>	ARF-like proteins
<b>COPI</b>	Cytosolic coatomer complex I
<b>TGN</b>	<i>trans</i> -Golgi network
<b>Dab-2</b>	Disabled-2
<b>AP-2</b>	Adaptor protein-2
<b>EE</b>	Early endosomes
<b>PKD1</b>	Protein kinase D1
<b>PNRC</b>	Perinuclear recycling compartment
<b>FBS</b>	Foetal bovine serum
<b>PFA</b>	Paraformaldehyde
<b>PBS</b>	Phosphate buffered saline
<b>PBS/T</b>	Phosphate buffered saline supplemented with Tween-20
<b>P/S</b>	penicillin/streptomycin
<b>EtOH</b>	Ethanol
<b>MACS</b>	Magnetic activated cell sorting
<b>PyMT</b>	polyoma-middle-T-antigen retrovirus
<b>dH<sub>2</sub>O</b>	Distilled water
<b>SDS</b>	Sodium dodecyl sulphate
<b>APS</b>	ammonium persulfate
<b>BSA</b>	Bovine serum albumin
<b>HRP</b>	Horseradish peroxidase
<b>Caspase-8</b>	Cysteine-aspartic proteases-8
<b>Caspase-9</b>	Cysteine-aspartic proteases-9
<b>GFP</b>	Green florescent proteins
<b>TCL</b>	Total cell lysate
<b>Mesna</b>	2-mercaptoethane sulfonate Na
<b>TCEP</b>	Tris-(2-carboxyethyl)phosphine
<b>Oligo</b>	Oligonucleotides
<b>mRNA</b>	Messenger RNA
<b>siRNAs</b>	Short interference Ribonucleic acids (RNA)

<b>shRNAs</b>	Short hairpin RNAs
<b>Ctrl-siRNA</b>	Control-short interference RNA
<b>NRP2-siRNA</b>	Neuropilin-short interference RNA
<b>pSico</b>	<u>Pl</u> asmid for <u>S</u> t <u>a</u> b <u>i</u> l <u>e</u> <u>I</u> n <u>t</u> e <u>r</u> f <u>e</u> r <u>e</u> n <u>c</u> e <u>C</u> o <u>n</u> d <u>i</u> t <u>i</u> o <u>n</u>
<b>pSicoR</b>	<u>Pl</u> asmid for <u>S</u> t <u>a</u> b <u>i</u> l <u>e</u> <u>I</u> n <u>t</u> e <u>r</u> f <u>e</u> r <u>e</u> n <u>c</u> e <u>C</u> o <u>n</u> d <u>i</u> t <u>i</u> o <u>n</u> Reverse
<b>OHT</b>	4-hydroxytamoxifen
<b>PLVAP</b>	Plasmalemma vesicle-associated protein
<b>ICC</b>	immunocytochemistry
<b>EHD2</b>	EH domain-containing protein 2
<b>Lamtor1</b>	Regulator complex protein LAMTOR1
<b>Scamp1</b>	Secretory carrier-associated membrane protein 1
<b>Scamp3</b>	Secretory carrier-associated membrane protein 3
<b><math>\alpha</math>-SNAP</b>	Alpha-soluble NSF attachment protein
<b>TCP1</b>	T-complex protein 1 subunit beta
<b>Arp1</b>	Alpha-centractin
<b>BiFC</b>	Biomolecular fluorescence complementation
<b>bp</b>	Base pair
<b>E</b>	Embryonic day
<b>EMT</b>	Epithelial-mesenchymal transition
<b>neo</b>	Neomycin
<b>p</b>	Phosphorylated
<b>Ig</b>	Immunoglobulin
<b>IP</b>	Immunoprecipitation
<b>p130Cas</b>	p130 CRK-associated substrate
<b>PDZ</b>	PSD-95/Dlg/ZO-1
<b>PMSF</b>	Phenylmethanesulfonylfluoride
<b>SDS-PAGE</b>	Sodium dodecyl sulphate polyacrylamide gel electrophoresis
<b>CRM assay</b>	Cell random motility assays
<b>WH assays</b>	Wound healing assays
<b>BAE assay</b>	Bovine aortic endothelial assay
<b>LFQ</b>	Label-Free quantitative
<b>MS</b>	Mass spectrometry
<b>DMEM</b>	Dulbecco's modified eagle medium
<b>FACS</b>	Fluorescence activated cell sorting
<b>CEB</b>	Cytoplasmic extraction buffer
<b>MEB</b>	Membrane extraction buffer
<b>NEB</b>	Nuclear extraction buffer
<b>PEB</b>	Pellet extraction buffer
<b>SBS</b>	Soerensen buffer
<b>EDTA</b>	Ethylenediaminetetraacetic acid
<b>TAE</b>	Buffer containing Tris base, acetic acid, and EDTA
<b>TE</b>	Tris-EDTA
<b>EB</b>	Elution buffer
<b>LB</b>	Lysogeny broth medium
<b>DAPI</b>	4',6-diamidino-2-phenylindole
<i>et.al</i>	er alia
<b>FITC</b>	Fluorescein-5-isothiocyanate
<b>PE</b>	Phycoerythrin

## References:

- Abhinand, C. S., et al. (2016). "VEGF-A/VEGFR2 signaling network in endothelial cells relevant to angiogenesis." Journal of cell communication and signaling **10**(4): 347-354.
- Achen, M. G., et al. (1998). "Vascular endothelial growth factor D (VEGF-D) is a ligand for the tyrosine kinases VEGF receptor 2 (Flk1) and VEGF receptor 3 (Flt4)." Proceedings of the National Academy of Sciences **95**(2): 548-553.
- Adair, B. D., et al. (2005). "Three-dimensional EM structure of the ectodomain of integrin  $\alpha$ V $\beta$ 3 in a complex with fibronectin." The Journal of cell biology **168**(7): 1109-1118.
- Adams, R. H. and K. Alitalo (2007). "Molecular regulation of angiogenesis and lymphangiogenesis." Nature reviews Molecular cell biology **8**(6): 464.
- Adams, R. H. and K. Alitalo (2007). "Molecular regulation of angiogenesis and lymphangiogenesis." Nature reviews Molecular cell biology **8**(6): 464-478.
- Aird, W. C. (2007). "Phenotypic heterogeneity of the endothelium: I. Structure, function, and mechanisms." Circulation research **100**(2): 158-173.
- Aird, W. C. (2012). "Endothelial cell heterogeneity." Cold Spring Harbor perspectives in medicine **2**(1): a006429.
- Akalu, A. and P. C. Brooks (2005). "Matrix, extracellular and interstitial." Reviews in Cell Biology and Molecular Medicine.
- Alghisi, G. C. and C. Rüegg (2006). "Vascular integrins in tumor angiogenesis: mediators and therapeutic targets." Endothelium **13**(2): 113-135.
- Almalki, S. G. and D. K. Agrawal (2017). "ERK signaling is required for VEGF-A/VEGFR2-induced differentiation of porcine adipose-derived mesenchymal stem cells into endothelial cells." Stem cell research & therapy **8**(1): 113.
- Almenar-Queralt, A., et al. (1999). "Tropomodulin assembles early in myofibrillogenesis in chick skeletal muscle: evidence that thin filaments rearrange to form striated myofibrils." Journal of cell science **112**(8): 1111-1123.
- Álvarez-Aznar, A., et al. (2017). VEGF receptor tyrosine kinases: key regulators of vascular function. Current topics in developmental biology, Elsevier. **123**: 433-482.

Armulik, A., et al. (2011). "Pericytes: developmental, physiological, and pathological perspectives, problems, and promises." Developmental cell **21**(2): 193-215.

Arroyo, J. A. and V. D. Winn (2008). Vasculogenesis and angiogenesis in the IUGR placenta. Seminars in perinatology, Elsevier.

Asahara, T., et al. (1999). "Bone marrow origin of endothelial progenitor cells responsible for postnatal vasculogenesis in physiological and pathological neovascularization." Circulation research **85**(3): 221-228.

Ascione, F., et al. (2016). "Comparison between fibroblast wound healing and cell random migration assays in vitro." Experimental cell research **347**(1): 123-132.

Ashby, W. J. and A. Zijlstra (2012). "Established and novel methods of interrogating two-dimensional cell migration." Integrative Biology **4**(11): 1338-1350.

Ata, R. and C. N. Antonescu (2017). "Integrins and cell metabolism: an intimate relationship impacting cancer." International journal of molecular sciences **18**(1): 189.

Atkinson, S. J., et al. (2018). "The  $\beta$ 3-integrin endothelial adhesome regulates microtubule-dependent cell migration." EMBO reports: e44578.

Autiero, M., et al. (2003). "Placental growth factor and its receptor, vascular endothelial growth factor receptor-1: novel targets for stimulation of ischemic tissue revascularization and inhibition of angiogenic and inflammatory disorders." Journal of Thrombosis and Haemostasis **1**(7): 1356-1370.

Avraamides, C. J., et al. (2008). "Integrins in angiogenesis and lymphangiogenesis." Nature Reviews Cancer **8**(8): 604.

Bachelder, R. E., et al. (2001). "Vascular endothelial growth factor is an autocrine survival factor for neuropilin-expressing breast carcinoma cells." Cancer research **61**(15): 5736-5740.

Bader, B. L., et al. (1998). "Extensive vasculogenesis, angiogenesis, and organogenesis precede lethality in mice lacking all  $\alpha$ v integrins." Cell **95**(4): 507-519.

Baker, M., et al. (2012). "Use of the mouse aortic ring assay to study angiogenesis." Nature protocols **7**(1): 89.

Balaji, S., et al. (2013). "The role of endothelial progenitor cells in postnatal vasculogenesis: implications for therapeutic neovascularization and wound healing." Advances in wound care **2**(6): 283-295.

Baldwin, M. E., et al. (2001). "The specificity of receptor binding by vascular endothelial growth factor-d is different in mouse and man." Journal of Biological Chemistry **276**(22): 19166-19171.

Baldwin, M. E., et al. (2005). "Vascular endothelial growth factor D is dispensable for development of the lymphatic system." Molecular and cellular biology **25**(6): 2441-2449.

Ballmer-Hofer, K., et al. (2011). "Neuropilin-1 promotes VEGFR-2 trafficking through Rab11 vesicles thereby specifying signal output." Blood: blood-2011-2001-328773.

Banks, R., et al. (1998). "Release of the angiogenic cytokine vascular endothelial growth factor (VEGF) from platelets: significance for VEGF measurements and cancer biology." British journal of cancer **77**(6): 956.

Bates, D. O. (2011). *An unexpected tail of VEGF and PlGF in pre-eclampsia*, Portland Press Limited.

Bazzoni, G. and E. Dejana (2004). "Endothelial cell-to-cell junctions: molecular organization and role in vascular homeostasis." Physiological reviews **84**(3): 869-901.

Becker, P. M., et al. (2005). "Neuropilin-1 regulates vascular endothelial growth factor-mediated endothelial permeability." Circulation research **96**(12): 1257-1265.

Bellomo, D., et al. (2000). "Mice lacking the vascular endothelial growth factor-B gene (Vegfb) have smaller hearts, dysfunctional coronary vasculature, and impaired recovery from cardiac ischemia." Circulation research **86**(2): e29-e35.

Benedito, R., et al. (2009). "The notch ligands Dll4 and Jagged1 have opposing effects on angiogenesis." Cell **137**(6): 1124-1135.

Benyair, R., et al. (2015). "Mammalian ER mannosidase I resides in quality control vesicles, where it encounters its glycoprotein substrates." Molecular biology of the cell **26**(2): 172-184.

Bergers, G. and S. Song (2005). "The role of pericytes in blood-vessel formation and maintenance." Neuro-oncology **7**(4): 452-464.

Berthois, Y., et al. (1986). "Phenol red in tissue culture media is a weak estrogen: implications concerning the study of estrogen-responsive cells in culture." Proceedings of the National Academy of Sciences **83**(8): 2496-2500.

Bhaskar, V., et al. (2007). "A function blocking anti-mouse integrin  $\alpha 5\beta 1$  antibody inhibits angiogenesis and impedes tumor growth in vivo." Journal of translational medicine **5**(1): 61.

Biçeroglu, S. and A. Memis (2005). "Gene therapy: applications in interventional radiology." Diagnostic and Interventional Radiology **11**(2): 113.

Bielenberg, D. R., et al. (2004). "Semaphorin 3F, a chemorepulsant for endothelial cells, induces a poorly vascularized, encapsulated, nonmetastatic tumor phenotype." The Journal of clinical investigation **114**(9): 1260-1271.

Blanco, R. and H. Gerhardt (2012). "VEGF and Notch in tip and stalk cell selection." Cold Spring Harbor perspectives in medicine: a006569.

Bökel, C. and N. H. Brown (2002). "Integrins in development: moving on, responding to, and sticking to the extracellular matrix." Developmental cell **3**(3): 311-321.

Borges, E., et al. (2000). "Platelet-derived growth factor receptor  $\beta$  and vascular endothelial growth factor receptor 2 bind to the  $\beta 3$  integrin through its extracellular domain." Journal of Biological Chemistry **275**(51): 39867-39873.

Borst, A. J., et al. (2017). "The Therapeutic Antibody LM609 Selectively Inhibits Ligand Binding to Human  $\alpha V\beta 3$  Integrin via Steric Hindrance." Structure **25**(11): 1732-1739. e1735.

Boudreau, N. J. and J. A. Varner (2004). "The homeobox transcription factor Hox D3 promotes integrin  $\alpha 5\beta 1$  expression and function during angiogenesis." Journal of Biological Chemistry **279**(6): 4862-4868.

Bouvard, D., et al. (2001). "Functional consequences of integrin gene mutations in mice." Circulation research **89**(3): 211-223.

Bouvrée, K., et al. (2012). "Semaphorin3A, Neuropilin-1, and PlexinA1 are required for lymphatic valve formation." Circulation research **111**(4): 437-445.

Breier, G., et al. (1992). "Expression of vascular endothelial growth factor during embryonic angiogenesis and endothelial cell differentiation." Development **114**(2): 521-532.

- Bretscher, M. S. (1989). "Endocytosis and recycling of the fibronectin receptor in CHO cells." The EMBO journal **8**(5): 1341.
- Bretscher, M. S. (1989). "Endocytosis and recycling of the fibronectin receptor in CHO cells." The EMBO journal **8**(5): 1341-1348.
- Bretscher, M. S. (1992). "Circulating integrins: alpha 5 beta 1, alpha 6 beta 4 and Mac-1, but not alpha 3 beta 1, alpha 4 beta 1 or LFA-1." The EMBO journal **11**(2): 405.
- Bretscher, M. S. and C. Aguado-Velasco (1998). "Membrane traffic during cell locomotion." Current opinion in cell biology **10**(4): 537-541.
- Bridgewater, R. E., et al. (2012). "Integrin trafficking at a glance." J Cell Sci **125**(16): 3695-3701.
- Broggi, E., et al. (1994). "Indirect angiogenic cytokines upregulate VEGF and bFGF gene expression in vascular smooth muscle cells, whereas hypoxia upregulates VEGF expression only." Circulation **90**(2): 649-652.
- Brooks, P. C., et al. (1994). "Requirement of vascular integrin alpha v beta 3 for angiogenesis." Science **264**(5158): 569-571.
- Brooks, P. C., et al. (1994). "Integrin  $\alpha v \beta 3$  antagonists promote tumor regression by inducing apoptosis of angiogenic blood vessels." Cell **79**(7): 1157-1164.
- Brooks, P. C., et al. (1995). "Antiintegrin alpha v beta 3 blocks human breast cancer growth and angiogenesis in human skin." The Journal of clinical investigation **96**(4): 1815-1822.
- Burek, M., et al. (2012). "Generation of an immortalized murine brain microvascular endothelial cell line as an in vitro blood brain barrier model." Journal of visualized experiments: JoVE(66).
- Burke, P. A., et al. (2002). "Cilengitide targeting of  $\alpha v \beta 3$  integrin receptor synergizes with radioimmunotherapy to increase efficacy and apoptosis in breast cancer xenografts." Cancer research **62**(15): 4263-4272.
- Burke, R. D. (1999). Invertebrate integrins: structure, function, and evolution. International review of cytology, Elsevier. **191**: 257-284.
- Cahill, P. A. and E. M. Redmond (2016). "Vascular endothelium—gatekeeper of vessel health." Atherosclerosis **248**: 97-109.

Cai, H. and R. R. Reed (1999). "Cloning and characterization of neuropilin-1-interacting protein: a PSD-95/Dlg/ZO-1 domain-containing protein that interacts with the cytoplasmic domain of neuropilin-1." Journal of Neuroscience **19**(15): 6519-6527.

Cai, Y., et al. (2011). "Multiple cytosolic and transmembrane determinants are required for the trafficking of SCAMP1 via an ER–Golgi–TGN–PM pathway." The Plant Journal **65**(6): 882-896.

Cain, R. J. and A. J. Ridley (2009). "Phosphoinositide 3-kinases in cell migration." Biology of the Cell **101**(1): 13-29.

Campbell, I. D. and M. J. Humphries (2011). "Integrin structure, activation, and interactions." Cold Spring Harbor perspectives in biology: a004994.

Cantley, L. C. (2002). "The phosphoinositide 3-kinase pathway." Science **296**(5573): 1655-1657.

Cao, Y., et al. (2013). "Neuropilin-2 promotes extravasation and metastasis by interacting with endothelial  $\alpha 5$  integrin." Cancer research **73**(14): 4579-4590.

Cao, Y., et al. (2008). "Neuropilin-1 upholds dedifferentiation and propagation phenotypes of renal cell carcinoma cells by activating Akt and sonic hedgehog axes." Cancer research **68**(21): 8667-8672.

Cardone, M. H., et al. (1998). "Regulation of cell death protease caspase-9 by phosphorylation." Science **282**(5392): 1318-1321.

Carmeliet, P. (2003). "Angiogenesis in health and disease." Nature medicine **9**(6): 653.

Carmeliet, P., et al. (1996). "Abnormal blood vessel development and lethality in embryos lacking a single VEGF allele." Nature **380**(6573): 435.

Carmeliet, P. and R. K. Jain (2011). "Molecular mechanisms and clinical applications of angiogenesis." Nature **473**(7347): 298-307.

Carmeliet, P. and R. K. Jain (2011). "Molecular mechanisms and clinical applications of angiogenesis." Nature **473**(7347): 298.

Carter, M. and J. Shieh (2015). Chapter 14 - Cell Culture Techniques. Guide to Research Techniques in Neuroscience (Second Edition). San Diego, Academic Press: 295-310.

Caserta, S., et al. (2013). "A methodology to study chemotaxis in 3-D collagen gels." AICHE Journal **59**(11): 4025-4035.

Caswell, P. and J. Norman (2008). "Endocytic transport of integrins during cell migration and invasion." Trends in cell biology **18**(6): 257-263.

Caswell, P. T. and J. C. Norman (2006). "Integrin trafficking and the control of cell migration." Traffic **7**(1): 14-21.

Caswell, P. T., et al. (2009). "Integrins: masters and slaves of endocytic transport." Nature reviews Molecular cell biology **10**(12): 843.

Caunt, M., et al. (2008). "Blocking neuropilin-2 function inhibits tumor cell metastasis." Cancer cell **13**(4): 331-342.

Chang, H. K., et al. (2007). "Oxidant generation by single infected monocytes after short-term fluorescence labeling of a protozoan parasite." Infection and immunity **75**(2): 1017-1024.

Chao, W.-T. and J. Kunz (2009). "Focal adhesion disassembly requires clathrin-dependent endocytosis of integrins." FEBS letters **583**(8): 1337-1343.

Chen, H., et al. (2000). "Neuropilin-2 regulates the development of select cranial and sensory nerves and hippocampal mossy fiber projections." Neuron **25**(1): 43-56.

Chen, H., et al. (1997). "Neuropilin-2, a novel member of the neuropilin family, is a high affinity receptor for the semaphorins Sema E and Sema IV but not Sema III." Neuron **19**(3): 547-559.

Chen, L., et al. (2009). "Analysis of allogenicity of mesenchymal stem cells in engraftment and wound healing in mice." PLoS One **4**(9): e7119.

Cheong, F. K. Y., et al. (2014). "Dynactin integrity depends upon direct binding of dynamitin to Arp1." Molecular biology of the cell **25**(14): 2171-2180.

Choi, S. H., et al. (2013). " $\alpha$ -Catenin interacts with APC to regulate  $\beta$ -catenin proteolysis and transcriptional repression of Wnt target genes." Genes & development **27**(22): 2473-2488.

- Chu, L.-Y., et al. (2013). "Thrombospondin-1 modulates VEGF signaling via CD36 by recruiting SHP-1 to VEGFR2 complex in microvascular endothelial cells." Blood **122**(10): 1822-1832.
- Claxton, S., et al. (2008). "Efficient, inducible Cre-recombinase activation in vascular endothelium." Genesis **46**(2): 74-80.
- Cleaver, O. and D. A. Melton (2003). "Endothelial signaling during development." Nature medicine **9**(6): 661.
- Cohen, T., et al. (2002). "Neuropilin-2 is a novel marker expressed in pancreatic islet cells and endocrine pancreatic tumours." The Journal of Pathology: A Journal of the Pathological Society of Great Britain and Ireland **198**(1): 77-82.
- Collet, G., et al. (2013). "Hypoxia-regulated overexpression of soluble VEGFR2 controls angiogenesis and inhibits tumor growth." Molecular cancer therapeutics.
- Contois, L., et al. (2009). Integrins as "functional hubs" in the regulation of pathological angiogenesis. Seminars in cancer biology, Elsevier.
- Conway, E. M., et al. (2001). "Molecular mechanisms of blood vessel growth." Cardiovascular research **49**(3): 507-521.
- Costache, M., et al. (2015). "VEGF expression in pancreatic cancer and other malignancies: a review of the literature." Romanian journal of internal medicine **53**(3): 199-208.
- Cox, C. M. and T. J. Poole (2000). "Angioblast differentiation is influenced by the local environment: FGF-2 induces angioblasts and patterns vessel formation in the quail embryo." Developmental dynamics: an official publication of the American Association of Anatomists **218**(2): 371-382.
- Cui, L., et al. (2009). "c-Abl kinase is required for  $\beta$ 2 integrin-mediated neutrophil adhesion." The Journal of Immunology **182**(5): 3233-3242.
- Curreli, S., et al. (2007). "Polysialylated neuropilin-2 is expressed on the surface of human dendritic cells and modulates dendritic cell-T lymphocyte interactions." Journal of Biological Chemistry **282**(42): 30346-30356.
- D'Amico, G., et al. (2010). "Endothelial-Rac1 is not required for tumor angiogenesis unless  $\alpha$ v $\beta$ 3-integrin is absent." PLoS One **5**(3): e9766.

D'andrea, L. D., et al. (2006). "Peptide-based molecules in angiogenesis." Chemical biology & drug design **67**(2): 115-126.

Dallas, N. A., et al. (2008). "Neuropilin-2-mediated tumor growth and angiogenesis in pancreatic adenocarcinoma." Clinical Cancer Research **14**(24): 8052-8060.

De Franceschi, N., et al. (2015). "Integrin traffic—the update." Journal of cell science **128**(5): 839-852.

de Oliveira, R. L., et al. (2011). "Growing tumor vessels: more than one way to skin a cat—implications for angiogenesis targeted cancer therapies." Molecular aspects of medicine **32**(2): 71-87.

De Pascalis, C. and S. Etienne-Manneville (2017). "Single and collective cell migration: the mechanics of adhesions." Molecular biology of the cell **28**(14): 1833-1846.

De Vries, L., et al. (1998). "GIPC, a PDZ domain containing protein, interacts specifically with the C terminus of RGS-GAIP." Proceedings of the National Academy of Sciences **95**(21): 12340-12345.

Deakin, N. O., et al. (2012). "Diverse roles for the paxillin family of proteins in cancer." Genes & cancer **3**(5-6): 362-370.

Decaestecker, C., et al. (2007). "Can anti-migratory drugs be screened in vitro? A review of 2D and 3D assays for the quantitative analysis of cell migration." Medicinal research reviews **27**(2): 149-176.

Dechantsreiter, M. A., et al. (1999). "N-Methylated cyclic RGD peptides as highly active and selective  $\alpha\beta_3$  integrin antagonists." Journal of medicinal chemistry **42**(16): 3033-3040.

Dehghanian, F., et al. (2014). "New insights into VEGF-A alternative splicing: key regulatory switching in the pathological process." Avicenna journal of medical biotechnology **6**(4): 192.

Dejana, E. (2004). "Endothelial cell–cell junctions: happy together." Nature reviews Molecular cell biology **5**(4): 261.

Dejana, E., et al. (2008). "The role of adherens junctions and VE-cadherin in the control of vascular permeability." Journal of cell science **121**(13): 2115-2122.

Delgoffe, G. M., et al. (2013). "Stability and function of regulatory T cells is maintained by a neuropilin-1–semaphorin-4a axis." Nature **501**(7466): 252.

Dell'Era Dosch, D. and K. Ballmer-Hofer (2010). "Transmembrane domain-mediated orientation of receptor monomers in active VEGFR-2 dimers." The FASEB Journal **24**(1): 32-38.

Dellinger, M. T. and R. A. Brekken (2011). "Phosphorylation of Akt and ERK1/2 is required for VEGF-A/VEGFR2-induced proliferation and migration of lymphatic endothelium." PLoS One **6**(12): e28947.

Demir, R., et al. (2006). "Sequential steps during vasculogenesis and angiogenesis in the very early human placenta." Placenta **27**(6-7): 535-539.

Demir, R., et al. (2010). "Vasculogenesis and angiogenesis in the endometrium during menstrual cycle and implantation." Acta histochemica **112**(3): 203-214.

Desgrosellier, J. S. and D. A. Cheresh (2010). "Integrins in cancer: biological implications and therapeutic opportunities." Nature Reviews Cancer **10**(1): 9-22.

Di Blasio, L., et al. (2010). "Protein Kinase D1 Regulates VEGF-A-Induced  $\alpha v\beta 3$  Integrin Trafficking and Endothelial Cell Migration." Traffic **11**(8): 1107-1118.

Dietrich, T., et al. (2007). "Inhibition of inflammatory lymphangiogenesis by integrin  $\alpha 5$  blockade." The American journal of pathology **171**(1): 361-372.

Dimmeler, S., et al. (1999). "Activation of nitric oxide synthase in endothelial cells by Akt-dependent phosphorylation." Nature **399**(6736): 601.

Djordjevic, S. and P. C. Driscoll (2013). "Targeting VEGF signalling via the neuropilin co-receptor." Drug discovery today **18**(9-10): 447-455.

Donaldson, J. G. and C. L. Jackson (2011). "ARF family G proteins and their regulators: roles in membrane transport, development and disease." Nature reviews Molecular cell biology **12**(6): 362.

Dong, Q. G., et al. (1997). "A general strategy for isolation of endothelial cells from murine tissues: characterization of two endothelial cell lines from the murine lung and subcutaneous sponge implants." Arteriosclerosis, thrombosis, and vascular biology **17**(8): 1599-1604.

Duffy, A. M., et al. (2004). "Vascular endothelial growth factor (VEGF) and its role in non-endothelial cells: autocrine signalling by VEGF." VEGF and Cancer: 133-144.

Dutta, S., et al. (2016). "NRP2 transcriptionally regulates its downstream effector WDFY1." Scientific reports **6**: 23588.

Echarri, A. and M. A. D. Pozo (2006). "Caveolae internalization regulates integrin-dependent signaling pathways." Cell cycle **5**(19): 2179-2182.

Eliceiri, B. P. (2001). "Integrin and growth factor receptor crosstalk." Circulation research **89**(12): 1104-1110.

Ellison, T. S., et al. (2015). "Suppression of  $\beta 3$ -integrin in mice triggers a neuropilin-1-dependent change in focal adhesion remodelling that can be targeted to block pathological angiogenesis." Disease models & mechanisms **8**(9): 1105-1119.

Elpek, G. Ö. (2015). "Angiogenesis and liver fibrosis." World journal of hepatology **7**(3): 377.

Eswarappa, S. M., et al. (2014). "Programmed translational readthrough generates antiangiogenic VEGF-Ax." Cell **157**(7): 1605-1618.

Evans, W. H., et al. (2006). "The gap junction cellular internet: connexin hemichannels enter the signalling limelight." Biochemical Journal **397**(1): 1-14.

Ezratty, E. J., et al. (2009). "Clathrin mediates integrin endocytosis for focal adhesion disassembly in migrating cells." The Journal of cell biology **187**(5): 733-747.

Fabbri, M., et al. (2005). "Dynamic partitioning into lipid rafts controls the endo-exocytic cycle of the  $\alpha L/\beta 2$  integrin, LFA-1, during leukocyte chemotaxis." Molecular biology of the cell **16**(12): 5793-5803.

Failla, C. M., et al. (2018). "Positive and Negative Regulation of Angiogenesis by Soluble Vascular Endothelial Growth Factor Receptor-1." International journal of molecular sciences **19**(5).

Fakhari, M., et al. (2002). "Selective upregulation of vascular endothelial growth factor receptors neuropilin-1 and-2 in human neuroblastoma." Cancer **94**(1): 258-263.

Falguières, T., et al. (2012). "Regulation of the MVB pathway by SCAMP3." Traffic **13**(1): 131-142.

- Fantin, A., et al. (2014). "Neuropilin 1 (NRP1) hypomorphism combined with defective VEGF-A binding reveals novel roles for NRP1 in developmental and pathological angiogenesis." Development: dev. 103028.
- Fantin, A., et al. (2011). "The cytoplasmic domain of neuropilin 1 is dispensable for angiogenesis, but promotes the spatial separation of retinal arteries and veins." Development: dev. 070037.
- Fantin, A., et al. (2013). "NRP1 acts cell autonomously in endothelium to promote tip cell function during sprouting angiogenesis." Blood: blood-2012-2005-424713.
- Fässler, R. and M. Meyer (1995). "Consequences of lack of beta 1 integrin gene expression in mice." Genes & development **9**(15): 1896-1908.
- Favero, G., et al. (2014). "Endothelium and its alterations in cardiovascular diseases: life style intervention." BioMed research international **2014**.
- Favier, B., et al. (2006). "Neuropilin-2 interacts with VEGFR-2 and VEGFR-3 and promotes human endothelial cell survival and migration." Blood **108**(4): 1243-1250.
- Fearnley, G. W., et al. (2014). "VEGF-A isoforms differentially regulate ATF-2-dependent VCAM-1 gene expression and endothelial-leukocyte interactions." Molecular biology of the cell **25**(16): 2509-2521.
- Fearnley, G. W., et al. (2016). "VEGF-A isoforms program differential VEGFR2 signal transduction, trafficking and proteolysis." Biology open: bio. 017434.
- Feil, S., et al. (2009). Inducible cre mice. Gene knockout protocols, Springer: 343-363.
- Félétou, M. (2011). The endothelium, Part I: Multiple functions of the endothelial cells--focus on endothelium-derived vasoactive mediators. Colloquium Series on Integrated Systems Physiology: From Molecule to Function, Morgan & Claypool Life Sciences.
- Ferrara, N., et al. (2003). "The biology of VEGF and its receptors." Nature medicine **9**(6): 669.
- Figlin, R., et al. (2006). "Phase II study of volociximab (M200), an  $\alpha 5\beta 1$  anti-integrin antibody in refractory metastatic clear cell renal cell cancer (RCC)." Journal of Clinical Oncology **24**(18\_suppl): 4535-4535.

Fischer, R. S., et al. (2003). "Pointed-end capping by tropomodulin3 negatively regulates endothelial cell motility." J Cell Biol **161**(2): 371-380.

Francis, S. E., et al. (2002). "Central roles of  $\alpha 5\beta 1$  integrin and fibronectin in vascular development in mouse embryos and embryoid bodies." Arteriosclerosis, thrombosis, and vascular biology **22**(6): 927-933.

Frankel, P., et al. (2008). "Chondroitin sulphate-modified neuropilin 1 is expressed in human tumour cells and modulates 3D invasion in the U87MG human glioblastoma cell line through a p130Cas-mediated pathway." EMBO reports **9**(10): 983-989.

Frantz, C., et al. (2010). "The extracellular matrix at a glance." Journal of cell science **123**(24): 4195-4200.

Friedrichs, K., et al. (1995). "High expression level of  $\alpha 6$  integrin in human breast carcinoma is correlated with reduced survival." Cancer research **55**(4): 901-906.

Fuh, G., et al. (2000). "The interaction of neuropilin-1 with vascular endothelial growth factor and its receptor flt-1." Journal of Biological Chemistry **275**(35): 26690-26695.

Fuh, G., et al. (1998). "Requirements for binding and signaling of the kinase domain receptor for vascular endothelial growth factor." Journal of Biological Chemistry **273**(18): 11197-11204.

Fujisawa, H., et al. (1997). "Roles of a neuronal cell-surface molecule, neuropilin, in nerve fiber fasciculation and guidance." Cell and tissue research **290**(2): 465-470.

Fujisawa, H., et al. (1995). "Growth-Associated Expression of a Membrane Protein, Neuropilin, in Xenopus Optic NerveFibers." Developmental neuroscience **17**(5-6): 343-349.

Fukahi, K., et al. (2004). "Aberrant expression of neuropilin-1 and-2 in human pancreatic cancer cells." Clinical Cancer Research **10**(2): 581-590.

Fukasawa, M., et al. (2007). "Neuropilin-1 interacts with integrin  $\beta 1$  and modulates pancreatic cancer cell growth, survival and invasion." Cancer biology & therapy **6**(8): 1184-1191.

Fukumura, D., et al. (2001). "Predominant role of endothelial nitric oxide synthase in vascular endothelial growth factor-induced angiogenesis and vascular permeability." Proceedings of the National Academy of Sciences **98**(5): 2604-2609.

Galley, H. F. and N. R. Webster (2004). "Physiology of the endothelium." British journal of anaesthesia **93**(1): 105-113.

Gaudry, M., et al. (1997). "Intracellular pool of vascular endothelial growth factor in human neutrophils." Blood **90**(10): 4153-4161.

Gaur, P., et al. (2009). "Role of class 3 semaphorins and their receptors in tumor growth and angiogenesis." Clinical Cancer Research **15**(22): 6763-6770.

Gaur, U., et al. (2009). "Leishmania donovani lacking the Golgi GDP-Man transporter LPG2 exhibit attenuated virulence in mammalian hosts." Experimental parasitology **122**(3): 182-191.

Gavard, J. and J. S. Gutkind (2006). "VEGF controls endothelial-cell permeability by promoting the  $\beta$ -arrestin-dependent endocytosis of VE-cadherin." Nature cell biology **8**(11): 1223.

Gehling, U. M., et al. (2000). "In vitro differentiation of endothelial cells from AC133-positive progenitor cells." Blood **95**(10): 3106-3112.

George, E. L., et al. (1993). "Defects in mesoderm, neural tube and vascular development in mouse embryos lacking fibronectin." Development **119**(4): 1079-1091.

Gerhardt, H. and C. Betsholtz (2003). "Endothelial-pericyte interactions in angiogenesis." Cell and tissue research **314**(1): 15-23.

German, A. E., et al. (2014). "Paxillin controls endothelial cell migration and tumor angiogenesis by altering neuropilin 2 expression." J Cell Sci **127**(8): 1672-1683.

Giger, R. J., et al. (2000). "Neuropilin-2 is required in vivo for selective axon guidance responses to secreted semaphorins." Neuron **25**(1): 29-41.

Gillingham, A. K. and S. Munro (2007). "The small G proteins of the Arf family and their regulators." Annu. Rev. Cell Dev. Biol. **23**: 579-611.

Ginsberg, M. H., et al. (2005). "Integrin regulation." Current opinion in cell biology **17**(5): 509-516.

Gluzman-Poltorak, Z., et al. (2000). "Neuropilin-2 and neuropilin-1 are receptors for VEGF165 and PLGF-2, but only neuropilin-2 functions as a receptor for VEGF145." Journal of Biological Chemistry.

Gluzman-Poltorak, Z., et al. (2000). "Neuropilin-2 is a receptor for the vascular endothelial growth factor (VEGF) forms VEGF-145 and VEGF-165 [corrected]." The Journal of biological chemistry **275**(24): 18040-18045.

Gluzman-Poltorak, Z., et al. (2001). "Vascular endothelial growth factor receptor-1 (VEGFR-1) and neuropilin-2 form complexes." Journal of Biological Chemistry.

Goel, H. L., et al. (2012). "VEGF/Neuropilin-2 regulation of Bmi-1 and consequent repression of IGF-1R define a novel mechanism of aggressive prostate cancer." Cancer discovery: CD-12-0085.

Goel, H. L. and A. M. Mercurio (2012). "Enhancing integrin function by VEGF/neuropilin signaling: implications for tumor biology." Cell adhesion & migration **6**(6): 554-560.

Goel, H. L., et al. (2013). "GLI1 regulates a novel neuropilin-2/ $\alpha$ 6 $\beta$ 1 integrin based autocrine pathway that contributes to breast cancer initiation." EMBO molecular medicine **5**(4): 488-508.

Goel, H. L., et al. (2012). "Neuropilin-2 regulates  $\alpha$ 6 $\beta$ 1 integrin in the formation of focal adhesions and signaling." Journal of cell science **125**(2): 497-506.

Goel, H. L., et al. (2012). "Neuropilin-2 regulates  $\alpha$ 6 $\beta$ 1 integrin in the formation of focal adhesions and signaling." J Cell Sci **125**(2): 497-506.

Goksoy, E., et al. (2008). "Structural basis for the autoinhibition of talin in regulating integrin activation." Molecular cell **31**(1): 124-133.

Gómez-Puertas, P., et al. (2004). "The substrate recognition mechanisms in chaperonins." Journal of Molecular Recognition **17**(2): 85-94.

Gong, Y., et al. (2013). "Sprouty4 regulates endothelial cell migration via modulating integrin  $\beta$ 3 stability through c-Src." Angiogenesis **16**(4): 861-875.

Goult, B. T., et al. (2013). "RIAM and vinculin binding to talin are mutually exclusive and regulate adhesion assembly and turnover." Journal of Biological Chemistry: jbc. M112. 438119.

Gourlaouen, M., et al. (2013). "Essential role for endocytosis in the growth factor stimulated activation of ERK1/2 in endothelial cells." Journal of Biological Chemistry: jbc. M112. 446401.

Gray, M. J., et al. (2008). "Therapeutic targeting of neuropilin-2 on colorectal carcinoma cells implanted in the murine liver." Journal of the National Cancer Institute **100**(2): 109-120.

Gu, C., et al. (2003). "Neuropilin-1 conveys semaphorin and VEGF signaling during neural and cardiovascular development." Developmental cell **5**(1): 45-57.

Gu, C., et al. (2005). "Semaphorin 3E and plexin-D1 control vascular pattern independently of neuropilins." Science **307**(5707): 265-268.

Gu, F., et al. (2013). "VEGF111b, a new member of VEGF<sub>xxx</sub>b isoforms and induced by mitomycin C, inhibits angiogenesis." Biochemical and biophysical research communications **441**(1): 18-24.

Gu, Z., et al. (2011). "Integrins traffic rapidly via circular dorsal ruffles and macropinocytosis during stimulated cell migration." The Journal of cell biology **193**(1): 61-70.

Guo, H.-F. and C. W. Vander Kooi (2015). "Neuropilin functions as an essential cell surface receptor." Journal of Biological Chemistry **290**(49): 29120-29126.

Guo, S., et al. (2010). "Vascular endothelial growth factor receptor-2 in breast cancer." Biochimica et Biophysica Acta (BBA)-Reviews on Cancer **1806**(1): 108-121.

Han, Y., et al. (2012). "Inhibition of ARNT severely compromises endothelial cell viability and function in response to moderate hypoxia." Angiogenesis **15**(3): 409-420.

Handa, A., et al. (2000). "Neuropilin-2 expression affects the increased vascularization and is a prognostic factor in osteosarcoma." International journal of oncology **17**(2): 291-296.

Harry, L. E. and E. M. Paleolog (2003). "From the cradle to the clinic: VEGF in developmental, physiological, and pathological angiogenesis." Birth Defects Research Part C: Embryo Today: Reviews **69**(4): 363-374.

Heinolainen, K., et al. (2017). "VEGFR3 modulates vascular permeability by controlling VEGF/VEGFR2 signaling." Circulation research: CIRCRESAHA. 116.310477.

Heitz, F., et al. (2014). "Heritable and inducible gene knockdown in astrocytes or neurons in vivo by a combined lentiviral and RNAi approach." Frontiers in cellular neuroscience **8**: 62.

Helker, C. S., et al. (2015). "The hormonal peptide Elabela guides angioblasts to the midline during vasculogenesis." Elife **4**: e06726.

Hellewell, A. L., et al. (2017). "A rapid, scalable method for the isolation, functional study, and analysis of cell-derived extracellular matrix." Journal of visualized experiments: JoVE(119).

Herrnberger, L., et al. (2012). "The role of plasmalemma vesicle-associated protein (PLVAP) in endothelial cells of Schlemm's canal and ocular capillaries." Experimental eye research **105**: 27-33.

Herzog, B., et al. (2011). "VEGF binding to NRP1 is essential for VEGF stimulation of endothelial cell migration, complex formation between NRP1 and VEGFR2, and signaling via FAK Tyr407 phosphorylation." Molecular biology of the cell **22**(15): 2766-2776.

Herzog, Y., et al. (2001). "Differential expression of neuropilin-1 and neuropilin-2 in arteries and veins." Mechanisms of development **109**(1): 115-119.

Hilmi, C. and M. Guyot (2012). "VEGF spliced variants: possible role of anti-angiogenesis therapy." Journal of nucleic acids **2012**.

Hiratsuka, S., et al. (2005). "Vascular endothelial growth factor A (VEGF-A) is involved in guidance of VEGF receptor-positive cells to the anterior portion of early embryos." Molecular and cellular biology **25**(1): 355-363.

Hirota, S., et al. (2015). "Neuropilin 1 balances  $\beta 8$  integrin-activated TGF $\beta$  signaling to control sprouting angiogenesis in the brain." Development **142**(24): 4363-4373.

Ho, Q. T. and C. J. Kuo (2007). "Vascular endothelial growth factor: biology and therapeutic applications." The international journal of biochemistry & cell biology **39**(7-8): 1349-1357.

Hodivala-Dilke, K. M., et al. (1999). " $\beta 3$ -integrin-deficient mice are a model for Glanzmann thrombasthenia showing placental defects and reduced survival." The Journal of clinical investigation **103**(2): 229-238.

Hodivala-Dilke, K. M., et al. (2003). "Integrins in angiogenesis: multitalented molecules in a balancing act." Cell and tissue research **314**(1): 131-144.

Hoernke, M., et al. (2017). "EHD2 restrains dynamics of caveolae by an ATP-dependent, membrane-bound, open conformation." Proceedings of the National Academy of Sciences **114**(22): E4360-E4369.

Hoffmann, C., et al. (2011). "Integrin-mediated uptake of fibronectin-binding bacteria." European journal of cell biology **90**(11): 891-896.

Holleran, E. A., et al. (1996). "Centractin (ARP1) associates with spectrin revealing a potential mechanism to link dynactin to intracellular organelles." The Journal of cell biology **135**(6): 1815-1829.

Holmes, D. I. and I. Zachary (2005). "The vascular endothelial growth factor (VEGF) family: angiogenic factors in health and disease." Genome biology **6**(2): 209.

Holmqvist, K., et al. (2004). "The adaptor protein shb binds to tyrosine 1175 in vascular endothelial growth factor (VEGF) receptor-2 and regulates VEGF-dependent cellular migration." Journal of Biological Chemistry **279**(21): 22267-22275.

Hood, J. D., et al. (1998). "VEGF upregulates ecNOS message, protein, and NO production in human endothelial cells." American Journal of Physiology-Heart and Circulatory Physiology **274**(3): H1054-H1058.

Hsieh, S., et al. (2008). "Galectin-1, a novel ligand of neuropilin-1, activates VEGFR-2 signaling and modulates the migration of vascular endothelial cells." Oncogene **27**(26): 3746.

Hu, P. and B. H. Luo (2013). "Integrin bi-directional signaling across the plasma membrane." Journal of cellular physiology **228**(2): 306-312.

Hubbard, T., et al. (2002). "The Ensembl genome database project." Nucleic acids research **30**(1): 38-41.

Humphries, J. D., et al. (2006). "Integrin ligands at a glance." Journal of cell science **119**(19): 3901-3903.

Hussein, H. A., et al. (2015). "Beyond RGD: virus interactions with integrins." Archives of virology **160**(11): 2669-2681.

Huttenlocher, A. and A. R. Horwitz (2011). "Integrins in cell migration." Cold Spring Harbor perspectives in biology **3**(9): a005074.

Hynes, R. (2007). "Cell-matrix adhesion in vascular development." Journal of Thrombosis and Haemostasis **5**(s1): 32-40.

Hynes, R. O. (2002). "Integrins: bidirectional, allosteric signaling machines." Cell **110**(6): 673-687.

Iivanainen, E., et al. (2003). "Endothelial cell–matrix interactions." Microscopy research and technique **60**(1): 13-22.

Ikuno, T., et al. (2017). "Efficient and robust differentiation of endothelial cells from human induced pluripotent stem cells via lineage control with VEGF and cyclic AMP." PLoS One **12**(3): e0173271.

Isner, J. M. and T. Asahara (1999). "Angiogenesis and vasculogenesis as therapeutic strategies for postnatal neovascularization." The Journal of clinical investigation **103**(9): 1231-1236.

Iyer, S. and K. R. Acharya (2011). "Tying the knot: The cystine signature and molecular-recognition processes of the vascular endothelial growth factor family of angiogenic cytokines." The FEBS journal **278**(22): 4304-4322.

Jagadeeswaran, R., et al. (2008). "Paxillin is a target for somatic mutations in lung cancer: implications for cell growth and invasion." Cancer research **68**(1): 132-142.

Jain, R. K. (2003). "Molecular regulation of vessel maturation." Nature medicine **9**(6): 685.

Jakobsson, L., et al. (2009). VEGFRs and Notch: a dynamic collaboration in vascular patterning, Portland Press Limited.

Jakobsson, L., et al. (2006). "Heparan sulfate in trans potentiates VEGFR-mediated angiogenesis." Developmental cell **10**(5): 625-634.

Jia, T., et al. (2018). "Heteromultivalent targeting of integrin  $\alpha v \beta 3$  and neuropilin 1 promotes cell survival via the activation of the IGF-1/insulin receptors." Biomaterials **155**: 64-79.

Jin, D., et al. (2017). "Vegfa signaling regulates diverse artery/vein formation in vertebrate vasculatures." Journal of Genetics and Genomics **44**(10): 483-492.

Jones, E. A., et al. (2008). "Separating genetic and hemodynamic defects in neuropilin 1 knockout embryos." Development **135**(14): 2479-2488.

Jung, J.-Y., et al. (2016). "Neuronal expression and cell-type-specific gene-silencing of Best1 in thalamic reticular nucleus neurons using pSico-Red System." Experimental neurobiology **25**(3): 120-129.

Jurisic, G., et al. (2012). "An unexpected role of semaphorin3A–neuropilin-1 signaling in lymphatic vessel maturation and valve formation." Circulation research **111**(4): 426-436.

Juriscic, G., et al. (2012). "An unexpected role of semaphorin3A/neuropilin-1 signaling in lymphatic vessel maturation and valve formation." Circulation research **111**(4): 426.

Kaipainen, A., et al. (1995). "Expression of the fms-like tyrosine kinase 4 gene becomes restricted to lymphatic endothelium during development." Proceedings of the National Academy of Sciences **92**(8): 3566-3570.

Kalluri, R. (2003). "Basement membranes: structure, assembly and role in tumour angiogenesis." Nature Reviews Cancer **3**(6): 422-433.

Kam, Y., et al. (2008). "A novel circular invasion assay mimics in vivo invasive behavior of cancer cell lines and distinguishes single-cell motility in vitro." BMC cancer **8**(1): 198.

Karkkainen, M. J., et al. (2004). "Vascular endothelial growth factor C is required for sprouting of the first lymphatic vessels from embryonic veins." Nature immunology **5**(1): 74.

Kärpänen, T., et al. (2006). "Functional interaction of VEGF-C and VEGF-D with neuropilin receptors." The FASEB Journal **20**(9): 1462-1472.

Kawakami, T., et al. (2002). "Neuropilin 1 and neuropilin 2 co-expression is significantly correlated with increased vascularity and poor prognosis in nonsmall cell lung carcinoma." Cancer: Interdisciplinary International Journal of the American Cancer Society **95**(10): 2196-2201.

Kawamura, H., et al. (2008). "Neuropilin-1 in regulation of VEGF-induced activation of p38MAPK and endothelial cell organization." Blood **112**(9): 3638-3649.

Kawasaki, T., et al. (1999). "A requirement for neuropilin-1 in embryonic vessel formation." Development **126**(21): 4895-4902.

Keck, B., et al. (2015). "Neuropilin-2 and its ligand VEGF-C predict treatment response after transurethral resection and radiochemotherapy in bladder cancer patients." International journal of cancer **136**(2): 443-451.

Kessler, O., et al. (2004). "Semaphorin-3F is an inhibitor of tumor angiogenesis." Cancer research **64**(3): 1008-1015.

Keuschnigg, J., et al. (2013). "Plasticity of blood-and lymphatic endothelial cells and marker identification." PLoS One **8**(9): e74293.

Keuschnigg, J., et al. (2012). "PV-1 is recognized by the PAL-E antibody and forms complexes with NRP-1." Blood **120**(1): 232-235.

Kim, S., et al. (2002). "Inhibition of endothelial cell survival and angiogenesis by protein kinase A." The Journal of clinical investigation **110**(7): 933-941.

Kim, S., et al. (2000). "Regulation of angiogenesis in vivo by ligation of integrin  $\alpha 5\beta 1$  with the central cell-binding domain of fibronectin." The American journal of pathology **156**(4): 1345-1362.

Kim, S., et al. (2000). "Regulation of integrin  $\alpha v\beta 3$ -mediated endothelial cell migration and angiogenesis by integrin  $\alpha 5\beta 1$  and protein kinase A." Journal of Biological Chemistry **275**(43): 33920-33928.

Kim, S. M., et al. (2017). "Overcoming key biological barriers to cancer drug delivery and efficacy." Journal of Controlled Release **267**: 15-30.

Kim, Y., et al. (2017). "Co-targeting of EGF receptor and neuropilin-1 overcomes cetuximab resistance in pancreatic ductal adenocarcinoma with integrin  $\beta 1$ -driven Src-Akt bypass signaling." Oncogene **36**(18): 2543.

Kitsukawa, T., et al. (1995). "Overexpression of a membrane protein, neuropilin, in chimeric mice causes anomalies in the cardiovascular system, nervous system and limbs." Development **121**(12): 4309-4318.

Klagsbrun, M. and M. A. Moses (1999). "Molecular angiogenesis." Chemistry & biology **6**(8): R217-R224.

Klagsbrun, M., et al. (2002). The role of neuropilin in vascular and tumor biology. Neuropilin: From Nervous System to Vascular and Tumor Biology, Springer: 33-48.

Klinge, S., et al. (2011). "Crystal structure of the eukaryotic 60S ribosomal subunit in complex with initiation factor 6." Science **334**(6058): 941-948.

Knight, B., et al. (2000). "Visualizing muscle cell migration in situ." Current Biology **10**(10): 576-585.

Koch, S. and L. Claesson-Welsh (2012). "Signal transduction by vascular endothelial growth factor receptors." Cold Spring Harbor perspectives in medicine **2**(7): a006502.

Koch, S. and L. Claesson-Welsh (2012). "Signal transduction by vascular endothelial growth factor receptors." Cold Spring Harbor perspectives in medicine: a006502.

Koch, S., et al. (2014). "NRP1 presented in trans to the endothelium arrests VEGFR2 endocytosis, preventing angiogenic signaling and tumor initiation." Developmental cell **28**(6): 633-646.

Kramer, N., et al. (2013). "In vitro cell migration and invasion assays." Mutation Research/Reviews in Mutation Research **752**(1): 10-24.

Krilleke, D., et al. (2007). "Molecular mapping and functional characterization of the VEGF164 heparin-binding domain." Journal of Biological Chemistry **282**(38): 28045-28056.

Kubis, N. and B. Levy (2003). "Vasculogenesis and Angiogenesis: Molecular and Cellular Controls: Part 1: Growth Factors." Interventional Neuroradiology **9**(3): 227-237.

Kwabi-Addo, B., et al. (2004). "The role of fibroblast growth factors and their receptors in prostate cancer." Endocrine-related cancer **11**(4): 709-724.

Lake, A. C., et al. (2006). "Low molecular weight fucoidan increases VEGF165-induced endothelial cell migration by enhancing VEGF165 binding to VEGFR-2 and NRP1." Journal of Biological Chemistry **281**(49): 37844-37852.

Lakshminarayan, R., et al. (2014). "Galectin-3 drives glycosphingolipid-dependent biogenesis of clathrin-independent carriers." Nature cell biology **16**(6): 592.

Lal, N., et al. (2017). "Loss of VEGFB and its signaling in the diabetic heart is associated with increased cell death signaling." American Journal of Physiology-Heart and Circulatory Physiology **312**(6): H1163-H1175.

Lal, N., et al. (2018). "Vascular endothelial growth factor B and its signaling." Frontiers in cardiovascular medicine **5**: 39.

Lam, S. K., et al. (2007). "Rice SCAMP1 defines clathrin-coated, trans-Golgi-located tubular-vesicular structures as an early endosome in tobacco BY-2 cells." The Plant Cell **19**(1): 296-319.

Lamallice, L., et al. (2006). "Phosphorylation of Tyr1214 within VEGFR-2 triggers the recruitment of Nck and activation of Fyn leading to SAPK2/p38 activation and endothelial cell migration in response to VEGF." Journal of Biological Chemistry **281**(45): 34009-34020.

Lamallice, L., et al. (2004). "Phosphorylation of tyrosine 1214 on VEGFR2 is required for VEGF-induced activation of Cdc42 upstream of SAPK2/p38." Oncogene **23**(2): 434.

Lampugnani, M. G., et al. (2006). "Vascular endothelial cadherin controls VEGFR-2 internalization and signaling from intracellular compartments." J Cell Biol **174**(4): 593-604.

Lampugnani, M. G., et al. (2003). "Contact inhibition of VEGF-induced proliferation requires vascular endothelial cadherin,  $\beta$ -catenin, and the phosphatase DEP-1/CD148." The Journal of cell biology **161**(4): 793-804.

Lamy, S., et al. (2010). "Propranolol suppresses angiogenesis in vitro: inhibition of proliferation, migration, and differentiation of endothelial cells." Vascular pharmacology **53**(5-6): 200-208.

Lamy, S., et al. (2014). "Olive oil compounds inhibit vascular endothelial growth factor receptor-2 phosphorylation." Experimental cell research **322**(1): 89-98.

Lanahan, A., et al. (2013). "The neuropilin 1 cytoplasmic domain is required for VEGF-A-dependent arteriogenesis." Developmental cell **25**(2): 156-168.

Lange, C., et al. (2016). "Vascular endothelial growth factor: a neurovascular target in neurological diseases." Nature Reviews Neurology **12**(8): 439.

Lantuéjoul, S., et al. (2003). "Expression of VEGF, semaphorin SEMA3F, and their common receptors neuropilins NP1 and NP2 in preinvasive bronchial lesions, lung tumours, and cell lines." The Journal of Pathology: A Journal of the Pathological Society of Great Britain and Ireland **200**(3): 336-347.

Laukaitis, C. M., et al. (2001). "Differential dynamics of  $\alpha 5$  integrin, paxillin, and  $\alpha$ -actinin during formation and disassembly of adhesions in migrating cells." The Journal of cell biology **153**(7): 1427-1440.

LaVallee, T. M., et al. (1998). "Activation of the MAP kinase pathway by FGF-1 correlates with cell proliferation induction while activation of the Src pathway correlates with migration." The Journal of cell biology **141**(7): 1647-1658.

Legate, K. R. and R. Fässler (2009). "Mechanisms that regulate adaptor binding to  $\beta$ -integrin cytoplasmic tails." Journal of cell science **122**(2): 187-198.

Leung, D. W., et al. (1989). "Vascular endothelial growth factor is a secreted angiogenic mitogen." Science **246**(4935): 1306-1309.

Lewis, J. M., et al. (1996). "Integrin regulation of c-Abl tyrosine kinase activity and cytoplasmic–nuclear transport." Proceedings of the National Academy of Sciences **93**(26): 15174-15179.

Lewis, J. M. and M. A. Schwartz (1998). "Integrins regulate the association and phosphorylation of paxillin by c-Abl." Journal of Biological Chemistry **273**(23): 14225-14230.

Li, J. and T. A. Springer (2017). "Integrin extension enables ultrasensitive regulation by cytoskeletal force." Proceedings of the National Academy of Sciences: 201704171.

Li, L., et al. (2012). "An angiogenic role for the  $\alpha 5\beta 1$  integrin in promoting endothelial cell proliferation during cerebral hypoxia." Experimental neurology **237**(1): 46-54.

Li, L., et al. (2010). "Absence of the  $\alpha v\beta 3$  integrin dictates the time-course of angiogenesis in the hypoxic central nervous system: accelerated endothelial proliferation correlates with compensatory increases in  $\alpha 5\beta 1$  integrin expression." Journal of Cerebral Blood Flow & Metabolism **30**(5): 1031-1043.

Li, S., et al. (2005). "Biochemistry and biomechanics of cell motility." Annu. Rev. Biomed. Eng. **7**: 105-150.

Li, X., et al. (2014). "Control of cellular motility by neuropilin-mediated physical interactions." Biomolecular concepts **5**(2): 157-166.

Li, X., et al. (2008). "Reevaluation of the role of VEGF-B suggests a restricted role in the revascularization of the ischemic myocardium." Arteriosclerosis, thrombosis, and vascular biology **28**(9): 1614-1620.

Lilja, J., et al. (2017). "SHANK proteins limit integrin activation by directly interacting with Rap1 and R-Ras." Nature cell biology **19**(4): 292.

Lippincott-Schwartz, J., et al. (2000). "Secretory protein trafficking and organelle dynamics in living cells." Annual review of cell and developmental biology **16**(1): 557-589.

Lizarbe, M. A., et al. (2013). "Annexin-phospholipid interactions. Functional implications." International journal of molecular sciences **14**(2): 2652-2683.

Llorca, O., et al. (1999). "Eukaryotic type II chaperonin CCT interacts with actin through specific subunits." Nature **402**(6762): 693.

- MacDonald, T. J., et al. (2001). "Preferential susceptibility of brain tumors to the antiangiogenic effects of an  $\alpha$ v integrin antagonist." Neurosurgery **48**(1): 151-157.
- Mackinnon, A. C., et al. (2010). "Paxillin expression and amplification in early lung lesions of high-risk patients, lung adenocarcinoma and metastatic disease." Journal of clinical pathology: jcp. 2010.075853.
- Mahabeleshwar, G. H., et al. (2008). "Integrin affinity modulation in angiogenesis." Cell cycle **7**(3): 335-347.
- Mahabeleshwar, G. H., et al. (2006). "Integrin signaling is critical for pathological angiogenesis." Journal of Experimental Medicine **203**(11): 2495-2507.
- Mahabeleshwar, G. H., et al. (2007). "Mechanisms of integrin–vascular endothelial growth factor receptor cross-activation in angiogenesis." Circulation research **101**(6): 570-580.
- Malek, M., et al. (2012). "LAMTOR1 depletion induces p53-dependent apoptosis via aberrant lysosomal activation." Cell death & disease **3**(4): e300.
- Mamluk, R., et al. (2005). "Soluble neuropilin targeted to the skin inhibits vascular permeability." Angiogenesis **8**(3): 217-227.
- Mana, G., et al. (2016). "PPFIA1 drives active  $\alpha$ 5 $\beta$ 1 integrin recycling and controls fibronectin fibrillogenesis and vascular morphogenesis." Nature communications **7**: 13546.
- Margadant, C., et al. (2011). "Mechanisms of integrin activation and trafficking." Current opinion in cell biology **23**(5): 607-614.
- Maric, G., et al. (2015). "GPNMB cooperates with neuropilin-1 to promote mammary tumor growth and engages integrin  $\alpha$  5  $\beta$  1 for efficient breast cancer metastasis." Oncogene **34**(43): 5494.
- Marugán, J. J., et al. (2005). "Design, synthesis, and biological evaluation of novel potent and selective  $\alpha$ v $\beta$ 3/ $\alpha$ v $\beta$ 5 integrin dual inhibitors with improved bioavailability. Selection of the molecular core." Journal of medicinal chemistry **48**(4): 926-934.
- Masson-Gadais, B., et al. (2003). "Integrin  $\alpha$ v $\beta$ 3 requirement for VEGFR2-mediated activation of SAPK2/p38 and for Hsp90-dependent phosphorylation of focal adhesion kinase in endothelial cells activated by VEGF." Cell stress & chaperones **8**(1): 37.

Matsumoto, T., et al. (2005). "VEGF receptor-2 Y951 signaling and a role for the adapter molecule TSAd in tumor angiogenesis." The EMBO journal **24**(13): 2342-2353.

Matsunaga, T., et al. (2014). Adhesion-dependent cell Regulation via Adhesion molecule, integrin: Therapeutic application of integrin activation-modulating factors. Colloid and Interface Science in Pharmaceutical Research and Development, Elsevier: 243-260.

McCarty, J. H., et al. (2002). "Defective associations between blood vessels and brain parenchyma lead to cerebral hemorrhage in mice lacking  $\alpha$ v integrins." Molecular and cellular biology **22**(21): 7667-7677.

McCleverty, C. J., et al. (2007). "Structure of the PTB domain of tensin1 and a model for its recruitment to fibrillar adhesions." Protein science **16**(6): 1223-1229.

McConnell, T. H. (2013). The nature of disease: pathology for the health professions, Lippincott Williams & Wilkins.

Menter, D. G. and R. N. DuBois (2012). "Prostaglandins in cancer cell adhesion, migration, and invasion." International journal of cell biology **2012**.

Mesquita, J., et al. (2018). "Vascular endothelial growth factors and placenta growth factor in retinal vasculopathies: Current research and future perspectives." Cytokine & growth factor reviews **39**: 102-115.

Meyer, M., et al. (1999). "A novel vascular endothelial growth factor encoded by Orf virus, VEGF-E, mediates angiogenesis via signalling through VEGFR-2 (KDR) but not VEGFR-1 (Flt-1) receptor tyrosine kinases." The EMBO journal **18**(2): 363-374.

Meyer, R. D., et al. (2008). "IQGAP1-dependent signaling pathway regulates endothelial cell proliferation and angiogenesis." PLoS One **3**(12): e3848.

Miao, H.-Q., et al. (1999). "Neuropilin-1 mediates collapsin-1/semaphorin III inhibition of endothelial cell motility: functional competition of collapsin-1 and vascular endothelial growth factor-165." The Journal of cell biology **146**(1): 233-242.

Miller, W. H., et al. (2000). "Identification and in vivo efficacy of small-molecule antagonists of integrin  $\alpha$  $\beta$ 3 (the vitronectin receptor)." Drug discovery today **5**(9): 397-408.

Milner, R., et al. (2008). "Increased expression of fibronectin and the  $\alpha$ 5 $\beta$ 1 integrin in angiogenic cerebral blood vessels of mice subject to hypobaric hypoxia." Molecular and Cellular Neuroscience **38**(1): 43-52.

- Mohan, J., et al. (2015). "Cavin3 interacts with cavin1 and caveolin1 to increase surface dynamics of caveolae." J Cell Sci **128**(5): 979-991.
- Monahan-Earley, R., et al. (2013). "Evolutionary origins of the blood vascular system and endothelium." Journal of Thrombosis and Haemostasis **11**(s1): 46-66.
- Morén, B., et al. (2012). "EHD2 regulates caveolar dynamics via ATP-driven targeting and oligomerization." Molecular biology of the cell **23**(7): 1316-1329.
- Morgan, M. R., et al. (2009). "Giving off mixed signals—distinct functions of  $\alpha 5\beta 1$  and  $\alpha v\beta 3$  integrins in regulating cell behaviour." IUBMB life **61**(7): 731-738.
- Mori, S., et al. (2008). "Direct binding of integrin  $\alpha v\beta 3$  to FGF1 plays a role in FGF1 signaling." Journal of Biological Chemistry **283**(26): 18066-18075.
- Moser, M., et al. (2008). "Kindlin-3 is essential for integrin activation and platelet aggregation." Nature medicine **14**(3): 325.
- Mu, Z., et al. (2017). "Structural insight into the Ragulator complex which anchors mTORC1 to the lysosomal membrane." Cell discovery **3**: 17049.
- Mucka, P., et al. (2016). "Inflammation and lymphedema are exacerbated and prolonged by neuropilin 2 deficiency." The American journal of pathology **186**(11): 2803-2812.
- Muders, M. H., et al. (2009). "Vascular endothelial growth factor-C protects prostate cancer cells from oxidative stress by the activation of mammalian target of rapamycin complex-2 and AKT-1." Cancer research **69**(15): 6042-6048.
- Muether, P. S., et al. (2007). "The role of integrin  $\alpha 5\beta 1$  in the regulation of corneal neovascularization." Experimental eye research **85**(3): 356-365.
- Mukai, H., et al. (2016). "PKN3 is the major regulator of angiogenesis and tumor metastasis in mice." Scientific reports **6**: 18979.
- Muller, Y. A., et al. (1997). "Vascular endothelial growth factor: crystal structure and functional mapping of the kinase domain receptor binding site." Proceedings of the National Academy of Sciences **94**(14): 7192-7197.
- Munde, P. B., et al. (2014). "Pericytes in Health and Disease." International Journal of Oral & Maxillofacial Pathology **5**(1).

Muñoz-Chápuli, R., et al. (2005). "The origin of the endothelial cells: an evo-devo approach for the invertebrate/vertebrate transition of the circulatory system." Evolution & development **7**(4): 351-358.

Murga, M., et al. (2005). "Neuropilin-1 regulates attachment in human endothelial cells independently of vascular endothelial growth factor receptor-2." Blood **105**(5): 1992-1999.

Naboulsi, W., et al. (2016). "Quantitative proteome analysis reveals the correlation between endocytosis-associated proteins and hepatocellular carcinoma dedifferentiation." Biochimica et Biophysica Acta (BBA)-Proteins and Proteomics **1864**(11): 1579-1585.

Nagano, M., et al. (2012). "Turnover of focal adhesions and cancer cell migration." International journal of cell biology **2012**.

Nakamura, F., et al. (1998). "Neuropilin-1 extracellular domains mediate semaphorin D/III-induced growth cone collapse." Neuron **21**(5): 1093-1100.

Nakayama, H., et al. (2015). "Regulation of mTOR signaling by semaphorin 3F-neuropilin 2 interactions in vitro and in vivo." Scientific reports **5**: 11789.

Nasarre, P., et al. (2013). "Neuropilin-2 is upregulated in lung cancer cells during TGF- $\beta$ 1-induced epithelial-mesenchymal transition." Cancer research.

Nayal, A., et al. (2006). "Paxillin phosphorylation at Ser273 localizes a GIT1-PIX-PAK complex and regulates adhesion and protrusion dynamics." The Journal of cell biology **173**(4): 587-589.

Neufeld, G., et al. (1999). "Vascular endothelial growth factor (VEGF) and its receptors." The FASEB Journal **13**(1): 9-22.

Neufeld, G., et al. (2002). "The neuropilins." Trends in cardiovascular medicine **12**(1): 13-19.

Neufeld, G., et al. (2002). "The neuropilins: multifunctional semaphorin and VEGF receptors that modulate axon guidance and angiogenesis." Trends in cardiovascular medicine **12**(1): 13-19.

Neufeld, G., et al. (2007). Semaphorins, plexins and neuropilins and their role in vasculogenesis and angiogenesis. Modern Concepts in Angiogenesis, World Scientific: 1-25.

Nevo, J. (2011). "Novel Players in the Integrin Signaling Orchestra: TCPTP and MDGI."

Ni, C.-W., et al. (2014). "Development of immortalized mouse aortic endothelial cell lines." Vascular cell **6**(1): 7.

Nicosia, R. (2009). "The aortic ring model of angiogenesis: a quarter century of search and discovery." Journal of cellular and molecular medicine **13**(10): 4113-4136.

Nicosia, R. F., et al. (1982). "Histotypic angiogenesis in vitro: light microscopic, ultrastructural, and radioautographic studies." In vitro **18**(6): 538-549.

Nisato, R. E., et al. (2003). " $\alpha$ v $\beta$ 3 and  $\alpha$ v $\beta$ 5 integrin antagonists inhibit angiogenesis in vitro." Angiogenesis **6**(2): 105-119.

Nishiya, N., et al. (2005). "An  $\alpha$ 4 integrin–paxillin–Arf-GAP complex restricts Rac activation to the leading edge of migrating cells." Nature cell biology **7**(4): 343-352.

Nissen, N. N., et al. (1998). "Vascular endothelial growth factor mediates angiogenic activity during the proliferative phase of wound healing." The American journal of pathology **152**(6): 1445.

Okazaki, T., et al. (2009). " $\alpha$ 5 $\beta$ 1 integrin blockade inhibits lymphangiogenesis in airway inflammation." The American journal of pathology **174**(6): 2378-2387.

Ong, H., et al. (2017). "Cytoplasmic neuropilin 2 is associated with metastasis and a poor prognosis in early tongue cancer patients." International journal of oral and maxillofacial surgery **46**(10): 1205-1219.

Orecchia, A., et al. (2003). "Vascular endothelial growth factor receptor-1 is deposited in the extracellular matrix by endothelial cells and is a ligand for the  $\alpha$ 5 $\beta$ 1 integrin." Journal of cell science **116**(17): 3479-3489.

Ou, J.-J., et al. (2015). "Neuropilin-2 mediates lymphangiogenesis of colorectal carcinoma via a VEGFC/VEGFR3 independent signaling." Cancer letters **358**(2): 200-209.

Palecek, S. P., et al. (1996). "Integrin dynamics on the tail region of migrating fibroblasts." Journal of cell science **109**(5): 941-952.

Pan, L., et al. (2016). "Research advances on structure and biological functions of integrins." Springerplus **5**(1): 1094.

Pan, Q., et al. (2007). "Blocking neuropilin-1 function has an additive effect with anti-VEGF to inhibit tumor growth." Cancer cell **11**(1): 53-67.

Pan, Q., et al. (2007). "Neuropilin-1 binds to VEGF121 and regulates endothelial cell migration and sprouting." Journal of Biological Chemistry **282**(33): 24049-24056.

Pankov, R., et al. (2000). "Integrin dynamics and matrix assembly: tensin-dependent translocation of  $\alpha 5 \beta 1$  integrins promotes early fibronectin fibrillogenesis." The Journal of cell biology **148**(5): 1075-1090.

Park-Windhol, C., et al. (2017). "Endomucin inhibits VEGF-induced endothelial cell migration, growth, and morphogenesis by modulating VEGFR2 signaling." Scientific reports **7**(1): 17138.

Park, S., et al. (2015). "PECAM-1 isoforms, eNOS and endoglin axis in regulation of angiogenesis." Clinical Science **129**(3): 217-234.

Parker, M. W., et al. (2012). "Function of members of the neuropilin family as essential pleiotropic cell surface receptors." Biochemistry **51**(47): 9437-9446.

Partanen, T. A., et al. (2000). "VEGF-C and VEGF-D expression in neuroendocrine cells and their receptor, VEGFR-3, in fenestrated blood vessels in human tissues." The FASEB Journal **14**(13): 2087-2096.

Pasapera, A. M., et al. (2010). "Myosin II activity regulates vinculin recruitment to focal adhesions through FAK-mediated paxillin phosphorylation." The Journal of cell biology **188**(6): 877-890.

Paul, N. R., et al. (2015). "Endocytic trafficking of integrins in cell migration." Current Biology **25**(22): R1092-R1105.

Peach, C. J., et al. (2018). "Molecular pharmacology of VEGF-A isoforms: binding and signalling at VEGFR2." International journal of molecular sciences **19**(4): 1264.

Pellet-Many, C., et al. (2011). "Neuropilin-1 mediates PDGF stimulation of vascular smooth muscle cell migration and signalling via p130Cas." Biochemical Journal **435**(3): 609-618.

Pellet-Many, C., et al. (2008). "Neuropilins: structure, function and role in disease." Biochemical Journal **411**(2): 211-226.

Peng, X., et al. (2012). " $\alpha$ -Catenin uses a novel mechanism to activate vinculin." Journal of Biological Chemistry **287**(10): 7728-7737.

Phng, L.-K. and H. Gerhardt (2009). "Angiogenesis: a team effort coordinated by notch." Developmental cell **16**(2): 196-208.

Pierini, L. M., et al. (2000). "Oriented endocytic recycling of  $\alpha 5\beta 1$  in motile neutrophils." Blood **95**(8): 2471-2480.

Plein, A., et al. (2014). "Neuropilin regulation of angiogenesis, arteriogenesis, and vascular permeability." Microcirculation **21**(4): 315-323.

Plow, E. F., et al. (2014). "Integrin function in vascular biology: a view from 2013." Current opinion in hematology **21**(3): 241.

Poltorak, Z., et al. (1997). "VEGF145, a secreted vascular endothelial growth factor isoform that binds to extracellular matrix." Journal of Biological Chemistry **272**(11): 7151-7158.

Posey, J. A., et al. (2001). "A pilot trial of Vitaxin, a humanized anti-vitronectin receptor (anti  $\alpha v \beta 3$ ) antibody in patients with metastatic cancer." Cancer Biotherapy and Radiopharmaceuticals **16**(2): 125-132.

Potente, M. and T. Mäkinen (2017). "Vascular heterogeneity and specialization in development and disease." Nature reviews Molecular cell biology **18**(8): 477.

Powelka, A. M., et al. (2004). "Stimulation-Dependent Recycling of Integrin  $\beta 1$  Regulated by ARF6 and Rab11." Traffic **5**(1): 20-36.

Praht, C., et al. (2008). "Neuropilin-1-VEGFR-2 complexing requires the PDZ-binding domain of neuropilin-1." Journal of Biological Chemistry **283**(37): 25110-25114.

Prud'homme, G. J. and Y. Glinka (2012). "Neuropilins are multifunctional coreceptors involved in tumor initiation, growth, metastasis and immunity." Oncotarget **3**(9): 921.

Pugsley, M. and R. Tabrizchi (2000). "The vascular system: An overview of structure and function." Journal of pharmacological and toxicological methods **44**(2): 333-340.

Purushothaman, A., et al. (2010). "Heparanase enhanced shedding of syndecan-1 by myeloma cells promotes endothelial invasion and angiogenesis." Blood: blood-2009-2007-234757.

Pytela, R., et al. (1985). "Identification and isolation of a 140 kd cell surface glycoprotein with properties expected of a fibronectin receptor." Cell **40**(1): 191-198.

Raghu, K. (2003). "Basement membranes: structure, assembly and role in tumor angiogenesis." Nat Med **3**: 442-433.

Raimondi, C., et al. (2014). "Imatinib inhibits VEGF-independent angiogenesis by targeting neuropilin 1–dependent ABL1 activation in endothelial cells." Journal of Experimental Medicine **211**(6): 1167-1183.

Ramsay, A. G., et al. (2007). "HS1-associated protein X-1 regulates carcinoma cell migration and invasion via clathrin-mediated endocytosis of integrin  $\alpha v \beta 6$ ." Cancer research **67**(11): 5275-5284.

Raper, J. A. (2000). "Semaphorins and their receptors in vertebrates and invertebrates." Current opinion in neurobiology **10**(1): 88-94.

Rauch, B. H., et al. (2007). "ICAM-1 and p38 MAPK mediate fibrinogen-induced migration of human vascular smooth muscle cells." European journal of pharmacology **577**(1-3): 54-57.

Ravelli, C., et al. (2013). "Involvement of  $\alpha v \beta 3$  integrin in gremlin-induced angiogenesis." Angiogenesis **16**(1): 235-243.

Regen, C. M. and A. F. Horwitz (1992). "Dynamics of beta 1 integrin-mediated adhesive contacts in motile fibroblasts." The Journal of cell biology **119**(5): 1347-1359.

Reinhart-King, C. A. (2008). "Endothelial cell adhesion and migration." Methods in enzymology **443**: 45-64.

Remacle, A., et al. (2003). "Membrane type I-matrix metalloproteinase (MT1-MMP) is internalised by two different pathways and is recycled to the cell surface." J Cell Sci **116**(19): 3905-3916.

Reuter, J. S. and D. H. Mathews (2010). "RNAstructure: software for RNA secondary structure prediction and analysis." BMC bioinformatics **11**(1): 129.

Rey-Gallardo, A., et al. (2010). "Polysialylated neuropilin-2 enhances human dendritic cell migration through the basic C-terminal region of CCL21." Glycobiology **20**(9): 1139-1146.

Reyes, M., et al. (2002). "Origin of endothelial progenitors in human postnatal bone marrow." The Journal of clinical investigation **109**(3): 337-346.

Reynolds, A., et al. (2004). "Rational siRNA design for RNA interference." Nature biotechnology **22**(3): 326.

Reynolds, A. R., et al. (2009). "Stimulation of tumor growth and angiogenesis by low concentrations of RGD-mimetic integrin inhibitors." Nature medicine **15**(4): 392.

Reynolds, A. R., et al. (2004). "Elevated Flk1 (vascular endothelial growth factor receptor 2) signaling mediates enhanced angiogenesis in  $\beta$ 3-integrin-deficient mice." Cancer research **64**(23): 8643-8650.

Reynolds, L. E. and K. M. Hodivala-Dilke (2006). Primary mouse endothelial cell culture for assays of angiogenesis. Breast Cancer Research Protocols, Springer: 503-509.

Reynolds, L. E., et al. (2002). "Enhanced pathological angiogenesis in mice lacking  $\beta$  3 integrin or  $\beta$  3 and  $\beta$  5 integrins." Nature medicine **8**(1): 27.

Riley, R. and A. Cournand (1951). "Analysis of factors affecting partial pressures of oxygen and carbon dioxide in gas and blood of lungs: theory." Journal of applied physiology **4**(2): 77-101.

Risau, W. and I. Flamme (1995). "Vasculogenesis." Annual review of cell and developmental biology **11**(1): 73-91.

Roberts, M., et al. (2001). "PDGF-regulated rab4-dependent recycling of  $\alpha$ v $\beta$ 3 integrin from early endosomes is necessary for cell adhesion and spreading." Current Biology **11**(18): 1392-1402.

Roberts, W. G. and G. E. Palade (1997). "Neovasculature induced by vascular endothelial growth factor is fenestrated." Cancer research **57**(4): 765-772.

Robinson, S. D., et al. (2009). "Alphavbeta3-integrin limits the contribution of neuropilin-1 to VEGF-induced angiogenesis." Journal of Biological Chemistry: jbc. M109. 030700.

Robinson, S. D., et al. (2009). " $\alpha$ v $\beta$ 3 integrin limits the contribution of neuropilin-1 to vascular endothelial growth factor-induced angiogenesis." Journal of Biological Chemistry **284**(49): 33966-33981.

Robinson, S. D., et al. (2004). " $\beta$ 3-Integrin Regulates Vascular Endothelial Growth Factor-A-Dependent Permeability." Arteriosclerosis, thrombosis, and vascular biology **24**(11): 2108-2114.

Rossignol, M., et al. (2000). "Genomic organization of human neuropilin-1 and neuropilin-2 genes: identification and distribution of splice variants and soluble isoforms." Genomics **70**(2): 211-222.

Rousseau, S., et al. (1997). "p38 MAP kinase activation by vascular endothelial growth factor mediates actin reorganization and cell migration in human endothelial cells." Oncogene **15**(18): 2169-2177.

Rubinson, D. A., et al. (2003). "A lentivirus-based system to functionally silence genes in primary mammalian cells, stem cells and transgenic mice by RNA interference." Nature genetics **33**(3): 401.

Rucker, H. K., et al. (2000). "Cellular mechanisms of CNS pericytes." Brain research bulletin **51**(5): 363-369.

Rüegg, C. and A. Mariotti (2003). "Vascular integrins: pleiotropic adhesion and signaling molecules in vascular homeostasis and angiogenesis." Cellular and Molecular Life Sciences CMLS **60**(6): 1135-1157.

Ruffini, F., et al. (2015). "Cilengitide downmodulates invasiveness and vasculogenic mimicry of neuropilin 1 expressing melanoma cells through the inhibition of  $\alpha v \beta 5$  integrin." International journal of cancer **136**(6).

Russell, W. M. S., et al. (1959). "The principles of humane experimental technique."

Rutanen, J., et al. (2003). "Vascular endothelial growth factor-D expression in human atherosclerotic lesions." Cardiovascular research **59**(4): 971-979.

Sampieri, C. L., et al. (2008). "Activation of p38 and JNK MAPK pathways abrogates requirement for new protein synthesis for phorbol ester mediated induction of select MMP and TIMP genes." Matrix biology **27**(2): 128-138.

Sanchez-Carbayo, M., et al. (2003). "Gene discovery in bladder cancer progression using cDNA microarrays." The American journal of pathology **163**(2): 505-516.

Sawano, A., et al. (1996). "Flt-1 but not KDR/Flk-1 tyrosine kinase is a receptor for placenta growth factor, which is related to vascular endothelial growth factor." Cell growth & differentiation: the molecular biology journal of the American Association for Cancer Research **7**(2): 213-221.

Schaffner, F., et al. (2013). "Integrin  $\alpha 5\beta 1$ , the fibronectin receptor, as a pertinent therapeutic target in solid tumors." Cancers **5**(1): 27-47.

Schiller, H. B., et al. (2011). "Quantitative proteomics of the integrin adhesome show a myosin II-dependent recruitment of LIM domain proteins." EMBO reports **12**(3): 259-266.

Schneider-Poetsch, T., et al. (2010). "Inhibition of eukaryotic translation elongation by cycloheximide and lactimidomycin." Nature chemical biology **6**(3): 209.

Schneller, M., et al. (1997). " $\alpha v\beta 3$  integrin associates with activated insulin and PDGF $\beta$  receptors and potentiates the biological activity of PDGF." The EMBO journal **16**(18): 5600-5607.

Schwarz, Q. and C. Ruhrberg (2010). "Neuropilin, you gotta let me know: should I stay or should I go?" Cell adhesion & migration **4**(1): 61-66.

Szcekan, M. M. and R. Juliano (1990). "Internalization of the fibronectin receptor is a constitutive process." Journal of cellular physiology **142**(3): 574-580.

Seguin, L., et al. (2015). "Integrins and cancer: regulators of cancer stemness, metastasis, and drug resistance." Trends in cell biology **25**(4): 234-240.

Sen, A., et al. (2012). "Paxillin mediates extranuclear and intranuclear signaling in prostate cancer proliferation." The Journal of clinical investigation **122**(7): 2469-2481.

Senger, D. R. and G. E. Davis (2011). "Angiogenesis." Cold Spring Harbor perspectives in biology **3**(8): a005090.

Serini, G., et al. (2013). "Class 3 semaphorins: physiological vascular normalizing agents for anti-cancer therapy." Journal of internal medicine **273**(2): 138-155.

Serini, G., et al. (2006). "Integrins and angiogenesis: a sticky business." Experimental cell research **312**(5): 651-658.

Setyawati, M. I., et al. (2015). "Understanding and exploiting nanoparticles' intimacy with the blood vessel and blood." Chemical Society Reviews **44**(22): 8174-8199.

Shah, N., et al. (2015). "Three  $\alpha$ SNAP and 10 ATP molecules are used in SNARE complex disassembly by N-ethylmaleimide-sensitive factor (NSF)." Journal of Biological Chemistry **290**(4): 2175-2188.

Shalaby, F., et al. (1995). "Failure of blood-island formation and vasculogenesis in Flk-1-deficient mice." Nature **376**(6535): 62.

Sharma, R., et al. (2004). "Gene therapy: Current concepts."

Shi, F. and J. Sottile (2008). "Caveolin-1-dependent  $\beta$ 1 integrin endocytosis is a critical regulator of fibronectin turnover." Journal of cell science **121**(14): 2360-2371.

Shibuya, M. (2006). "Differential roles of vascular endothelial growth factor receptor-1 and receptor-2 in angiogenesis." BMB Reports **39**(5): 469-478.

Shibuya, M. (2011). "Vascular endothelial growth factor (VEGF) and its receptor (VEGFR) signaling in angiogenesis: a crucial target for anti-and pro-angiogenic therapies." Genes & cancer **2**(12): 1097-1105.

Shintani, Y., et al. (2006). "Glycosaminoglycan modification of neuropilin-1 modulates VEGFR2 signaling." The EMBO journal **25**(13): 3045-3055.

Shraga-Heled, N., et al. (2007). "Neuropilin-1 and neuropilin-2 enhance VEGF121 stimulated signal transduction by the VEGFR-2 receptor." The FASEB Journal **21**(3): 915-926.

Silverio, A., et al. (2015). "Aortic dissection in patients with autosomal dominant polycystic kidney disease: a series of two cases and a review of the literature." Nephrology **20**(4): 229-235.

Sivarapatna, A., et al. (2015). "Arterial specification of endothelial cells derived from human induced pluripotent stem cells in a biomimetic flow bioreactor." Biomaterials **53**: 621-633.

Small, J. V., et al. (1998). "Assembling an actin cytoskeleton for cell attachment and movement." Biochimica Et Biophysica Acta (BBA)-Molecular Cell Research **1404**(3): 271-281.

Smith, G. A., et al. (2015). "The cellular response to vascular endothelial growth factors requires co-ordinated signal transduction, trafficking and proteolysis." Bioscience reports: BSR20150171.

Soker, S., et al. (1996). "Characterization of novel vascular endothelial growth factor (VEGF) receptors on tumor cells that bind VEGF via its exon 7-encoded domain." Journal of Biological Chemistry **271**(10): 5761-5767.

- Soker, S., et al. (2002). "VEGF165 mediates formation of complexes containing VEGFR-2 and neuropilin-1 that enhance VEGF165-receptor binding." Journal of cellular biochemistry **85**(2): 357-368.
- Soker, S., et al. (1998). "Neuropilin-1 is expressed by endothelial and tumor cells as an isoform-specific receptor for vascular endothelial growth factor." Cell **92**(6): 735-745.
- Soldi, R., et al. (1999). "Role of  $\alpha v \beta 3$  integrin in the activation of vascular endothelial growth factor receptor-2." The EMBO journal **18**(4): 882-892.
- Somanath, P. R., et al. (2009). "Integrin and growth factor receptor alliance in angiogenesis." Cell biochemistry and biophysics **53**(2): 53-64.
- Somanath, P. R., et al. (2009). "Cooperation between integrin  $\alpha v \beta 3$  and VEGFR2 in angiogenesis." Angiogenesis **12**(2): 177-185.
- Somanath, P. R., et al. (2006). "Akt1 in endothelial cell and angiogenesis." Cell cycle **5**(5): 512-518.
- Sottile, J. and J. Chandler (2005). "Fibronectin matrix turnover occurs through a caveolin-1-dependent process." Molecular biology of the cell **16**(2): 757-768.
- Srichai, M. B. and R. Zent (2010). Integrin structure and function. Cell-extracellular matrix interactions in cancer, Springer: 19-41.
- Stalmans, I., et al. (2002). "Arteriolar and venular patterning in retinas of mice selectively expressing VEGF isoforms." The Journal of clinical investigation **109**(3): 327-336.
- Stanton, M. J., et al. (2012). "Autophagy control by the VEGF-C/NRP-2 axis in cancer and its implication for treatment resistance." Cancer research.
- Stenbeck, G. (1998). "Soluble NSF-attachment proteins." The international journal of biochemistry & cell biology **30**(5): 573-577.
- Stenn, K. S., et al. (1989). "Dispase, a neutral protease from *Bacillus polymyxa*, is a powerful fibronectinase and type IV collagenase." Journal of investigative dermatology **93**(2): 287-290.
- Stephens, L. E., et al. (1995). "Deletion of beta 1 integrins in mice results in inner cell mass failure and peri-implantation lethality." Genes & development **9**(15): 1883-1895.

Steri, V., et al. (2014). "Acute Depletion of Endothelial  $\beta$ 3-Integrin Transiently Inhibits Tumor Growth and Angiogenesis in Mice Novelty and Significance." Circulation research **114**(1): 79-91.

Stoeber, M., et al. (2012). "Oligomers of the ATPase EHD2 confine caveolae to the plasma membrane through association with actin." The EMBO journal **31**(10): 2350-2364.

Streuli, C. (1999). "Extracellular matrix remodelling and cellular differentiation." Current opinion in cell biology **11**(5): 634-640.

Strieth, S., et al. (2006). "Antiangiogenic combination tumor therapy blocking  $\alpha$ v-integrins and VEGF-receptor-2 increases therapeutic effects in vivo." International journal of cancer **119**(2): 423-431.

Stupp, R., et al. (2014). "Cilengitide combined with standard treatment for patients with newly diagnosed glioblastoma with methylated MGMT promoter (CENTRIC EORTC 26071-22072 study): a multicentre, randomised, open-label, phase 3 trial." The lancet oncology **15**(10): 1100-1108.

Suarez, S. C., et al. (2006). "A VEGF-A splice variant defective for heparan sulfate and neuropilin-1 binding shows attenuated signaling through VEGFR-2." Cellular and Molecular Life Sciences CMLS **63**(17): 2067-2077.

Sun, X.-z., et al. (2011). "Over-expression of VEGF165 in the adipose tissue-derived stem cells via the lentiviral vector." Chinese Medical Journal-Beijing **124**(19): 3093.

Sun, Y., et al. (2004). "Increased Severity of Cerebral Ischemic Injury in Vascular Endothelial Growth Factor-B-Deficient Mice." Journal of Cerebral Blood Flow & Metabolism **24**(10): 1146-1152.

Susanto, J., et al. (2008). "Porphyrin homeostasis maintained by ABCG2 regulates self-renewal of embryonic stem cells." PLoS One **3**(12): e4023.

Suzuki, K., et al. (2008). "Semaphorins and their receptors in immune cell interactions." Nature immunology **9**(1): 17.

Suzuki, Y., et al. (2007). "BMPs promote proliferation and migration of endothelial cells via stimulation of VEGF-A/VEGFR2 and angiopoietin-1/Tie2 signalling." Journal of biochemistry **143**(2): 199-206.

Swartz, M. A. (2001). "The physiology of the lymphatic system." Advanced drug delivery reviews **50**(1-2): 3-20.

Tabatabai, G. and M. Weller (2013). Role of integrins in angiogenesis. Biochemical Basis and Therapeutic Implications of Angiogenesis, Springer: 79-91.

Takagi, S., et al. (1991). "The A5 antigen, a candidate for the neuronal recognition molecule, has homologies to complement components and coagulation factors." Neuron **7**(2): 295-307.

Takagi, S., et al. (1987). "Specific cell surface labels in the visual centers of *Xenopus laevis* tadpole identified using monoclonal antibodies." Developmental biology **122**(1): 90-100.

Takahashi, H. and M. Shibuya (2005). "The vascular endothelial growth factor (VEGF)/VEGF receptor system and its role under physiological and pathological conditions." Clinical Science **109**(3): 227-241.

Takahashi, T., et al. (1999). "VEGF activates protein kinase C-dependent, but Ras-independent Raf-MEK-MAP kinase pathway for DNA synthesis in primary endothelial cells." Oncogene **18**(13): 2221.

Takahashi, T., et al. (2001). "A single autophosphorylation site on KDR/Flk-1 is essential for VEGF-A-dependent activation of PLC- $\gamma$  and DNA synthesis in vascular endothelial cells." The EMBO journal **20**(11): 2768-2778.

Takashima, S., et al. (2002). "Targeting of both mouse neuropilin-1 and neuropilin-2 genes severely impairs developmental yolk sac and embryonic angiogenesis." Proceedings of the National Academy of Sciences **99**(6): 3657-3662.

Tamagnone, L., et al. (1999). "Plexins are a large family of receptors for transmembrane, secreted, and GPI-anchored semaphorins in vertebrates." Cell **99**(1): 71-80.

Tamkun, J. W., et al. (1986). "Structure of integrin, a glycoprotein involved in the transmembrane linkage between fibronectin and actin." Cell **46**(2): 271-282.

Tammela, T., et al. (2005). "The biology of vascular endothelial growth factors." Cardiovascular research **65**(3): 550-563.

Tan, W. H., et al. (2013). "Computational model of VEGFR2 pathway to ERK activation and modulation through receptor trafficking." Cellular signalling **25**(12): 2496-2510.

Tanjore, H., et al. (2008). " $\beta$ 1 integrin expression on endothelial cells is required for angiogenesis but not for vasculogenesis." Developmental dynamics **237**(1): 75-82.

Tannenbaum, J. and B. T. Bennett (2015). "Russell and Burch's 3Rs then and now: the need for clarity in definition and purpose." Journal of the American Association for Laboratory Animal Science **54**(2): 120-132.

Tasaki, Y., et al. (2010). "Expression of VEGF and its receptors in the bovine endometrium throughout the estrous cycle: effects of VEGF on prostaglandin production in endometrial cells." Journal of Reproduction and Development **56**(2): 223-229.

Taverna, D. and R. O. Hynes (2001). "Reduced blood vessel formation and tumor growth in  $\alpha 5$ -integrin-negative teratocarcinomas and embryoid bodies." Cancer research **61**(13): 5255-5261.

Teckchandani, A., et al. (2009). "Quantitative proteomics identifies a Dab2/integrin module regulating cell migration." The Journal of cell biology **186**(1): 99-111.

Teran, M. and M. A. Nugent (2015). "Synergistic binding of vascular endothelial growth factor-A and its receptors to heparin selectively modulates complex affinity." Journal of Biological Chemistry: jbc. M114. 627372.

Terryn, C., et al. (2009). "Video-microscopic imaging of cell spatio-temporal dispersion and migration." Critical reviews in oncology/hematology **69**(2): 144-152.

Theocharis, A. D., et al. (2016). "Extracellular matrix structure." Advanced drug delivery reviews **97**: 4-27.

Tillo, M., et al. (2015). "VEGF189 binds NRP1 and is sufficient for VEGF/NRP1-dependent neuronal patterning in the developing brain." Development **142**(2): 314-319.

Tiwari, A., et al. (2012). Membrane trafficking and endothelial-cell dynamics during angiogenesis. Hematology-Science and Practice, InTech.

Tomizawa, Y., et al. (2001). "Inhibition of lung cancer cell growth and induction of apoptosis after reexpression of 3p21. 3 candidate tumor suppressor gene SEMA3B." Proceedings of the National Academy of Sciences **98**(24): 13954-13959.

Triantafilou, K. and M. Triantafilou (2001). "Mechanisms of integrin-mediated virus attachment and internalization process." Critical Reviews<sup>TM</sup> in Immunology **21**(4).

Umeda, N., et al. (2006). "Suppression and regression of choroidal neovascularization by systemic administration of an  $\alpha 5\beta 1$  integrin antagonist." Molecular pharmacology.

Vadakekolathu, J., et al. (2018). "MTSS1 and SCAMP1 cooperate to prevent invasion in breast cancer." Cell death & disease **9**(3): 344.

Vadasz, Z., et al. (2012). "Semaphorin 3A is a marker for disease activity and a potential immunoregulator in systemic lupus erythematosus." Arthritis research & therapy **14**(3): R146.

Vailhé, B., et al. (2001). "In vitro models of vasculogenesis and angiogenesis." Laboratory investigation **81**(4): 439.

Valdembri, D., et al. (2009). "Neuropilin-1/GIPC1 signaling regulates  $\alpha 5\beta 1$  integrin traffic and function in endothelial cells." PLoS Biol **7**(1): e1000025.

Valdembri, D. and G. Serini (2012). "Regulation of adhesion site dynamics by integrin traffic." Current opinion in cell biology **24**(5): 582-591.

Vales, A., et al. (2007). "Myeloid leukemias express a broad spectrum of VEGF receptors including neuropilin-1 (NRP-1) and NRP-2." Leukemia & lymphoma **48**(10): 1997-2007.

van der Flier, A., et al. (2010). "Endothelial  $\alpha 5$  and  $\alpha v$  integrins cooperate in remodeling of the vasculature during development." Development **137**(14): 2439-2449.

Velling, T., et al. (1996). "Distinct  $\alpha 7A\beta 1$  and  $\alpha 7B\beta 1$  integrin expression patterns during mouse development:  $\alpha 7A$  is restricted to skeletal muscle but  $\alpha 7B$  is expressed in striated muscle, vasculature, and nervous system." Developmental dynamics **207**(4): 355-371.

Vellon, L., et al. (2006). "A bidirectional " $\alpha v\beta 3$  integrin-ERK1/ERK2 MAPK" connection regulates the proliferation of breast cancer cells." Molecular carcinogenesis **45**(10): 795-804.

Vempati, P., et al. (2014). "Extracellular regulation of VEGF: isoforms, proteolysis, and vascular patterning." Cytokine & growth factor reviews **25**(1): 1-19.

Ventura, A., et al. (2004). "Cre-lox-regulated conditional RNA interference from transgenes." Proceedings of the National Academy of Sciences of the United States of America **101**(28): 10380-10385.

Vlodavsky, I. and D. Gospodarowicz (1981). "Respective roles of laminin and fibronectin in adhesion of human carcinoma and sarcoma cells." Nature **289**(5795): 304-306.

Vlodavsky, I., et al. (1980). "Morphological appearance, growth behavior and migratory activity of human tumor cells maintained on extracellular matrix versus plastic." Cell **19**(3): 607-616.

Wallez, Y. and P. Huber (2008). "Endothelial adherens and tight junctions in vascular homeostasis, inflammation and angiogenesis." Biochimica et Biophysica Acta (BBA)-Biomembranes **1778**(3): 794-809.

Wang, J. and R. Milner (2006). "Fibronectin promotes brain capillary endothelial cell survival and proliferation through  $\alpha 5\beta 1$  and  $\alpha v\beta 3$  integrins via MAP kinase signalling." Journal of neurochemistry **96**(1): 148-159.

Wang, L., et al. (2006). "C terminus of RGS-GAIP-interacting protein conveys neuropilin-1-mediated signaling during angiogenesis." The FASEB Journal **20**(9): 1513-1515.

Wang, L., et al. (2003). "Neuropilin-1-mediated vascular permeability factor/vascular endothelial growth factor-dependent endothelial cell migration." Journal of Biological Chemistry **278**(49): 48848-48860.

Wang, Y.-N., et al. (2010). "COPI-mediated retrograde trafficking from the Golgi to the ER regulates EGFR nuclear transport." Biochemical and biophysical research communications **399**(4): 498-504.

Ward, T. H., et al. (2001). "Maintenance of Golgi structure and function depends on the integrity of ER export." The Journal of cell biology **155**(4): 557-570.

Webb, D. J., et al. (2002). "Adhesion assembly, disassembly and turnover in migrating cells—over and over and over again." Nature cell biology **4**(4): E97-E100.

Węsierska-Gądek, J., et al. (2007). "Phenol red in the culture medium strongly affects the susceptibility of human MCF-7 cells to roscovitine." Cellular & molecular biology letters **12**(2): 280.

West, X. Z., et al. (2012). "Integrin  $\beta 3$  crosstalk with VEGFR accommodating tyrosine phosphorylation as a regulatory switch." PLoS One **7**(2): e31071.

Wewer, U. M., et al. (1997). "The integrin alpha 6 beta 1 promotes the survival of metastatic human breast carcinoma cells in mice." The American journal of pathology **151**(5): 1191.

Whitaker, G. B., et al. (2001). "Vascular endothelial growth factor receptor-2 and neuropilin-1 form a receptor complex that is responsible for the differential signaling potency of VEGF165 and VEGF121." Journal of Biological Chemistry **276**(27): 25520-25531.

Wijelath, E. S., et al. (2002). "Novel vascular endothelial growth factor binding domains of fibronectin enhance vascular endothelial growth factor biological activity." Circulation research **91**(1): 25-31.

Wilder, R. (2002). "Integrin alpha V beta 3 as a target for treatment of rheumatoid arthritis and related rheumatic diseases." Annals of the rheumatic diseases **61**(suppl 2): ii96-ii99.

Wittmann, P., et al. (2015). "Neuropilin-2 induced by transforming growth factor- $\beta$  augments migration of hepatocellular carcinoma cells." BMC cancer **15**(1): 909.

Wollebo, H. S., et al. (2013). Lentiviral transduction of neuronal cells. Neuronal Cell Culture, Springer: 141-146.

Woodard, A. S., et al. (1998). "The synergistic activity of  $\alpha v \beta 3$  integrin and PDGF receptor increases cell migration." Journal of cell science **111**(4): 469-478.

Woods, A. J., et al. (2004). "PKD1/PKC $\mu$  promotes  $\alpha v \beta 3$  integrin recycling and delivery to nascent focal adhesions." The EMBO journal **23**(13): 2531-2543.

Woolard, J., et al. (2009). "Molecular diversity of VEGF-A as a regulator of its biological activity." Microcirculation **16**(7): 572-592.

Woolard, J., et al. (2004). "VEGF165b, an inhibitory vascular endothelial growth factor splice variant: mechanism of action, in vivo effect on angiogenesis and endogenous protein expression." Cancer research **64**(21): 7822-7835.

Wu, H., et al. (2014). "Imaging Integrin  $\alpha v \beta 3$  and NRP-1 Positive Gliomas with a Novel Fluorine-18 Labeled RGD-ATWLPPR Heterodimeric Peptide Probe." Molecular Imaging and Biology **16**(6): 781-792.

Wu, L.-W., et al. (2000). "VRAP is an adaptor protein that binds KDR, a receptor for vascular endothelial cell growth factor." Journal of Biological Chemistry **275**(9): 6059-6062.

Xu, L., et al. (2018). "New microtubulin inhibitor MT189 suppresses angiogenesis via the JNK-VEGF/VEGFR2 signaling axis." Cancer letters **416**: 57-65.

Xu, Y., et al. (2010). "Neuropilin-2 mediates VEGF-C-induced lymphatic sprouting together with VEGFR3." The Journal of cell biology **188**(1): 115-130.

Yakkundi, A., et al. (2015). "FKBPL is a critical antiangiogenic regulator of developmental and pathological angiogenesis." Arteriosclerosis, thrombosis, and vascular biology: ATVBAHA. 114.304539.

Yamaji, S., et al. (2010). "A novel fibroblast growth factor-1 (FGF1) mutant that acts as an FGF antagonist." PLoS One **5**(4): e10273.

Yamaoka-Tojo, M., et al. (2006). "IQGAP1 mediates VE-cadherin-based cell-cell contacts and VEGF signaling at adherence junctions linked to angiogenesis." Arteriosclerosis, thrombosis, and vascular biology **26**(9): 1991-1997.

Yamazaki, Y., et al. (2009). "Snake venom Vascular Endothelial Growth Factors (VEGF-Fs) exclusively vary their structures and functions among species." Journal of Biological Chemistry.

Yang, C., et al. (2018). "Lipid raft-associated  $\beta$ -adducin participates in neutrophil migration." Molecular medicine reports **18**(2): 1353-1360.

Yang, J. T., et al. (1993). "Embryonic mesodermal defects in alpha 5 integrin-deficient mice." Development **119**(4): 1093-1105.

Yang, K. and A. Proweller (2011). "Vascular smooth muscle Notch signals regulate endothelial cell sensitivity to angiogenic stimulation." Journal of Biological Chemistry **286**(15): 13741-13753.

Yang, S., et al. (2017). "Diverse functions and mechanisms of pericytes in ischemic stroke." Current neuropharmacology **15**(6): 892-905.

Yasuoka, H., et al. (2009). "Neuropilin-2 expression in breast cancer: correlation with lymph node metastasis, poor prognosis, and regulation of CXCR4 expression." BMC cancer **9**(1): 220.

Yazdani, U. and J. R. Terman (2006). "The semaphorins." Genome biology **7**(3): 211.

Yazji, S., et al. (2007). "Final results from phase II study of volociximab, an  $\alpha 5\beta 1$  anti-integrin antibody, in refractory or relapsed metastatic clear cell renal cell carcinoma (mCCRCC)." Journal of Clinical Oncology **25**(18\_suppl): 5094-5094.

Yoon, S.-O., et al. (2005). "Hypoxia stimulates carcinoma invasion by stabilizing microtubules and promoting the Rab11 trafficking of the  $\alpha 6\beta 4$  integrin." Cancer research **65**(7): 2761-2769.

Yuan, L., et al. (2002). "Abnormal lymphatic vessel development in neuropilin 2 mutant mice." Development **129**(20): 4797-4806.

Zachary, I. (2014). Neuropilins: role in signalling, angiogenesis and disease. Angiogenesis, Lymphangiogenesis and Clinical Implications, Karger Publishers. **99**: 37-70.

Zachary, I. C., et al. (2009). The role of neuropilins in cell signalling, Portland Press Limited.

Zaidel-Bar, R., et al. (2003). "Early molecular events in the assembly of matrix adhesions at the leading edge of migrating cells." Journal of cell science **116**(22): 4605-4613.

Zaidel-Bar, R., et al. (2007). "A paxillin tyrosine phosphorylation switch regulates the assembly and form of cell-matrix adhesions." Journal of cell science **120**(1): 137-148.

Zal, T. (2008). Visualization of protein interactions in living cells. Multichain Immune Recognition Receptor Signaling, Springer: 183-197.

Zhang, C., et al. (2018). "Targeting VEGF/VEGFRs Pathway in the Antiangiogenic Treatment of Human Cancers by Traditional Chinese Medicine." Integrative cancer therapies: 1534735418775828.

Zhang, J. and D. Castle (2011). "Regulation of fusion pore closure and compound exocytosis in neuroendocrine PC12 cells by SCAMP1." Traffic **12**(5): 600-614.

Zhang, X., et al. (2005). "Extracellular matrix regulates endothelial functions through interaction of VEGFR-3 and integrin  $\alpha 5\beta 1$ ." Journal of cellular physiology **202**(1): 205-214.

Zhen, Y. and H. Stenmark (2015). "Cellular functions of Rab GTPases at a glance." J Cell Sci **128**(17): 3171-3176.

Zimmermann-Geller, B., et al. (2016). "Influence of extracellular RNAs, released by rheumatoid arthritis synovial fibroblasts, on their adhesive and invasive properties." The Journal of Immunology: 1501580.

Zovein, A. C., et al. (2010). " $\beta 1$  integrin establishes endothelial cell polarity and arteriolar lumen formation via a Par3-dependent mechanism." Developmental cell **18**(1): 39-51.

